

UCSF

UC San Francisco Electronic Theses and Dissertations

Title

FUNCTIONAL ANALYSIS OF LEUCINE-RICH AMELOGENIN PEPTIDE AND ITS MMP-20-MEDIATED PROTEOLYTIC PRODUCTS IN TOOTH FORMATION

Permalink

<https://escholarship.org/uc/item/5jh2p956>

Author

Le, Thuan Quoc

Publication Date

2007-03-16

Peer reviewed|Thesis/dissertation

Functional Analysis of Leucine-rich Amelogenin Peptide and Its MMP-20-Mediated
Proteolytic Products in Tooth Formation

by

Thuan Quoc Le

DISSERTATION

Submitted in partial satisfaction of the requirements for the degree of

DOCTOR OF PHILOSOPHY

in

Oral and Craniofacial Sciences

in the

GRADUATE DIVISION

of the

UNIVERSITY OF CALIFORNIA, SAN FRANCISCO

UMI Number: 3251929



UMI Microform 3251929

Copyright 2007 by ProQuest Information and Learning Company.
All rights reserved. This microform edition is protected against
unauthorized copying under Title 17, United States Code.

ProQuest Information and Learning Company
300 North Zeeb Road
P.O. Box 1346
Ann Arbor, MI 48106-1346

Acknowledgements

I would like to express my special thanks to Dr. Pam Den Besten and Dr. Wu Li, who were my primary mentors throughout my entire graduate school training. These two individuals have given me with a unique opportunity to be a member in their lab. They have taught me so much scientific knowledge while I was a Ph.D. student and provided me with invaluable guidance and motivation for me to pursue a future academic career. They were absolutely instrumental for whom I am becoming today.

I also want to thank all members in the lab: Cen Gao, Ling Ye, He Liu, Yan Zhang, Zhu Li, Kotaro Tanimoto, Shengwu Wang and James Chen for all their technical support, candid criticism and advice in my experimental designs and data analysis. These people are personable, intelligent, unselfish and the hardest-working researchers that I know and with whom I have had the privilege of becoming their friend and colleague. These special people truly made my daily training experiences most enjoyable in a highly intellectual environment.

I wish to thank my thesis committee members of world-renown scientists: Dr. Caroline Damsky, Dr. Pam Den Besten, Dr. John Featherstone, and Dr. Randall Kramer, who were willing to spend valuable time out of their extremely busy schedule to serve on my thesis committee. These faculty have provided me with excellent critique, advice and guidance during my oral qualifying exam and the writing of my thesis.

I thank Drs. Grayson and Sally Marshall, and Dr. Stefan Habelitz for allowing me to use the AFM instrument in their lab and the technical training for the use of these equipments. In addition, I thank them for giving me the opportunity to complete my highly-interesting research rotation in their lab to study and analyze the surface of dento-enamel junction (DEJ) using scanning electron microscopy (SEM).

I thank Dr. John Featherstone for allowing me to use the apatite synthesis instruments in his lab during my early research lab rotation. He has helped me so much with data interpretation and analysis throughout my training. He has introduced and taught me in areas of FTIR, X-ray diffraction and isothermal titration microcalorimetry (ITC). His input and guidance were instrumental for the success of the completion of this thesis.

I want thank Dr. Miriam Gochin for helping me with the interpretation of NMR and CD data to determine amelogenin structural information. I also want to thank Ewa Witkowska for assisting me in understanding the results of mass spectrometric analysis of the purified amelogenins and amelogenin proteolytic products.

And last but not least, I thank NIDCR training grants K16-DE00386 and T32-DE07306-09 for providing me with generous financial support throughout my 7.5 years of training as a dentist scientist candidate in Pediatric Dentistry and Oral & Craniofacial Sciences Graduate Program at the University of California at San Francisco.

Table of Contents:

Chapter 1. General Introduction and Summary.	Page 1-9
Chapter 2. Literature Review of Amelogenin Functions and Significance.	Page 10-31
Chapter 3. Preparation and Characterization of Enamel-like Synthetic Carbonated Hydroxyapatite.	Page 32-45
Chapter 4. Expression, Purification and Characterization of Full-length Amelogenin and Other Amelogenin Isoforms.	Page 46-61
Chapter 5. The Role of Carboxyl-terminal Domains of Amelogenins in Modulating <i>In Vitro</i> Enamel-like Crystal Growth.	Page 62-88
Chapter 6. Comparative Calcium Binding of Leucine-Rich Amelogenin Peptide and Full-Length Amelogenin.	Page 89-116
Chapter 7. Structural Determination of Leucine-rich Amelogenin Peptide Using Nuclear Magnetic Resonance (NMR) and Circular Dichroism (CD)	Page 117-131
Chapter 8. Amelogenins in Human Developing and Mature Dental Pulp, and the Effects of Amelogenins on Dental Pulp Cell Proliferation.	Page 132-153
Chapter 9. Proteolytic Processing of Leucine-rich Amelogenin Peptide and Functional Analysis of Its Proteolytic Products.	Page 154-182
Chapter 10. The Effect of Leucine-rich Amelogenin Peptide on Ameloblast-lineage Cell Differentiation.	Page 183-197

List of Figures and Tables:

Chapter 2. Literature Review of Amelogenin Functions and Significance.	Page 30-31
Chapter 3. Preparation and Characterization of Enamel-like Synthetic Carbonated Hydroxyapatite.	Page 40-45
Chapter 4. Expression, Purification and Characterization of Full-length Amelogenin and Other Amelogenin Isoforms.	Page 56-61
Chapter 5. The Carboxyl-terminal Domains of Full-length Amelogenin and LRAP Bind Synthetic Carbonated Hydroxyapatite to Modulate <i>In Vitro</i> Enamel-like Crystal Growth.	Page 79-88
Chapter 6. Comparative Calcium Binding of Leucine-Rich Amelogenin Peptide and Full-Length Amelogenin.	Page 104-116
Chapter 7. Structural Determination of Leucine-rich Amelogenin Peptide Using Nuclear Magnetic Resonance (NMR) and Circular Dichroism (CD)	Page 128-131
Chapter 8. Amelogenins in Human Developing and Mature Dental Pulp, and the Effects of Amelogenins on Dental Pulp Cell Proliferation.	Page 149-153
Chapter 9. Proteolytic Processing of Leucine-rich Amelogenin Peptide and Functional Analysis of Its Proteolytic Products.	Page 175-182
Chapter 10. The Effect of Leucine-rich Amelogenin Peptide on Ameloblast-lineage Cell Differentiation.	Page 194-197

Abstract:

Title: Functional Analysis of Leucine-rich Amelogenin Peptide and Its MMP-20-Mediated Proteolytic Products in Tooth Formation.

Name: Thuan Q. Le

Signature of Dissertation Advisor:



Amelogenins make up over 90% of the secretory enamel proteins and play a critical role in tooth enamel formation. There are several amelogenin isoforms identified within the enamel extracellular matrix as a result of proteolysis and alternative splicing of the primary amelogenin mRNA transcript. Leucine-rich amelogenin peptide (LRAP) is one of the major alternatively spliced amelogenins, whose function in tooth formation remains unclear. The purpose of this thesis is to explore the role and mechanism of LRAP and its MMP-20-mediated proteolytic products in enamel biomineralization, and their biological effects on odontogenic cell (i.e. dental pulp cell and ameloblast-lineage cell) proliferation and/or differentiation. The purified recombinant LRAP was hydrolyzed by active MMP-20. LRAP proteolytic products were analyzed by mass spectrometry to identify specific cleavage sites. Subsequently, LRAP and its proteolytic products were allowed to interact with synthetic carbonate hydroxyapatites (CAP) *in vitro* to determine the binding mechanism. After binding on the apatite substrates, these peptides were incubated in supersaturated calcium phosphate solution, similar to secretory stage enamel-like fluid, to study their ability to promote enamel-like crystal growth. In addition, LRAP and its proteolytic fragments were also exogenously added to human dental pulp cell and primary ameloblast-lineage cell cultures to study their effects

proliferation and/or differentiation. Expressions of regulatory genes and cell-surface receptors associated with these specific pathways were also identified by gene arrays, reverse-transcription PCR and immunohistochemistry. LRAP is a specific substrate for MMP-20 hydrolysis to cleave its C-terminal domain, which was responsible for the binding of LRAP directly onto the surface of CAP by ionic interactions. Unlike its parent amelogenin, LRAP did not function as a structural protein to promote crystal formation *in vitro*; however, it acted as a cell-signaling molecule to affect odontoblast cell proliferation and ameloblast-lineage cell differentiation by up-regulating and interacting with its cell membrane receptor lysosome-associated membrane glycoprotein 1 (LAMP-1). Therefore, LRAP functions in the early stages of cell development to control odontogenesis and amelogenesis. These are novel findings that allow us for the first time to understand how the alternatively spliced amelogenin protein, LRAP and its MMP-20 hydrolysis products, interact with cells and mineral in the developing tooth. This knowledge is critical for further studies of tooth regeneration and the use of amelogenins in biomineralization.

Chapter 1. General Introduction and Summary

Leucine-rich amelogenin peptide (LRAP) is one of the most abundant alternatively spliced amelogenins among the tooth enamel matrix proteins. LRAP is synthesized and secreted by both ameloblasts and odontoblasts, which suggests that this protein has a role in both tooth enamel and dentin formation. Currently, there is evidence to suggest that LRAP functions as a cell-signaling molecule, LRAP was shown to regulate non-odontogenic mesenchymal-derived cell (i.e. mouse embryonic myoblasts) proliferation and/or differentiation (Tompkins and Veis, 2002; Tompkins *et al.*, 2005; Tompkins *et al.*, 2006; Veis *et al.*, 2000; Veis, 2003). In addition, LRAP is also believed to interact with hydroxyapatite surface *in vitro* to regulate enamel biomineralization (Shaw *et al.*, 2004). However, the precise functional mechanisms of how LRAP affects human tooth development remain largely unknown. I hypothesize that LRAP does not function as a structural protein to promote enamel-like crystal formation; however, it acts as a cell-signaling molecule to affect odontoblast and ameloblast cell proliferation and/or differentiation processes that control dentin and enamel biomineralization. The objectives of my thesis were to determine the effects of LRAP and its MMP-20 (matrix metalloproteinase 20 or enamelysin)-mediated proteolytic products on the processes and development of cells that regulate odontogenesis and amelogenesis. Therefore, this thesis is focused in two primary directions.

First, the mechanism of interaction between LRAP and enamel-like synthetic carbonated hydroxyapatite (CAP) was analyzed. Functional domains were identified in crystal growth experiments to identify protein-apatite interaction that plays a role in regulating

enamel formation. Secondly, the effects of LRAP and its MMP-20-mediated proteolytic products on human dental pulp cell (DPC) and ameloblast-lineage cell (ALC) proliferation and/or differentiation were elucidated to understand the functions of LRAP in the early stages of cell developments that control odontogenesis and amelogenesis. Understanding the mechanism of LRAP function in enamel and dentin formation is critical for further advancement of the field of tooth development.

Additional literature review and background information regarding the current-known functions of enamel matrix proteins with specific emphasis on amelogenins, from which LRAP is one of the major alternatively spliced protein components, are reviewed in chapter 2. This information was necessary for understanding the basis and rationale of this thesis project.

The materials (i.e. synthetic carbonated apatites), recombinant full-length and several alternatively spliced amelogenins, antibodies (i.e. full-length amelogenin and LRAP antibodies) and odontogenic cells (i.e. dental pulp fibroblasts and ameloblast-lineage cells) used for this project were not available commercially, I had to synthesize these tools. Although the procedures required to make these materials were labor-intensive, it would not have been possible to complete the studies outlined in this thesis without them. In addition, these materials will be useful for further research on enamel development and biomineralization.

In my initial studies of LRAP-apatite interaction, enamel-like synthetic carbonated hydroxyapatite was synthesized using aqueous precipitation reaction according to previously published methods (Nelson and Featherstone, 1982) (chapter 3). The synthetic apatite was then characterized using Fourier Transform Infrared Spectroscopy (FTIR) and X-ray diffraction, and was found to be similar to synthetic carbonated hydroxyapatite found in dental enamel (Nelson and Featherstone, 1982). Therefore, this synthetic apatite could be used as a substitute for enamel.

The parent full-length amelogenin and several other amelogenin isoforms, resulting from alternative splicing and proteolysis, were either commercially synthesized or recombinantly expressed in bacteria *E. coli*, purified by affinity chromatography and reverse-phase HPLC, and finally characterized by SDS-PAGE, Western blots, and mass spectrometry analysis (chapter 4). After obtaining the synthetic carbonated hydroxyapatite and purified amelogenin proteins, the molecular mechanism of protein-apatite interaction was carefully investigated to determine the specific binding domain(s) of the full-length amelogenin and LRAP to the surface of apatite substrate (chapter 5).

A previous report using NMR methodology indicated that the carboxyl-terminal domain of LRAP appeared to orient toward the surface of hydroxyapatite (Shaw *et al.*, 2004). However, no details regarding mechanisms of interaction were provided. In chapter 5, I determined that full-length amelogenin and LRAP bind directly to the surface of synthetic carbonated hydroxyapatite by the hydrophilic carboxyl-terminal domains. This domain contains the last 11 C-terminal amino acids, STDKTKREEVD. I then used

isothermal titration microcalorimetry (ITC) to show that the interaction between an apatite substrate and the LRAP C-terminal motif was mediated by ionic interaction between the calcium ions on the surface of the apatite and the hydrophilic charged carboxyl termini of amelogenins (chapter 6). This type of ionic interaction between calcium ions and a negatively charged surface was also investigated as calcium ions interacted with highly phosphorylated proteins such as phosvitin (chapter 6). The use of ITC to determine interaction between calcium and phosvitin was used to optimize parameters for calcium-protein interactions, allowing the study of calcium binding to amelogenin. The principles and illustration of ITC use were discussed in more details in chapter 6.

The effect of calcium binding on the structure of LRAP was studied using circular dichroism (CD) and ^1H - ^{15}N NMR (chapter 7). In the presence of calcium ions, LRAP appeared to change from one random-coiled structure to an alternate random coiled structure with only a few amino acids could be well resolved in the ^1H - ^{15}N NMR spectrum. This spectrum could not be used to identify a well-defined secondary structure such as α -helix or β -sheet. This may be attributed to the fact that LRAP is a hydrophobic molecule that exists as a random coil in the aqueous environment used in our studies. Future studies to optimize the buffer conditions that mimic the *in vivo* environment in order to determine the true structural conformation of LRAP will allow further interpretation of these results. In general, the highly hydrophobic nature of amelogenins has resulted in major difficulties in determining a structure for this protein. The results of calcium binding to full-length amelogenin and LRAP, and their structural determination

were presented at the Enamel Symposium VII, 2005, and subsequently published in the European Journal of Oral Sciences (Le *et al.*, 2006).

The abilities of full-length amelogenin and its MMP-20-mediated proteolytic products to regulate enamel-like crystal formation *in vitro* using simulated secretory enamel-like fluid (Aoba and Moreno, 1987) were also studied. The crystals formed under these conditions were investigated by atomic force microscopy (AFM) imaging to determine the bioactive domains of amelogenins, responsible for promoting crystal growth (chapter 5). We found that full-length amelogenin clearly promoted enamel-like crystal formation on the surfaces of fluorapatite substrates. However, amelogenin proteolytic products (amino- and carboxyl-terminal peptides resulting from MMP-20 proteolysis) failed to stimulate crystal growth. This result suggests that full-length amelogenin possesses a specific conformation that is necessary for promoting mineralization, while its proteolytic products are deprived of such required structural information to direct crystal growth. As a result, amelogenin proteolytic peptides lack the ability to stimulate enamel-like crystal formation.

Similarly, our group has reported that LRAP also failed to promote enamel-like crystal formation *in vitro* (Habelitz *et al.*, 2006). The effects of full-length amelogenin and LRAP on regulation of crystal growth suggests that the central domain of full-length amelogenin is an important motif, playing a critical role in promoting crystal formation, because LRAP lacks the central domain of the full-length protein.

To attain the second major objective of determining cell-signaling functions of alternatively spliced amelogenins, I isolated LRAP and LRAP+exon4 cDNA's from dental pulp cells, and subsequently cloned, expressed and purified LRAP and LRAP+exon4. Both LRAP and LRAP+exon4 significantly stimulated dental pulp cell proliferation by up-regulating cell-cycle related genes expression (chapter 8). However, LRAP and LRAP+exon4 had no apparent effect on dental pulp cell differentiation (chapter 8). Since the effect of LRAP and LRAP+exon4 on cell proliferation and differentiation was not significantly different, I decided to use LRAP, instead of LRAP+exon4, for the subsequent functional analysis because LRAP can be recombinantly synthesized with much higher yield than LRAP+exon4. This difference is likely due to the greater hydrophilicity of LRAP, lacking the more hydrophobic exon 4. The results in chapter 8 lead to my co-authorship on a recent publication (Ye *et al.*, 2006).

To determine the specific bioactive domain of LRAP, it was first important to determine the process of MMP-20-mediated proteolysis of LRAP and study the protein self-assembly properties of LRAP proteolytic products using progressive time-controlled digestion (chapter 9). The LRAP proteolytic products and specific cleavage sites were analyzed by SDS-PAGE and mass spectrometric analysis. These studies showed that LRAP contains three specific MMP-20 cleavage sites, AWP/STD, DLT/LEA and PLP/PML. Progressive proteolysis revealed that MMP-20 sequentially cleaved LRAP beginning at the end of carboxyl terminus and proceeding upstream of the amino acid sequence. The self-assembly property of LRAP proteolytic products was also examined

by using turbidity assay (absorbance at λ 340 nm), and the sizes of LRAP nanospheres were analyzed by dynamic light scattering (DLS).

I studied the effects of LRAP and its N- and C-terminal proteolytic peptide on ameloblast-lineage cell *in vitro*. These studies showed that LRAP and N-terminal proteolytic peptide, but not C-terminal proteolytic domain, induced ameloblast-lineage cell differentiation by up-regulating amelogenin, while down-regulating Notch1 synthesis (chapter 9).

Recently, Tompkins and coworkers reported that lysosome-associated membrane protein 1 (LAMP-1) in mesenchymal-derived mouse myoblasts is the cell-surface receptor of LRAP (Tompkins *et al.*, 2006). Epithelial-derived keratinocytes and mammary cells also expressed LAMP-1, correlated with different stages of cell differentiation (Cella *et al.*, 1996; Sarafian *et al.*, 2006), leading me to first determine whether ameloblast-lineage cells synthesize LAMP-1, and the effect of LRAP on this surface receptor. In chapter 10, I showed by reverse-transcription PCR that epithelial-derived ameloblast-lineage cells expressed LAMP-1 mRNA. Moreover, addition of LRAP induced ameloblast-lineage cell differentiation by up-regulating LAMP-1 synthesis and other differentiation protein markers.

In conclusion (chapter 11), I thoroughly investigated the functional analysis of LRAP. The results of these studies suggest that, rather than a structural role in enamel formation, LRAP stimulates dental pulp cell proliferation and signals early epithelial-derived

ameloblast-lineage cell differentiation, suggesting that LRAP plays critical roles in dentinogenesis and amelogenesis. These findings are novel, and allowing us for the first time to understand how the alternatively spliced amelogenin protein, LRAP and its MMP-20 hydrolysis products, interact with cells and mineral in the developing tooth.

References:

Aoba T, Moreno EC (1987). The enamel fluid in the early secretory stage of porcine amelogenesis: chemical composition and saturation with respect to enamel mineral. *Calcif Tissue Int* 41(2):86-94.

Cella N, Cornejo-Uribe RR, Montes GS, Hynes NE, Chammas R (1996). The lysosomal-associated membrane protein LAMP-1 is a novel differentiation marker for HC11 mouse mammary epithelial cells. *Differentiation* 61(2):113-20.

Habelitz S, Denbesten PK, Marshall SJ, Marshall GW, Li W (2006). Self-assembly and effect on crystal growth of the leucine-rich amelogenin peptide. *Eur J Oral Sci* 114 Suppl 1(315-9).

Le TQ, Gochin M, Featherstone JD, Li W, Denbesten PK (2006). Comparative calcium binding of leucine-rich amelogenin peptide and full-length amelogenin. *Eur J Oral Sci* 114 Suppl 1(320-6).

Nelson DG, Featherstone JD (1982). Preparation, analysis, and characterization of carbonated apatites. *Calcif Tissue Int* 34 Suppl 2(S69-81).

Sarafian V, Jans R, Poumay Y (2006). Expression of lysosome-associated membrane protein 1 (Lamp-1) and galectins in human keratinocytes is regulated by differentiation. *Arch Dermatol Res* 298(2):73-81.

Shaw WJ, Campbell AA, Paine ML, Snead ML (2004). The COOH terminus of the amelogenin, LRAP, is oriented next to the hydroxyapatite surface. *J Biol Chem* 279(39):40263-6.

Tompkins K, Veis A (2002). Polypeptides translated from alternatively spliced transcripts of the amelogenin gene, devoid of the exon 6a, b, c region, have specific effects on tooth germ development in culture. *Connect Tissue Res* 43(2-3):224-31.

Tompkins K, Alvares K, George A, Veis A (2005). Two related low molecular mass polypeptide isoforms of amelogenin have distinct activities in mouse tooth germ differentiation in vitro. *J Bone Miner Res* 20(2):341-9.

Tompkins K, George A, Veis A (2006). Characterization of a mouse amelogenin [A-4]/M59 cell surface receptor. *Bone* 38(2):172-180.

Veis A, Tompkins K, Alvares K, Wei K, Wang L, Wang XS, Brownell AG, Jengh SM, Healy KE (2000). Specific amelogenin gene splice products have signaling effects on cells in culture and in implants in vivo. *J Biol Chem* 275(52):41263-72.

Veis A (2003). Amelogenin gene splice products: potential signaling molecules. *Cell Mol Life Sci* 60(1):38-55.

Ye L, Le TQ, Zhu L, Butcher K, Schneider RA, Li W, Besten PK (2006). Amelogenins in human developing and mature dental pulp. *J Dent Res* 85(9):814-8.

Chapter 2. Literature Review of Amelogenin Functions and Significance

I. Introduction to enamel extracellular matrix proteins

Dental enamel is formed within a unique enamel extracellular matrix (ECM), which is established by the synthesis and secretion of proteins by the epithelial-derived ameloblast cells. These secreted enamel proteins are mainly composed of amelogenins, ameloblastin, enamelin, tuftelin, in addition to two proteases: enamelysin (or matrix metalloproteinase 20, MMP-20) and kallikrein 4 (KLK-4). However, amelogenins represent greater than 90% of the proteins in the developing enamel ECM (Termine *et al.*, 1980). Amelogenins are highly conserved among divergent species. Both amino acid and cDNA sequences for bovine, human, mouse and porcine amelogenins have revealed greater than 80% conservation (Deutsch, 1989). Purified amelogenins from developing porcine enamel matrix have been shown to be phosphorylated at Ser-16 due to post-translational modification (Fincham *et al.*, 1994a; Salih *et al.*, 1998). The importance of this single Ser-16 phosphorylation in amelogenin is currently unknown. It has been hypothesized that Ser-16 phosphorylation may serve as a potential crystal nucleation site; while others suggested that it could have an important function in cell signaling. However, currently there is no strong evidence supporting either of these hypotheses.

In the developing enamel matrix, several isoforms of amelogenins ranging from 5 to 28 kDa have been reported. The heterogeneity of amelogenins is due to alternative splicing of the primary pre-mRNA transcript into multiple spliced variants (Fincham *et al.*,

1994b). Moreover, the proteolysis of amelogenins by MMP-20 (Bartlett *et al.*, 1998; Bartlett and Simmer, 1999) and KLK-4 (Simmer and Hu, 2002) also further contributes to this heterogeneity, and thus increases functional complexity of amelogenins. In contrast to the developing enamel, in the fully mature enamel amelogenins are almost completely absent from the mineralized matrix. Thus, amelogenins have been proposed to play structural roles directing enamel crystal growth by allowing mineral deposition to occur in spaces initially occupied by amelogenins. This “space-filling model” hypothesis for amelogenin functions has not been proven.

However, several studies have shown that amelogenins regulate biomineralization of enamel-like crystals *in vitro*, though the results are conflicting. Some investigators have reported that full-length amelogenin promotes enamel-like crystal formation (Habelitz *et al.*, 2004; Habelitz *et al.*, 2005; Iijima *et al.*, 2002; Iijima and Moradian-Oldak, 2005; Moradian-Oldak, 2001; Moradian-Oldak *et al.*, 2003), while others have shown that full-length amelogenin inhibits crystal growth (Beniash *et al.*, 2005; Iijima and Moradian-Oldak, 2004). This apparent discrepancy maybe the result of different experimental methods (i.e. concentrations of amelogenins, lengths of incubation) and conditions of the mineralization solutions used (i.e. differences in concentrations of calcium, phosphate, pH's and ionic strengths).

More recently, amelogenin alternatively spliced products (i.e. leucine-rich amelogenin peptide or LRAP) were reported to have specific cell-signaling functions to effect mesenchymal-derived cell proliferation and/or differentiation (Nebgen *et al.*, 1999;

Tompkins and Veis, 2002; Tompkins *et al.*, 2005; Tompkins *et al.*, 2006; Veis *et al.*, 2000; Veis, 2003; Ye *et al.*, 2006). Therefore, the current literature supports that amelogenins in the enamel matrix function both as structural molecules to guide enamel crystal growth and cell signaling proteins.

II. Amelogenins function as structural molecules to regulate enamel-like crystal growth *in vitro* and amelogenesis *in vivo*

Enamel is the hardest mineralized tissue in mammalian species. The mature enamel crystallites are composed mainly of carbonated hydroxyapatite (CAP) crystals, which are oriented into long and highly organized rods or prisms, extending from the dentino-enamel junction to the enamel surface of the tooth (Simmer and Fincham, 1995). Dental enamel forms by matrix-mediated biomineralization. Amelogenins, the predominant (> 90%) extracellular enamel matrix protein components, play critical functions in amelogenesis (Fincham *et al.*, 1999).

There is both *in vitro* and *in vivo* evidence indicating that alterations of the amelogenin amino acid sequence, results in defects in enamel crystal formation. Recombinant full-length amelogenins (the most predominant amelogenin isoform) have the ability to undergo self-assembly into nanospheres (radius ~ 20 nm) and nanochains that might serve as scaffolding proteins to regulate *in vitro* biomineralization of enamel-like crystals (Du *et al.*, 2005; Habelitz *et al.*, 2004; Iijima and Moradian-Oldak, 2005; Moradian-Oldak, 2001; Moradian-Oldak *et al.*, 2003; Wen *et al.*, 1999). There is also an *in vivo*

evidence to show that these amelogenin nanospheres align along the c-axis of the developing enamel rods, inhibiting crystal growth in width (Fincham *et al.*, 1995). Amelogenin-null mice experience disorganized hypoplastic (thin) enamel defect, suggesting the critical roles of amelogenin in the normal enamel development (Gibson *et al.*, 2001). In humans, different mutations of the amelogenin gene on the X chromosome results in a heterogeneous group of inherited disorders characterized by defects of the enamel biomineralization, called X-linked amelogenesis imperfecta (Collier *et al.*, 1997; Kim *et al.*, 2004; Kindelan *et al.*, 2000; Lagerstrom *et al.*, 1990; Lench and Winter, 1995).

One of the first documented amelogenin mutations is a missense mutation of C → T in exon 6, resulting in Pro41 converting into Thr41 (P41T), which gives rise to hypomaturational type of X-linked amelogenesis imperfecta (Collier *et al.*, 1997). Our group showed definitively that P41T mutation significantly reduces the rate of mutated amelogenin proteolysis by MMP-20, resulting in protein retention in the mineralizing enamel matrix (Li *et al.*, 2003). This finding also established the pathological mechanism underlining this specific type of hypomaturational amelogenesis imperfecta. Subsequently, additional amelogenin mutations have also been reported including two missense mutations of M1T and W4S in exon 2 encoded for the signaling peptide that affect the translation initiation codon and/or the secretion of amelogenin, resulting in rough and pitted hypoplastic enamel (Kim *et al.*, 2004).

Two published nonsense amelogenin mutations result in truncation of the hydrophilic carboxyl-terminal domains, lacking the last 12- and 18-amino-acid carboxyl termini, causing an identical phenotype of both hypomineralization and hypoplasia (Kindelan *et al.*, 2000; Lench and Winter, 1995). It has been reported that the amino-acid sequence of carboxyl-terminal domain is highly conserved across many species, suggesting that this domain plays critical role in the proper enamel formation (Toyosawa *et al.*, 1998). However, the specific mechanism of amelogenin carboxyl-terminal functions has not been well understood. In this thesis, I investigated the interaction of amelogenin carboxyl domains with enamel-like carbonated hydroxyapatites and their effects on crystal growth *in vitro*, in hopes to provide new insights into functions of the carboxyl termini in regulation of enamel crystal growth.

During the early enamel development, ameloblasts secrete amelogenins into the extracellular matrix, where the proteins undergo proteolytic processing by MMP-20 (matrix metalloproteinase 20 or enamelysin). Mass spectrometric analysis of proteolytic amelogenins obtained from developing enamel matrix of different species reveals that MMP-20 specifically hydrolyzed the carboxyl-terminal motif of amelogenin (Fincham and Moradian-Oldak, 1996). The truncated amelogenin lacking the hydrophilic carboxyl-terminus is one of the most predominant amelogenin components, comprising 50% of the enamel protein matrix (Yamakoshi *et al.*, 1994).

Amelogenins lacking the hydrophilic carboxyl-terminal domains have been shown to form a larger nanospheres, most likely due to hydrophobic-hydrophobic interactions of

the amino-terminal domains. The affinity of the truncated amelogenins to apatite significantly lower than that of the full-length amelogenins, suggesting the carboxyl terminus plays an important function in apatite interactions and enamel biomineralization (Moradian-Oldak *et al.*, 2002). *In vivo*, when the amelogenin carboxyl terminus is missing, amelogenesis is abnormal (Kindelan *et al.*, 2000; Lench and Winter, 1995).

A completely intact amelogenin is encoded by 7 exons, including the signal peptide in bovine (Shimokawa *et al.*, 1987a; Shimokawa *et al.*, 1987b) and human (Salido *et al.*, 1992). However, the most predominant secreted amelogenin isoform isolated from the human enamel matrix is encoded by exons 2 to 7, minus exon 4 (Fig. 1). I refer to this particular amelogenin variant as human full-length amelogenin (H174, MW ~ 20 kDa) throughout my thesis. In contrast, other amelogenin isoforms containing the encoded sequence of exon 4 (exon 4 coded for 14 amino acids, NSHSQAINVDRTAL) are extremely minor components within the matrix, and quite difficult to detect. Majority of published reports in the literature studied this most predominant amelogenin isoform, and conventionally called it “full-length amelogenin”. Thus, I adopted the same name of “full-length amelogenin” or H174 (human 174-residue amelogenin), referring to human amelogenin variant encoded by exons 2 to 7, but lacking exon 4.

Interestingly, only in mouse and rodent, but not in human and bovine, there are two additional exons, 8 and 9, down stream of exon 7 (Li *et al.*, 1998; Papagerakis *et al.*, 2005). The roles of exons 8 and 9 remain an enigma. However, one possibility is that exon 8 and 9 may function as signaling molecules to regulate the continuous eruption of

mouse and rodent incisors that is not observed in bovine and human teeth. Further studies are needed to identify the function of these additional exons in rodents.

Human amelogenins undergo alternative splicing of the primary mRNA transcript to produce 6.8-kDa leucine-rich amelogenin peptide (LRAP), whose sequence contains 58 residues (Gibson *et al.*, 1991). LRAP is encoded by exons 2, 3, 5, 6d (3' end of exon 6) and 7, corresponding to the first 33 and the last 25 amino acids of the parent full-length amelogenin (Fig. 2). Thus, LRAP is identical to the full-length amelogenin at its amino and carboxyl termini, but lacks a large segment from the central region (encoded by a long nucleotide sequence located at the 5'-end of exon 6) of the full-length protein (see Fig. 1 and 2 for primary sequence comparison). LRAP can also self-assemble into nanospheres via its hydrophobic N-terminal regions, while the highly hydrophilic carboxyl-terminal domains are exposed on the surface of the nanospheres (Moradian-Oldak *et al.*, 2001). Moreover, the charged hydrophilic carboxyl-terminal region of LRAP has been shown to oriented next to the surface of hydroxyapatite, suggesting that the carboxyl-terminal domain of LRAP may have a role in modulating enamel biomineralization, similar to full-length amelogenin (Shaw *et al.*, 2004).

LRAP and full-length amelogenin appear to have many similar characteristics. Both of these proteins are bipolar and form nanospheres. They both contain identical charged carboxyl-terminal regions that may interact with hydroxyapatite, suggesting their roles in regulating enamel biomineralization. Despite their importance in the normal amelogenesis, the specific molecular mechanisms of LRAP and the parent amelogenin in

enamel biomineralization have not been determined. In this thesis, the function of amelogenin carboxyl termini was studied in details to determine the molecular mechanism of carboxyl-terminal mediated amelogenin-apatite interaction. In addition, I investigated the ability of amelogenin carboxyl-terminal motif to regulate enamel-like crystal growth *in vitro*.

III. Amelogenins function as signaling molecules to regulate mesenchymal-derived cell proliferation and/or differentiation

Amelogenins are comprised of several alternatively spliced and proteolytic peptides isoforms encoded by a single gene on X-chromosome. Understanding the functions of amelogenins has been particularly difficult because amelogenin primary mRNA transcript undergo extensive alternative splicing, producing more than 14 mRNAs, which encode various amelogenin isoforms with different combinations of exon concatenation (Gibson, 1999; Hu *et al.*, 1997; Simmer, 1995). It is possible that additional alternatively spliced patterns of amelogenins have not yet been discovered.

Amelogenins are found to be expressed by both ameloblasts and odontoblasts. Amelogenins (originally thought to be enamel-specific) have been detected via immunohistochemistry within odontoblasts (Inai *et al.*, 1991; Nakamura *et al.*, 1994). Amelogenins are also reported to be transiently expressed by premature odontoblasts during the stage of reciprocal interaction between preodontoblasts and preameloblasts to regulate cell proliferation and differentiation (Papagerakis *et al.*, 2003). A study

conducted by Viswanathan and co-workers showed that *in situ* hybridization and immunohistochemical analysis of sections from amelogenin-null mice revealed a dramatic reduction in expression of bone sialoprotein (BSP) mRNA and protein in cementoblasts and surrounding osteoblasts (Viswanathan *et al.*, 2003). They concluded that amelogenins may be critical signaling molecules required for appropriate development of cells of periodontium. In addition, amelogenin-null mice also exhibited cementum defects characterized by the presence of multinucleated osteoclasts, cementicles, and upregulation of receptor activator of the nuclear factor- κ B (RANKL) (Hatakeyama *et al.*, 2003). This suggests that amelogenins play a role in regulation of genes associated with root formation.

The cell-signaling functions of amelogenins has been proposed as an explanation for the therapeutic effects of a commercial product Emdogain® (EMD), an amelogenin-rich extract from developing porcine enamel (Hammarstrom, 1997; Hammarstrom *et al.*, 1997). Application of EMD into periodontal defects resulted in significant gains in both attachment and alveolar bone growth (Jepsen *et al.*, 2004; Sculean *et al.*, 2004). The bioactive components of EMD are not known, and along with enamel matrix proteins such as amelogenins, may also be due to the presence of other factors in the developing enamel, such TGF- β (Kawase *et al.*, 2002). It is important to determine which amelogenin isoforms contain the biological activities that are responsible for cell signaling effects.

The amelogenin gene was originally thought to contain 7 exons and associated introns (Simmer *et al.*, 1994). However, in rat two additional exons have been identified further downstream of exon 7, namely exon 8 and 9 (Li *et al.*, 1998). *In situ* hybridization and immunohistochemical analysis revealed that exon 8 and 9 were detected in both ameloblasts and odontoblasts of the enamel organ (Baba *et al.*, 2002; Papagerakis *et al.*, 2005). However, the functions of peptides coded by exon 8 and 9 are still largely unknown. Since exon 8 and 9 represent minor components of amelogenins, the encoded proteins are most likely to play roles in cell signaling to regulate tooth development. This led to my co-authorship of a recent publication to report that peptide encoded by exon 8 and 9 significantly enhanced dental pulp fibroblast proliferation *in vitro* (Ye *et al.*, 2006).

IV. Leucine-rich amelogenin peptide (LRAP) functions as a signaling molecule through its receptor LAMP-1

Nebgen and coworkers identified low-molecular-mass peptides extracted from bovine dentin that induced chondrogenesis and osteogenesis at ectopic sites when implanted *in vivo*, as well as in cultures of embryonic muscle-derived fibroblasts *in vitro* (Nebgen *et al.*, 1999). The isolated peptides were identified to be approximately 6-10 kDa amelogenins. These peptides included leucine-rich amelogenin peptide (LRAP).

LRAP (~6.8 kDa) is composed of 58-residue peptide, which is an alternatively spliced amelogenin product translated from primary mRNA containing exon 2, 3, 5, 6d (3'-end nucleotide segment of exon 6), and 7 (Fig. 2). Amelogenin had historically been

described as an ameloblast “specific” protein, which is now known to be inaccurate. The presence of amelogenin proteins in dentin and amelogenin mRNA in odontoblasts has been confirmed by others (Oida *et al.*, 2002; Papagerakis *et al.*, 2003).

Recent interesting work on the functions of alternatively spliced amelogenins has turned in an unanticipated and exciting direction. Particularly, Veis and coworkers identified the presence of LRAP cDNA from a rat incisor odontoblast and pulp cDNA library using PCR amplification (Veis *et al.*, 2000). Furthermore, they amplified two isoforms of LRAP, with and without exon 4 (LRAP+exon4 and LRAP), which were encoded by cDNA’s derived from exons 2, 3, 4, 5, 6d, 7 and 2, 3, 5, 6d, 7, respectively. Exon 4 is encoded for additional 14 amino acids, NSHSQAINVDRTAL. The addition of these recombinant peptides to cultured embryonic rat muscle fibroblasts, induced enhanced sulfate incorporation into proteoglycans, production of type II collagen, as well as expression of chondrogenic markers Sox9 and Cbfa1 (Veis *et al.*, 2000; Veis, 2003). These studies showed a cell-signaling role for both recombinant LRAP and LRAP+exon4. Thus, recombinant LRAP and LRAP+exon4 proteins were able to recapitulate the *in vitro* chondrogenic conversion of embryonic mouse fibroblasts seen using the amelogenin protein extracted from dentin that was previously discussed (Nebgen *et al.*, 1999). Moreover, when LRAP and LRAP+exon4 conjugated to a polymer matrix were implanted into rat thigh muscle, there were expressions of bone-related proteins BSP and BAG-75, which were characteristic of mineralized tissues (Veis *et al.*, 2000).

However, the biological activity of LRAP and LRAP+exon4 are not always identical depending on varying with different cell types. Although structurally related, LRAP and LRAP+exon4 differ by the presence or absence of the 14 amino acid sequence, which is primarily encoded by exon 4 (Gibson *et al.*, 1991). Interesting, the presence of this quite hydrophobic exon-4-encoded region can also result in distinct differences in signaling activities between LRAP and LRAP+exon4 (Goldberg *et al.*, 2003; Tompkins and Veis, 2002; Tompkins *et al.*, 2005). Mouse mandibular molar tooth germs cultured with either LRAP or LRAP+exon4 showed significant differences in signaling effects on ameloblast and odontoblast differentiation in tooth development. Treatment of LRAP+exon4 significantly stimulated cell differentiation with evidence of well-polarized odontoblasts and ameloblasts, associating with robust dentin matrix protein 2 (DMP-2) expression. In contrast, addition of LRAP inhibited ameloblast differentiation, resulting in disorganization of preameloblasts. Moreover, the treatment of LRAP also reduced odontoblast polarization and decreased DMP-2 expression as compared to LRAP+exon4 (Tompkins *et al.*, 2005). When LRAP-conjugated beads were implanted into the intentionally exposed pulps of rat upper molars, the result was a complete obliteration of the pulpal chamber and the radicular canals (Goldberg *et al.*, 2003). However, similar implantation of LRAP+exon4-conjugated beads resulted in a physiological dentin bridge formation and occluded the pulpal perforation (Goldberg *et al.*, 2003). Though the cell-signaling effects of alternatively spliced amelogenin isoforms LRAP and LRAP+exon4 are clearly seen, the transduction mechanisms by which this signaling activity is initiated still remain obscure.

A recent break-through finding reported the identification of the cell-surface receptor of LRAP (Tompkins *et al.*, 2006). These investigators utilized radioactive-labeled LRAP and found that ³H-labeled LRAP was initially bound, then internalized from the cell surface of embryonic mouse myoblasts. These authors used “Far Western” immunohistochemical labeling of sections of embryonic mouse incisors and molars with biotin-labeled LRAP as the primary ligand, showing that LRAP was localized in stratum intermedium and the inner enamel epithelium of the developing teeth. Furthermore, they reported that LRAP was specifically bound to a 95-kDa cell-surface protein. Tandem MS (MS/MS) sequencing was used to discover that the LRAP receptor was a 95-kDa transmembrane protein, called lysosomal-associated membrane protein 1 (LAMP-1), also found at the cell surface (Tompkins *et al.*, 2006).

V. Rationale and Significance:

Despite evidence to support that alternatively spliced amelogenins such as LRAP, LRAP+exon4 are involved in cell signaling, the active domain(s) of these proteins and their effects on human dental pulp fibroblasts and ameloblast-lineage cell developments are not known. In this thesis, progressive proteolysis of LRAP by MMP-20 was done to identify the proteolytic fragments, and determine their effects on ameloblast and odontoblast cell proliferation and/or differentiation.

Currently, there is evidence in the literature to support the hypothesis that amelogenins function both as structural proteins to guide enamel crystal formation and as cell-

signaling molecules to regulate mesenchymal-derived cell proliferation and/or differentiation. However, the molecular mechanism by which amelogenins direct tooth formation is not clear. The overall goal of my thesis was to better understand the role of amelogenins in tooth formation. Several important questions were addressed. First, I investigated the molecular mechanism by which of LRAP and full-length amelogenin interact with enamel-like synthetic carbonated hydroxyapatite substrate. This information provided direct evidence of specific matrix-crystal interactions, mediated through the C-terminus of amelogenin proteins. The information gained from this aim enhanced our understanding of what may be required for amelogenins to function as structural proteins to promote enamel biomineralization.

A second goal was to gain additional knowledge regarding the functions of LRAP as a cell-signaling molecule. Because LRAP is hydrolyzed within the mineralizing enamel matrix, it was important to understand how MMP-20 hydrolyzes LRAP, and the functions of its proteolytic peptides in stimulating odontoblast and ameloblast proliferation and/or differentiation. The effect of LRAP on expression of the LRAP receptor LAMP-1 and other specific regulatory genes and/or proteins responsible for controlling tooth formation was investigated.

References

Baba O, Takahashi N, Terashima T, Li W, DenBesten PK, Takano Y (2002). Expression of alternatively spliced RNA transcripts of amelogenin gene exons 8 and 9 and its end products in the rat incisor. *J Histochem Cytochem* 50(9):1229-36.

- Bartlett JD, Ryu OH, Xue J, Simmer JP, Margolis HC (1998). Enamelysin mRNA displays a developmentally defined pattern of expression and encodes a protein which degrades amelogenin. *Connect Tissue Res* 39(1-3):101-9; discussion 141-9.
- Bartlett JD, Simmer JP (1999). Proteinases in developing dental enamel. *Crit Rev Oral Biol Med* 10(4):425-41.
- Beniash E, Simmer JP, Margolis HC (2005). The effect of recombinant mouse amelogenins on the formation and organization of hydroxyapatite crystals in vitro. *J Struct Biol* 149(2):182-90.
- Collier PM, Sauk JJ, Rosenbloom SJ, Yuan ZA, Gibson CW (1997). An amelogenin gene defect associated with human X-linked amelogenesis imperfecta. *Arch Oral Biol* 42(3):235-42.
- Deutsch D (1989). Structure and function of enamel gene products. *Anat Rec* 224(2):189-210.
- Du C, Falini G, Fermani S, Abbott C, Moradian-Oldak J (2005). Supramolecular assembly of amelogenin nanospheres into birefringent microribbons. *Science* 307(5714):1450-4.
- Fincham AG, Moradian-Oldak J, Sarte PE (1994a). Mass-spectrographic analysis of a porcine amelogenin identifies a single phosphorylated locus. *Calcif Tissue Int* 55(5):398-400.
- Fincham AG, Moradian-Oldak J, Simmer JP, Sarte P, Lau EC, Diekwisch T, Slavkin HC (1994b). Self-assembly of a recombinant amelogenin protein generates supramolecular structures. *J Struct Biol* 112(2):103-9.
- Fincham AG, Moradian-Oldak J, Diekwisch TG, Lyaruu DM, Wright JT, Bringas P, Jr., Slavkin HC (1995). Evidence for amelogenin "nanospheres" as functional components of secretory-stage enamel matrix. *J Struct Biol* 115(1):50-9.
- Fincham AG, Moradian-Oldak J (1996). Comparative mass spectrometric analyses of enamel matrix proteins from five species suggest a common pathway of post-secretory proteolytic processing. *Connect Tissue Res* 35(1-4):151-6.
- Fincham AG, Moradian-Oldak J, Simmer JP (1999). The structural biology of the developing dental enamel matrix. *J Struct Biol* 126(3):270-99.
- Gibson CW, Golub E, Ding WD, Shimokawa H, Young M, Termine J, Rosenbloom J (1991). Identification of the leucine-rich amelogenin peptide (LRAP) as the translation product of an alternatively spliced transcript. *Biochem Biophys Res Commun* 174(3):1306-12.

Gibson CW (1999). Regulation of amelogenin gene expression. *Crit Rev Eukaryot Gene Expr* 9(1):45-57.

Gibson CW, Yuan ZA, Hall B, Longenecker G, Chen E, Thyagarajan T, Sreenath T, Wright JT, Decker S, Piddington R, Harrison G, Kulkarni AB (2001). Amelogenin-deficient mice display an amelogenesis imperfecta phenotype. *J Biol Chem* 276(34):31871-5.

Goldberg M, Six N, Decup F, Lasfargues JJ, Salih E, Tompkins K, Veis A (2003). Bioactive molecules and the future of pulp therapy. *Am J Dent* 16(1):66-76.

Habelitz S, Kullar A, Marshall SJ, DenBesten PK, Balooch M, Marshall GW, Li W (2004). Amelogenin-guided crystal growth on fluoroapatite glass-ceramics. *J Dent Res* 83(9):698-702.

Habelitz S, Denbesten PK, Marshall SJ, Marshall GW, Li W (2005). Amelogenin control over apatite crystal growth is affected by the pH and degree of ionic saturation. *Orthod Craniofac Res* 8(4):232-8.

Hammarstrom L (1997). The role of enamel matrix proteins in the development of cementum and periodontal tissues. *Ciba Found Symp* 205(246-55; discussion 255-60).

Hammarstrom L, Heijl L, Gestrelus S (1997). Periodontal regeneration in a buccal dehiscence model in monkeys after application of enamel matrix proteins. *J Clin Periodontol* 24(9 Pt 2):669-77.

Hatakeyama J, Sreenath T, Hatakeyama Y, Thyagarajan T, Shum L, Gibson CW, Wright JT, Kulkarni AB (2003). The receptor activator of nuclear factor-kappa B ligand-mediated osteoclastogenic pathway is elevated in amelogenin-null mice. *J Biol Chem* 278(37):35743-8.

Hu CC, Ryu OH, Qian Q, Zhang CH, Simmer JP (1997). Cloning, characterization, and heterologous expression of exon-4-containing amelogenin mRNAs. *J Dent Res* 76(2):641-7.

Iijima M, Moriwaki Y, Wen HB, Fincham AG, Moradian-Oldak J (2002). Elongated growth of octacalcium phosphate crystals in recombinant amelogenin gels under controlled ionic flow. *J Dent Res* 81(1):69-73.

Iijima M, Moradian-Oldak J (2004). Interactions of amelogenins with octacalcium phosphate crystal faces are dose dependent. *Calcif Tissue Int* 74(6):522-31.

Iijima M, Moradian-Oldak J (2005). Control of apatite crystal growth in a fluoride containing amelogenin-rich matrix. *Biomaterials* 26(13):1595-603.

- Inai T, Kukita T, Ohsaki Y, Nagata K, Kukita A, Kurisu K (1991). Immunohistochemical demonstration of amelogenin penetration toward the dental pulp in the early stages of ameloblast development in rat molar tooth germs. *Anat Rec* 229(2):259-70.
- Jepsen S, Heinz B, Jepsen K, Arjomand M, Hoffmann T, Richter S, Reich E, Sculean A, Gonzales JR, Bodeker RH, Meyle J (2004). A randomized clinical trial comparing enamel matrix derivative and membrane treatment of buccal Class II furcation involvement in mandibular molars. Part I: Study design and results for primary outcomes. *J Periodontol* 75(8):1150-60.
- Kawase T, Okuda K, Yoshie H, Burns DM (2002). Anti-TGF-beta antibody blocks enamel matrix derivative-induced upregulation of p21WAF1/cip1 and prevents its inhibition of human oral epithelial cell proliferation. *J Periodontol Res* 37(4):255-62.
- Kim JW, Simmer JP, Hu YY, Lin BP, Boyd C, Wright JT, Yamada CJ, Rayes SK, Feigal RJ, Hu JC (2004). Amelogenin p.M1T and p.W4S mutations underlying hypoplastic X-linked amelogenesis imperfecta. *J Dent Res* 83(5):378-83.
- Kindelan SA, Brook AH, Gangemi L, Lench N, Wong FS, Fearne J, Jackson Z, Foster G, Stringer BM (2000). Detection of a novel mutation in X-linked amelogenesis imperfecta. *J Dent Res* 79(12):1978-82.
- Lagerstrom M, Dahl N, Iselius L, Backman B, Pettersson U (1990). Mapping of the gene for X-linked amelogenesis imperfecta by linkage analysis. *Am J Hum Genet* 46(1):120-5.
- Lench NJ, Winter GB (1995). Characterisation of molecular defects in X-linked amelogenesis imperfecta (AIH1). *Hum Mutat* 5(3):251-9.
- Li W, Mathews C, Gao C, DenBesten PK (1998). Identification of two additional exons at the 3' end of the amelogenin gene. *Arch Oral Biol* 43(6):497-504.
- Li W, Gao C, Yan Y, DenBesten P (2003). X-linked amelogenesis imperfecta may result from decreased formation of tyrosine rich amelogenin peptide (TRAP). *Arch Oral Biol* 48(3):177-83.
- Moradian-Oldak J (2001). Amelogenins: assembly, processing and control of crystal morphology. *Matrix Biol* 20(5-6):293-305.
- Moradian-Oldak J, Jimenez I, Maltby D, Fincham AG (2001). Controlled proteolysis of amelogenins reveals exposure of both carboxy- and amino-terminal regions. *Biopolymers* 58(7):606-16.
- Moradian-Oldak J, Bouropoulos N, Wang L, Gharakhanian N (2002). Analysis of self-assembly and apatite binding properties of amelogenin proteins lacking the hydrophilic C-terminal. *Matrix Biol* 21(2):197-205.

Moradian-Oldak J, Iijima M, Bouropoulos N, Wen HB (2003). Assembly of amelogenin proteolytic products and control of octacalcium phosphate crystal morphology. *Connect Tissue Res* 44 Suppl 1(58-64).

Nakamura M, Bringas P, Jr., Nanci A, Zeichner-David M, Ashdown B, Slavkin HC (1994). Translocation of enamel proteins from inner enamel epithelia to odontoblasts during mouse tooth development. *Anat Rec* 238(3):383-96.

Nebgen DR, Inoue H, Sabsay B, Wei K, Ho CS, Veis A (1999). Identification of the chondrogenic-inducing activity from bovine dentin (bCIA) as a low-molecular-mass amelogenin polypeptide. *J Dent Res* 78(9):1484-94.

Oida S, Nagano T, Yamakoshi Y, Ando H, Yamada M, Fukae M (2002). Amelogenin gene expression in porcine odontoblasts. *J Dent Res* 81(2):103-8.

Papagerakis P, MacDougall M, Hotton D, Bailleul-Forestier I, Oboeuf M, Berdal A (2003). Expression of amelogenin in odontoblasts. *Bone* 32(3):228-40.

Papagerakis P, Ibarra JM, Inozentseva N, DenBesten P, MacDougall M (2005). Mouse amelogenin exons 8 and 9: sequence analysis and protein distribution. *J Dent Res* 84(7):613-7.

Salido EC, Yen PH, Koprivnikar K, Yu LC, Shapiro LJ (1992). The human enamel protein gene amelogenin is expressed from both the X and the Y chromosomes. *Am J Hum Genet* 50(2):303-16.

Salih E, Huang JC, Strawich E, Gouverneur M, Glimcher MJ (1998). Enamel specific protein kinases and state of phosphorylation of purified amelogenins. *Connect Tissue Res* 38(1-4):225-35; discussion 241-6.

Sculean A, Windisch P, Chiantella GC (2004). Human histologic evaluation of an intrabony defect treated with enamel matrix derivative, xenograft, and GTR. *Int J Periodontics Restorative Dent* 24(4):326-33.

Shaw WJ, Campbell AA, Paine ML, Snead ML (2004). The COOH terminus of the amelogenin, LRAP, is oriented next to the hydroxyapatite surface. *J Biol Chem* 279(39):40263-6.

Shimokawa H, Ogata Y, Sasaki S, Sobel ME, McQuillan CI, Termine JD, Young MF (1987a). Molecular cloning of bovine amelogenin cDNA. *Adv Dent Res* 1(2):293-7.

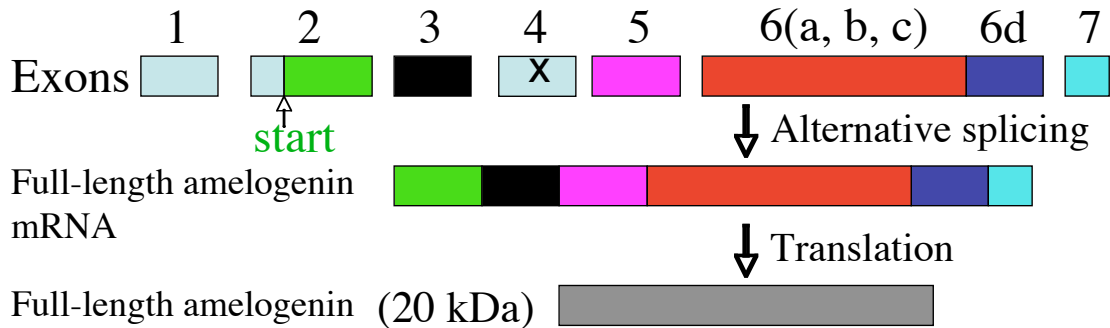
Shimokawa H, Sobel ME, Sasaki M, Termine JD, Young MF (1987b). Heterogeneity of amelogenin mRNA in the bovine tooth germ. *J Biol Chem* 262(9):4042-7.

- Simmer JP, Hu CC, Lau EC, Sarte P, Slavkin HC, Fincham AG (1994). Alternative splicing of the mouse amelogenin primary RNA transcript. *Calcif Tissue Int* 55(4):302-10.
- Simmer JP (1995). Alternative splicing of amelogenins. *Connect Tissue Res* 32(1-4):131-6.
- Simmer JP, Fincham AG (1995). Molecular mechanisms of dental enamel formation. *Crit Rev Oral Biol Med* 6(2):84-108.
- Simmer JP, Hu JC (2002). Expression, structure, and function of enamel proteinases. *Connect Tissue Res* 43(2-3):441-9.
- Termine JD, Belcourt AB, Christner PJ, Conn KM, Nylén MU (1980). Properties of dissociatively extracted fetal tooth matrix proteins. I. Principal molecular species in developing bovine enamel. *J Biol Chem* 255(20):9760-8.
- Tompkins K, Veis A (2002). Polypeptides translated from alternatively spliced transcripts of the amelogenin gene, devoid of the exon 6a, b, c region, have specific effects on tooth germ development in culture. *Connect Tissue Res* 43(2-3):224-31.
- Tompkins K, Alvares K, George A, Veis A (2005). Two related low molecular mass polypeptide isoforms of amelogenin have distinct activities in mouse tooth germ differentiation in vitro. *J Bone Miner Res* 20(2):341-9.
- Tompkins K, George A, Veis A (2006). Characterization of a mouse amelogenin [A-4]/M59 cell surface receptor. *Bone* 38(2):172-180.
- Toyosawa S, O'Huigin C, Figueroa F, Tichy H, Klein J (1998). Identification and characterization of amelogenin genes in monotremes, reptiles, and amphibians. *Proc Natl Acad Sci U S A* 95(22):13056-61.
- Veis A, Tompkins K, Alvares K, Wei K, Wang L, Wang XS, Brownell AG, Jengh SM, Healy KE (2000). Specific amelogenin gene splice products have signaling effects on cells in culture and in implants in vivo. *J Biol Chem* 275(52):41263-72.
- Veis A (2003). Amelogenin gene splice products: potential signaling molecules. *Cell Mol Life Sci* 60(1):38-55.
- Viswanathan HL, Berry JE, Foster BL, Gibson CW, Li Y, Kulkarni AB, Snead ML, Somerman MJ (2003). Amelogenin: a potential regulator of cementum-associated genes. *J Periodontol* 74(10):1423-31.
- Wen HB, Moradian-Oldak J, Fincham AG (1999). Modulation of apatite crystal growth on Bioglass by recombinant amelogenin. *Biomaterials* 20(18):1717-25.

Yamakoshi Y, Tanabe T, Fukae M, Shimizu M (1994). Porcine amelogenins. *Calcif Tissue Int* 54(1):69-75.

Ye L, Le TQ, Zhu L, Butcher K, Schneider RA, Li W, Besten PK (2006). Amelogenins in human developing and mature dental pulp. *J Dent Res* 85(9):814-8.

Human Amelogenin Primary Transcript



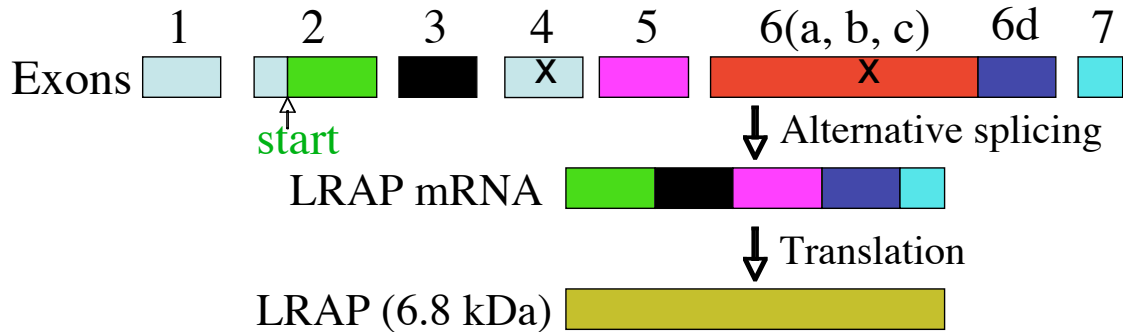
MPLPPHPGHPGYINFSYEVLTKWYQSIRPPYPSYGYE
 PMGGWLHHQIIPVLSQQHPPHTLQPHHHIPVVPAQQPV
 IPQQPMMPVPGQHSMTPIQHHQPNLPPPAQQPYQPQPV
 QPQPHQPMQPQPPVHPMQPLPPQPPLPPMFPMQPLPML
 PDLTLEAWPSTDKTKREEVD (FL amelogenin sequence)

Figure 1.

Human full-length amelogenin (H174) and its amino acid sequence.

The most predominant secreted amelogenin isoform isolated from the human enamel matrix is encoded by exons 2 to 7, minus exon 4 (marked as X). This particular amelogenin variant is referred to as “human full-length amelogenin” (H174, MW ~ 20 kDa) in this thesis. Amelogenin isoforms containing exon-4-coded sequence are extremely minute in quantities and very difficult to detect in the developing enamel extracellular matrix.

Human Amelogenin Primary Transcript



MPLPPHPGHPGYINFSYEVLTPLKWKYQSIRPPPLP
 PMLPDLTLEAWPSTDKTKREEVD (LRAP sequence)

Figure 2.

Alternatively spliced pattern of human LRAP and its amino acid sequence.

LRAP is encoded by exons 2, 3, 5, 6d (3'-end of exon 6) and 7, resulting in a 58-residue alternatively spliced peptide, whose amino acid sequence is identical to the first 33 and the last 25 residues of the full-length amelogenin (H174). Thus, LRAP is identical to H174 at the amino- and carboxyl-terminal domains, but lacking the large central domain (indicated as X) encoded by the majority of 5'-nucleotide segment of exon 6 (exon 6a, b and c).

Chapter 3. Preparation and Characterization of Enamel-like Synthetic Carbonated Hydroxyapatite

INTRODUCTION

The inorganic or mineral content of human dental enamel and bone is a highly substituted form of hydroxyapatite (HAP), $\text{Ca}_{10}(\text{PO}_4)_6(\text{OH})_2$, commonly referred to as carbonated hydroxyapatite (CAP)(Simpson, 1972; Young, 1974). In the normal dental enamel, carbonate component is approximately 3-5% by weight, and mostly substitutes for the phosphate ions in the crystal structure (Curzon and Featherstone, 1983). Stoichiometric analysis suggests that four carbonate groups replace three phosphate groups within the crystal lattice of CAP (Nelson and Featherstone, 1982). Further analysis by Nelson and Featherstone (Nelson and Featherstone, 1982) suggests that sodium and hydroxyl ions can also replace carbonate ions. The carbonate component in the enamel has been related to dental caries progression and is believed to enhance the dissolution of CAP in an acidic environment (Nelson *et al.*, 1983). Preferential demineralization of CAP in enamel has been documented in the initial stages of dental caries process (Featherstone *et al.*, 1978; Hallsworth *et al.*, 1973).

There has always been some variation in terms of the compositional properties of enamel between tooth types and different human subjects. Thus, it has been a major challenge to obtain large amounts of CAP from human dental enamel, with uniform physical and chemical properties. Therefore, to allow the studies of amelogenin-mineral interaction, it was necessary to prepare and characterize synthetic CAP, with a composition and characteristics similar to that of human dental enamel.

Synthetic CAP is prepared by aqueous precipitation at a high temperature, adopting methods published previously (Nelson and Featherstone, 1982). The synthetic CAP is analyzed and characterized using X-ray diffraction (XRD) and Fourier Transform Infrared (FTIR) spectroscopy.

MATERIALS AND METHODS

A. Synthesis of carbonated hydroxyapatite (CAP)

The methods used for synthesizing CAP were described previously (Featherstone *et al.*, 1983; Nelson and Featherstone, 1982). All chemical solutions were prepared using boiling double-distilled water (DDW) to remove excess CO₂. Ca(NO₃)₂·4H₂O (Baker, Phillipsburg, NJ, USA) of 14.16 g was dissolved in 200 mL of boiling DDW, and filtered through Whatman filter paper #1 (Whatman Inc., Florham Park, NJ, USA) into 1-L reaction vessel containing a stir bar. A condenser, pH Ross electrode, thermometer and NaOH delivery line were connected to the reaction vessel as shown in Fig. 1. Na₂HPO₄ of 5.2 g (Baker) was dissolved in 200 mL of boiling DDW and filtered into a 500-mL conical flask. To prepare additive solution containing carbonate, NaHCO₃ of 2.2 g was dissolved in a final volume of 25 mL of boiling DDW. To synthesize 3% carbonated hydroxyapatite (CAP), 2 mL of the above NaHCO₃ solution was added into 18 mL of DDW to make 20 mL, which was then added to the solution of Na₂HPO₄ prepared previously in the conical flask.

A solution containing of Na_2HPO_4 and NaHCO_3 was added drop-wise (60 drops/min) to 200 mL of $\text{Ca}(\text{NO}_3)_2 \cdot 4\text{H}_2\text{O}$ in a 1-L reaction vessel with constant stirring. The reaction was placed under reflux at 92 °C using a glass condenser. A pH Stat was set to end point 9.1 using a pH Stat device (718 STAT Titrino, Metrohm, Herisau, Switzerland), titrating with NaOH solution (2.5 M) (Fisher scientific, Fair Lawn, NJ, USA). During addition of phosphate, pH of the reaction was maintained by the pH Stat between 8.9 to 9.1.

After the addition of the reactants was completed (approximately 1.5 to 2 h), the system was refluxed for an additional 2 h at 100 °C. The synthetic CAP was filtered with Whatman filter paper #42 (Whatman), then thoroughly washed with 1-L of boiling DDW to remove NO_3 contaminants, and dried overnight at 120 °C. The dried CAP samples were crushed using a mortar and pestle, and then sequentially screened through 60- μm and 30- μm mesh nylon filters (Spectrum Laboratories, Inc., Rancho Dominguez, CA, USA). Sample powder with a diameter between 30 μm to 60 μm was characterized to determine specific surface areas and used for further studies. A detailed illustration of carbonated hydroxyapatite synthesis is shown in Fig. 2.

B. Specific surface area determination for synthetic CAP

The surface area determination was analyzed by Micromeritics Analytical Services (Norcross, GA, USA). In this analysis, the exposed surface areas of CAP were measured with a gas adsorption apparatus according to the Brunauer-Emmet-Teller (BET) method using a Micromeritics TriStar 3000 (Micromeritics instrument, Norcross, GA, USA). The CAP samples were prepared for analysis by heating them to 200 °C for 960 min. Warm

and cold free space was measured with helium gas. Samples were measured by taking 11 data points between a relative pressure of 0.05 and 0.3 psi. Equilibration time was 10 seconds. Sample weight ranged from 0.74 g to 1.16 g. Saturation pressure was set to measure every 2 h. These measurements showed that CAP had surface area of $74.68 \pm 0.31 \text{ m}^2/\text{g}$ for this particular batch of CAP.

C. Characterization of synthetic CAP by X-ray diffractometer (XRD) and Fourier Transform Infrared Spectroscopy (FTIR)

The crystal phases of the synthetic CAP and human enamel powder were analyzed by X-ray diffraction (XRD) using Philips APD 10 microprocessor-controlled diffractometer system operated at 40 kV and 35 mA with an angle-controlled divergence slit and graphite monochromator, ranging from $2\theta = 15$ to 60 degrees.

Synthetic CAP and human enamel was also characterized using an Analect RFX-30 FTIR spectrometer (Applied Instrument Technologies, Pomona, CA, USA). One mg of powdered sample was pressed into pellets with approximately 400 mg of spectroscopic-graded KBr (Fisher Scientific, Pittsburgh, PA, USA) using an applied load of 8000 kg, under 0.5 torr vacuum. KBr without apatite was used as a background. FTIR spectra were scanned in reflectance mode in the range between 4000 and 400 cm^{-1} at 2 cm^{-1} resolution, averaging of 50 scans, under purges of dry CO_2 -free nitrogen. The spectra were analyzed using an Igor Pro. 5.03 software (WaveMetrix, Portland, OR, USA).

RESULTS AND DISCUSSION

Characterization of synthetic carbonated hydroxyapatite (CAP) and human enamel powder using XRD

Both CAP and human dental enamel were characterized using X-ray diffractometry (XRD). The results showed that human enamel and CAP powders had the identical reflections with characteristic peaks appearing at specific locations of 2θ (degree) values, representing specific planes with labeled coordinate values (hkl) and corresponding dots (●) as indicated in Fig. 3A and 3B, respectively. These results confirmed that synthetic CAP was successfully synthesized and comparable to human enamel.

Characterization of synthetic CAP and human enamel powder using FTIR

Synthetic CAP and human enamel powder were prepared and characterized using FTIR, and compared to commercial HAP. Human enamel and synthetic CAP showed the typical phosphate (PO_4), hydroxyl (OH) and carbonate (CO_3) infrared band positions. These were similar to those of commercial HAP (Rehman and Bonfield, 1997) (Fig. 4A and 4B) and Table 1. Theoretically, a pure commercial HAP should not have any carbonate constituents. However, the commercial HAP used in Rehman and Bonfield's study clearly contained carbonate components, which may be a result of atmospheric carbon dioxide contaminants. Hydroxyl stretch was observed at 3580 cm^{-1} and $610 - 640\text{ cm}^{-1}$ in both human enamel and CAP spectra. However, the OH band of synthetic CAP at 3580 cm^{-1} had a higher intensity than that of human enamel (Fig. 4A and B). The greater OH band intensity of CAP may be attributed to lesser amount of CO_3 substitution as compared to human enamel. In other words, human enamel may contain higher

carbonate content than that of the synthetic CAP. The OH band intensity of CAP has been reported to be greater than commercial HAP, suggesting increase in CO₃ substitution in CAP (Elliott *et al.*, 1985). In both CAP and human enamel spectra, there were four PO₄ ions vibrational modes (ν_1 , ν_2 , ν_3 and ν_4). The most intense was ν_3 bands present at 1090 - 1100 cm⁻¹ and 1030 - 1040 cm⁻¹. The ν_1 mode was detected at 961 cm⁻¹, while the ν_4 mode was present in the region of 560 cm⁻¹- 640 cm⁻¹. The ν_2 mode typically appeared at 470 cm⁻¹ as seen in human enamel spectrum. However, the ν_2 mode was not shown in CAP spectrum because it was an instrumental out-of-range. The band positions obtained from Fig. 4A and B were summarized in Table 1.

Synthetic CAP and human enamel also revealed the same carbonate (CO₃) infrared band positions (Fig. 4A and 4B). Typically, carbonate ions show 4 vibrational modes (ν_1 , ν_2 , ν_3 and ν_4), three of which were observed in the infrared spectrum (Nelson and Featherstone, 1982). The carbonate ν_1 and ν_4 bands have very low intensity and are rarely detected in the FTIR (el Feki *et al.*, 1991). The ν_2 and ν_3 vibrational modes were observed in infrared spectrum. Carbonate ions occupied two different sites in synthetic CAP and human enamel. Carbonate ions ν_3 mode peaked at 1450 - 1460 cm⁻¹ and 1420 - 1415 cm⁻¹, while ν_2 mode was detected at 870 - 880 cm⁻¹. These values representing ν_2 and ν_3 vibrational modes were consistent with those previously reported (Nelson and Featherstone, 1982). The occupancy of ν_3 sites resulted from the competition for replacement between PO₄ and CO₃ ions (Elliott *et al.*, 1985; Nelson and Featherstone, 1982). When the synthetic CAP product was not properly washed with boiled de-ionized water, there was evidence of nitrate (NO₃) contamination as an extra peak at 1385 cm⁻¹

(Fig. 4C). Potassium bromide (KBr) was used as a background for FTIR and was eventually subtracted from all CAP samples (Fig. 4D). Table 1 summarizes the results of synthetic CAP and human enamel FTIR data as compared to the commercial HAP standard.

CONCLUSION

The analysis of synthetic CAP using X-ray diffraction and FTIR spectroscopy showed that the synthetic product has physiochemical characteristics consistent with those of human enamel. Furthermore, the synthetic CAP is relatively pure, free of nitrate ions (NO_3) contaminant. Specific surface area analysis indicated that synthetic CAP has an average surface area of $74.68 \pm 0.31 \text{ m}^2/\text{g}$. However, the specific surface area of human enamel powder was not determined because only CAP, not human enamel powder, will be used for the future experiments of protein-mineral interactions.

REFERENCES

- Curzon MEJ, Featherstone JDB (1983). Chemical composition of enamel. In: Chemical composition of enamel. FL Boca Raton editor: CRC Press, pp. 123-135.
- el Feki H, Rey C, Vignoles M (1991). Carbonate ions in apatites: infrared investigations in the $\nu_4 \text{ CO}_3$ domain. *Calcif Tissue Int* 49(4):269-74.
- Elliott JC, Holcomb DW, Young RA (1985). Infrared determination of the degree of substitution of hydroxyl by carbonate ions in human dental enamel. *Calcif Tissue Int* 37(4):372-5.
- Featherstone JD, Duncan JF, Cutress TW (1978). Crystallographic changes in human tooth enamel during in-vitro caries simulation. *Arch Oral Biol* 23(5):405-13.
- Featherstone JD, Mayer I, Driessens FC, Verbeeck RM, Heijligers HJ (1983). Synthetic apatites containing Na, Mg, and CO_3 and their comparison with tooth enamel mineral. *Calcif Tissue Int* 35(2):169-71.

Hallsworth AS, Weatherell JA, Robinson C (1973). Loss of carbonate during the first stages of enamel caries. *Caries Res* 7(4):345-8.

Nelson DG, Featherstone JD (1982). Preparation, analysis, and characterization of carbonated apatites. *Calcif Tissue Int* 34 Suppl 2(S69-81).

Nelson DG, Featherstone JD, Duncan JF, Cutress TW (1983). Effect of carbonate and fluoride on the dissolution behaviour of synthetic apatites. *Caries Res* 17(3):200-11.

Rehman I, Bonfield W (1997). Characterization of hydroxyapatite and carbonated apatite by photo acoustic FTIR spectroscopy. *J Mater Sci Mater Med* 8(1):1-4.

Simpson DR (1972). Problems of the composition and structure of the bone minerals. *Clin Orthop Relat Res* 86(260-86).

Young RA (1974). Implications of atomic substitutions and other structural details in apatites. *J Dent Res* 53(2):193-203.

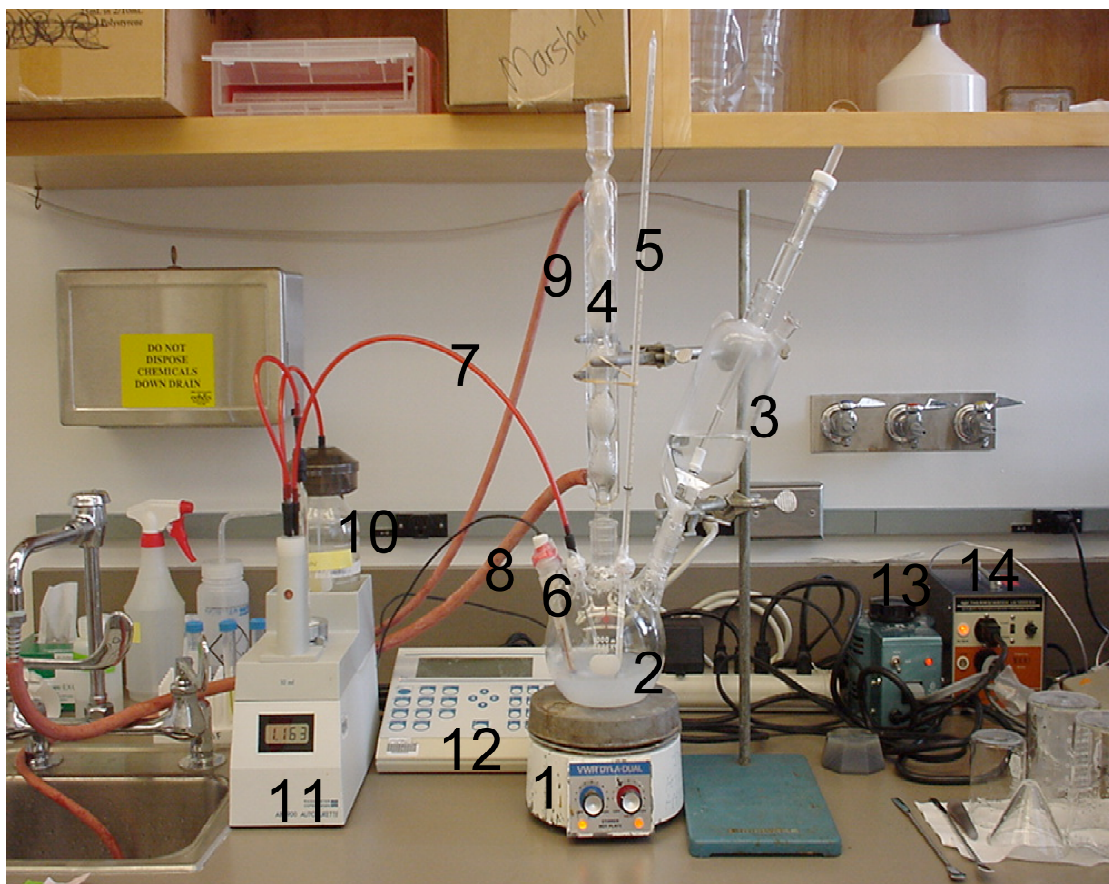


Figure 1.

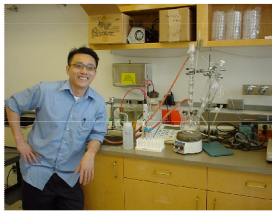
Experimental apparatus set-up for the synthesis of carbonated hydroxyapatite.

1) Heating plate and a stirring unit. 2) Reaction vessel containing $\text{Ca}(\text{NO}_3)_2 \cdot 4\text{H}_2\text{O}$ and drop-wise addition of a mixture of Na_2HPO_4 and NaHCO_3 . 3) Addition funnel containing a mixture of Na_2HPO_4 and NaHCO_3 . 4) Condenser allowing reflux. 5) Thermometer. 6) pH electrode. 7) NaOH addition line. 8) Water line carrying water into the condenser. 9) Water line carrying water out of the condenser. 10) NaOH reservoir. 11) pH stat. 12) pH-control unit and monitor. 13) Thermostat controls for a constant temperature. 14) A power source.



Process of CAP Synthesis

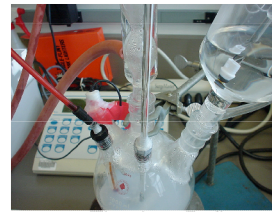
92 °C
pH 9.1



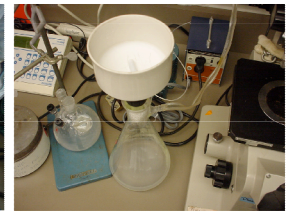
1. Instruments preparation



2. Autoburette



3. Titration~Reflux



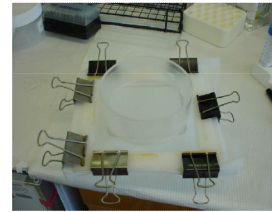
4. Wash



5. Dry



6. Crush apatite



7. Filtration

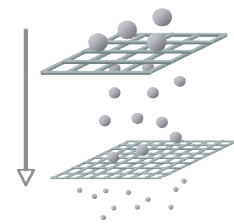


Figure 2.

Detailed illustrations of CAP synthesis process.

1) Instruments preparation was set-up according to Fig. 1 above. 2) Autoburette unit controlled the addition of NaOH (2.5 N) to maintain a constant pH of 9.1 throughout the synthesis. 3) After titration of Na_2HPO_4 and NaHCO_3 into $\text{Ca}_2.4\text{H}_2\text{O}$ solution to produce apatites, the system was placed under reflux for 2 h. 4) Newly-synthesized apatites were filtered and washed with boiling water. 5) Apatites were dried in oven overnight at 120 °C. 6) Apatite powders were obtained using mortar and pestle. 7) Apatite powders were screened through 60- μm and 30- μm nylon mesh.

Fig. 3A

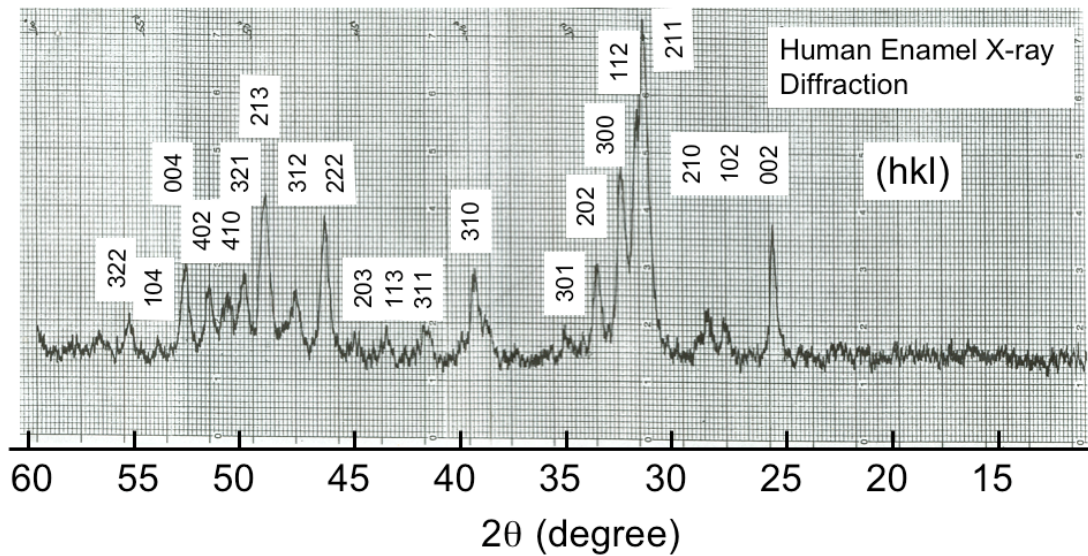


Fig. 3B

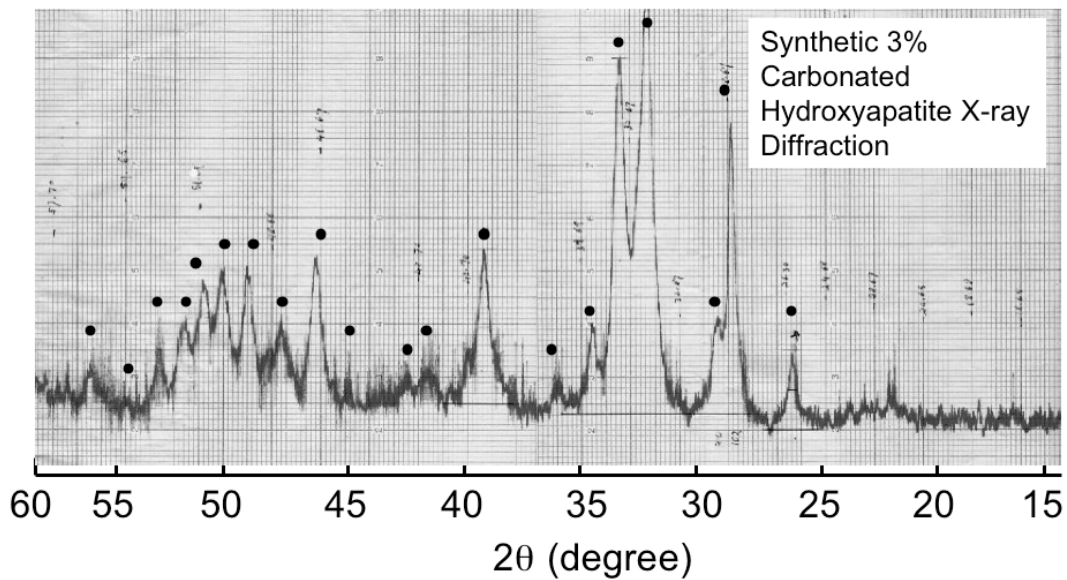


Figure 3.

X-ray diffraction pattern of human enamel and synthetic CAP powder.

A) Labeled peaks with coordinates (hkl) represent the X-ray diffraction powder reflections of human enamel in the range of $2\theta = 15^\circ - 60^\circ$, indicating carbonated hydroxyapatite spectrum. B) X-ray diffraction of synthetic CAP powder with peaks labeled with dots (•) matching those peaks of human enamel X-ray reflections.

Fig. 4A

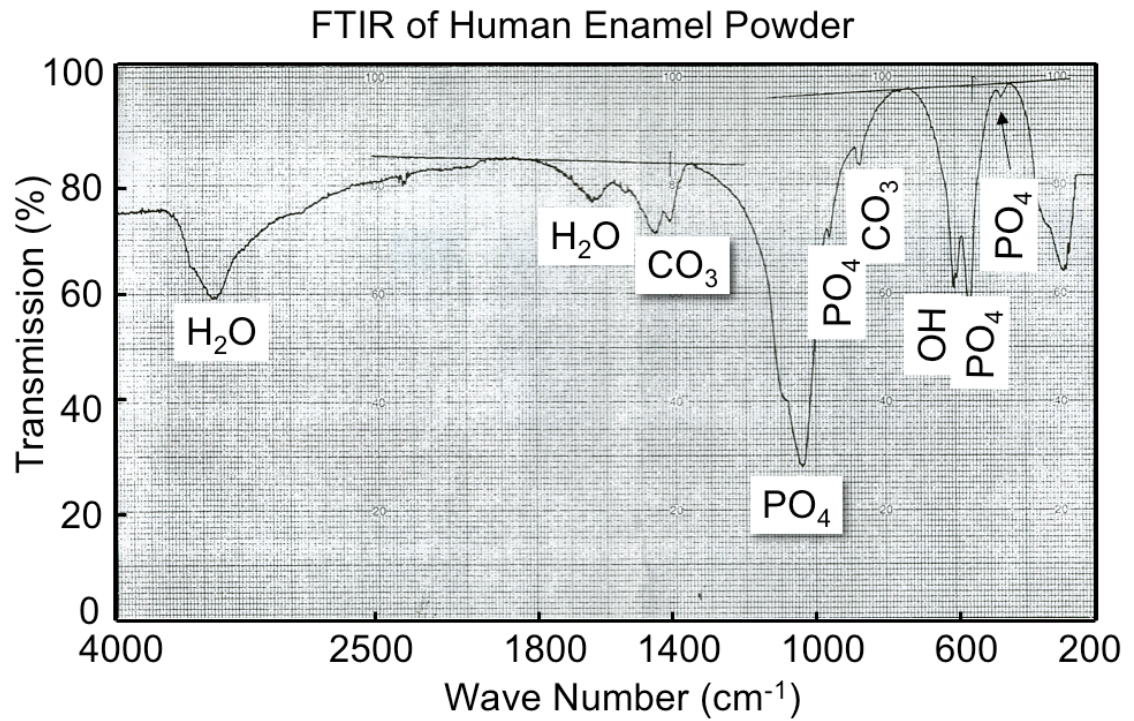


Fig. 4B

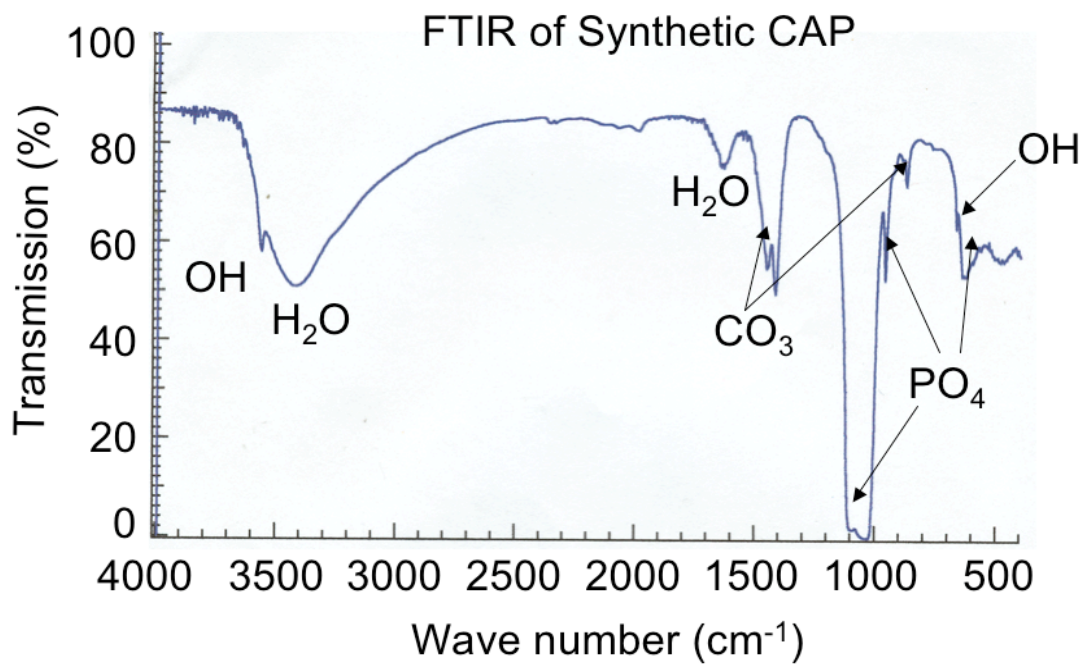


Fig. 4C

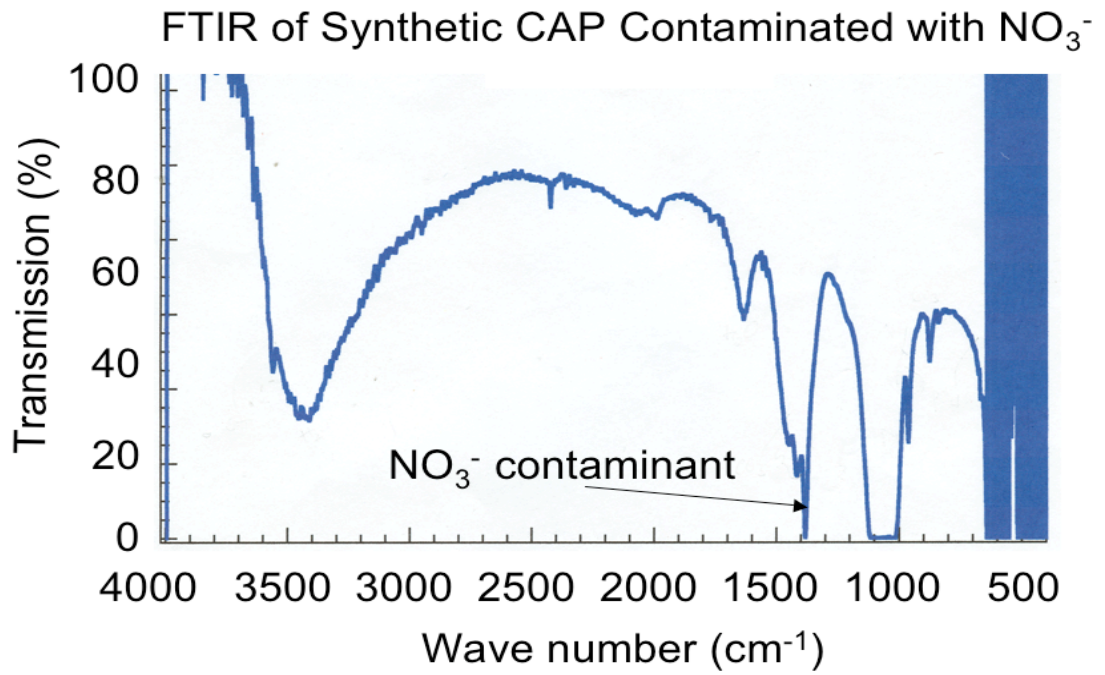


Fig. 4D

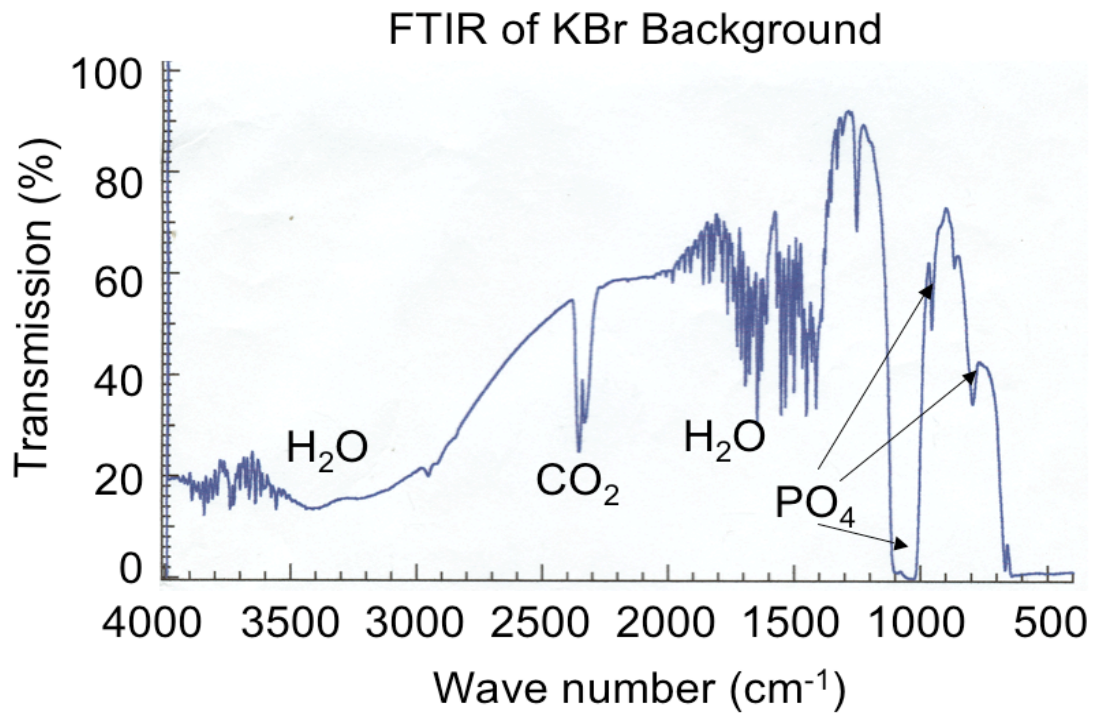


Fig. 4.

Fourier Transform Infrared Spectroscopy (FTIR) of human enamel and synthetic carbonated hydroxyapatite in KBr background.

A) FTIR of a human enamel sample, showing characteristic of carbonated substituted hydroxyapatite. B) FTIR of synthetic carbonated hydroxyapatites, resembling those features of human enamel. C) FTIR of carbonated hydroxyapatites contaminated with NO_3 , showing extra NO_3 peak in the spectrum. D) A typical FTIR spectrum of KBr background that was subtracted from the spectrum of carbonated hydroxyapatite samples.

Table 1.

Peak assignments	Synthetic CAP (cm^{-1})	Human enamel (cm^{-1})	Commercial HAP (cm^{-1}) (Rehman et al., 1997)
Hydroxyl stretch	3580, 640	3580, 610	3570, 632
Phosphate ν_3	1100, 1030	1090, 1040	1091, 1042
Phosphate ν_1	960	960	962
Phosphate ν_4	640	560	660 - 560
Phosphate ν_2	-----	470	472
Carbonate ν_3	1450, 1415	1460, 1420	1455, 1417
Carbonate ν_2	880	870	877

Table 1.

Observed FTIR band positions (cm^{-1}) for human enamel, synthetic carbonated hydroxyapatite, and commercial hydroxyapatite.

Chapter 4. Expression, Purification and Characterization of Full-length Amelogenin and Other Amelogenin Isoforms

INTRODUCTION

Amelogenins, secreted by epithelially-derived ameloblasts, are the predominant proteins in the developing enamel extracellular matrix (ECM), representing greater than 90% of the total protein in the secretory-stage enamel matrix (Termine *et al.*, 1980). Moreover, amelogenins have been localized in the dentin (Inai *et al.*, 1991; Nakamura *et al.*, 1994), and synthesized and secreted by mesenchymally-derived odontoblasts (Papagerakis *et al.*, 2003). We showed amelogenin mRNA expression by odontoblasts (Ye *et al.*, 2006), and immunochemical staining for amelogenin shows amelogenin secreted between these two cell types (Fig. 1).

Amelogenins are highly conserved among divergent species. Both amino acid and cDNA sequences for bovine, human, mouse and porcine amelogenins have revealed greater than 80% conservation (Deutsch, 1989). In the developing enamel matrix, amelogenins are believed to function in modulating the enamel crystal growth. There is both *in vitro* and *in vivo* evidence indicating that alterations of amelogenin amino acid sequences result in defects in enamel crystal formation.

Recombinant full-length amelogenins from different species have the ability to undergo self-assembly into nanospheres (radius ~ 20 nm) and nanochains that might serve as scaffolding proteins to regulate *in vitro* biomineralization of enamel-like crystals (Du *et*

al., 2005; Habelitz *et al.*, 2004; Iijima and Moradian-Oldak, 2005; Moradian-Oldak, 2001; Moradian-Oldak *et al.*, 2003; Wen *et al.*, 1999). There is also an *in vivo* evidence to show that these amelogenin nanospheres align along the c-axis of the developing enamel rods, inhibiting crystal growth in width (Fincham *et al.*, 1995).

Amelogenin-null mice experience disorganized hypoplastic (thin) enamel, suggesting the critical roles of amelogenin in the normal enamel development (Gibson *et al.*, 2001). In humans, mutations of amelogenin gene on the X-chromosome result in a heterogeneous group of inherited disorders characterized by defective of the enamel biomineralization, called X-linked amelogenesis imperfecta (Collier *et al.*, 1997; Kim *et al.*, 2004; Kindelan *et al.*, 2000; Lagerstrom *et al.*, 1990; Lench and Winter, 1995).

Several isoforms of amelogenins ranging from 5 to 28 kDa have been reported. In human, the most the predominant amelogenin isoform found in the developing enamel matrix is encoded by exons 2 to 7, except lacking exon 4 (Fig. 2); I refer to this particular amelogenin variant as human full-length amelogenin (H174, MW ~ 20 kDa) throughout my thesis. In contrast, the quantities of amelogenin isoforms containing the encoded sequence of exon 4 (exon 4 coded for 14 amino acids, NSHSQAINVDRTAL) are very minute within the matrix, and quite difficult to detect. The heterogeneity of amelogenins is due to alternative splicing of the primary pre-mRNA into multiple spliced variants (Simmer *et al.*, 1994). Moreover, the hydrolysis of amelogenins by matrix metalloproteinase 20 (MMP-20 or enamelysin) (Bartlett *et al.*, 1998; Bartlett and Simmer, 1999) and kallikrein-4 (KLK-4 or enamel matrix serine protease 1, EMSP1)

(Simmer and Hu, 2002) also contributes to this heterogeneity. One of the most studied amelogenin alternatively spliced variants of the primary transcript is 6.8-kDa leucine-rich amelogenin peptide (LRAP), whose sequence contains 58 residues (Gibson *et al.*, 1991). LRAP is encoded by exons 2, 3, 5, 6d (only 3' end of exon 6) and 7, corresponding to the first 33 and the last 25 amino acids of the full-length amelogenin. As a result, LRAP and full-length amelogenin are different because LRAP sequence lacks the central domain of the full-length amelogenin that is encoded by the large 5'-segment of exon 6. The primary architecture of full-length amelogenin and its alternatively spliced LRAP are presented in Fig. 2. LRAP can also self-assemble into nanospheres via its hydrophobic N-terminal regions, while the highly hydrophilic C-terminal tails (identical to those of the parent full-length amelogenins) are exposed on the surface of the nanospheres (Moradian-Oldak *et al.*, 2001). Moreover, the charged hydrophilic C-terminal region of LRAP has been shown to oriented next to the surface of hydroxyapatite, suggesting that this C-terminal domain may play roles in modulating mineralization (Shaw *et al.*, 2004). Furthermore, LRAP has been shown to induce chondrogenesis and odontogenesis (Nebgen *et al.*, 1999). Therefore, LRAP seems to have both structural functions to guide enamel growth and cell-signaling functions in dental mesenchyme and epithelium.

LRAP and full-length amelogenin appear to have many similar characteristics. Both of these proteins are bipolar and form nanospheres. They both contain the identical charged C-terminal regions that may interact with hydroxyapatite, suggesting their roles in regulating enamel biomineralization. However, LRAP functions as a cell-signaling molecule, but currently there is no report of similar functions in full-length amelogenin.

Despite their important in amelogenesis, the specific molecular mechanisms of LRAP and the full-length amelogenin in enamel biomineralization and cell signaling have not been well determined.

The purpose of this study was to synthesize several alternatively spliced recombinant amelogenins. These amelogenins include human full-length amelogenin (rH174, sequence containing 174 residues) and its several isoforms such as C-terminal truncated amelogenin (rH163, sequence lacking 11 residues of the C-terminal motif), LRAP and C-terminal truncated or short LRAP (sLRAP) were synthesized using the bacteria *E. coli*, while the C-terminal peptide was commercially synthesized. In the subsequent chapters, these recombinant and synthetic amelogenins were used in my investigations of the mechanisms of protein-apatite interaction, as well as the role of amelogenins in cell signaling.

MATERIALS AND METHODS

A. Expression and purification of rH174 and rH163

Expression and purification of recombinant human full-length amelogenin (rH174) were performed as described previously (Li *et al.*, 2003). A full-length amelogenin H174 cDNA (GI: 6715562 in Genebank), including exons 2-7, without the signal peptide was amplified from a human enamel-organ cDNA library. In addition, a truncated H163 cDNA was created from H174 cDNA, lacking the 3' nucleotide sequence encoded for the last 11 amino acids (STDKTKREEVD) of the rH174. Both H174 and H163 cDNA's were cloned into pRSET vectors (Invitrogen, Carlsbad, CA, USA), and transformed into

BL21 (DE3) pLysS competent *E. coli* (Stratagene, La Jolla, CA, USA). Transformed bacteria were plated onto LB agarose plates containing 100 µg/ml ampicillin and incubated overnight at 37 °C. Single colonies were isolated and cultured in 10-ml of LB starter cultures (EMD Chemicals Inc., Gibbstown, NJ, USA) supplemented with 100 µg/ml ampicillin (EMD Chemical Inc.) and cultured at 37 °C overnight in a shaker incubator. The overnight cultures were added to 1L of LB broth containing the same antibiotic concentration, and incubated at 37 °C. To express rH174 and rH163, at bacterial O.D._{600nm} of 0.8, the cells were induced for protein expressions using 0.8 mM of isopropyl-1-thio-β-D-galactopyranoside (IPTG) (Invitrogen) at 28 °C overnight. The bacteria were harvested, resuspended in 6 M Guanidine, and lysed by sonication. The supernatants were collected by centrifugation and further diluted 10 times with 5% formic acid. Both rH174 and rH163 were purified using 2-time 15% (NH₄)₂SO₄ precipitation.

The precipitated proteins were re-dissolved in 30% acetonitrile (ACN) + 0.1% trifluoroacetic acid (TFA), and added to C4-beads (GraceVyDac, Hesperia, CA, USA) in solution. The beads were poured into a column, and the protein was eluted from the beads with 80% acetonitrile (ACN) + 0.1% trifluoroacetic acid (TFA).

B. Expression and purification of LRAP and sLRAP

LRAP cDNA was amplified from a human ameloblast cDNA library. In addition, short LRAP (sLRAP) cDNA was made from LRAP cDNA, lacking the 3' nucleotide sequence encoded for the last 11 residues (STDKTKREEVD) of the LRAP. Both LRAP and

sLRAP cDNA's were inserted separately into pGEX-4T-1 vectors (Amersham Biosciences, Piscataway, NJ, USA) and transformed into BL21 (DE3) pLysS competent *E. coli* (Stratagene). Transformed bacteria were plated onto LB agarose plates containing 100 µg/ml ampicillin and incubated overnight at 37 °C. Single colonies were isolated and cultured in 10-ml of LB starter culture overnight at 37 °C. The overnight cultures were resuspended in fresh LB broth (1 L) with 100 µg/ml ampicillin. At bacterial O.D._{600nm} of 0.6, the cells were induced for 24 h, 225 r.p.m., at 28 °C to express GST-LRAP or GST-sLRAP fusion protein using 0.2 mM of IPTG (Invitrogen). The cells were harvested by centrifugation, resuspended in lysis buffer comprised of 0.5% sarkosyl and 1% Triton X-100 in 1X PBS solution, supplemented with protease inhibitor cocktails (Roche, Indianapolis, IN, USA), at pH 7.4, and lysed by sonication.

Cell debris was removed by centrifugation, and the soluble fractions of GST-LRAP or GST-sLRAP supernatant was loaded on a glutathione-sepharose beads (Amersham Biosciences) column that had been pre-equilibrated with 1X PBS. The column was washed extensively with 1X PBS, and the fusion protein was then digested with 100 U of thrombin (Amersham Biosciences) at 25 °C for 4 h, and eluted with PBS. However, sLRAP is a highly hydrophobic proteins, thus 30% acetonitrile (ACN) was subsequently used for elution after PBS. The eluted LRAP or sLRAP was further purified by reverse-phase HPLC on a C18 column (Varian, Lake Forest, CA, USA) eluting with a gradient of ACN + 0.1% TFA.

C. Characterization of purified rH174, rH163, LRAP, sLRAP and synthetic C-terminal domain

The purified rH174, rH163, LRAP and sLRAP were visualized by SDS-PAGE, reconfirmed by Western blots and mass spectrometry (MS). After separation by SDS-PAGE, rH174, rH163, LRAP and sLRAP were transferred onto nitrocellulose membranes, NitroBind (Osmonics Inc, Minnetonka, MN, USA) for Western blots.

The membranes were blocked with 5% skim milk (Oxoid Ltd, Basingstoke, Hampshire, England) and incubated with 1:1000 dilution of rabbit anti-human amelogenin or LRAP antibody, respectively. Anti-rabbit IgG conjugated with horse radish peroxidase (1:1000 dilution) was applied as a secondary antibody. The immunoreactivity was visualized using an ECL Western Blotting Analysis System (Amersham Biosciences, Piscataway, NJ, USA).

MS analyses were performed by matrix-assisted laser desorption ionization time-of-flight (MALDI-TOF). The predicted average masses were determined using a computer program Protein Prospector 3.1.1 (Mass Spectrometry Facility, University of California, San Francisco, CA, USA).

C-terminal domain (the last 11 C-terminal amino acids, STDKTKREEVD) of rH174 and LRAP was commercially synthesized, purified by HPLC (purity > 96.5%). The size was measured by mass spectrometry to be 1308.40 Da as compared to the predicted mass of 1307.64 Da (GeneScript Corporation, Piscataway, NJ, U.S.A.)

RESULTS

Expression, purification and characterization of rH174, rH163, LRAP and sLRAP

After expression and purification, rH174, rH163, LRAP and sLRAP were analyzed using SDS-PAGE and Western blots. Purified rH174 and rH163 appeared as ~20 kDa and ~18 kDa, respectively (Fig. 3A, B), while LRAP and sLRAP had apparent molecular weights of ~6.8 kDa and ~5.5 kDa, respectively (Fig. 4A, B). The identities of rH174, rH163, LRAP and sLRAP were also reconfirmed by mass spectrometry analysis to be 19806.10, 18516.70, 6838.68 and 5546.84, respectively. These measured mass values matched well with the predicted mass values indicated in Table 1. The synthetic C-terminal peptide predicted and measured mass values were also reported in Table 1.

CONCLUSION

Recombinant human amelogenins rH174, rH163, LRAP and sLRAP were successfully produced from bacteria *E. coli*, then purified and characterized by SDS-PAGE, Western blots and mass spectrometric analysis. Synthetic C-terminal amelogenin peptide was also synthesized, purified and characterized by mass spectrometric analysis. These purified amelogenins will be used for future experiments to determine the mechanisms of protein-apatite interaction and their ability to modulate enamel-like crystal growth.

In addition, the functional mechanisms of these amelogenins as signaling molecules to regulate odontoblast and ameloblast proliferation and/or differentiation will also be

thoroughly investigated. These recombinant amelogenins are necessary for studies to understand the role of these proteins in tooth formation and enamel biomineralization.

REFERENCES

- Bartlett JD, Ryu OH, Xue J, Simmer JP, Margolis HC (1998). Enamelysin mRNA displays a developmentally defined pattern of expression and encodes a protein which degrades amelogenin. *Connect Tissue Res* 39(1-3):101-9; discussion 141-9.
- Bartlett JD, Simmer JP (1999). Proteinases in developing dental enamel. *Crit Rev Oral Biol Med* 10(4):425-41.
- Collier PM, Sauk JJ, Rosenbloom SJ, Yuan ZA, Gibson CW (1997). An amelogenin gene defect associated with human X-linked amelogenesis imperfecta. *Arch Oral Biol* 42(3):235-42.
- Deutsch D (1989). Structure and function of enamel gene products. *Anat Rec* 224(2):189-210.
- Du C, Falini G, Fermani S, Abbott C, Moradian-Oldak J (2005). Supramolecular assembly of amelogenin nanospheres into birefringent microribbons. *Science* 307(5714):1450-4.
- Fincham AG, Moradian-Oldak J, Diekwisch TG, Lyaruu DM, Wright JT, Bringas P, Jr., Slavkin HC (1995). Evidence for amelogenin "nanospheres" as functional components of secretory-stage enamel matrix. *J Struct Biol* 115(1):50-9.
- Gibson CW, Golub E, Ding WD, Shimokawa H, Young M, Termine J, Rosenbloom J (1991). Identification of the leucine-rich amelogenin peptide (LRAP) as the translation product of an alternatively spliced transcript. *Biochem Biophys Res Commun* 174(3):1306-12.
- Gibson CW, Yuan ZA, Hall B, Longenecker G, Chen E, Thyagarajan T, Sreenath T, Wright JT, Decker S, Piddington R, Harrison G, Kulkarni AB (2001). Amelogenin-deficient mice display an amelogenesis imperfecta phenotype. *J Biol Chem* 276(34):31871-5.
- Habelitz S, Kullar A, Marshall SJ, DenBesten PK, Balooch M, Marshall GW, Li W (2004). Amelogenin-guided crystal growth on fluoroapatite glass-ceramics. *J Dent Res* 83(9):698-702.

- Iijima M, Moradian-Oldak J (2005). Control of apatite crystal growth in a fluoride containing amelogenin-rich matrix. *Biomaterials* 26(13):1595-603.
- Inai T, Kukita T, Ohsaki Y, Nagata K, Kukita A, Kurisu K (1991). Immunohistochemical demonstration of amelogenin penetration toward the dental pulp in the early stages of ameloblast development in rat molar tooth germs. *Anat Rec* 229(2):259-70.
- Kim JW, Simmer JP, Hu YY, Lin BP, Boyd C, Wright JT, Yamada CJ, Rayes SK, Feigal RJ, Hu JC (2004). Amelogenin p.M1T and p.W4S mutations underlying hypoplastic X-linked amelogenesis imperfecta. *J Dent Res* 83(5):378-83.
- Kindelan SA, Brook AH, Gangemi L, Lench N, Wong FS, Fearne J, Jackson Z, Foster G, Stringer BM (2000). Detection of a novel mutation in X-linked amelogenesis imperfecta. *J Dent Res* 79(12):1978-82.
- Lagerstrom M, Dahl N, Iselius L, Backman B, Pettersson U (1990). Mapping of the gene for X-linked amelogenesis imperfecta by linkage analysis. *Am J Hum Genet* 46(1):120-5.
- Lench NJ, Winter GB (1995). Characterisation of molecular defects in X-linked amelogenesis imperfecta (AIH1). *Hum Mutat* 5(3):251-9.
- Li W, Gao C, Yan Y, DenBesten P (2003). X-linked amelogenesis imperfecta may result from decreased formation of tyrosine rich amelogenin peptide (TRAP). *Arch Oral Biol* 48(3):177-83.
- Moradian-Oldak J (2001). Amelogenins: assembly, processing and control of crystal morphology. *Matrix Biol* 20(5-6):293-305.
- Moradian-Oldak J, Jimenez I, Maltby D, Fincham AG (2001). Controlled proteolysis of amelogenins reveals exposure of both carboxy- and amino-terminal regions. *Biopolymers* 58(7):606-16.
- Moradian-Oldak J, Iijima M, Bouropoulos N, Wen HB (2003). Assembly of amelogenin proteolytic products and control of octacalcium phosphate crystal morphology. *Connect Tissue Res* 44 Suppl 1(58-64).
- Nakamura M, Bringas P, Jr., Nanci A, Zeichner-David M, Ashdown B, Slavkin HC (1994). Translocation of enamel proteins from inner enamel epithelia to odontoblasts during mouse tooth development. *Anat Rec* 238(3):383-96.
- Nebgen DR, Inoue H, Sabsay B, Wei K, Ho CS, Veis A (1999). Identification of the chondrogenic-inducing activity from bovine dentin (bCIA) as a low-molecular-mass amelogenin polypeptide. *J Dent Res* 78(9):1484-94.
- Papagerakis P, MacDougall M, Hotton D, Bailleul-Forestier I, Oboeuf M, Berdal A (2003). Expression of amelogenin in odontoblasts. *Bone* 32(3):228-40.

Shaw WJ, Campbell AA, Paine ML, Snead ML (2004). The COOH terminus of the amelogenin, LRAP, is oriented next to the hydroxyapatite surface. *J Biol Chem* 279(39):40263-6.

Simmer JP, Lau EC, Hu CC, Aoba T, Lacey M, Nelson D, Zeichner-David M, Snead ML, Slavkin HC, Fincham AG (1994). Isolation and characterization of a mouse amelogenin expressed in *Escherichia coli*. *Calcif Tissue Int* 54(4):312-9.

Simmer JP, Hu JC (2002). Expression, structure, and function of enamel proteinases. *Connect Tissue Res* 43(2-3):441-9.

Termine JD, Belcourt AB, Christner PJ, Conn KM, Nylén MU (1980). Properties of dissociatively extracted fetal tooth matrix proteins. I. Principal molecular species in developing bovine enamel. *J Biol Chem* 255(20):9760-8.

Wen HB, Moradian-Oldak J, Fincham AG (1999). Modulation of apatite crystal growth on Bioglass by recombinant amelogenin. *Biomaterials* 20(18):1717-25.

Ye L, Le TQ, Zhu L, Butcher K, Schneider RA, Li W, Besten PK (2006). Amelogenins in human developing and mature dental pulp. *J Dent Res* 85(9):814-8.

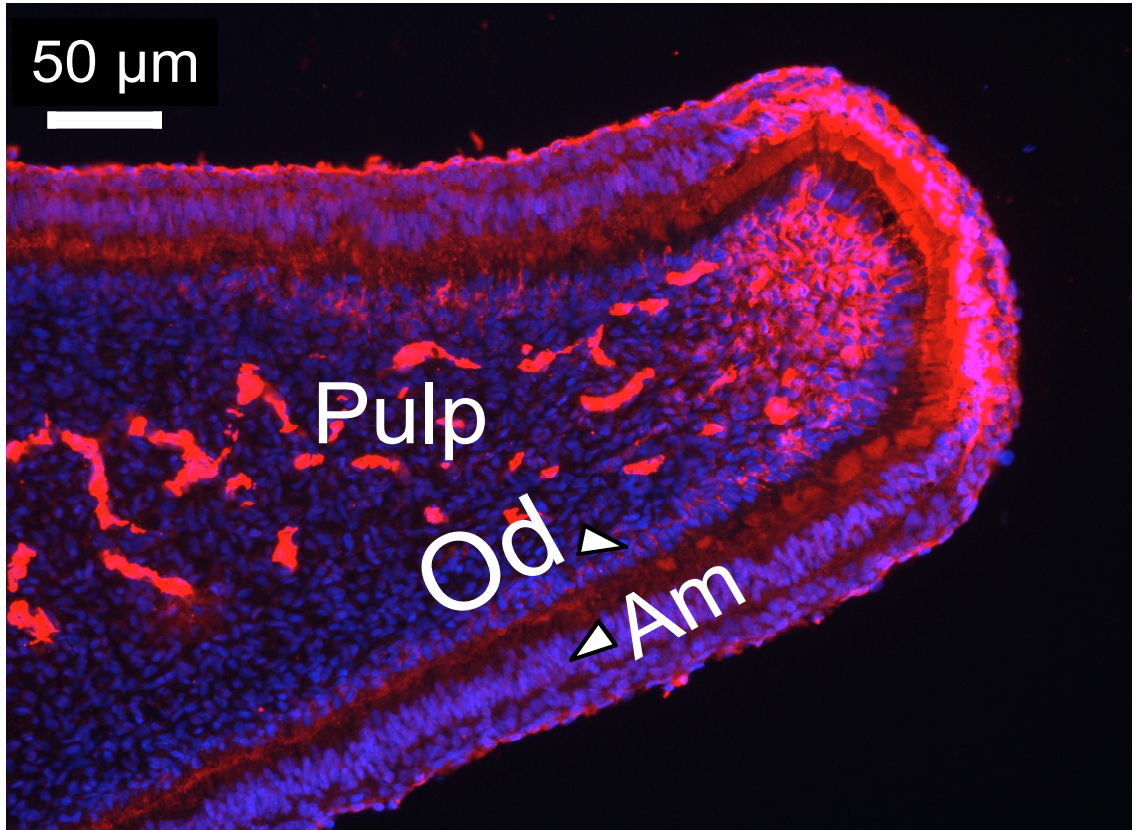
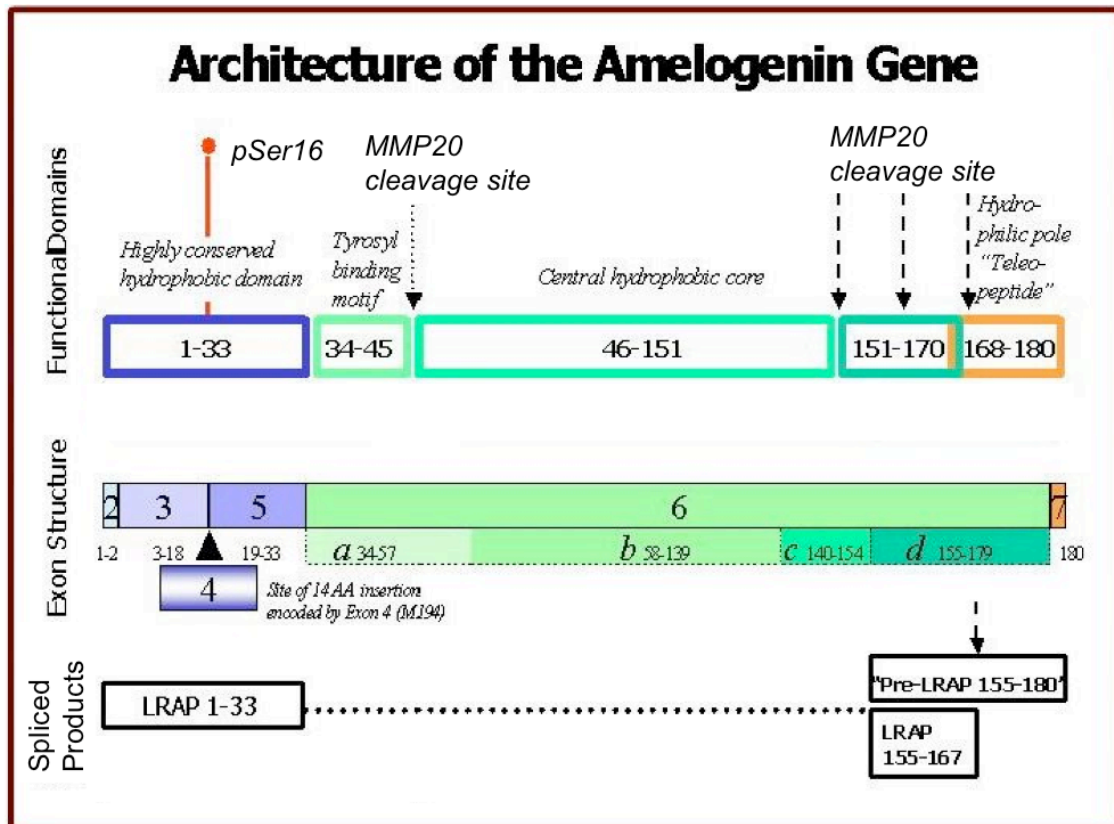


Figure 1

***In vivo* immunostaining for amelogenins in a developing human incisor**

Human fetal (21-week old) incisor immunofluorescent staining for amelogenin (red) showed that both odontoblasts (Od.) and ameloblasts (Am.) synthesized and secreted amelogenins. DAPI (blue) stained for cell nuclei. Endothelial cells lining the blood vessels in the pulp appeared to be non-specifically stained by amelogenin antibody as well. Bar = 50 μ m.



<http://dentistry.uic.edu/CraniofacialGenetics/ResearchTED.htm>

Figure 2.

The primary architecture of the parent full-length amelogenin and leucine-rich amelogenin peptide (LRAP).

The most predominant secreted human amelogenin isoform is called the “full-length amelogenin”, which is encoded by exons 2 to 7, except lacking exon 4, resulting in ~20 kDa, 174-residue protein (rH174) after cleaving the C-terminal teleopeptide. Amelogenin undergoes extensive proteolysis and alternative splicing, yielding many peptide isoforms. One of the most studied alternatively spliced variant is leucine-rich amelogenin peptide (LRAP, ~6.8 kDa), which is encoded by exon 2, 3, 5 and 6d (3'-end of exon 6) and 7, corresponding to the first 33 and the last 25 amino acids of the full-length amelogenin, except lacking the central region (encoded by exon 6a, b, c). As a result, full-length amelogenin and LRAP have many similar characteristics, including highly hydrophilic charged C-terminal domains (11-residue sequence) and hydrophobic N-terminal regions. The functions of these N- and C-terminal domains are some of the major subjects of my thesis.

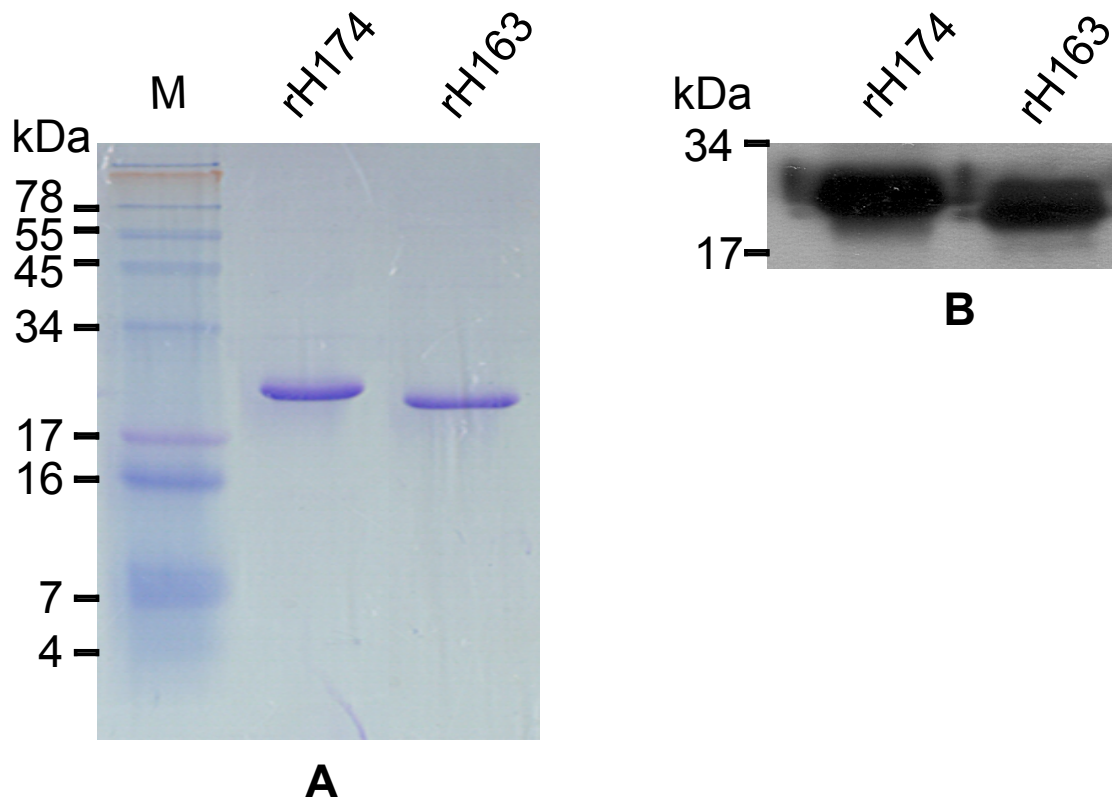


Figure 3.

Characterization of the purified human full-length amelogenin (rH174) and its C-terminal truncated isoforms (rH163).

A) SDS-PAGE and B) Western blot of purified rH174 (19.8 kDa) and rH163 (18.6 kDa) using rabbit anti-human amelogenin antibody. The C-terminal truncated rH163 lacks the last 11 amino acids (STDKTKREEVD). M, SeeBlue Plus2 marker (Invitrogen).

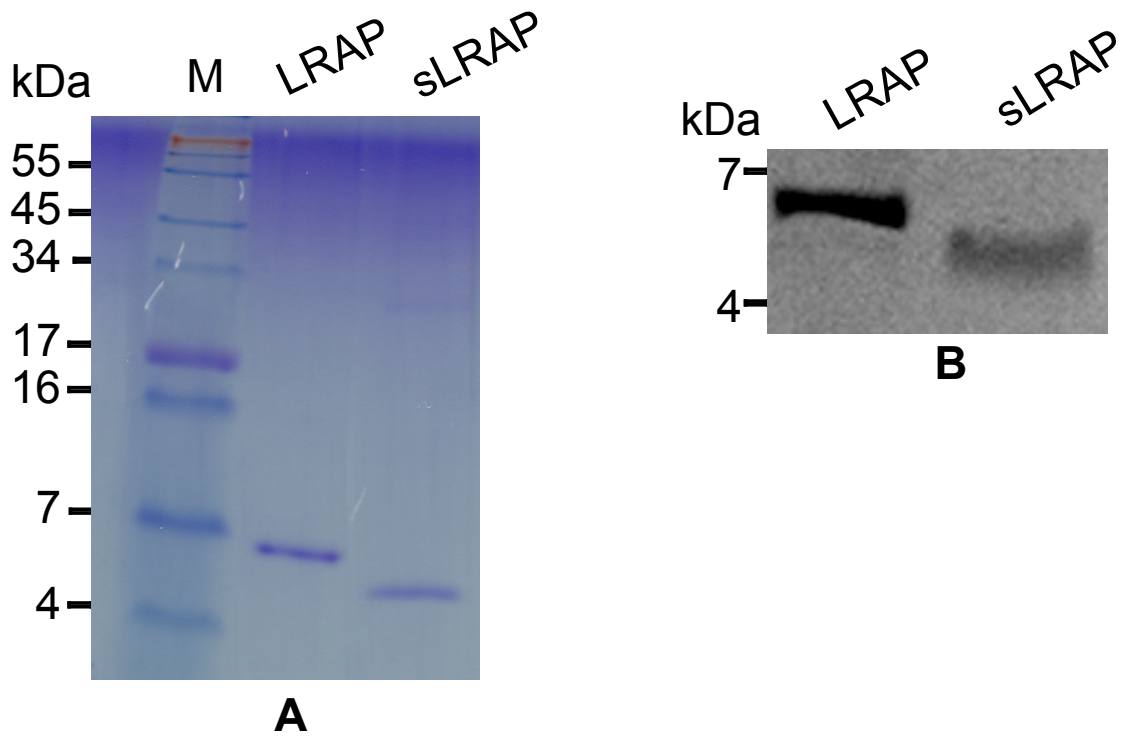


Figure 4.

Characterization of the purified human leucine-rich amelogenin peptide (LRAP) and its C-terminal truncated or short LRAP (sLRAP).

A) SDS-PAGE and B) Western blot of purified LRAP (6.8 kDa) and sLRAP (5.5 kDa) using rabbit anti-human LRAP antibody. The C-terminal truncated sLRAP lacks the last 11 amino acids (STDKTKREEVD). M, SeeBlue Plus2 marker (Invitrogen).

Amelogenin	Measured m/z (Da)	Predicted m/z (Da)
rH174	19806.10	19804.89
rH163	18516.70	18515.52
LRAP	6838.68	6838.48
sLRAP	5546.84	5546.851
C-term motif	1308.40	1307.64

Table 1.

Mass spectrometric analysis of recombinant and synthetic amelogenins.

The measured mass values of recombinant proteins (rH174, rH163, LRAP and sLRAP) and synthetic peptide (C-terminal motif, STDKTKREEVD) matched their respective predicted theoretical values.

Chapter 5: The Role of Carboxyl-terminal Domains of Amelogenins in Modulating *In Vitro* Enamel-like Crystal Growth

INTRODUCTION

Enamel is the hardest mineralized tissue in mammalian species. Mature enamel crystallites are composed mainly of carbonated hydroxyapatite crystals, which are oriented into long and highly organized rods or prisms, extending from the dentino-enamel junction (DEJ) to the enamel surface of the tooth (Simmer and Fincham, 1995).

Dental enamel forms by matrix-mediated biomineralization. Amelogenins are the predominant (> 90%) extracellular enamel matrix proteins, (Fincham *et al.*, 1999).

Amelogenin-null mice experience disorganized hypoplastic (thin) enamel, suggesting that amelogenins serve a critical function in the normal enamel development (Gibson *et al.*, 2001). There is both *in vitro* and *in vivo* evidence showing that even single amino acid alterations of the amelogenin sequence result in defects of enamel crystal formation.

These various mutations of the amelogenin gene on the X-chromosome result in a heterogeneous group of inherited disorders characterized by defective of the enamel biomineralization, called X-linked amelogenesis imperfecta (Collier *et al.*, 1997; Kim *et al.*, 2004; Kindelan *et al.*, 2000; Lagerstrom *et al.*, 1990; Lench and Winter, 1995).

In vitro studies show that recombinant full-length amelogenin (the most predominant secreted amelogenin isoform encoded by exons 2, 3, 5, 6 and 7, but lacking exon 4) has the ability to undergo self-assembly into nanospheres (radius ~ 20 nm) and nanochains

that might serve as scaffolding proteins to regulate enamel biomineralization (Du *et al.*, 2005; Habelitz *et al.*, 2004; Iijima and Moradian-Oldak, 2005; Moradian-Oldak, 2001; Moradian-Oldak *et al.*, 2003; Wen *et al.*, 1999). There is also an *in vivo* evidence to show that these amelogenin nanospheres align parallel to the c-axis of the developing enamel rods, playing a potential role in inhibiting crystal growth in width (Fincham *et al.*, 1995).

Beginning early in enamel matrix formation, ameloblasts secrete matrix metalloproteinase 20 (MMP-20 or enamelysin) at the same time amelogenins are secreted. Mass spectrometric analysis of proteolytic amelogenins obtained from developing human enamel matrix reveals that MMP-20 specifically hydrolyzes the full-length amelogenin (H174, 174 residue protein) at the carboxyl terminus, removing 11 C-terminal amino acids (STDKTKREEVD) from the end of the protein (Fincham and Moradian-Oldak, 1996). Thus, the cleavage of C-terminal domain creates another amelogenin isoform called C-terminal truncated amelogenin (H163, lacking the last 11 C-terminal residues of H174). Post-secretion, the truncated amelogenin lacking the hydrophilic carboxyl terminus is one of the most predominant proteolytic amelogenin components, comprising 50% of the enamel protein matrix (Yamakoshi *et al.*, 1994).

Amelogenins lacking the hydrophilic C-terminal domains form larger nanospheres than amelogenins with an intact carboxyl terminus. This is likely due to enhanced hydrophobic-hydrophobic interactions between the more hydrophobic truncated amelogenins. Moradian-Oldak and co-workers showed that the affinity of the truncated

full-length amelogenin to apatite was significantly lower than that of the intact full-length amelogenin, suggesting the carboxyl terminus plays important functions in enamel biomineralization (Moradian-Oldak *et al.*, 2002). An early *in vitro* study reported that the C-terminal domain inhibits apatite crystal growth in a supersaturated calcium phosphate solution having ionic composition similar to that of secretory-stage enamel fluid (Aoba *et al.*, 1989). Two amelogenin mutations that result in truncation of the hydrophilic C-terminal domains, lacking the last 12- and 18-amino-acid carboxyl terminus, result in the formation of both hypomineralized and hypoplastic enamel (Kindelan *et al.*, 2000; Lench and Winter, 1995). The importance of the C-terminal amelogenin sequence is evidenced by the conservation of this sequence across many species (Toyosawa *et al.*, 1998).

Amelogenins also undergo alternative splicing of the primary mRNA transcript to produce 6.8-kDa leucine-rich amelogenin peptide (LRAP), whose sequence contains 58 residues (Gibson *et al.*, 1991). LRAP is encoded by exons 2, 3, 5, 6d (3' end of exon 6) and 7, corresponding to the first 33 and the last 25 amino acids of the full-length amelogenin. Therefore, similar to full-length amelogenin, LRAP also contains MMP-20 cleavage site at the carboxyl terminus. MMP-20-mediated proteolysis of LRAP results in a C-terminal truncated or short LRAP (sLRAP), lacking the last 11 C-terminal residues (STDKTKREEVD) of the LRAP. Like full-length amelogenin, LRAP can also self-assemble into nanospheres via its hydrophobic N-terminal regions, while the highly hydrophilic C-terminal domains are exposed on the surface of the nanospheres (Moradian-Oldak *et al.*, 2001). Moreover, the charged hydrophilic C-terminal region of

LRAP has been shown to orient toward the surface of hydroxyapatite, suggesting that this carboxyl-terminal domain may modulate mineralization (Shaw *et al.*, 2004).

LRAP and full-length amelogenin differ in that LRAP lacks the central amino acid segment, which is encoded by a long nucleotide sequence located at 5'-end of exon 6 (exon 6a, b, c) of the full-length protein. Yet, these amelogenins still share many similar characteristics. Both of these proteins are bipolar and form nanospheres. They both contain the identical charged carboxyl-terminal regions that may interact with hydroxyapatite. These proteins differ in their hydrophobicity, and despite their importance in amelogenesis, the specific molecular mechanisms of LRAP and the full-length amelogenin in enamel biomineralization have not been determined. The purpose of this study is to investigate the role of C-terminal domain to mediate the binding between LRAP and full-length amelogenin to the surface of synthetic carbonated hydroxyapatite, and the abilities of these proteins to promote enamel-like crystal growth *in vitro*. The results of these studies provide direct evidence of specific matrix-crystal interactions, which guide enamel mineralization.

MATERIALS AND METHODS

1. Amelogenins and synthetic carbonated hydroxyapatite (CAP) binding experiments

A. Dose-dependent binding of human full-length amelogenin (rH174) and LRAP to CAP

Excess amount of purified rH174 (20 μ l of 0.86 μ g/ μ l, or 17.2 μ g) or LRAP (20 μ l of 0.51 μ g/ μ l, or 10.2 μ g) were incubated with various amounts of synthetic CAP (0, 20, 40, 120 and 200 μ g) in a final volume of 40 μ l of Tris/HCl (20 mM), pH 7.5, for 2 h at 25 °C, allowing protein-apatite interaction. These assays were done in duplicate reaction sets, and each set was done in triplicate. The reaction tubes were manually mixed every 30 min. The samples were then centrifuged at 12,000 r.p.m. for 5 min, and carefully washed 4 times with 300 μ l Tris/HCl (20 mM), pH 7.5 to remove the unbound proteins in the supernatants, while avoiding disturbing the pellets. The collected protein-bound CAP samples were freeze-dried under vacuum. In one set of reactions, de-ionized water (15 μ l) was used to resuspend the pellets, which were then added to 15 μ l of 2X SDS loading buffer. The samples were heated at 100 °C for 5 min, and 20 μ l was loaded per well for SDS-PAGE analysis. Bound rH174 (15 μ l) and bound LRAP (20 μ l) were loaded into SDS-PAGE sample well, separated by electrophoresis, and stained with Coomassie blue.

In a second set of reactions, 15 μ l of 0.5 % TFA was used to completely dissolve protein-bound CAP. The samples were neutralized using 15 μ l of 0.25 mM Tris/HCl, pH 8.0. The quantity of bound proteins was determined by Bradford protein assay kit according to manufacturer's instruction (Bio-Rad Lab, Inc., Hercules, CA, USA). Statistical analysis was done with unpaired t-test with $p < 0.05$ ($n=3$) to be considered significant, using an InStat software (GraphPad software, Inc., San Diego, CA, USA).

B. Determining the binding saturation of rH174 and LRAP to a fixed amount of synthetic CAP

Using the information obtained from experiments in part 1A, a fixed amount of synthetic CAP (150 μg) was chosen and incubated with various amounts of purified rH174 (0, 2, 4, 10, 17 μg) or LRAP (0, 1, 2, 5, 10 μg) in a final volume of 40 μl of Tris/HCl (20 mM), pH 7.5, for 2 h at 25 $^{\circ}\text{C}$, allowing protein-apatite interactions. The protein mineral complex was then characterized as described in part 1A above. These experiments were used to identify the maximum amount of rH174 or LRAP to bind to a to a specific amount of CAP.

C. Carboxyl-terminal domain binding to synthetic CAP

The 11 amino acids sequence (STDKTKREEVD) corresponding to the carboxyl-terminal fragment of both full-length amelogenin (rH174) and LRAP, which is cleaved from the protein by MMP-20, were commercially synthesized by (GeneScript Corporation, Piscataway, NJ, U.S.A.). The synthetic CAP used for all of the binding experiments was from the same batch, which was previously characterized in chapter 3.

An excess amount of synthetic C-terminal peptide (150 μl of 1.6 $\mu\text{g}/\mu\text{l}$ or 240 μg) was incubated with 3 mg of synthetic CAP in a final volume of 450 μl of Tris/HCl (20 mM), pH 7.5, for 2 h at 25 $^{\circ}\text{C}$, allowing peptide-apatite interaction. For a control, CAP (3 mg) was suspended in 450 μl of Tris/HCl (20 mM), pH 7.5 without the addition of C-terminal peptide. After the binding, the samples were centrifuged at 12,000 r.p.m. for 5 min. The supernatants (150 μl) containing the unbound C-terminal domains were removed for bicinchoninic acid (BCA) protein assay using BCA kit (Pierce, Rockford, IL, USA).

Determining the amount of unbound C-terminal peptide in supernatant allows the indirect

calculation of the amount of bound C-terminal peptide on apatites. For direct calculation of the amount of bound C-terminal peptide, the C-terminal bound CAP was carefully washed 4 times with 500 μl of 20 mM Tris/HCl, pH 7.5. The washed apatites were resuspended in a final total volume of 300 μl of the same Tris/HCl buffer ($\sim 10 \mu\text{g}$ CAP/ μl Tris buffer). The amounts of bound C-terminal domains on CAP were also quantified by BCA protein assay (Pierce). Bradford protein assay could not be used to determine the concentration of C-terminal domains because C-terminal sequence does not contain any aromatic and basic amino acids that can be recognized and bind by the acidic Coomassie Brilliant Blue G-250 dye. These C-terminal bound CAP were used for the subsequent binding experiments with full-length recombinant human amelogenin (rH174), C-terminal truncated full-length amelogenin (rH163), leucine-rich amelogenin peptide (LRAP), and C-terminal truncated or short LRAP (sLRAP).

D. Carboxyl-terminal domain mediated the binding of rH174 and LRAP to synthetic CAP

CAP (30 mg) or C-term bound CAP (30 mg) was suspended separately in 4.5 ml of 20 mM Tris/HCl, pH 7.5 to make $6.67 \mu\text{g}/\mu\text{l}$. Concurrently, LRAP, sLRAP, rH174 or rH163 were also dissolved each separately in 20 mM Tris/HCl, pH 7.5 to create $1 \mu\text{g}/\mu\text{l}$.

After optimization for the proper amount of CAP and proteins used, the free CAP (22.5 μl of $6.67 \mu\text{g}/\mu\text{l}$, or 150 μg) and C-terminal bound CAP suspensions (22.5 μl of $6.67 \mu\text{g}/\mu\text{l}$, or 150 μg) were incubated separately with LRAP (7.65 μl of $1 \mu\text{g}/\mu\text{l}$, or 7.65 μg) and sLRAP (7.65 μl of $1 \mu\text{g}/\mu\text{l}$, or 7.65 μg). The final total volume of 40 μl was obtained

by adding 9.85 μl of 20 mM Tris/HCl, pH 7.5, and incubated for 2 h at 25 °C to facilitate the binding interactions. Similarly, the free CAP (22.5 μl of 6.67 $\mu\text{g}/\mu\text{l}$, or 150 μg) and C-terminal bound CAP (22.5 μl of 6.67 $\mu\text{g}/\mu\text{l}$, or 150 μg) were also incubated separately with rH174 (15.3 μl of 1 $\mu\text{g}/\mu\text{l}$, or 15.3 μg) or rH163 (22.5 μl of 6.67 $\mu\text{g}/\mu\text{l}$, or 15.3 μg). The final total volume of 40 μl was obtained by adding 2.2 μl of 20 mM Tris/HCl, pH 7.5, and incubated for 2 h at 25 °C to facilitate the binding interactions.

The subsequent binding and analyzing procedures were followed according to methods described in part 1A above. Bradford protein assay (Bio-Rad) was an ideal assay to quantify the amount of bound proteins (i.e. LRAP and sLRAP, rH174 and rH163) to CAP substrates. Because the Bradford protein assay does not recognize the pre-bound C-terminal peptides for reasons indicated in part 1C, the bound C-terminal peptides did not interfere with the quantification of bound amelogenins.

E. Atomic force microscopy (AFM) imaging of rH174, rH163, LRAP, sLRAP and carboxyl-terminal peptide binding to a mineral (fluoroapatite) substrate

Fluoroapatite (FAP) glass-ceramic disks were prepared and polished according to previously published methods (Habelitz *et al.*, 2004). Polished FAP glass-ceramic substrates were incubated separately with 100 μl of 80 μM of rH174, rH163, LRAP, sLRAP or C-terminal peptide in 20 mM Tris/HCl, pH 7.5 at 25 °C for 2 h. After incubation, the FAP substrates were rinsed thoroughly with de-ionized water to remove unbound proteins, and gently dried with dust-free air. Evidence of protein binding to FAP was detected using an atomic force microscope (AFM, Nanoscope III, Digital

Instruments, Santa Barbara, CA, USA) in tapping mode with high aspect-ratio Si-tips (r~5 nm, l~125 μ m) (Nanosensors, Neuchatel, Switzerland) operating at approximately 300 kHz.

2. Amelogenin-guided crystal growth *in vitro* using rH174, and MMP-20-mediated amelogenin proteolytic products, rH163 and C-terminal domain

Amelogenin-guided crystal growth *in vitro* experiments were conducted on fluoroapatite (FAP) glass-ceramic substrates. Amelogenins were incubated in mineralizing calcium phosphate solutions containing rH174, rH163, or the C-terminal domain (11-residue fragment of rH174), in the presence of the FAP surface. FAP and protein samples preparation, and experimental procedures were done as previously described by Habelitz *et al.* (Habelitz *et al.*, 2004; Habelitz *et al.*, 2005). Briefly, rH174, rH163 or C-term fragment, each at 80.8 μ M, were incubated in the presence of a polished FAP substrate in a final volume of 400 μ l of mineralizing solution. This solution composition was comparable to the secretory enamel fluid (Aoba and Moreno, 1987), and contained $[\text{Ca}^{2+}] = 0.5 \text{ mM}$, $[\text{PO}_4^{3-}] = 2.45 \text{ mM}$, $[\text{KCl}] = 150 \text{ mM}$, $[\text{Tris/Cl}] = 50 \text{ mM}$, pH 7.5 at 37 $^\circ\text{C}$. Samples were incubated in a horizontal shaker, shaking at 225 r.p.m. at 37 $^\circ\text{C}$ for 24 h. After the incubation, FAP substrates were rinsed with de-ionized water, and carefully dried with dust-free air. Evidence of amelogenin-guided enamel-like crystal growth on FAP substrate was analyzed using AFM (Nanoscope III, Digital Instruments) in tapping mode with high aspect-ratio siliconized tips (r ~ 5 nm, l ~ 125 μ m) (Nanosensors).

RESULTS

Dose-dependending binding of rH174 and LRAP to carbonated hydroxyapatite (CAP)

SDS-PAGE (Fig 1A, B) and Bradford protein assays (Fig 1C, D) both showed that synthetic CAP (0, 20, 40, 120, 200 μg) was incubated with an excess amount of rH174 (17.2 μg) or LRAP (10.2 μg) in 40 μl of Tris/HCl (20 mM), pH 7.5, the amounts of bound rH174 (Fig. 1A, C) or LRAP (Fig. 1B, D) increased proportionally with the amounts of CAP substrate. These data showed specific interactions between rH174 or LRAP and synthetic CAP, and directed further experiments to define the maximum amount of amelogenin protein (rH174 or LRAP) that would bind with a fixed amount of synthetic CAP (150 μg).

Determining the binding saturation of rH174 and LRAP to fixed amount of CAP (150 μg)

Various amount of rH174 (0, 2, 4, 10, 17 μg) or LRAP (0, 1, 2, 5, 10 μg) were incubated with 150 μg CAP substrate in a final volume of 40 μl of Tris/HCl (20 mM), pH 7.5, for 2 h at 25 °C. The maximal amounts of bound rH174 and bound LRAP were 8.72 μg rH174/150 μg CAP (58.13 μg rH174/mg CAP) and 4.34 μg LRAP/150 μg CAP (28.93 μg LRAP/mg CAP), respectively (Fig. 2C and D). This quantification of bound rH174 and bound LRAP was visualized by SDS-PAGE (Fig. 2A and B).

Carboxyl-terminal domain binding to synthetic CAP

BCA protein assay showed that $210.2 \pm 9.7 \mu\text{g}$ of unbound C-terminal peptide in the supernatant, while $18.9 \pm 2.19 \mu\text{g}$ of C-terminal peptide bound to 3 mg of synthetic CAP

(Fig. 3). Therefore, approximately 6.3 μg of C-terminal domain bound and saturated all binding sites of 1 mg CAP ($\sim 6.3 \mu\text{g}/\text{mg}$, or $84.3 \mu\text{g}/\text{m}^2$, or $0.064 \mu\text{mol}/\text{m}^2$). A total of 229.1 μg (210.2 μg unbound + 18.9 μg bound C termini) of C-terminal peptide was measured as compared to 240 μg originally added. Thus, there was 4.5 % error.

Carboxyl-terminal domain mediated binding of LRAP and rH174 to synthetic CAP

The amount of bound LRAP ($23.52 \pm 2.98 \mu\text{g}/\text{mg CAP}$) was significantly greater than that of bound sLRAP ($2.67 \pm 1.13 \mu\text{g}/\text{mg CAP}$), showing increased binding by more than 88% (Fig. 4A, B and Fig. 5A, B). Pre-treatment CAP with the C-terminal peptide significantly reduced the binding of LRAP ($5.04 \pm 1.54 \mu\text{g}/\text{mg CAP}$) by 79%, but it did not greatly affect the binding of sLRAP ($2.58 \pm 0.80 \mu\text{g}/\text{mg CAP}$) as compared to the untreated CAP substrate (Fig. 4A, B and Fig. 5A, B).

Similarly, the amount of bound rH174 ($78.89 \pm 10.18 \mu\text{g}/\text{mg CAP}$) was significantly greater than that of bound rH163 ($42.06 \pm 4.34 \mu\text{g}/\text{mg CAP}$), indicating increased binding by more than 46% (Fig. 6A, B and Fig. 7A, B). The pre-treatment of C-terminal domains to CAP significantly reduced the binding of rH174 ($37.01 \pm 7.07 \mu\text{g}/\text{mg CAP}$) by 53%; however, it did not significantly affect the binding of rH163 ($41.15 \pm 4.04 \mu\text{g}/\text{mg CAP}$) as compared to the untreated CAP sample (Fig. 6A, B and Fig. 7A, B). These results provided strong evidence that LRAP and rH174 directly bind synthetic CAP through the C-terminal domain.

AFM imaging of rH174, rH163, LRAP, sLRAP and carboxyl terminus binding fluoroapatite (FAP) glass-ceramic disks

AFM imaging showed direct evidence of different amounts of rH174, rH163, LRAP and sLRAP bound onto the surface of FAP substrates (Fig. 8). Comparisons of rH174 and rH163 binding to FAP showed that more rH174 bound to the FAP substrate (Fig. 8B and C). Similarly, more LRAP bound to FAP as compared to sLRAP (Fig. 8D and E). The bound C-terminal peptide was difficult to detect because the fragments were very small (Fig. 8F). A well-polished surface of FAP glass-ceramic disk was provided as a control for comparison (Fig. 8A), showing the hexagonal shapes identifying the locations of FAP.

Amelogenin-guided crystal growth *in vitro* using rH174, rH163 and C-terminal domain

rH174, rH163 and C-terminal domain were incubated in calcium phosphate (CaP) mineralizing solutions, pH 7.4, in the presence of polished FAP substrates for amelogenin-guided crystal growth experiments at 37 °C. The AFM results indicated that rH163 (C-terminal truncation of rH174) and C-terminal domain failed to stimulate enamel-like crystal formation (Fig. 9E and F). Interestingly, only rH174 had the ability to promote enamel-like crystal growth (Fig. 9D). These enamel-like crystals were $\sim 400 \pm 56$ nm in length. In the negative controls of FAP incubated with or without BSA, showed no evidence of enamel-like crystal formation (Fig. 9B and C).

DISCUSSION

Apatite binding to recombinant full-length amelogenin (rH174) and LRAP experiments definitively showed that these proteins interact with the surface of synthetic carbonated hydroxyapatite by carboxyl-terminal motif (Fig. 4-7). When apatites were pre-treated with the C-terminal peptide, the protein binding was reduced. In addition, amelogenins without the C-terminal domains also had reduced apatite binding. The specificity of apatites binding by the C-terminal domain suggests that the C-terminus of amelogenin is involved in matrix-mediated enamel biomineralization. These studies confirmed previous investigations (Aoba *et al.*, 1989; Shaw *et al.*, 2004). Since the C-terminal domain contains two Asp's and two Glu's, these acidic amino acids may be responsible for binding the amelogenins to the surface of CAP by directly interacting with the calcium ions on the surface of the apatites via ionic interaction.

Aoba *et al.* suggested that the role of the C-terminus was to inhibit mineralization, as demonstrated in *in-vitro* studies of apatite-peptide interactions in solution. (Aoba *et al.*, 1989). However, our studies using a FAP surface showed no effect of LRAP in mediating crystal formation when incubated in simulated secretory enamel fluid (Habelitz *et al.*, 2006). An *in vivo* study reported that an LRAP knock-in has failed to rescue the hypoplastic enamel defect of amelogenin-null mice (Chen *et al.*, 2003). These results suggest that either LRAP does not have a role in enamel crystal growth, or that in some way it acts in concert with other amelogenin, such as the full-length amelogenin described in these studies.

The full-length amelogenin, rH174 can promote *in vitro* enamel-like crystal growth (Habelitz *et al.*, 2004; Habelitz *et al.*, 2005). This amelogenin and LRAP differ in that LRAP lacks the central hydrophobic amino acid sequence coded for by exon 6. This leads to the question as to whether an amelogenin with the central hydrophobic sequence, but lacking the C-terminus, could promote crystal growth. To test the hypothesis that the central core is the primary domain required to promote crystal growth, we used the AFM to compare rH163 (C-terminal truncation of rH174) mediated crystal growth on the FAP substrate, as compared to rH174. We found that amelogenin missing the C-terminus failed to promote crystal growth. Crystals also did not grow in the presence of a synthetic C-terminal domain (the last 11 hydrophilic charged residues, STDKTKREEVD) alone (Fig. 9E and F). Only rH174 successfully promoted enamel-like crystal growth (Fig. 9D).

These data suggest that amelogenin must have both an intact C-terminus as well the central hydrophobic amino acid sequence to stimulate enamel-like crystal formation. We propose that the C-terminal domain is required for rH174 to interact directly to hydroxyapatite surface, allowing the N-terminal region to facilitate the passage of calcium and phosphate ions via 1-Å β -spiral internal channel, which is made up of 27-residues, repeating of (Gln-Pro-X)₉ (Renugopalakrishnan *et al.*, 1989; Renugopalakrishnan, 2002) within the hydrophobic central domain. This structure would create a supersaturated calcium phosphate microenvironments in the areas between hydroxyapatite surfaces and the adjacent charged hydrophilic C-terminal domains on the surface of amelogenin assembly, promoting localized mineral precipitation required for

crystal growth. Therefore, lacking either the C- or N-terminal domain would deprive the rH174 molecule the necessary structures for performing its designated functions. It is interesting to note another unique difference between the C- and N-terminal regions is that the C-terminal domain contains 2 Asp's and 2 Glu's closely positioned within its 11-residue sequence; however, the much longer N-terminal motif contains no Asp and only 2 Glu's, which are distantly located from each other. The presence of several acidic amino acids within the short C-terminal domain results in a much higher degree of hydrophilicity as compared to the more hydrophobic N-terminal sequence. This hydrophilic C-terminal domain allows the amelogenin to bind to the surface of apatites to promote crystal growth *in vitro*.

It has been well documented that immobilized dentin matrix proteins on a surface (i.e. type I collagen, or agarose beads) result in some three-dimensional conformations that would initiate mineralization (Saito *et al.*, 1997). Base on this information, it is also possible that the immobilized hydrophobic N-terminal domain or rH163 (lacking the C-terminal end) would also promote mineral formation, similar to that observed in the intact rH174. Thus, the function of the N-terminal sequence requires additional study.

These studies have provided important new information on the structure-function relationships of amelogenins as they mediate crystal growth. We found that the carboxyl terminus is required for initial crystal formation on a charged surface, such as FAP. However, the C-terminus alone can not nucleate mineral formation. Mineralization requires an intact hydrophobic core. The role of this hydrophobic core in mineralization

is not known, but it is likely to form a unique structure that promotes localization of mineral ions, creating an environment of supersaturation and crystal nucleation to form the building blocks of enamel crystal growth. Clearly, further studies are needed to better understand this unique and interesting model of amelogenin-mediated crystal growth.

REFERENCES

Aoba T, Moreno EC (1987). The enamel fluid in the early secretory stage of porcine amelogenesis: chemical composition and saturation with respect to enamel mineral. *Calcif Tissue Int* 41(2):86-94.

Aoba T, Moreno EC, Kresak M, Tanabe T (1989). Possible roles of partial sequences at N- and C-termini of amelogenin in protein-enamel mineral interaction. *J Dent Res* 68(9):1331-6.

Chen E, Yuan ZA, Wright JT, Hong SP, Li Y, Collier PM, Hall B, D'Angelo M, Decker S, Piddington R, Abrams WR, Kulkarni AB, Gibson CW (2003). The small bovine amelogenin LRAP fails to rescue the amelogenin null phenotype. *Calcif Tissue Int* 73(5):487-95.

Collier PM, Sauk JJ, Rosenbloom SJ, Yuan ZA, Gibson CW (1997). An amelogenin gene defect associated with human X-linked amelogenesis imperfecta. *Arch Oral Biol* 42(3):235-42.

Du C, Falini G, Fermani S, Abbott C, Moradian-Oldak J (2005). Supramolecular assembly of amelogenin nanospheres into birefringent microribbons. *Science* 307(5714):1450-4.

Fincham AG, Moradian-Oldak J, Diekwisch TG, Lyaruu DM, Wright JT, Bringas P, Jr., Slavkin HC (1995). Evidence for amelogenin "nanospheres" as functional components of secretory-stage enamel matrix. *J Struct Biol* 115(1):50-9.

Fincham AG, Moradian-Oldak J (1996). Comparative mass spectrometric analyses of enamel matrix proteins from five species suggest a common pathway of post-secretory proteolytic processing. *Connect Tissue Res* 35(1-4):151-6.

Fincham AG, Moradian-Oldak J, Simmer JP (1999). The structural biology of the developing dental enamel matrix. *J Struct Biol* 126(3):270-99.

Gibson CW, Golub E, Ding WD, Shimokawa H, Young M, Termine J, Rosenbloom J (1991). Identification of the leucine-rich amelogenin peptide (LRAP) as the translation

product of an alternatively spliced transcript. *Biochem Biophys Res Commun* 174(3):1306-12.

Gibson CW, Yuan ZA, Hall B, Longenecker G, Chen E, Thyagarajan T, Sreenath T, Wright JT, Decker S, Piddington R, Harrison G, Kulkarni AB (2001). Amelogenin-deficient mice display an amelogenesis imperfecta phenotype. *J Biol Chem* 276(34):31871-5.

Habelitz S, Kullar A, Marshall SJ, DenBesten PK, Balooch M, Marshall GW, Li W (2004). Amelogenin-guided crystal growth on fluoroapatite glass-ceramics. *J Dent Res* 83(9):698-702.

Habelitz S, Denbesten PK, Marshall SJ, Marshall GW, Li W (2005). Amelogenin control over apatite crystal growth is affected by the pH and degree of ionic saturation. *Orthod Craniofac Res* 8(4):232-8.

Habelitz S, Denbesten PK, Marshall SJ, Marshall GW, Li W (2006). Self-assembly and effect on crystal growth of the leucine-rich amelogenin peptide. *Eur J Oral Sci* 114 Suppl 1(315-9).

Iijima M, Moradian-Oldak J (2005). Control of apatite crystal growth in a fluoride containing amelogenin-rich matrix. *Biomaterials* 26(13):1595-603.

Kim JW, Simmer JP, Hu YY, Lin BP, Boyd C, Wright JT, Yamada CJ, Rayes SK, Feigal RJ, Hu JC (2004). Amelogenin p.M1T and p.W4S mutations underlying hypoplastic X-linked amelogenesis imperfecta. *J Dent Res* 83(5):378-83.

Kindelan SA, Brook AH, Gangemi L, Lench N, Wong FS, Fearne J, Jackson Z, Foster G, Stringer BM (2000). Detection of a novel mutation in X-linked amelogenesis imperfecta. *J Dent Res* 79(12):1978-82.

Lagerstrom M, Dahl N, Iselius L, Backman B, Pettersson U (1990). Mapping of the gene for X-linked amelogenesis imperfecta by linkage analysis. *Am J Hum Genet* 46(1):120-5.

Lench NJ, Winter GB (1995). Characterisation of molecular defects in X-linked amelogenesis imperfecta (AIH1). *Hum Mutat* 5(3):251-9.

Moradian-Oldak J (2001). Amelogenins: assembly, processing and control of crystal morphology. *Matrix Biol* 20(5-6):293-305.

Moradian-Oldak J, Jimenez I, Maltby D, Fincham AG (2001). Controlled proteolysis of amelogenins reveals exposure of both carboxy- and amino-terminal regions. *Biopolymers* 58(7):606-16.

Moradian-Oldak J, Bouropoulos N, Wang L, Gharakhanian N (2002). Analysis of self-assembly and apatite binding properties of amelogenin proteins lacking the hydrophilic C-terminal. *Matrix Biol* 21(2):197-205.

Moradian-Oldak J, Iijima M, Bouropoulos N, Wen HB (2003). Assembly of amelogenin proteolytic products and control of octacalcium phosphate crystal morphology. *Connect Tissue Res* 44 Suppl 1(58-64).

Renugopalakrishnan V, Pattabiraman N, Prabhakaran M, Strawich E, Glimcher MJ (1989). Tooth enamel protein, amelogenin, has a probable beta-spiral internal channel, Gln112-Leu138, within a single polypeptide chain: preliminary molecular mechanics and dynamics studies. *Biopolymers* 28(1):297-303.

Renugopalakrishnan V (2002). A 27-mer tandem repeat polypeptide in bovine amelogenin: synthesis and CD spectra. *J Pept Sci* 8(4):139-43.

Saito T, Arsenault AL, Yamauchi M, Kuboki Y, Crenshaw MA (1997). Mineral induction by immobilized phosphoproteins. *Bone* 21(4):305-11.

Shaw WJ, Campbell AA, Paine ML, Snead ML (2004). The COOH terminus of the amelogenin, LRAP, is oriented next to the hydroxyapatite surface. *J Biol Chem* 279(39):40263-6.

Simmer JP, Fincham AG (1995). Molecular mechanisms of dental enamel formation. *Crit Rev Oral Biol Med* 6(2):84-108.

Toyosawa S, O'HUigin C, Figueroa F, Tichy H, Klein J (1998). Identification and characterization of amelogenin genes in monotremes, reptiles, and amphibians. *Proc Natl Acad Sci U S A* 95(22):13056-61.

Wen HB, Moradian-Oldak J, Fincham AG (1999). Modulation of apatite crystal growth on Bioglass by recombinant amelogenin. *Biomaterials* 20(18):1717-25.

Yamakoshi Y, Tanabe T, Fukae M, Shimizu M (1994). Porcine amelogenins. *Calcif Tissue Int* 54(1):69-75.

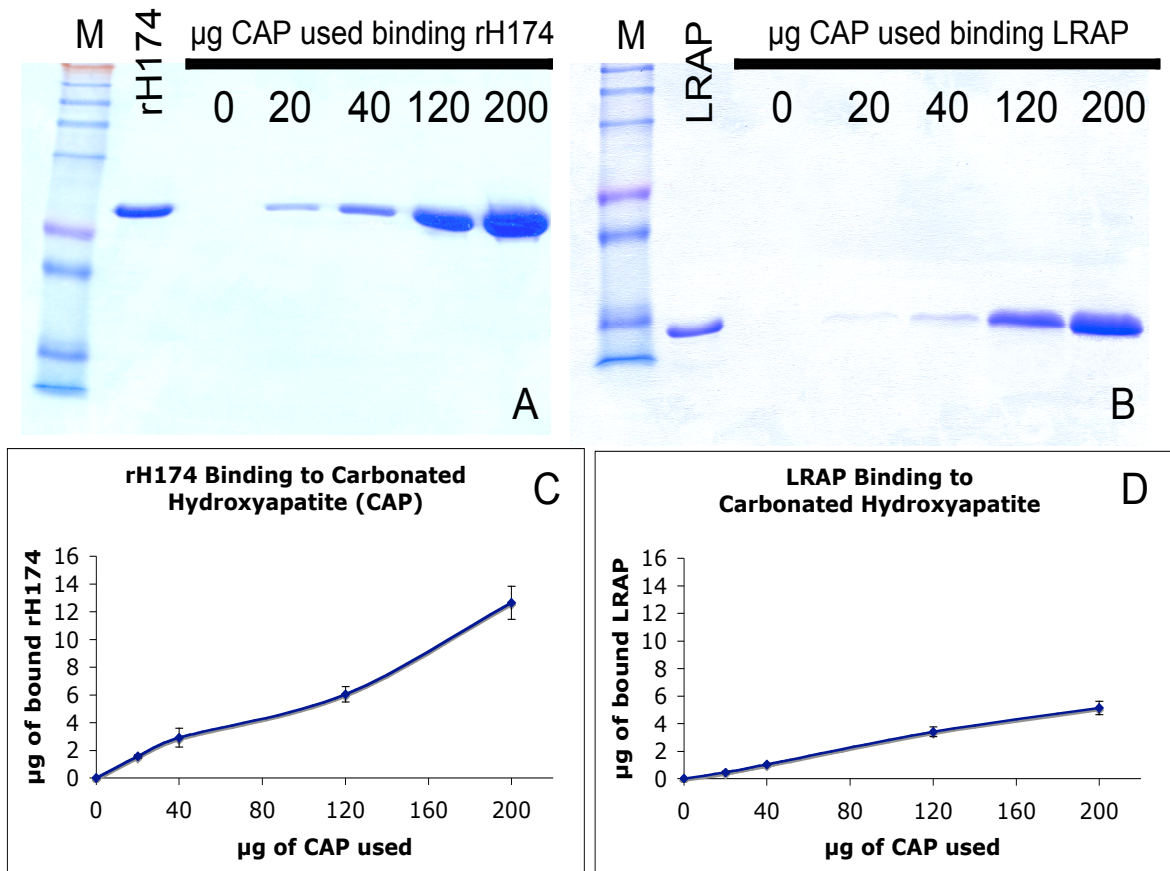


Figure 1.
Dose-dependent binding of full-length recombinant human amelogenin (rH174) and LRAP to carbonated hydroxyapatite (CAP)
 Various amounts of synthetic CAP (0, 20, 40, 120 and 200 µg) were incubated with excess amount of rH174 (17.2 µg) or LRAP (10.2 µg) in Tris/HCl (20 mM), pH 7.5. The amounts of bound rH174 were analyzed using SDS-PAGE (A) and quantified by Bradford protein assay (C). Similarly, the amounts of bound LRAP were also analyzed using SDS-PAGE (B) and quantified by Bradford protein assay (D). The amounts of bound rH174 or LRAP increased proportionally with the amounts of CAP substrates.

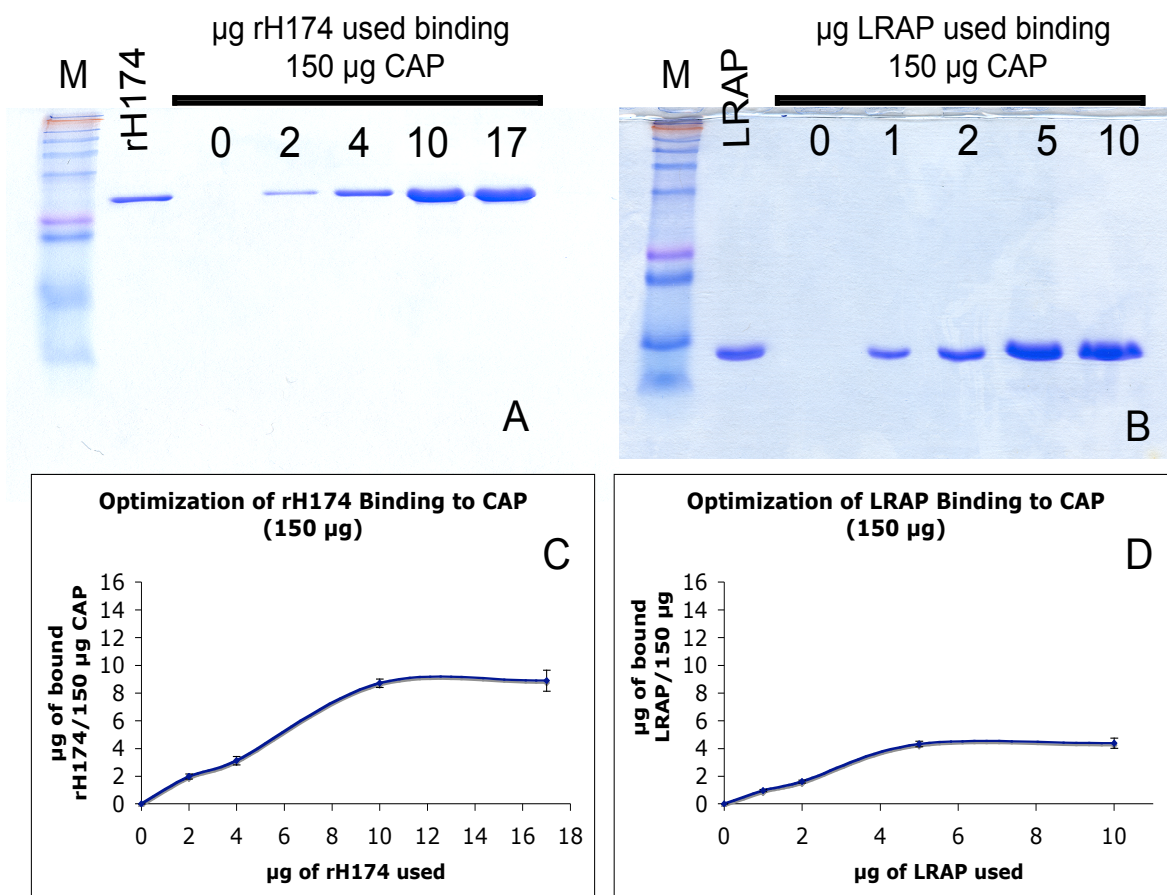


Figure 2.

Determining the binding saturation of rH174 and LRAP to a fixed amount of synthetic carbonated hydroxyapatite, CAP (150 µg)

Various amounts of rH174 (0, 2, 4, 10, 17 µg) and LRAP (0, 1, 2, 5, 10 µg) were allowed to interact and bind to a fixed amount of CAP (150 µg). The amounts of bound rH174 were analyzed using SDS-PAGE (A) and quantified by Bradford protein assay (C). Similarly, the amounts of bound LRAP were also analyzed using SDS-PAGE (B) and quantified by Bradford protein assay (D).

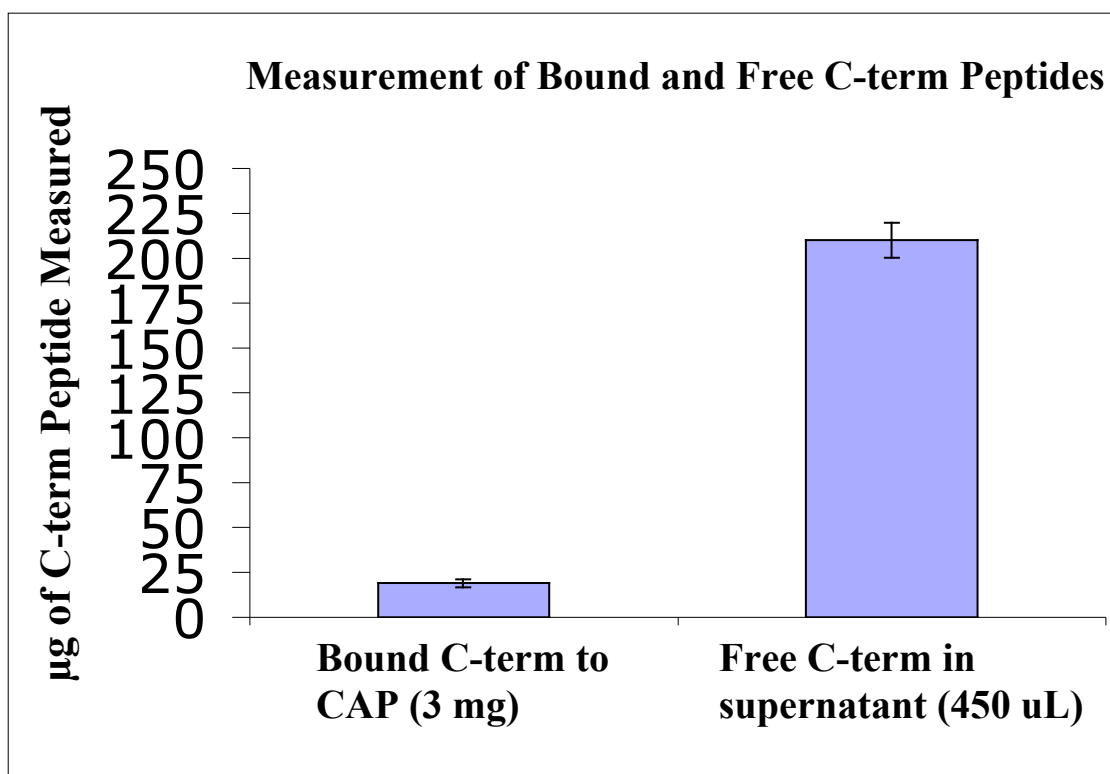


Figure 3.
Determination of the amount of bound carboxyl-terminal peptide to the surface of carbonated hydroxyapatite, CAP (3 mg).
 CAP (3 mg) was allowed to interact and bind with an excess amount of C-terminal peptide. Subsequently, the amount of bound C-terminal peptide was measured using Bicinchoninic acid (BCA) protein assay. In addition, the amount of unbound peptide in the supernatant was also analyzed.

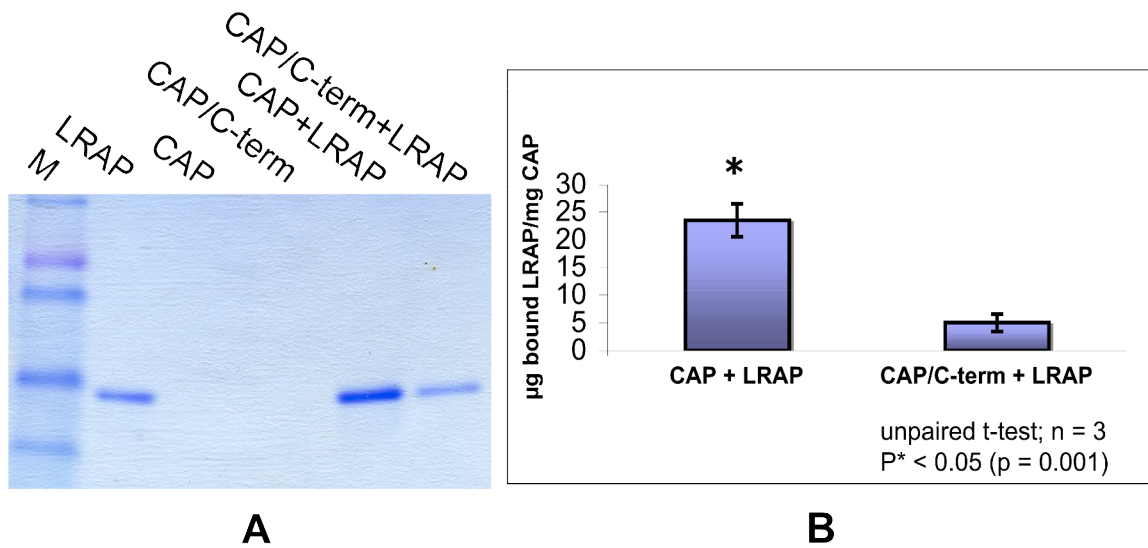


Figure 4.
Carboxyl-terminal peptides reduced the binding of LRAP to carbonated hydroxyapatite (CAP).
 LRAP was allowed to bind CAP and C-terminal peptide pre-treated CAP (CAP/C-term). The bound LRAP was analyzed using SDS-PAGE (A) and quantified by Bradford protein assay (B). Results represented the mean ± S.E. P* < 0.05 showed significant difference.

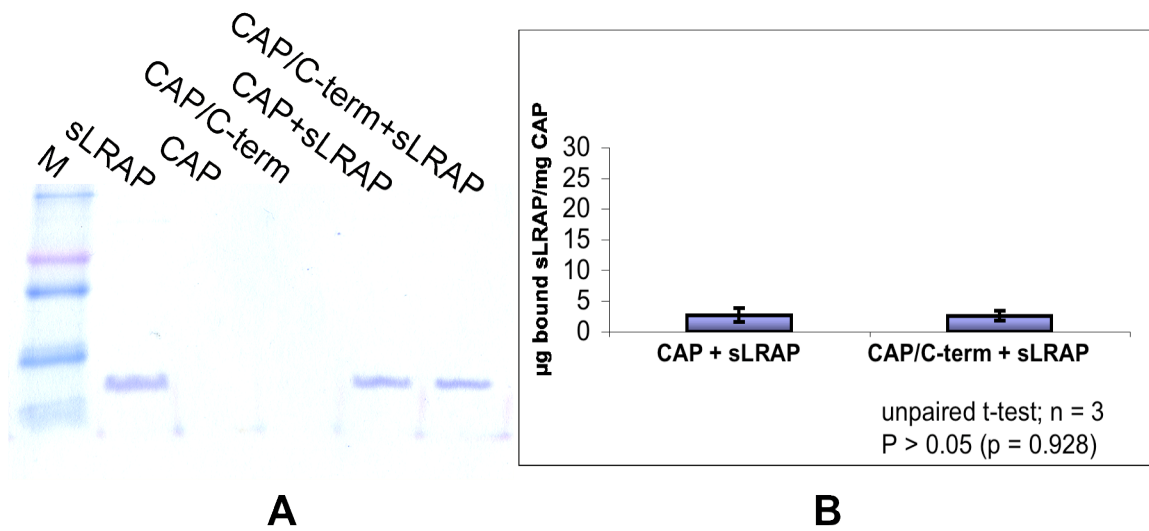


Figure 5.

Carboxyl-terminal peptides had no effects on the binding of C-terminal truncated LRAP (sLRAP) to carbonated hydroxyapatite (CAP).

sLRAP was allowed to bind CAP and C-terminal peptide pre-treated CAP (CAP/C-term). The bound sLRAP was analyzed using SDS-PAGE (A) and quantified by Bradford protein assay (B). Results represented the mean \pm S.E. $P^* > 0.05$ showed no significant difference.

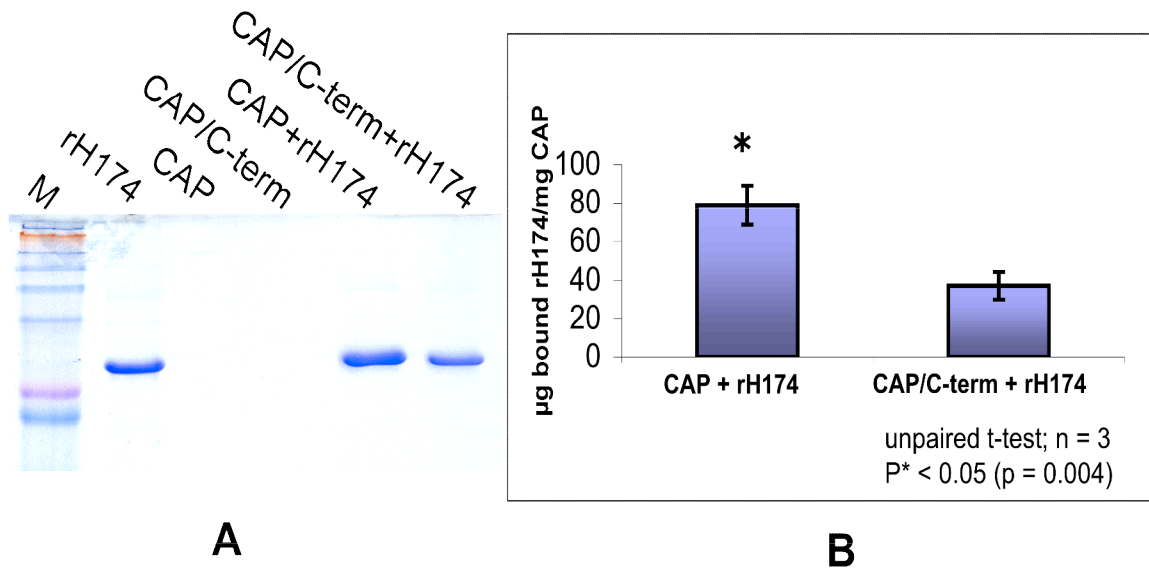


Figure 6.
Carboxyl-terminal peptides reduced the binding of full-length amelogenin (rH174) to carbonated hydroxyapatite (CAP).
 rH174 was allowed to bind CAP and C-terminal peptide pre-treated CAP (CAP/C-term). The bound rH174 was analyzed using SDS-PAGE (A) and quantified by Bradford protein assay (B). Results represented the mean \pm S.E. $P^* < 0.05$ showed significant difference.

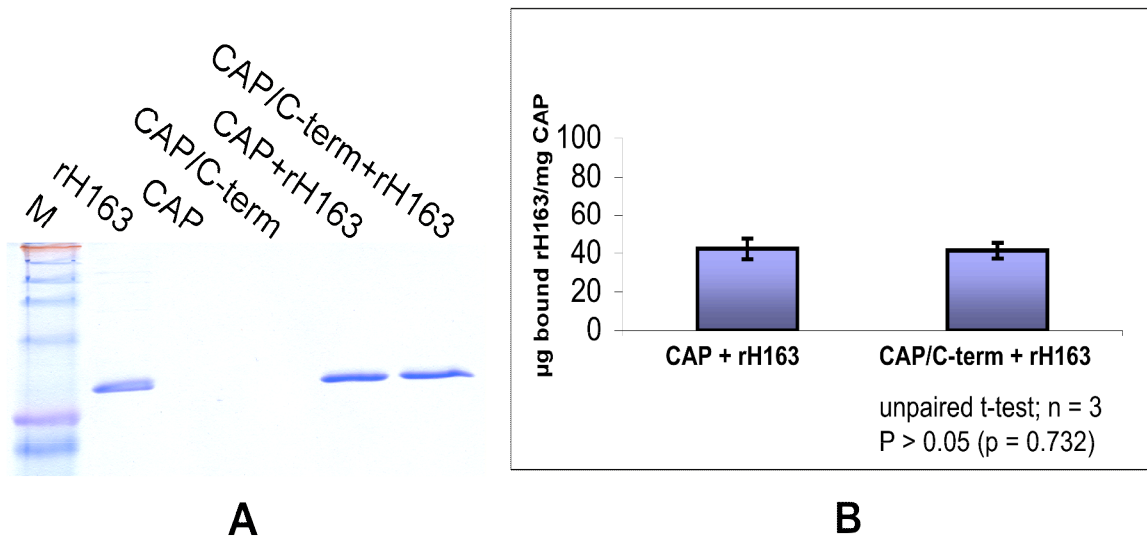


Figure 7.

Carboxyl-terminal peptides had no effects on the binding of C-terminal truncated full-length amelogenin (rH163) to carbonated hydroxyapatite (CAP).

rH163 was allowed to bind CAP and C-terminal peptide pre-treated CAP (CAP/C-term).

The bound rH163 was analyzed using SDS-PAGE (A) and quantified by Bradford protein assay (B). Results represented the mean ± S.E. $P^* > 0.05$ showed no significant difference.

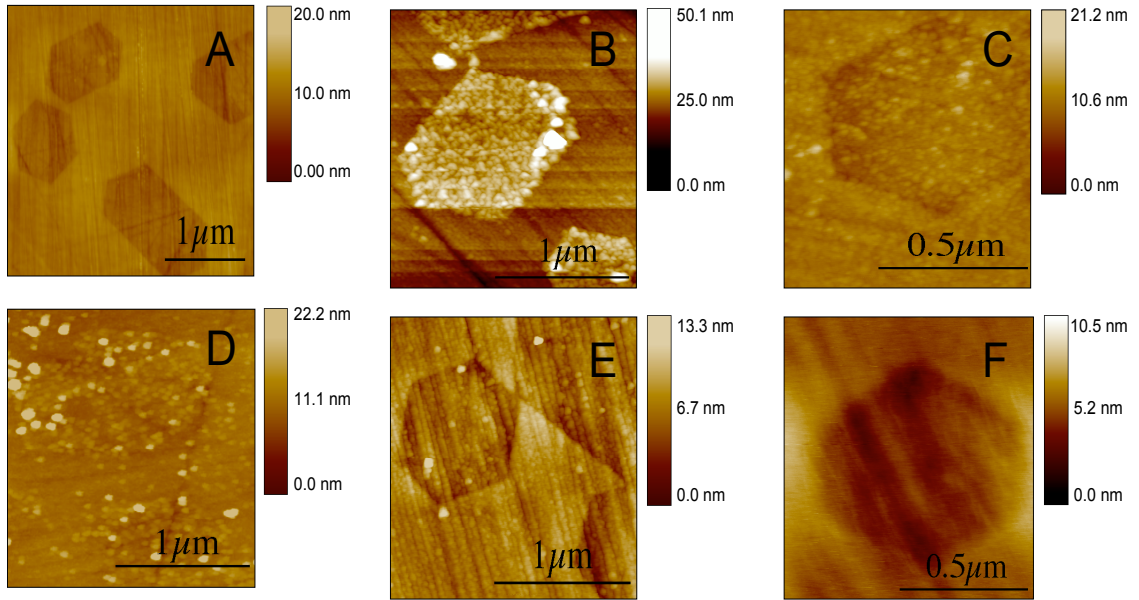


Figure 8.

Atomic force microscopy (AFM) imaging of rH174, rH163, LRAP, sLRAP and C-terminal peptide binding to fluorapatite (FAP).

A) Polished surface of glass ceramic embedded FAP. B) rH174, C) rH163, D) LRAP, E) sLRAP and F) C-terminal domain binding to the surface of FAP.

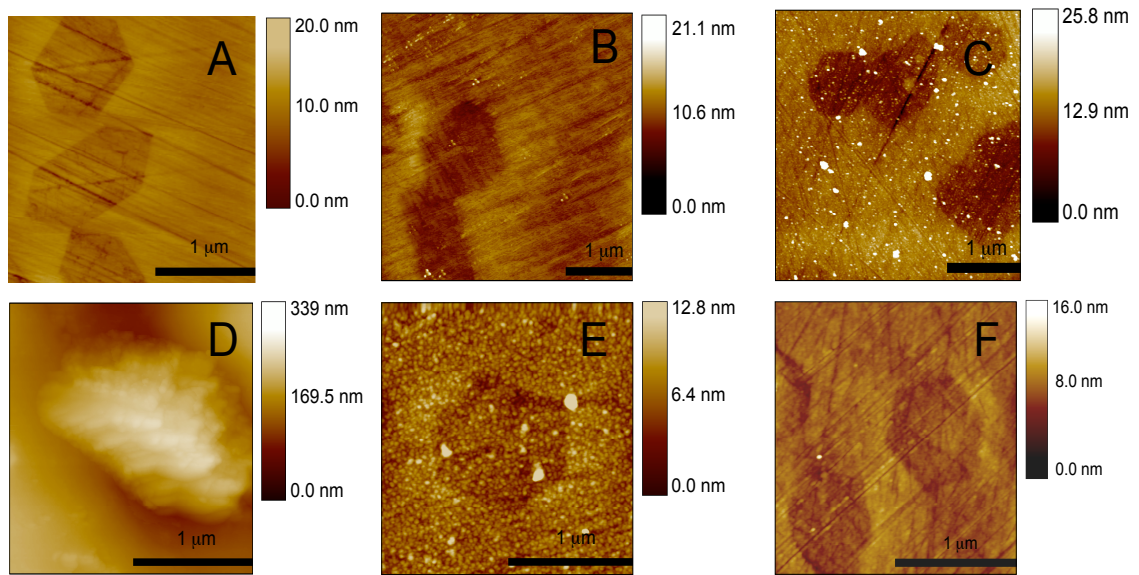


Figure 9.

Full-length amelogenin (rH174) promoted enamel-like crystal growth on the surface of fluorapatite (FAP) when incubated in mineralizing calcium/phosphate (CaP) solution that is similar to enamel-secretory fluid.

A) A Polished surface of FAP. B) FAP incubated in CaP solution, without any proteins. C) FAP incubated in CaP solution in the presence of BSA. D) FAP incubated in CaP solution in the presence of rH174 promoted enamel-like crystal growth, whose dimension was measured to be 400 ± 56 nm long. E) FAP incubated in CaP solution in the presence of rH163. F) FAP incubated in CaP solution in the presence of C-terminal peptide. Bars = $1 \mu\text{m}$.

Chapter 6: Comparative Calcium Binding of Leucine-Rich Amelogenin Peptide and Full-length Amelogenin

INTRODUCTION

During the early enamel mineralization, ameloblasts, which differentiate from the inner enamel epithelium, secrete enamel matrix proteins. Greater than 90% of the proteins present in the secretory stage enamel matrix are amelogenins (Fincham *et al.*, 1999).

Two of the most predominant amelogenin isoforms detected within the human developing enamel matrix are the full-length amelogenin (H174, 174-residue protein) encoded by exons 2 to 7, but minus exon 4, and leucine-rich amelogenin peptide (LRAP). The difference in the primary structures of H174 and LRAP was discussed in chapter 2.

The full-length amelogenin has the ability to undergo self-assembly into nanospheres, nanochains, and micro-ribbons, suggesting their potential roles as scaffolding proteins to direct enamel crystal growth (Du *et al.*, 2005). There is also an *in vivo* evidence to show that these amelogenin nanospheres align along the c-axis of the developing enamel rods, inhibiting crystal growth in the a-b plane (Fincham *et al.*, 1995). Amelogenin nanospheres formed from human recombinant full-length amelogenin (rH174) bind directly to the surface of synthetic carbonated hydroxyapatite via the C-terminal domain to promote enamel-like crystal formation *in vitro* (see chapter 5).

The so-called leucine-rich amelogenin peptide (LRAP) is a 58-residue alternatively spliced amelogenin variant (Gibson *et al.*, 1991). LRAP is encoded by exons 2, 3, 5, 6d

(3'-end segment of exon 6) and 7, corresponding to the first 33 and the last 25 amino acids of the full-length amelogenin (see chapter 2). Thus, both LRAP and full-length amelogenin are bipolar with hydrophobic N-terminal and highly hydrophilic C-terminal regions. The full-length amelogenins have been reported to form nanospheres, with the carboxyl regions exposed to the surface of the nanospheres (Moradian-Oldak *et al.*, 2001). Since the 25-residue C-terminal domains of both full-length amelogenin and LRAP are identical, the C-terminus of LRAP would be expected to behave similarly to that of full-length amelogenin. Moreover, the hydrophilic charged C-terminal region of LRAP has been shown to orient toward (Shaw *et al.*, 2004) and bind directly to the surface of hydroxyapatite (chapter 5), suggesting that this C-terminal domain may have a role in regulating mineralization.

The mechanisms by which amelogenins interact with apatites are largely unknown. It is possible that amelogenins bind calcium on the surface of apatites with a function in modulating enamel crystal growth. Interactions between calcium and amelogenins are not well understood. It is possible that calcium/amelogenin interactions are important in biomineralization, including initial crystal nucleation and post-nucleation growth.

The acidic, noncollagenous phosphoproteins of extracellular matrix (ECM) are also thought to regulate matrix-mediated mineralization on bone and dentin (Boskey, 1989a; Boskey, 1989b; Gorski, 1992; Linde and Lussi, 1989). One of the most extensively studied mineral inducers is phosvitin (PV) that is isolated from egg yolk. Phosvitin is a polyanionic protein, which contains predominantly phosphoserine residues that have been

demonstrated to interact with calcium phosphate mineralizing solution to induce crystal nucleation and growth *in vitro* (Linde *et al.*, 1989; Saito *et al.*, 1997). In contrast, bovine serum albumin (BSA) is a non-phosphorylated protein, but can interact with calcium ions via negatively charged residues (Wassell *et al.*, 1995). However, BSA functions to inhibit mineral formation *in vitro* (Linde *et al.*, 1989; Saito *et al.*, 1997). Thus, BSA is often used as a negative control for mineral induction experiments. Base on these studies, it is suggested that specific binding of calcium to phosphoproteins is an important event to understand the mechanism of crystal nucleation and biomineralization.

In this study, isothermal titration microcalorimetry (ITC) was used to determine the thermodynamic values of Ca^{+2} binding to LRAP and full-length recombinant human amelogenin (rH174). Calcium bindings to phosphorylated (phosvitin, PV) and non-phosphorylated (bovine serum albumin, BSA) proteins were used as controls for comparison. The raw heat of the reactions generated from Ca^{+2} /protein interactions is directly measured by ITC, and subsequently used to determine affinity constant (K_a) and enthalpy (ΔH) values. Moreover, entropy (ΔS) was also calculated by using the following equations: $\Delta G = -RT\ln K_a$, and $\Delta G = \Delta H - T\Delta S$; where ΔG is Gibb's free energy, $R = 8.314 \text{ J/K}^{-1}\text{mol}^{-1}$ (gas constant), and T is temperature in degree Kelvin.

MATERIALS AND METHODS

Expression, purification and characterization of recombinant human full-length amelogenin (rH174) and leucine-rich amelogenin peptide (LRAP)

Full-length amelogenin (H174) and LRAP cDNA's were amplified from a human ameloblast cDNA library, cloned into pRSET (Invitrogen, Carlsbad, CA, USA) and pGEX-4T-1 vectors (Amersham Biosciences, Piscataway, NJ, USA), respectively, and transformed into the *E. coli* BL21 (DE3) (Invitrogen). Transformed bacteria were cultured separately in 1 L of fresh LB medium containing 100 µg/mL ampicillin and incubated at 37 °C. At bacterial OD_{600nm} of 0.8, the cells were induced for protein expression using 0.8 mM of isopropyl-1-thio-β-D-galactopyranoside (IPTG) (Invitrogen) at 25 °C overnight. The bacteria were harvested by centrifugation.

For rH174 purification, bacterial pellets were resuspended in 6 M Guanidine, and lysed by sonication. The supernatant was collected by centrifugation and further diluted 10X with 5% formic acid. rH174 was purified using 2-time 15% (NH₄)₂SO₄ precipitation. The precipitated proteins were re-dissolved in 30% acetonitrile + 0.1% TFA, and applied to C4-bead (GraceVydac, Hesperia, CA, USA), and eluted in a column with 80% acetonitrile + 0.1% TFA.

To purify LRAP, bacterial pellets were resuspended in lysis buffer comprised of 1% Triton X-100 and 1.5% sarkosyl in 1X PBS solution supplemented with protease inhibitor cocktails, pH 7.4, and lysed by sonication. Cell debris was removed by centrifugation, and the soluble fraction of GST-LRAP supernatant was loaded on a glutathione-Sepharose beads (Amersham Biosciences) column that had been equilibrated with 1X PBS. The column was washed extensively with 1X PBS, and the fusion protein was then digested with 100 U thrombin (Amersham Biosciences) at 25 °C for 4 h. LRAP

was further purified by reverse-phase HPLC on a C18 column (Varian, Lake Forest, CA, USA), and eluted with a gradient of acetonitrile + 0.1% TFA.

Both purified rH174 and LRAP were confirmed by SDS-PAGE, Western blots and mass spectrometry analysis.

Isothermal Titration Calorimetry (ITC) analysis of calcium binding to phosphorylated (Phosvitin) and non-phosphorylated (Bovine Serum Albumin) proteins

Phosvitin (PV, Sigma, St. Louis, MO, USA) and bovine serum albumin (BSA, Sigma) were dialyzed overnight against HEPES [10 mM], pH 7.5 at 4 °C. The final protein concentrations were determined by Bio-Rad Protein Assay (Bio-Rad Lab, Hercules, CA, USA). PV and BSA binding to Ca²⁺ were measured by ITC (Microcal, Northampton, MA, USA). The instrument and its use have been described previously (Wiseman *et al.*, 1989). After optimization, CaCl₂ [15 mM], PV [0.011 mM] and BSA [0.057 mM] were prepared using the same dialyzed HEPES [10 mM], pH 7.5. All samples then were degassed for 5 min. at 25 °C using ThermoVac (MicroCal). CaCl₂ (10 µL/injection) was incrementally injected into 1.8 mL of PV or BSA solution at 25 °C using isothermal titration microcalorimetry (ITC) that has been pre-programmed and equipped with a computer-controlled injection (MicroCal). Reference data were also obtained by titrating CaCl₂ into dialyzed HEPES buffer [10 mM], pH 7.5. The heat of reactions generated per injection as Ca⁺² bound to the proteins was automatically recorded and presented as differential power (µcal/sec) vs. time (min). The areas under the peaks were integrated

and displayed as kcal/mol of injectant vs. molar ratio. After subtracting the reference data, the result was analyzed using Origin 7.0 Software provided with the ITC (OriginLab, Northampton, MA, USA) to determine K_a , ΔH , ΔS and N values. The detailed illustrations and principle of ITC operation and data analysis was provided in Fig. 1A and B.

ITC analysis of calcium binding to LRAP and rH174

Similarly, purified LRAP and rH174 were dialyzed against HEPES [10 mM], pH 7.5 at 4 °C overnight. After optimization, CaCl_2 [5-15 mM] was titrated (10 μL /injection) into 1.4 mL of LRAP or rH174 [0.064 – 0.12 mM] in dialyzed HEPES [10 mM], pH 7.5 at 25 °C. The heat generated per injection as calcium ions bound to amelogenins was recorded and displayed as differential power ($\mu\text{cal}/\text{sec}$) vs. time (min). The area under each injection peak was integrated and presented as kcal/mol of injectant vs. the molar ratio of $[\text{Ca}^{2+}]/[\text{protein}]$. Reference data was obtained by titrating the same concentration of CaCl_2 into dialyzed HEPES [10 mM] without protein at pH 7.5, and the value was then subtracted from the raw heat of the reaction to obtain the effective heat of binding. The resulting titration data were analyzed and fitted using Origin 7.0 for ITC software (OriginLab). The best-fitting of the experimental data was obtained using ‘the one-set of sites model’ of ITC to obtain the thermodynamic values such as N, K_a , ΔH , ΔS of calcium binding to LRAP or rH174. These thermodynamic values of calcium binding to LRAP and rH174 were compared, along with those values of calcium binding to phosvitin (PV) and bovine serum albumin (BSA).

RESULTS

Characterization of purified LRAP and rH174

LRAP and rH174 were expressed in *E. coli*. After purification, LRAP and rH174 analyzed by SDS-PAGE had apparent molecular weights of 6.8 kDa and 20 kDa, respectively (Fig. 2A). The identity of LRAP (Fig. 2B) and rH174 (Fig. 2C) were reconfirmed by Western blots. It should be noted that because thrombin was used to cleavage the GST-LRAP fusion protein, the resultant two additional residues, Gly and Ser, should be added to the N-terminal of the recombinant peptides. The mass spectrometric results showed that the measured average mass values of LRAP and rH174 were 6838.68 and 19806.10 Da (Fig. 2D), which matched the theoretical average mass of 6838.48 and 19804.89 Da for both proteins, respectively (Table 1).

Calcium binding to Phosvitin and Bovine Serum Albumin

The heat measured from the binding reactions of calcium to phosvitin (PV) and to bovine serum albumin (BSA) were positive values ($\mu\text{cal}/\text{sec}$), indicating that the reactions were endothermic (Fig. 3A and 4A). Reference baseline data were also obtained by injecting calcium ions into HEPES buffer only, showing very small amount of heat of dilution produced (Fig. 3B and 4B). The raw heat data obtained from Ca^{2+}/PV or $\text{Ca}^{2+}/\text{BSA}$ binding reactions and reference data were superimposed to show that Ca^{2+} and proteins interactions absorbed much greater amount of heat as compared to the amount heat generated from the reference (Fig. 3C and 4C). Integration of Ca^{2+}/PV and reference data (Fig. 3D) or integration of $\text{Ca}^{2+}/\text{BSA}$ and reference data (Fig. 4D) determined the area under peaks and represented as kcal/mole of injectant vs. molar ratio. After subtracting

the reference data, the net effective integrated data of Ca^{2+}/PV and $\text{Ca}^{2+}/\text{BSA}$ interactions were analyzed using Origin 7 Software, showing thermodynamic properties of calcium binding to these proteins (Fig. 3E and 4E). Calcium binding affinity to PV ($K_a = 1.414 \times 10^4 \text{ M}^{-1}$) was 8.5 times greater than binding to BSA ($K_a = 1.654 \times 10^3 \text{ M}^{-1}$). The values of ΔH and ΔS of calcium binding to PV ($\Delta H = 3.533 \text{ kcal/mol}$; $\Delta S = 30.84 \text{ cal/mol}^\circ\text{K}$) were also greater than those of BSA ($\Delta H = 1.203 \text{ kcal/mol}$; $\Delta S = 18.76 \text{ cal/mol}^\circ\text{K}$). Approximately 54 ($N = 53.6$) and 7 ($N = 6.76$) calcium-binding sites per one molecule of PV and one molecule of BSA, respectively. These results were summarized for comparison in Table 2.

Calcium binding to LRAP and rH174, and compare to calcium binding to PV and BSA

The raw heat of binding reactions associated with each injection of calcium ions into LRAP and rH174 solutions was recorded (data not shown). The area under each peak of the raw heat data was integrated and superimposed with the integrated data of the background reference (Figs. 5A, 6A). After subtracting the reference, the final data representing the effective binding isotherms of $\text{Ca}^{2+}/\text{LRAP}$ and $\text{Ca}^{2+}/\text{rH174}$ interactions were analyzed by determining the best least-squares fit of the data. This analysis of thermodynamic values showed that LRAP had ~ 6.4 times greater Ca^{2+} -binding affinity than rH174 (Figs. 5B, 6B). The affinity constants (K_a) of $\text{Ca}^{2+}/\text{LRAP}$ and $\text{Ca}^{2+}/\text{rH174}$ were found to be $8.551 \times 10^3 \text{ M}^{-1} \pm 365$ and $1.332 \times 10^3 \text{ M}^{-1} \pm 131$, respectively.

When these calcium-amelogenin binding properties were compared to those of phosvitin (PV) and bovine serum albumin (BSA), Ca²⁺/PV interaction had the highest affinity ($K_a = 1.414 \times 10^4 \text{ M}^{-1} \pm 242$), while Ca²⁺/BSA affinity ($K_a = 1.654 \times 10^3 \text{ M}^{-1} \pm 142$) was somewhat similar to that of Ca²⁺/rH174 ($K_a = 1.332 \times 10^3 \text{ M}^{-1} \pm 131$). The values of enthalpy and entropy changes of Ca²⁺/LRAP ($\Delta H = 0.1109 \pm 0.01 \text{ kcal/mol}$; $\Delta S = 18.35 \text{ cal/mol/ } ^\circ\text{K}$) and Ca²⁺/rH174 ($\Delta H = 0.462 \pm 0.1 \text{ kcal/mol}$; $\Delta S = 15.78 \text{ cal/mol/ } ^\circ\text{K}$) were relatively small, indicating ionic interactions. There were approximately 4 ($N = 4.024 \pm 0.86$) and 6 ($N = 6.449 \pm 1.26$) calcium ions bound to each molecule of LRAP and rH174, respectively (Fig 5B, 6B). However, these stoichiometry values did not appear to be significantly different. In contrast, Ca²⁺/PV interaction showed a significantly higher number of bound Ca²⁺ per molecule of PV ($N = 53.6 \pm 0.21$). All of these thermodynamic results were summarized in Table 2.

DISCUSSION

LRAP and full-length amelogenin are two of the most predominant proteins in the developing enamel extracellular matrix (Fincham *et al.*, 1999). These proteins are thought to play important roles in amelogenesis. A complete knock-out of amelogenin gene in mice results in amelogenesis imperfecta phenotype (Gibson *et al.*, 2001). Yet, LRAP knock-in has failed to rescue this amelogenin-null phenotype (Chen *et al.*, 2003). The exact function of LRAP in amelogenesis has remained largely obscured. LRAP and rH174 share many common characteristics. The 58-residue LRAP consists of the first 33 and the last 25 amino acids from the rH174. These two proteins are both bipolar with hydrophobic N-terminal and highly hydrophilic C-terminal regions. Moradian-Oldak *et*

al. reported that full-length mouse amelogenin forms nanospheres, with the carboxyl regions exposed on the surface of the nanospheres (Moradian-Oldak *et al.*, 2001). Since the 25-residue C-terminal domains of both rH174 and LRAP are identical, it is reasonable to expect that the C-terminus of LRAP should behave similarly. These hydrophilic charged C-terminal domains can also bind directly with hydroxyapatite surfaces (chapter 5), suggesting a function in enamel biomineralization (Moradian-Oldak *et al.*, 2002; Shaw *et al.*, 2004).

In this study, I showed that LRAP and rH174 interacted with calcium ions via ionic interactions, shown by their thermodynamic properties obtained in real-time measurements (Table 2). The low enthalpy (ΔH) and entropy (ΔS) values of calcium binding reactions to LRAP and rH174 suggested that these were ionic interactions. Ionic interactions were also observed for calcium binding PV and BSA. If there were any other types of interactions such as van der Waals forces, ΔH values would have been much greater (at least 5 to 10 times greater) than those obtained in Table 2 (Meador *et al.*, 1992). It is possible that these ionic interactions can occur between the calcium ions and the charged acidic groups of amino acids (i.e. Asp, Glu, phosphorylated Ser). In my experiments, the stoichiometry (N) values showed that the number of calcium ions binding to each molecule LRAP or rH174 was not significantly different, in the range of 4 to 6 calcium ions for each protein molecule.

This result suggests that binding may occur on either the C-terminal or the N-terminal regions. Since the C-terminus is much more hydrophilic due to the presence of several

acidic amino acids (i.e. Asp, Glu) and the calcium binding is an ionic interaction, it is predicted that the C-terminal regions of LRAP and rH174 are the most likely calcium-binding motif. Preliminary ITC data obtained from injecting calcium ions into solution of synthetic C-terminal peptide (the last 11 C-terminal residues of both LRAP and rH174, STDKTKREEVD) showed that the each molecule of C-terminal peptide contains approximately 1.5 calcium-binding sites (data not shown).

Although the affinity constants (K_a) for both Ca^{2+} /LRAP ($K_a = 8.551 \times 10^3 \text{ M}^{-1}$) and Ca^{2+} /rH174 ($K_a = 1.332 \times 10^3 \text{ M}^{-1}$) interactions were relatively weaker than that of Ca^{2+} /PV ($K_a = 1.414 \times 10^4 \text{ M}^{-1}$), LRAP has ~ 6.4 times greater Ca^{2+} -binding affinity than that of rH174. The structural basis for the significant difference in Ca^{2+} affinity for LRAP and rH174 is not yet understood. However, the fact that Ca^{2+} has an affinity for both LRAP and rH174 may suggest that Ca^{2+} potentially can activate specific functions in these proteins by inducing structural changes, which may also be responsible for the magnitude of K_a values. This type of conformational change and functional activation in the presence of calcium occurs in the protein calmodulin (Finn *et al.*, 1995). Similar to LRAP and rH174, calmodulin, has 4 Ca^{2+} binding sites, and a Ca^{2+} affinity constant of $2.5 \times 10^4 \text{ M}^{-1}$ to $3.0 \times 10^4 \text{ M}^{-1}$ (Wintrod and Privalov, 1997). Whether the presence of calcium would induce structural and conformational changes of LRAP is a subject of investigation in the next chapter.

The ITC data showed that Ca^{2+} had the greatest affinity for PV ($K_a = 1.414 \times 10^4 \text{ M}^{-1}$) as compared to LRAP ($K_a = 8.551 \times 10^3 \text{ M}^{-1}$), rH174 ($K_a = 1.332 \times 10^3 \text{ M}^{-1}$) and BSA ($K_a =$

$1.654 \times 10^3 \text{ M}^{-1}$). In addition, a significantly greater number of Ca^{2+} bound per molecule of PV ($N = 53.6 \pm 0.21$) were detected as compared to LRAP, rH174 or BSA due to ionic interactions between calcium ions and several negatively-charged phosphorylated Ser residues on the PV protein (Saito *et al.*, 1997). PV is a highly phosphorylated protein isolated from egg yolk, and is a well-known mineral inducer *in vitro* (Saito *et al.*, 1997). An effective mineral inducer like PV should bind Ca^{2+} with high affinity constant and possess a great number of Ca^{2+} binding sites. Since Ca^{2+} binding properties of LRAP, rH174, BSA and even calmodulin apparently do not satisfy these two specific criteria, they are predicted not to be good and effective mineral inducers or nucleators.

It is interesting to note that though these results support the fact that rH174 and LRAP are not effective mineral nucleators, when a nucleating surface such as fluoroapatite is present, rH174 but not LRAP can promote crystal growth (Habelitz *et al.*, 2004; Habelitz *et al.*, 2006)(see chapter 5). This suggests that the central hydrophobic core of rH174, which is absent from LRAP, directs crystal growth once nucleation is initiated. It is possible that the C-terminus of rH174 may serve as an anchor to attach this mineral growth promoting protein to the growing crystal surface.

Current literature supports the notion that LRAP functions in cell signaling (Tompkins and Veis, 2002; Veis *et al.*, 2000; Veis, 2003). However, there has been no indication that full-length amelogenins function as cell-signaling molecules. Thus, LRAP and rH174 may have different biological functions. Understanding the structures of LRAP and rH174 may explain some of the functional differences between these two proteins.

REFERENCES

- Boskey AL (1989a). Noncollagenous matrix proteins and their role in mineralization. *Bone Miner* 6(2):111-23.
- Boskey AL (1989b). What's in a name? The function of the mineralized tissue matrix proteins. *J Dent Res* 68(2):159.
- Chen E, Yuan ZA, Wright JT, Hong SP, Li Y, Collier PM, Hall B, D'Angelo M, Decker S, Piddington R, Abrams WR, Kulkarni AB, Gibson CW (2003). The small bovine amelogenin LRAP fails to rescue the amelogenin null phenotype. *Calcif Tissue Int* 73(5):487-95.
- Du C, Falini G, Fermani S, Abbott C, Moradian-Oldak J (2005). Supramolecular assembly of amelogenin nanospheres into birefringent microribbons. *Science* 307(5714):1450-4.
- Fincham AG, Moradian-Oldak J, Diekwisch TG, Lyaruu DM, Wright JT, Bringas P, Jr., Slavkin HC (1995). Evidence for amelogenin "nanospheres" as functional components of secretory-stage enamel matrix. *J Struct Biol* 115(1):50-9.
- Fincham AG, Moradian-Oldak J, Simmer JP (1999). The structural biology of the developing dental enamel matrix. *J Struct Biol* 126(3):270-99.
- Finn BE, Evenas J, Drakenberg T, Waltho JP, Thulin E, Forsen S (1995). Calcium-induced structural changes and domain autonomy in calmodulin. *Nat Struct Biol* 2(9):777-83.
- Gibson CW, Golub E, Ding WD, Shimokawa H, Young M, Termine J, Rosenbloom J (1991). Identification of the leucine-rich amelogenin peptide (LRAP) as the translation product of an alternatively spliced transcript. *Biochem Biophys Res Commun* 174(3):1306-12.
- Gibson CW, Yuan ZA, Hall B, Longenecker G, Chen E, Thyagarajan T, Sreenath T, Wright JT, Decker S, Piddington R, Harrison G, Kulkarni AB (2001). Amelogenin-deficient mice display an amelogenesis imperfecta phenotype. *J Biol Chem* 276(34):31871-5.
- Gorski JP (1992). Acidic phosphoproteins from bone matrix: a structural rationalization of their role in biomineralization. *Calcif Tissue Int* 50(5):391-6.
- Habelitz S, Kullar A, Marshall SJ, DenBesten PK, Balooch M, Marshall GW, Li W (2004). Amelogenin-guided crystal growth on fluoroapatite glass-ceramics. *J Dent Res* 83(9):698-702.

Habelitz S, Denbesten PK, Marshall SJ, Marshall GW, Li W (2006). Self-assembly and effect on crystal growth of the leucine-rich amelogenin peptide. *Eur J Oral Sci* 114 Suppl 1(315-9).

Linde A, Lussi A (1989). Mineral induction by polyanionic dentin and bone proteins at physiological ionic conditions. *Connect Tissue Res* 21(1-4):197-202; discussion 203.

Linde A, Lussi A, Crenshaw MA (1989). Mineral induction by immobilized polyanionic proteins. *Calcif Tissue Int* 44(4):286-95.

Meador WE, Means AR, Quioco FA (1992). Target enzyme recognition by calmodulin: 2.4 A structure of a calmodulin-peptide complex. *Science* 257(5074):1251-5.

Moradian-Oldak J, Jimenez I, Maltby D, Fincham AG (2001). Controlled proteolysis of amelogenins reveals exposure of both carboxy- and amino-terminal regions. *Biopolymers* 58(7):606-16.

Moradian-Oldak J, Bouropoulos N, Wang L, Gharakhanian N (2002). Analysis of self-assembly and apatite binding properties of amelogenin proteins lacking the hydrophilic C-terminal. *Matrix Biol* 21(2):197-205.

Saito T, Arsenault AL, Yamauchi M, Kuboki Y, Crenshaw MA (1997). Mineral induction by immobilized phosphoproteins. *Bone* 21(4):305-11.

Shaw WJ, Campbell AA, Paine ML, Snead ML (2004). The COOH terminus of the amelogenin, LRAP, is oriented next to the hydroxyapatite surface. *J Biol Chem* 279(39):40263-6.

Tompkins K, Veis A (2002). Polypeptides translated from alternatively spliced transcripts of the amelogenin gene, devoid of the exon 6a, b, c region, have specific effects on tooth germ development in culture. *Connect Tissue Res* 43(2-3):224-31.

Veis A, Tompkins K, Alvares K, Wei K, Wang L, Wang XS, Brownell AG, Jengh SM, Healy KE (2000). Specific amelogenin gene splice products have signaling effects on cells in culture and in implants in vivo. *J Biol Chem* 275(52):41263-72.

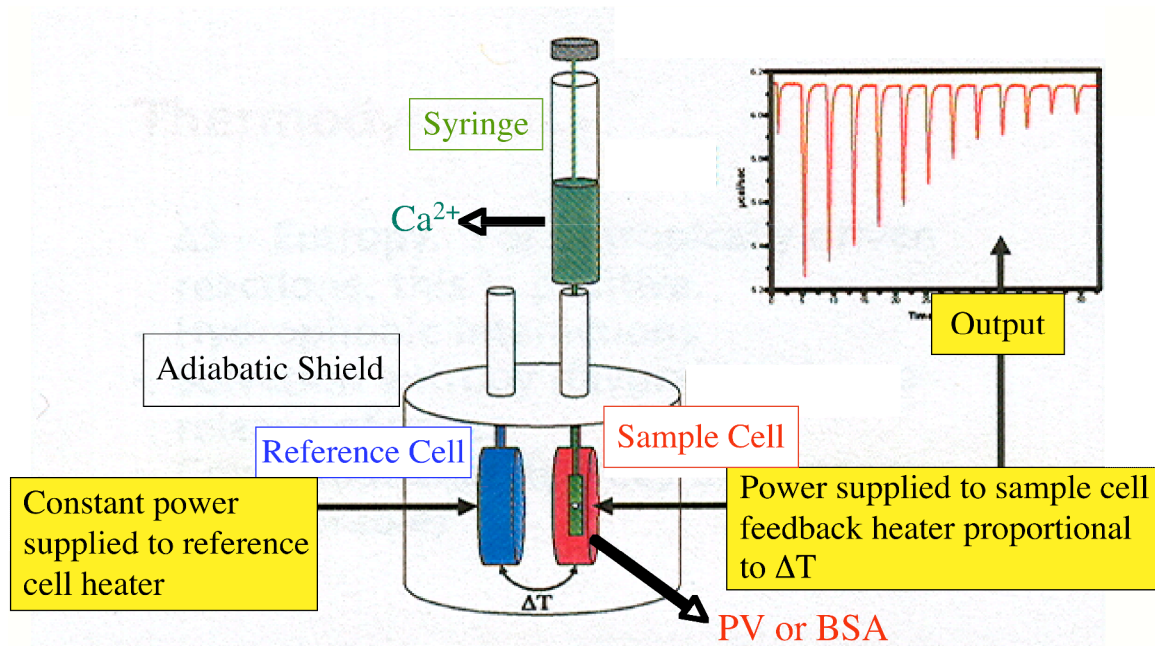
Veis A (2003). Amelogenin gene splice products: potential signaling molecules. *Cell Mol Life Sci* 60(1):38-55.

Wassell DT, Hall RC, Embery G (1995). Adsorption of bovine serum albumin onto hydroxyapatite. *Biomaterials* 16(9):697-702.

Wintrode PL, Privalov PL (1997). Energetics of target peptide recognition by calmodulin: a calorimetric study. *J Mol Biol* 266(5):1050-62.

Wiseman T, Williston S, Brandts JF, Lin LN (1989). Rapid measurement of binding constants and heats of binding using a new titration calorimeter. *Anal Biochem* 179(1):131-7.

A.



B.

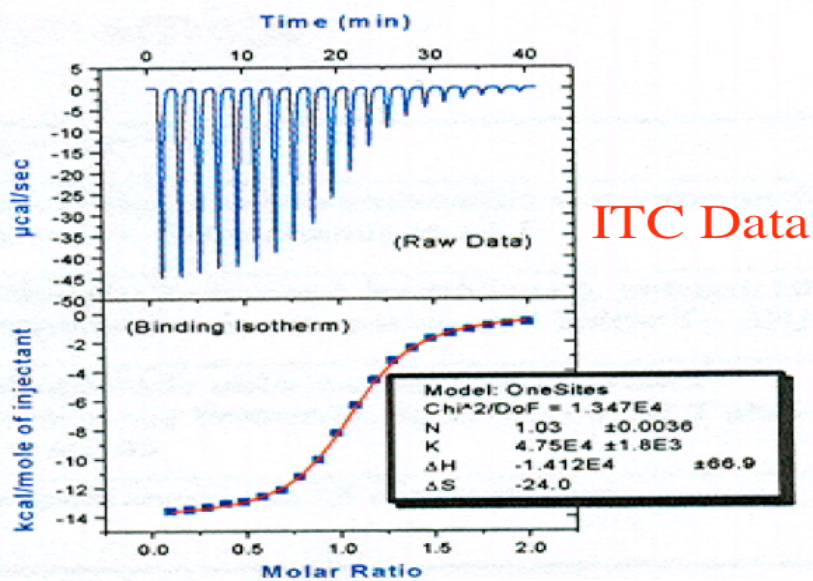


Figure 1.
Principle of isothermal titration microcalorimetry (ITC) operation and data analysis.

A) ITC is operated based on a cell feedback network, which is designed to measure the differential heat effects between a sample and reference cell. This is known as

differential power compensation. The temperature difference between these two cells is constantly monitored and a constant power is applied to the reference cell, which activates the feedback network to apply a variable power to the sample cell in order to maintain very small temperature difference between the cells. This feedback power is the baseline level in the absence of any reaction. However, when calcium ions were placed in the syringe, which incrementally injected into a sample cell containing protein solutions (phosvitin or BSA), a binding reaction occurred between calcium ions and the protein. This reaction is accompanied with a temperature change due to heat released or absorbed through an exothermic or endothermic reaction in the sample cell, which resulted in a temperature difference (ΔT) between the sample and reference cell. This is detected by the calorimeter, and the power applied by cell feedback is adjusted. Exothermic reactions will trigger a temporary decrease in the feedback power, while the endothermic reactions will produce an increased feedback. B) The heat evolved or absorbed by the reaction is then obtained by integration of these deflections from baselines with respect to time. The calculation is done by Origin 7 analysis software to automatically determine K_a , ΔH , ΔS and N values in one single experiment.

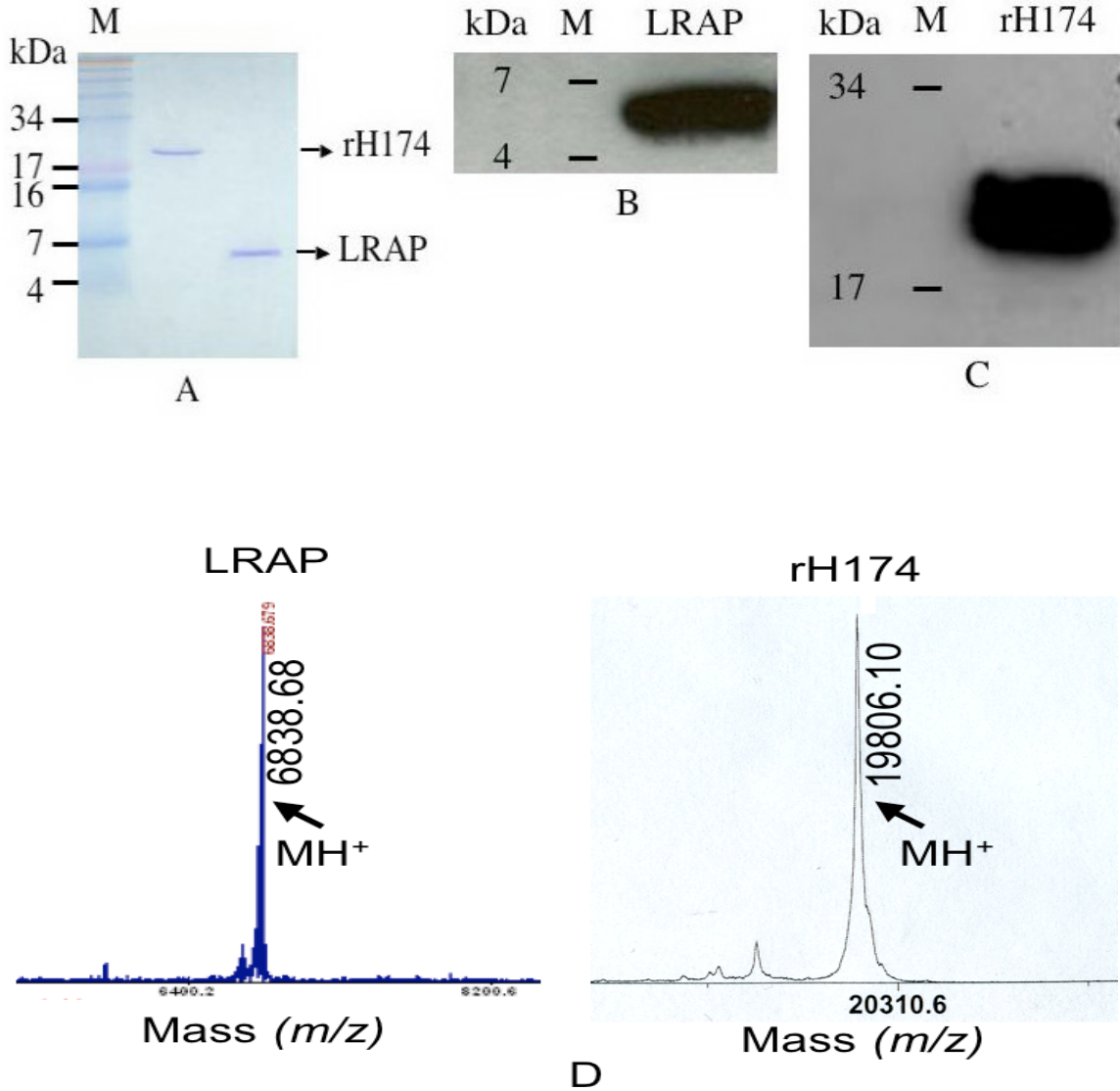


Figure 2.

Characterization of purified recombinant human full-length amelogenin (rH174) and leucine-rich amelogenin peptide (LRAP).

A) SDS-PAGE of LRAP and rH174. B) Western blot to confirm the identity of purified LRAP. C) Western blot to confirm the identity of purified rH174. D) Mass spectrometric analysis of LRAP and rH174. M, SeeBlue Plus2 marker standard (Invitrogen).

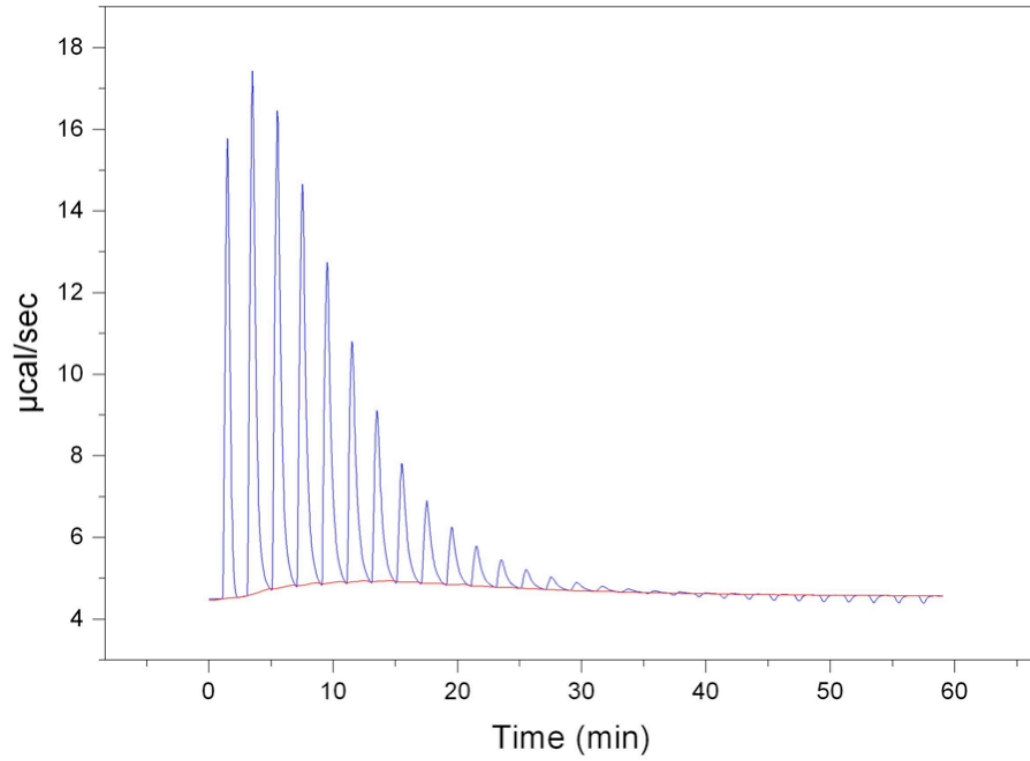
Amelogenin	Measured <i>m/z</i> (Da)	Predicted <i>m/z</i> (Da)
LRAP	6838.68	6838.48
rH174	19806.10	19804.89

Table 1.

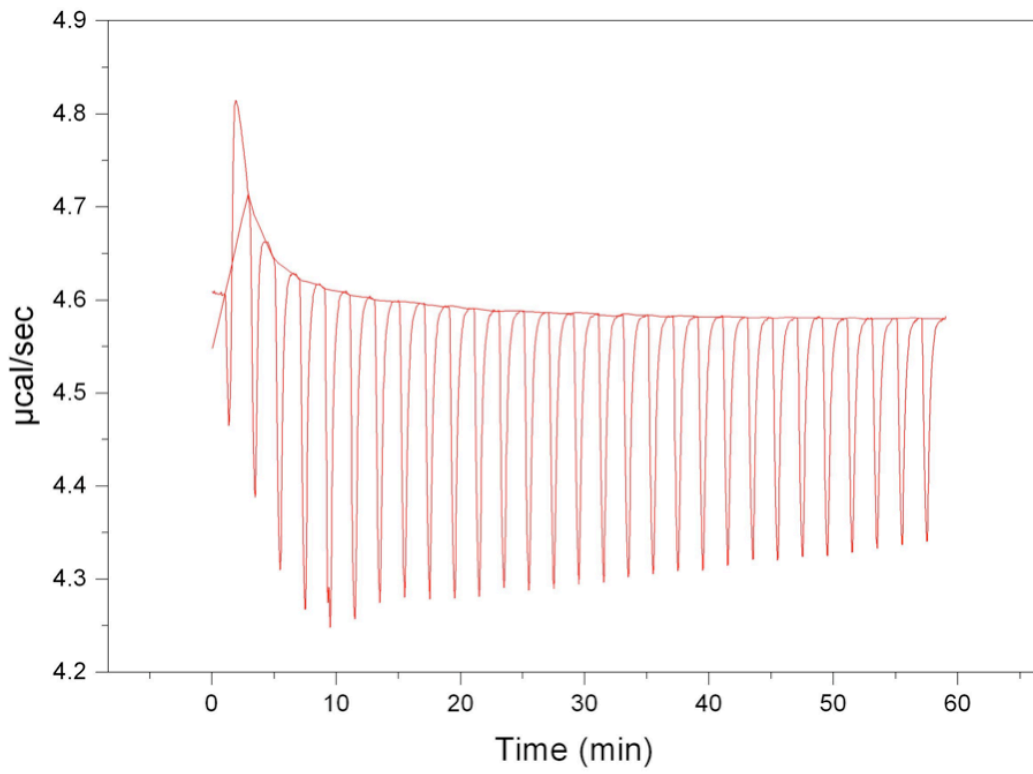
Mass spectrometric analysis of purified recombinant human LRAP and full-length amelogenin (rH174).

The measured mass values of LRAP and rH174 matched their respective predicted theoretical values.

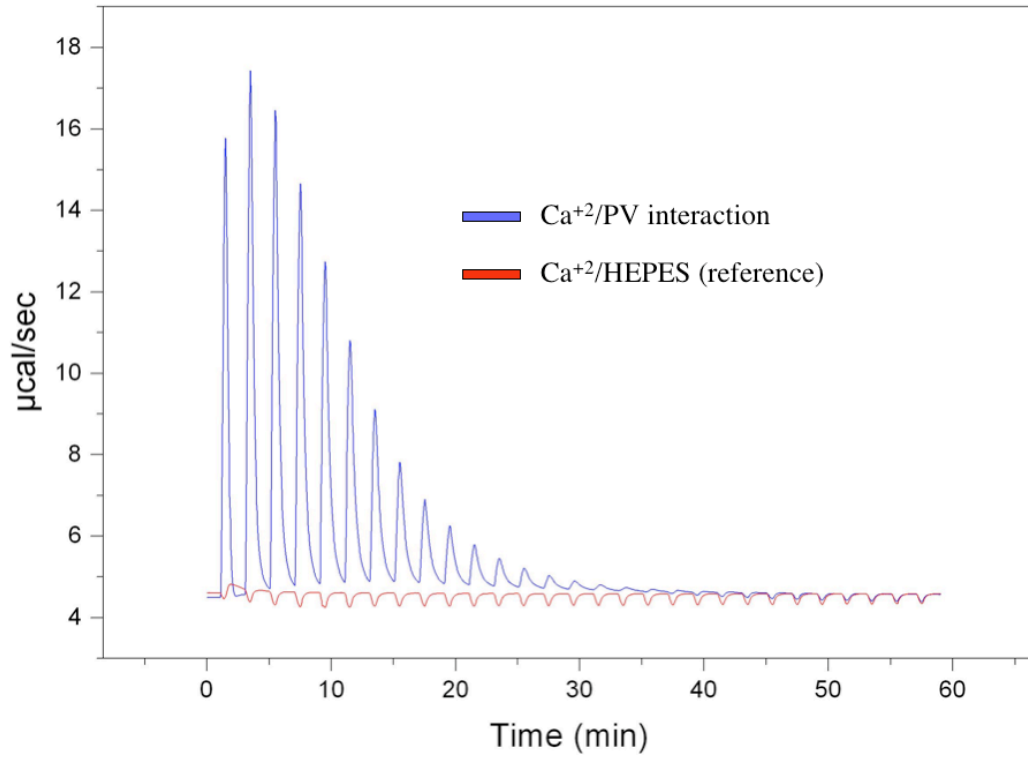
A.



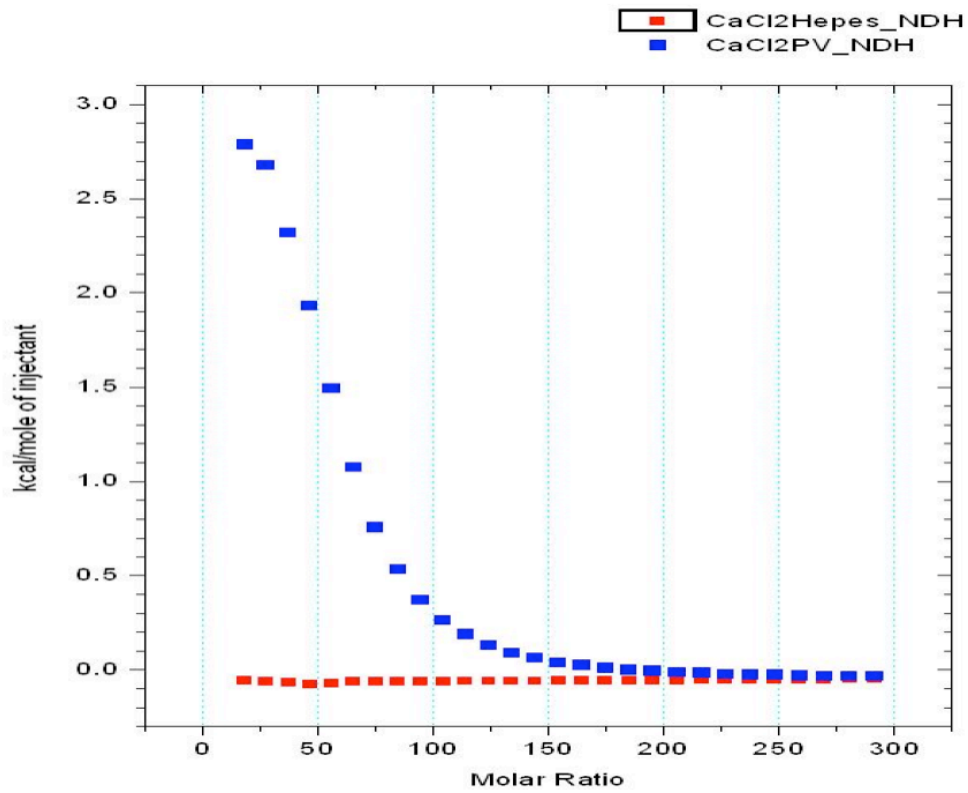
B.



C.



D.



E.

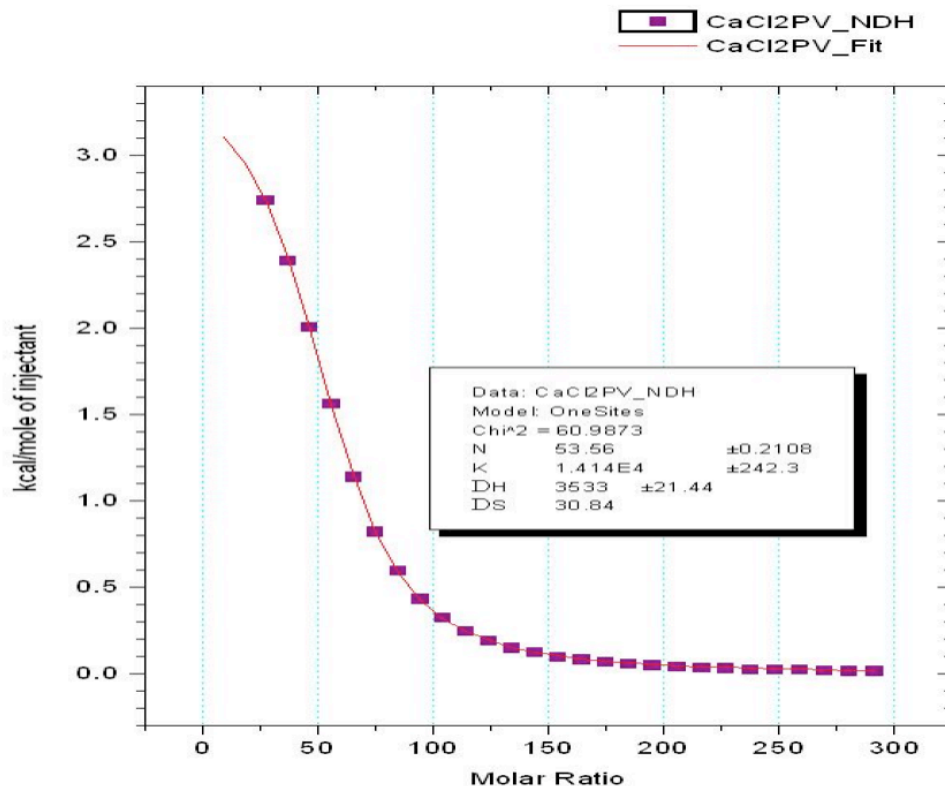
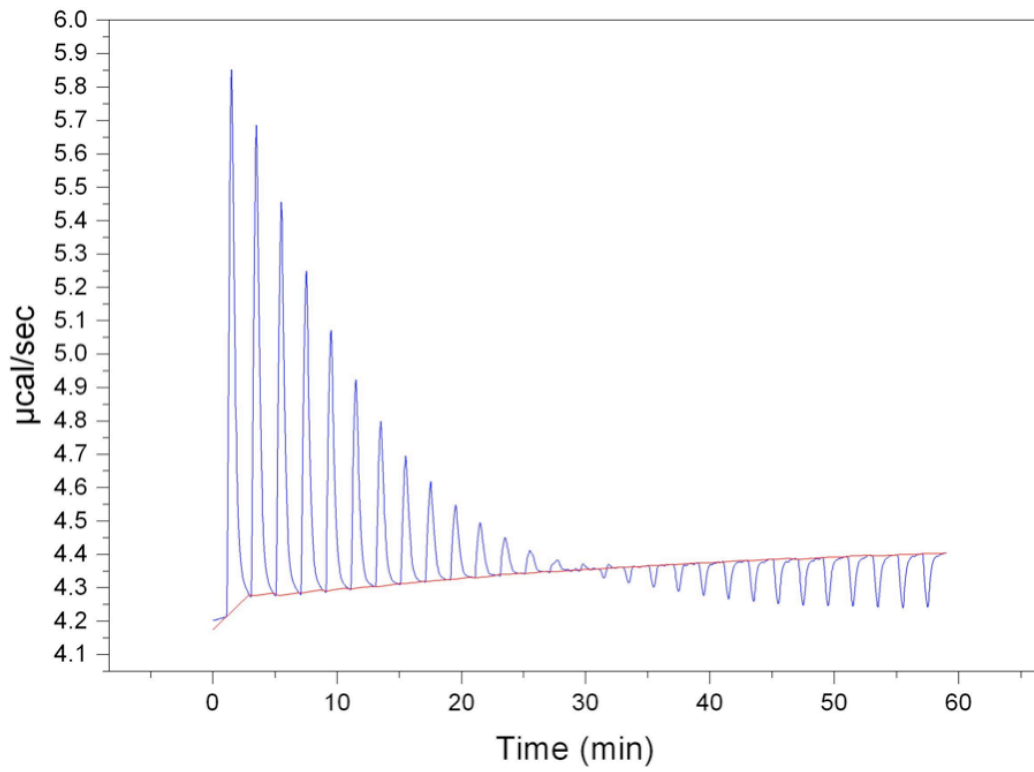


Figure 3.

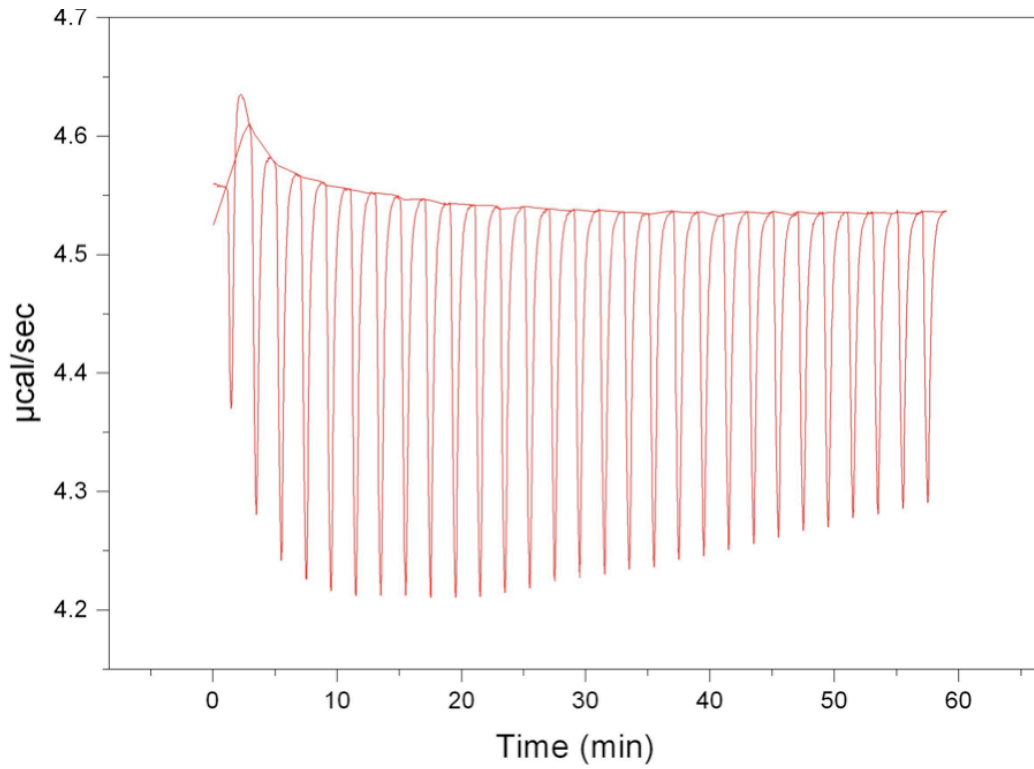
Microcalorimetric analysis of calcium binding to phosvitin (PV).

A) CaCl_2 (15 mM) titrated at $10 \mu\text{L}/\text{injection}$ into 1.8 mL of PV (0.0114 mM) in HEPES (10 mM), pH 7.5 indicates that Ca^{2+}/PV interaction is an endothermic reaction. B) A reference base line is obtained by injecting CaCl_2 (15 mM) into 1.8 mL of HEPES (10 mM), pH 7.5 shows small amount of heat of dilution generated. C) Superimposition of Ca^{2+}/PV reaction and reference raw heat data shows that Ca^{2+}/PV binding has much greater amount of heat absorbed as compared to the insignificant heat released when Ca^{2+} titrated into HEPES buffer only. D) Integration of Ca^{2+}/PV and reference raw data to determine the area under peaks represents as kcal/mole of injectant vs. molar ratio. E) After subtracting the reference data, the integrated data of Ca^{2+}/PV interaction is analyzed using Origin 7 Software, showing thermodynamic properties of calcium binding PV.

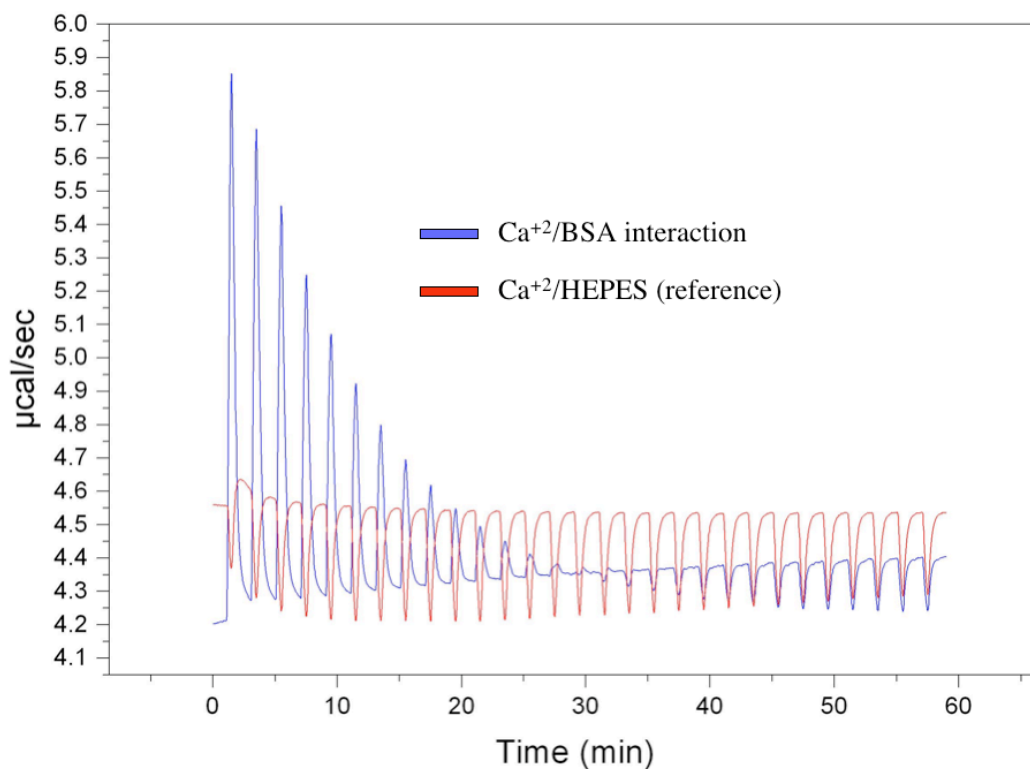
A.



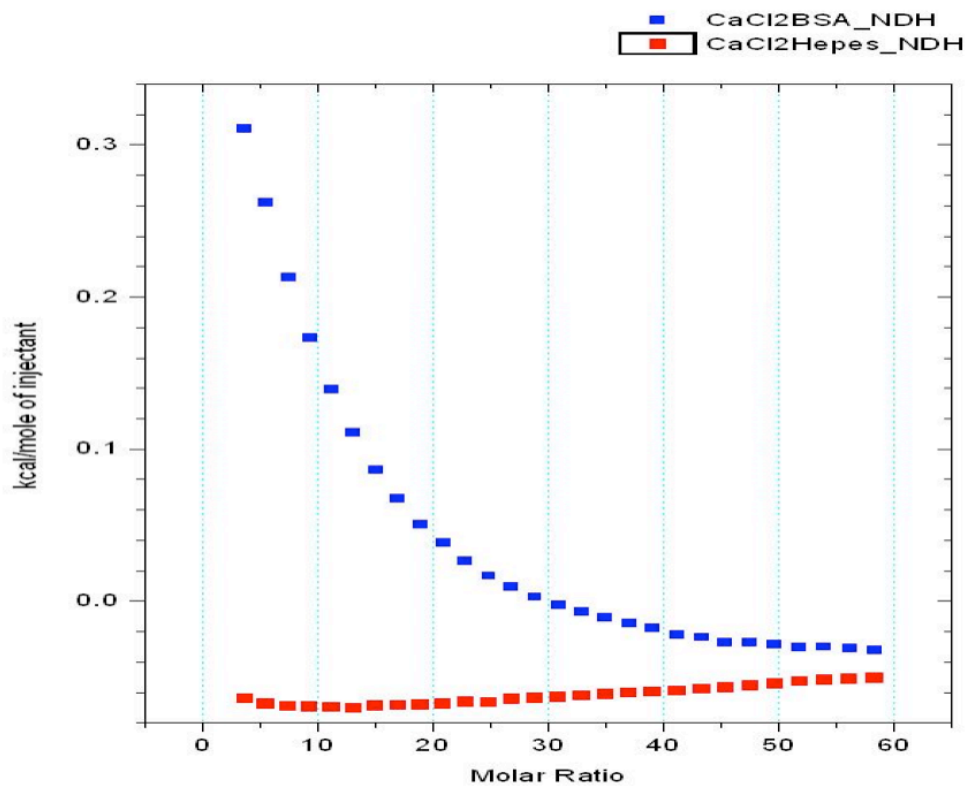
B.



C.



D.



E.

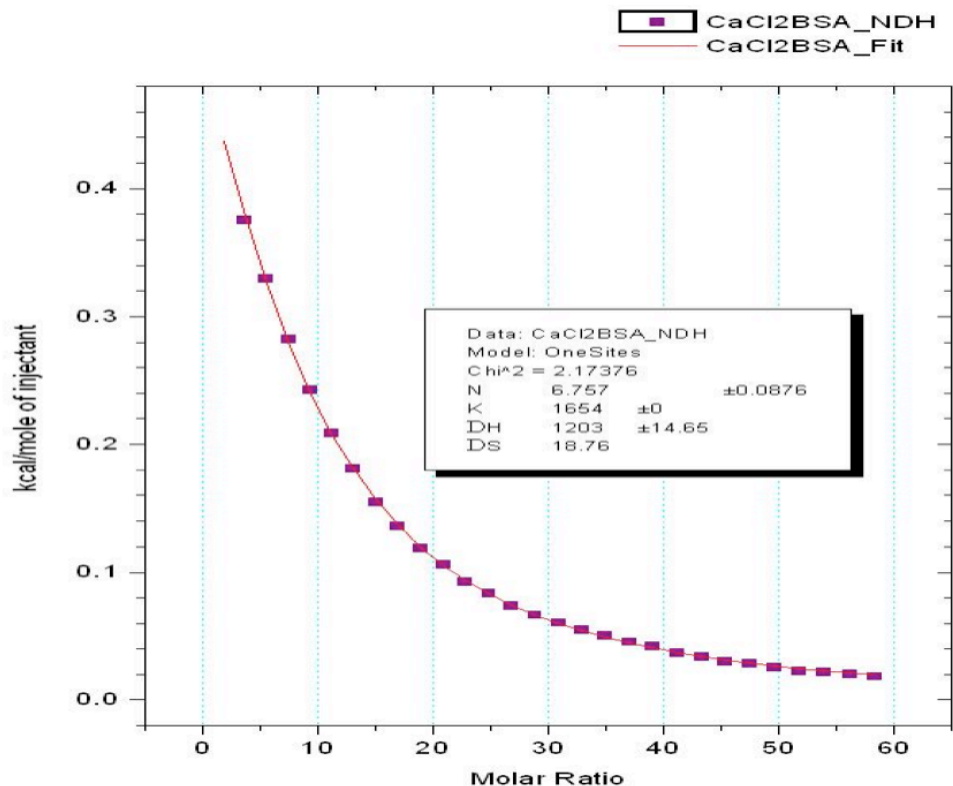


Figure 4.

Microcalorimetric analysis of calcium binding to bovine serum albumin (BSA).

A) CaCl_2 (15 mM) titrated at $10 \mu\text{L}$ /injection into 1.8 mL of BSA (0.057 mM) in HEPES (10 mM), pH 7.5 indicates that Ca^{2+} /BSA interaction is an endothermic reaction. B) A reference base line is obtained by injecting CaCl_2 (15 mM) into 1.8 mL of HEPES (10 mM), pH 7.5 shows small amount of heat of dilution generated. C) Superimposition of Ca^{2+} /BSA interaction and reference raw heat data shows that Ca^{2+} /BSA binding absorbs greater amount of heat as compared to the smaller amount of heat released when Ca^{2+} titrated into HEPES buffer only. D) Integration of Ca^{2+} /BSA and reference raw heat data to determine the area under peaks represents as kcal/mole of injectant vs. molar ratio. E) After subtracting the reference data, the integrated data of Ca^{2+} /BSA interaction is analyzed using Origin 7 Software, showing thermodynamic properties of calcium binding BSA.

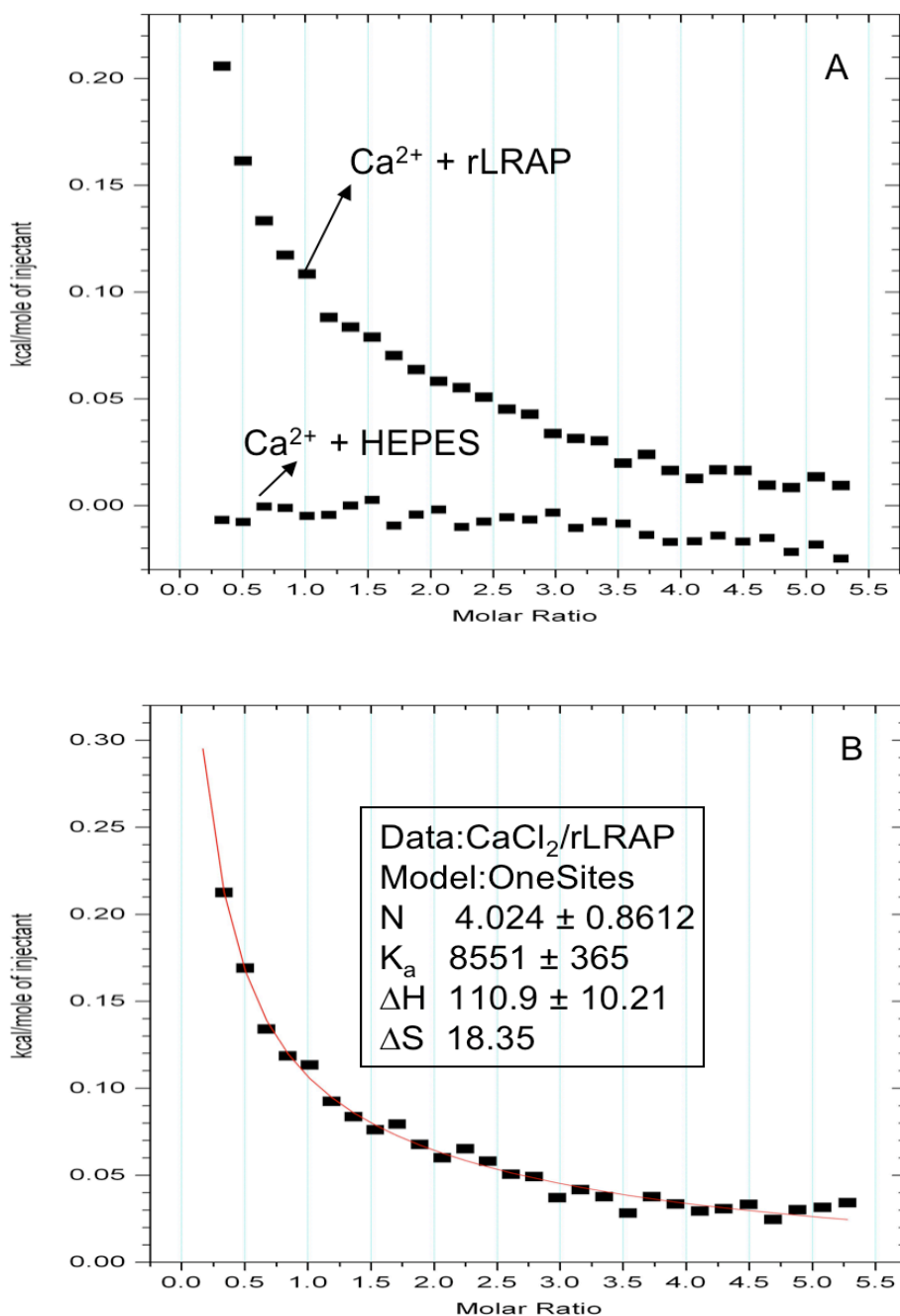


Figure 5.

Binding of Ca²⁺ to recombinant leucine-rich amelogenin peptide (rLRAP) by ITC.

A) The graph showed the integrated data of heat change (raw heat data not shown) associated with Ca²⁺ titrated into rLRAP, and the control reference data of Ca²⁺ titrated into buffer only. Calcium chloride [5 mM] was titrated (10 μL/injection) into 1.4 mL of rLRAP [0.12 mM] in HEPES [10 mM], pH 7.5. B) The integrated data of heat change of Ca²⁺/rLRAP after subtracting the reference was analyzed by determining the best least-squares fit of the data. The thermodynamic properties of Ca²⁺ binding to rLRAP were shown in the box insert.

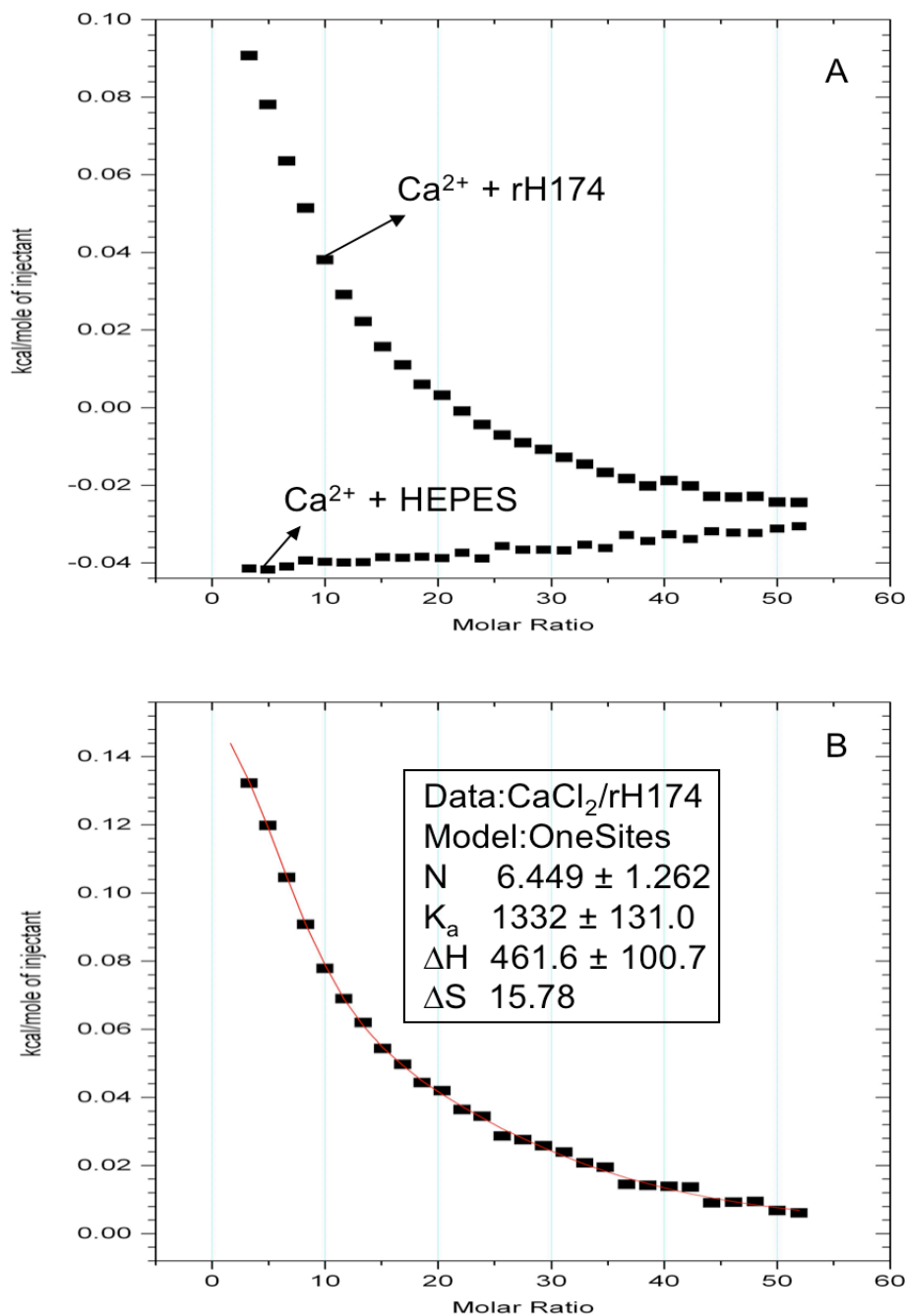


Figure 6.
Binding of Ca²⁺ to recombinant human full-length amelogenin (rH174) by ITC.
 A) The graph showed the integrated data of heat change (raw heat data not shown) associated with Ca²⁺ titrated into rH174, and the control reference data of Ca²⁺ titrated into buffer only. Calcium chloride [15 mM] was titrated (10 μL/injection) into 1.4 mL of rH174 [0.064 mM] in HEPES [10 mM], pH 7.5. B) The integrated data of heat change of Ca²⁺/rH174 after subtracting the reference was analyzed by determining the best least-squares fit of the data. The thermodynamic properties of Ca²⁺ binding to rH174 were shown in the box insert.

Thermodynamic Properties	Ca ²⁺ / PV	Ca ²⁺ / rLRAP	Ca ²⁺ / rH174	Ca ²⁺ / BSA
K_a (M ⁻¹)	1.414 x 10 ⁴ ± 242	8.551 x 10 ³ ± 365	1.332 x 10 ³ ± 131	1.654 x 10 ³ ± 142
ΔH (kcal/mol)	3.533 ± 0.021	0.1109 ± 0.01	0.462 ± 0.1	1.203 ± 0.014
ΔS (cal/mol/°K)	30.84	18.35	15.78	18.76
N (sites/molecule)	53.6 ± 0.21	4.024 ± 0.86	6.449 ± 1.26	6.7 ± 0.09

Table 2.

Comparison of Ca²⁺/LRAP and Ca²⁺/rH174 interactions.

The results showed that Ca²⁺ binding to LRAP and rH174 via ionic interactions indicated by relatively small values of enthalpy (ΔH) and entropy (ΔS) changes. The affinity constant (K_a) of Ca²⁺/LRAP is ~ 6.4 times greater than that of Ca²⁺/rH174. The stoichiometry values (N) of calcium binding were not significantly difference between LRAP and rH174. Thermodynamic values of calcium binding to bovine serum albumin (BSA) and phosvitin (PV) were also provided for comparison. Interestingly, calcium binding to PV resulted in highest affinity, and that PV contained the greatest number of calcium binding sites (N), which contributed to the unique property of PV as a highly effective mineral inducer *in vitro*.

Chapter 7. Structural Determination of Leucine-rich Amelogenin Peptide Using Nuclear Magnetic Resonance (NMR) and Circular Dichroism (CD)

INTRODUCTION

Amelogenins are the most predominant components, greater than 90% of the total enamel extracellular matrix (Fincham *et al.*, 1999). Amelogenins have the ability to undergo self-assembly into nanospheres, nanochains, and micro-ribbons, suggesting their potential roles as scaffolding proteins to direct enamel crystal growth (Du *et al.*, 2005). Both *in vivo* (Gibson *et al.*, 2001) and *in vitro* studies (Habelitz *et al.*, 2004; Habelitz *et al.*, 2005) show that amelogenins play a critical role in enamel formation.

The primary structures of several mammalian (i.e. murine, bovine, porcine and human) full-length amelogenins have been determined, and the core domain of the protein is well conserved across species. The bovine full-length amelogenin has been known to contain a 27-mer tandem repeats of (Gln-Pro-X)₉, where X could be His, Leu or Met. This unique sequence of Gln₁₁₂-Leu₁₃₈ results in a secondary structure of repetitive β -turns and β -spiral, whose function has been suggested to potentially facilitate the passage of calcium ions to directly regulate the enamel mineralization (Renugopalakrishnan *et al.*, 1989; Renugopalakrishnan, 2002).

Within the enamel matrix, there are several amelogenin isoforms (5-28 kDa) due to proteolysis and alternative splicing (Fincham *et al.*, 1999). Two 5-kDa amelogenins are present in the enamel matrix. One of these, the N-terminal proteolytic product of full-length amelogenins, is the tyrosine-rich amelogenin peptide (TRAP), whose structure

contains a β -sheet with a possible role in mineral formation (Goto *et al.*, 1993). The second 5-kDa amelogenin is the 58-residue alternatively spliced amelogenin peptide, called the leucine-rich amelogenin peptide (LRAP) (Gibson *et al.*, 1991). LRAP is encoded by exons 2, 3, 5, 6d and 7, corresponding to the first 33 and the last 25 amino acids of the full-length amelogenin (Fig. 1). LRAP and full-length amelogenin are both bipolar with hydrophobic N-terminal and highly hydrophilic C-terminal regions.

Despite domain similarity at the N- and C-termini, several reports show different functions between LRAP and full-length amelogenins, suggesting that there may be structural differences between these proteins. Studies of full-length amelogenin show that it regulates enamel mineralization (Beniash *et al.*, 2005; Du *et al.*, 2005; Habelitz *et al.*, 2004), while LRAP has been reported to function as a cell signaling molecule (Tompkins *et al.*, 2005; Veis *et al.*, 2000; Veis, 2003). Although full-length amelogenin contains repetitive β -turns and β -spiral structure, LRAP secondary structure is currently unknown. In chapter 6, I reported that both LRAP and full-length amelogenin bind calcium ions. The binding of calcium to LRAP may induce specific conformational changes, resulting in specific protein structure that gives rise to its biological activity.

The purpose of this study was to elucidate the secondary structure of LRAP *in vitro* by using ^1H - ^{15}N -nuclear magnetic resonance (NMR) and circular dichroism (CD) spectrometry in the absence and presence of calcium ions, pH 7.5 and 4.0 at 25 °C. Structural differences between LRAP and full-length amelogenin may provide some new insights into functional differences between these two proteins in enamel formation.

MATERIALS AND METHODS

Expression and purification of unlabeled and ¹⁵N-labeled recombinant LRAP

LRAP cDNA was amplified from a human ameloblast cDNA library, cloned pGEX-4T-1 vectors (Amersham Biosciences, Piscataway, NJ, USA) and transformed into the *E. coli* BL21 (DE3) (Invitrogen). To express the unlabeled or ¹⁵N-labeled recombinant LRAP, the transformed bacteria were cultured in LB (1 L) + 100 µg/mL ampicillin, or M9 medium (1 L) supplemented with 100 µg/mL ampicillin, ¹⁵NH₄Cl (1g/L) (Isotec, Miamisburg, OH, USA) and Isogrow Powder-Growth Medium (1g/L) (Isotec). At optical density OD_{600nm} of 0.8, the cells were induced for 4 h, 225 r.p.m., at 37 °C to express glutathione S-transferase (GST)-LRAP fusion protein using 0.8 mM of IPTG (Invitrogen). The cells were harvested by centrifugation, resuspended in lysis buffer comprised of 1% Triton X-100 and 1.5% sarkosyl in 1X PBS solution supplemented with protease inhibitor cocktails, pH 7.4, and lysed by sonication. Cell debris was removed by centrifugation, and the soluble fraction of GST-LRAP supernatant was loaded on a glutathione-Sepharose beads (Amersham Biosciences) column that had been equilibrated with 1X PBS. The column was washed extensively with 1X PBS, and the fusion protein was then digested with 100 U thrombin (Amersham Biosciences) at 25 °C for 4 h. LRAP's were further purified by reverse-phase HPLC on a C18 column (Varian, Lake Forest, CA, USA), and eluted with a gradient of acetonitrile + 0.1% TFA. The purified LRAP and ¹⁵N-LRAP were analyzed by mass spectrometry analysis.

NMR spectroscopy

A sample of 250 μL ^{15}N -LRAP [40 μM] was prepared in D_4 -acetate solution [10 mM], pH 4.0. At pH 7.5, ^{15}N -LRAP [40 μM] was partially precipitated in pH 7.5, so further measurements by NMR at neutral pH were not possible. ^{15}N -heteronuclear single quantum coherence (^{15}N -HSQC) spectrum of ^{15}N -LRAP was recorded on a Bruker Avance 800-MHz. Spectrometer (Bruker BioSpin, Fremont, CA, USA) at 25 °C.

Circular Dichroism (CD) spectroscopy

Samples of 500 μL of unlabeled LRAP [28 μM] were prepared in HEPES [10 mM], pH 7.5 and in acetate [10 mM], pH 4.0. For CD studies, a much lower concentration [28 μM] of LRAP was required. At this low concentration, LRAP was soluble at both pH 7.5 and 4.0. CD spectroscopy was measured at 25 °C on a Jasco spectropolarimeter (Model J-715; Jasco, Easton, MD, USA) using a quartz cell with 1-mm path length. In the far-UV range of 250 nm – 190 nm, data points were recorded with a separation of 1 nm. Each data point was an average of 4 readings at every wavelength position. CD experiments were conducted using LRAP in the absence and presence of calcium ions (by adding 4 μL of 50 mM of CaCl_2). CD data were displayed as observed ellipticity θ (mdeg) vs. wavelength (nm).

RESULTS

Characterization of purified ^{15}N -labeled and unlabeled recombinant LRAP

After purification, recombinant ^{15}N -LRAP and unlabeled LRAP were analyzed by mass spectrometry analysis. Both labeled and unlabeled LRAP's were recombinantly expressed as GST-LRAP fusion proteins. When these fusion proteins were cleaved by

thrombin, two additional residues, Gly and Ser, were added to the N-terminal of both ^{15}N -LRAP and LRAP (total 60 residues). The mass spectrometry measurement showed that the measured mass values of LRAP was 6838.68 Da, which matched the predicted mass of 6838.48 (Table 1).

Similarly, mass spectrometric analysis of ^{15}N -LRAP showed that the measured mass of ^{15}N -LRAP was 6908.34 Da (Table 1). The LRAP sequence contains a total of 77 nitrogens, with a predicted mass of ^{15}N -LRAP to be ~ 6915.14 Da, which is ~ 77 Da higher than the predicted mass of non-labeled ^{14}N -LRAP (~ 6838.48 Da) if all nitrogens were labeled. Thus, approximately 70 ($= 6908.34 - 6838.68$) out of 77 nitrogens were ^{15}N -labeled, for a 90.9% labeling efficiency.

NMR and CD studies of LRAP structure

The structural properties of the purified ^{15}N -LRAP were studied at pH 4.0 using NMR spectroscopy. The NMR spectrum of ^{15}N -LRAP (Fig. 2) indicated a very limited chemical shift distribution. However, the majority of the backbone amide NMR signals of ^{15}N -LRAP amino acid sequence was detected (47 signals detected, excluding the 13 prolines scattering through the LRAP sequence). These backbone amide signals were mostly localized at 7.8 ppm – 8.4 ppm in the ^1H -axis. This limited signal distribution pattern represented a random-coiled protein (Warnmark *et al.*, 2001). However, a few other signals were well resolved in the spectrum. The signals of side-chain NH_2 of Gln resulted in two peaks (7.5 ppm, 116 ppm) and (6.9 ppm, 116 ppm). Similarly, the signals of side-chain NH_2 of Asn were also seen at the approximate coordinates. The side-chain

NH₂ of Arg signaled as a pair of peaks (7.1 ppm, 118 ppm) and (7.2 ppm, 118 ppm). Additionally, two indole NH signals of the two Trp's were also detected (10.08 ppm, 129 ppm) and (10.14 ppm, 130 ppm) (data not shown, out of range). Thus, all side chain amides of ¹⁵N-LRAP were observed in the spectrum.

CD measurements were also used to further determine the secondary conformation of LRAP at pH 4.0, as well as at pH 7.5 without calcium. CD measurements at pH 4.0 agreed well with the findings from the NMR study. A random-coiled structure produced a CD spectrum having a sharp negative ellipticity with a minimum at 200 nm - 204 nm (Greenfield, 1996; Warnmark *et al.*, 2001). The recorded CD spectrum of LRAP showed this characteristic profile (Fig. 3). Therefore, the CD data reconfirmed the conclusion from NMR results that LRAP had a random-coiled structure in aqueous solution at pH 4.0. A similar structure was also obtained at pH 7.5 (Fig. 3)

CD study of LRAP structure in the absence and presence of calcium ions

To determine whether the calcium interaction with LRAP would induce a folding mechanism to form a more defined and stabilized structure (i.e. β -sheet or α -helix), CD spectra of Ca²⁺/LRAP interaction at pH 7.5 and pH 4.0 with and without calcium were recorded (Fig. 3). In the absence of calcium ions, LRAP had random-coiled conformations at the two different pH's indicated by the negative ellipticity at minimum of 200 nm and 204 nm, respectively (Greenfield, 1996; Warnmark *et al.*, 2001). The addition of calcium ions into LRAP did not induce any major conformational change into a more stabilized structure (Fig. 3).

DISCUSSION

Current literature supports the notion that LRAP functions in cell signaling (Tompkins and Veis, 2002; Veis *et al.*, 2000; Veis, 2003). LRAP does not appear to play a direct structural role in modulating enamel mineralization (Chen *et al.*, 2003b). In contrast, full-length amelogenin has been known to be important in regulation of mineralization *in vitro* (Beniash *et al.*, 2005; Du *et al.*, 2005; Habelitz *et al.*, 2004) and *in vivo* (Gibson *et al.*, 2001), respectively. However, there has been no indication that full-length amelogenin functions as a cell-signaling molecule. Therefore, LRAP and full-length amelogenin have a distinctly different biological function, which maybe a result of their intrinsic structural differences. A partial secondary structure of full-length amelogenin has been determined, containing β -sheet domain (Renugopalakrishnan *et al.*, 1989; Renugopalakrishnan, 2002). However, secondary structure of LRAP is completely unknown.

In chapter 6, I showed definitively that Ca^{2+} has an affinity for LRAP, suggesting that Ca^{2+} potentially can activate specific functions in this protein by inducing structural changes. This type of conformational change in the presence of calcium occurs in the protein, calmodulin (Finn *et al.*, 1995). Similar to LRAP, calmodulin, has 4 Ca^{2+} binding sites (Wintrode and Privalov, 1997). When activated by binding Ca^{2+} , calmodulin is capable of interacting with a number of intracellular proteins (i.e. smooth muscle myosin light chain kinase) to regulate various processes of muscle contraction and cytoskeletal activity (Wintrode and Privalov, 1997).

The NMR and CD data both confirmed that LRAP had a random-coiled conformation at pH 7.5 and 4.0 (Figs. 2 and 3). Some intrinsically random-coiled proteins become folded into more defined structures upon recruitment and binding with their proper interaction partners (i.e. other target proteins, metal ions). Calmodulin is a good example of such properties. Calmodulin in solution is substantially disordered (random-coil) in the unbound state; however, in the bound state (with myosin light chain kinase and/or Ca^{2+}), calmodulin undergoes conformational changes into a well-ordered structure (Finn *et al.*, 1995; Meador *et al.*, 1992).

In this study, we tested the hypothesis that binding of calcium ions would induce a certain conformational change of LRAP. The CD results revealed that calcium ions failed to induce LRAP to form any more stable structure at both pH 7.5 and pH 4.0 (Fig. 3). The slight shift of the CD spectrum to the right suggested that at different pH's, calcium may induce LRAP to change from one random-coiled to another random-coiled structure. Yet, it is still possible that under the conditions that exist in the developing enamel matrix, LRAP may be induced to fold into a defined structure. However, the results of this study suggest that calcium binding to LRAP does not induce structural folding, and we suggest that because calcium binding locations are likely to be similar in the full-length amelogenin that the structure of amelogenins in general are not affected by calcium binding.

The secondary structure of bovine full-length amelogenin has been determined to contain repetitive β -turns forming an internal β -spiral channel (diameter of $\sim 1\text{\AA}$),

suggesting a potential function to facilitate calcium ion passage to regulate mineralization (Renugopalakrishnan *et al.*, 1989; Renugopalakrishnan, 2002). It is possible that the structural difference between LRAP (random-coil) and full-length amelogenin (β -spiral) maybe responsible for their ultimate differences in biological activities and functions in enamel biomineralization. Functional and structural differences between LRAP and full-length amelogenin are summarized in Table 2.

To better relate the role of amelogenin structure to protein function, future studies should aim at determining the specific conditions that would allow LRAP to fold into a specific structure (i.e. α -helix and /or β -sheet). Toward this goal, LRAP crystallization for X-ray crystallography study is a logical research pursuit. If the conditions allowing LRAP crystallization were identified, then it may be possible to use this information to promote crystallization of the full-length amelogenin protein, an important and elusive goal in elucidated structure-function relationships of amelogenins.

REFERENCES

- Beniash E, Simmer JP, Margolis HC (2005). The effect of recombinant mouse amelogenins on the formation and organization of hydroxyapatite crystals in vitro. *J Struct Biol* 149(2):182-90.
- Chen E, Yuan ZA, Wright JT, Hong SP, Li Y, Collier PM, Hall B, D'Angelo M, Decker S, Piddington R, Abrams WR, Kulkarni AB, Gibson CW (2003a). The small bovine amelogenin LRAP fails to rescue the amelogenin null phenotype. *Calcif Tissue Int* 73(5):487-95.
- Chen E, Yuan ZA, Wright JT, Hong SP, Li Y, Collier PM, Hall B, D'Angelo M, Decker S, Piddington R, Abrams WR, Kulkarni AB, Gibson CW (2003b). The Small Bovine Amelogenin LRAP Fails to Rescue the Amelogenin Null Phenotype. *Calcif Tissue Int*.

- Du C, Falini G, Fermani S, Abbott C, Moradian-Oldak J (2005). Supramolecular assembly of amelogenin nanospheres into birefringent microribbons. *Science* 307(5714):1450-4.
- Fincham AG, Moradian-Oldak J, Simmer JP (1999). The structural biology of the developing dental enamel matrix. *J Struct Biol* 126(3):270-99.
- Finn BE, Evenas J, Drakenberg T, Waltho JP, Thulin E, Forsen S (1995). Calcium-induced structural changes and domain autonomy in calmodulin. *Nat Struct Biol* 2(9):777-83.
- Gibson CW, Golub E, Ding WD, Shimokawa H, Young M, Termine J, Rosenbloom J (1991). Identification of the leucine-rich amelogenin peptide (LRAP) as the translation product of an alternatively spliced transcript. *Biochem Biophys Res Commun* 174(3):1306-12.
- Gibson CW, Yuan ZA, Hall B, Longenecker G, Chen E, Thyagarajan T, Sreenath T, Wright JT, Decker S, Piddington R, Harrison G, Kulkarni AB (2001). Amelogenin-deficient mice display an amelogenesis imperfecta phenotype. *J Biol Chem* 276(34):31871-5.
- Goto Y, Kogure E, Takagi T, Aimoto S, Aoba T (1993). Molecular conformation of porcine amelogenin in solution: three folding units at the N-terminal, central, and C-terminal regions. *J Biochem (Tokyo)* 113(1):55-60.
- Greenfield NJ (1996). Methods to estimate the conformation of proteins and polypeptides from circular dichroism data. *Anal Biochem* 235(1):1-10.
- Habelitz S, Kullar A, Marshall SJ, DenBesten PK, Balooch M, Marshall GW, Li W (2004). Amelogenin-guided crystal growth on fluoroapatite glass-ceramics. *J Dent Res* 83(9):698-702.
- Habelitz S, Denbesten PK, Marshall SJ, Marshall GW, Li W (2005). Amelogenin control over apatite crystal growth is affected by the pH and degree of ionic saturation. *Orthod Craniofac Res* 8(4):232-8.
- Meador WE, Means AR, Quijcho FA (1992). Target enzyme recognition by calmodulin: 2.4 A structure of a calmodulin-peptide complex. *Science* 257(5074):1251-5.
- Moradian-Oldak J, Jimenez I, Maltby D, Fincham AG (2001). Controlled proteolysis of amelogenins reveals exposure of both carboxy- and amino-terminal regions. *Biopolymers* 58(7):606-16.
- Moradian-Oldak J, Bouropoulos N, Wang L, Gharakhanian N (2002). Analysis of self-assembly and apatite binding properties of amelogenin proteins lacking the hydrophilic C-terminal. *Matrix Biol* 21(2):197-205.

Rajender S, Rajani V, N JG, Chakravarty B, Singh L, Thangaraj K (2006). SRY-negative 46,XX male with normal genitals, complete masculinization and infertility. *Mol Hum Reprod*.

Renugopalakrishnan V, Pattabiraman N, Prabhakaran M, Strawich E, Glimcher MJ (1989). Tooth enamel protein, amelogenin, has a probable beta-spiral internal channel, Gln112-Leu138, within a single polypeptide chain: preliminary molecular mechanics and dynamics studies. *Biopolymers* 28(1):297-303.

Renugopalakrishnan V (2002). A 27-mer tandem repeat polypeptide in bovine amelogenin: synthesis and CD spectra. *J Pept Sci* 8(4):139-43.

Saito T, Arsenault AL, Yamauchi M, Kuboki Y, Crenshaw MA (1997). Mineral induction by immobilized phosphoproteins. *Bone* 21(4):305-11.

Shaw WJ, Campbell AA, Paine ML, Snead ML (2004). The COOH terminus of the amelogenin, LRAP, is oriented next to the hydroxyapatite surface. *J Biol Chem* 279(39):40263-6.

Tompkins K, Veis A (2002). Polypeptides translated from alternatively spliced transcripts of the amelogenin gene, devoid of the exon 6a, b, c region, have specific effects on tooth germ development in culture. *Connect Tissue Res* 43(2-3):224-31.

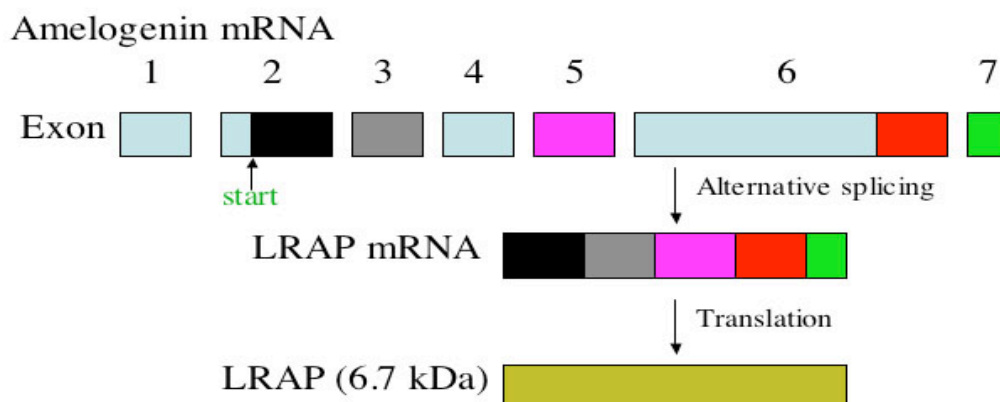
Tompkins K, Alvares K, George A, Veis A (2005). Two related low molecular mass polypeptide isoforms of amelogenin have distinct activities in mouse tooth germ differentiation in vitro. *J Bone Miner Res* 20(2):341-9.

Veis A, Tompkins K, Alvares K, Wei K, Wang L, Wang XS, Brownell AG, Jengh SM, Healy KE (2000). Specific amelogenin gene splice products have signaling effects on cells in culture and in implants in vivo. *J Biol Chem* 275(52):41263-72.

Veis A (2003). Amelogenin gene splice products: potential signaling molecules. *Cell Mol Life Sci* 60(1):38-55.

Warnmark A, Wikstrom A, Wright AP, Gustafsson JA, Hard T (2001). The N-terminal regions of estrogen receptor alpha and beta are unstructured in vitro and show different TBP binding properties. *J Biol Chem* 276(49):45939-44.

Wintrade PL, Privalov PL (1997). Energetics of target peptide recognition by calmodulin: a calorimetric study. *J Mol Biol* 266(5):1050-62.



MPLPPHPGHPGYINFSYEVLTPWKYQSIRPPPLPPMLPD
LTLEAWPSTDKTKREEVD (LRAP Sequence)

Figure 1.

Alternatively spliced pattern of human LRAP and its amino acid sequence.

LRAP is encoded by exons 2, 3, 5, 6d and 7, resulting in a 58-residue alternatively spliced peptide, whose amino acid sequence is identical to the first 32 and the last 26 residues of H174.

Peptides	Measured <i>m/z</i> (Da)	Predicted <i>m/z</i> (Da)
LRAP	6838.68	6838.48
¹⁵ N-LRAP	6908.34	6915.14

Table 1.

Mass spectrometry analysis of LRAP and ¹⁵N-LRAP.

Mass measurements confirmed the correct identity of unlabeled LRAP and ¹⁵N-LRAP. ¹⁵N-LRAP was successfully labeled with 90.9% efficiency. The LRAP sequence (total 60 amino acids) used for mass analysis contained two more residues (Gly and Ser) added to the N-terminal of the peptide as a result of thrombin cleavage.

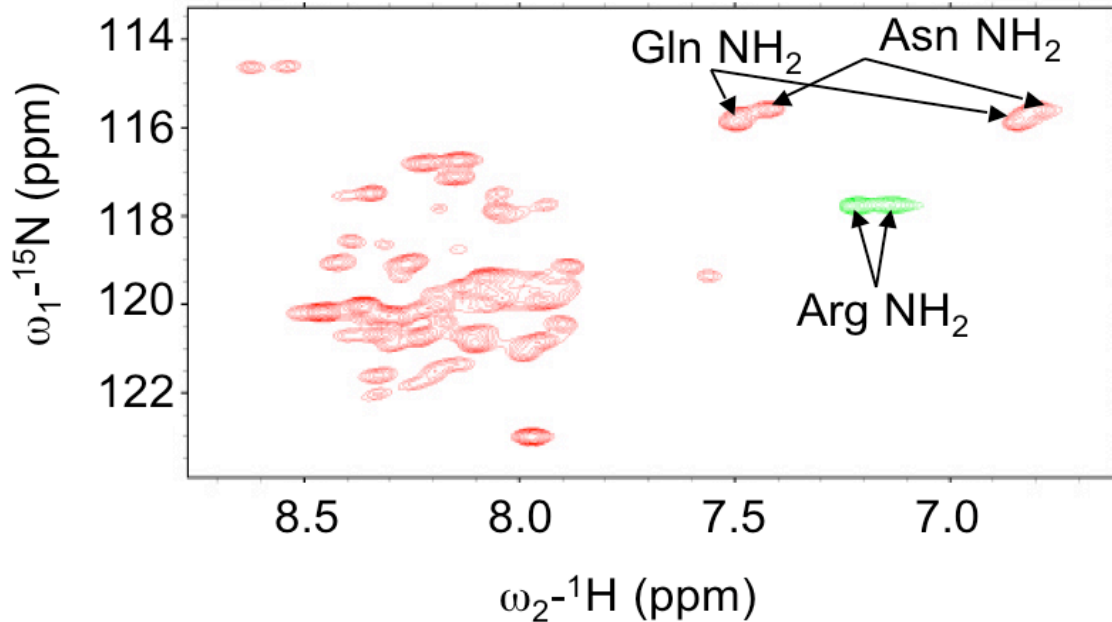


Figure 2.

Nuclear magnetic resonance (NMR) analysis of N^{15} -labeled recombinant human leucine-rich amelogenin peptide (N^{15} -LRAP) structure.

The 800-MHz ^1H - ^{15}N heteronuclear single quantum coherence (HSQC) spectrum of N^{15} -LRAP [40 μM] in D_4 -acetate [10 mM], pH 4.0, at 25 $^\circ\text{C}$. All backbone amides NMR signals of N^{15} -LRAP were detected. The spectrum revealed a limited signal distribution profile of N^{15} -LRAP, mostly coalesced at 7.8 ppm – 8.4 ppm (^1H -axis), indicating a random-coiled structure. However, a few signals were well resolved, representing the side-chain NH_2 's of Gln and Asn as two pairs of peaks at coordinates (7.5 ppm, 116 ppm) and (7.1 ppm, 116 ppm). The side-chain NH_2 of Arg signal was detected as a pair of peaks at (7.1 ppm, 118 ppm) and (7.2 ppm, 118 ppm). Two indole NH signals of the two Trp's were also observed at (10.08 ppm, 129 ppm) and (10.14 ppm, 130 ppm) (data not shown due to out of range).

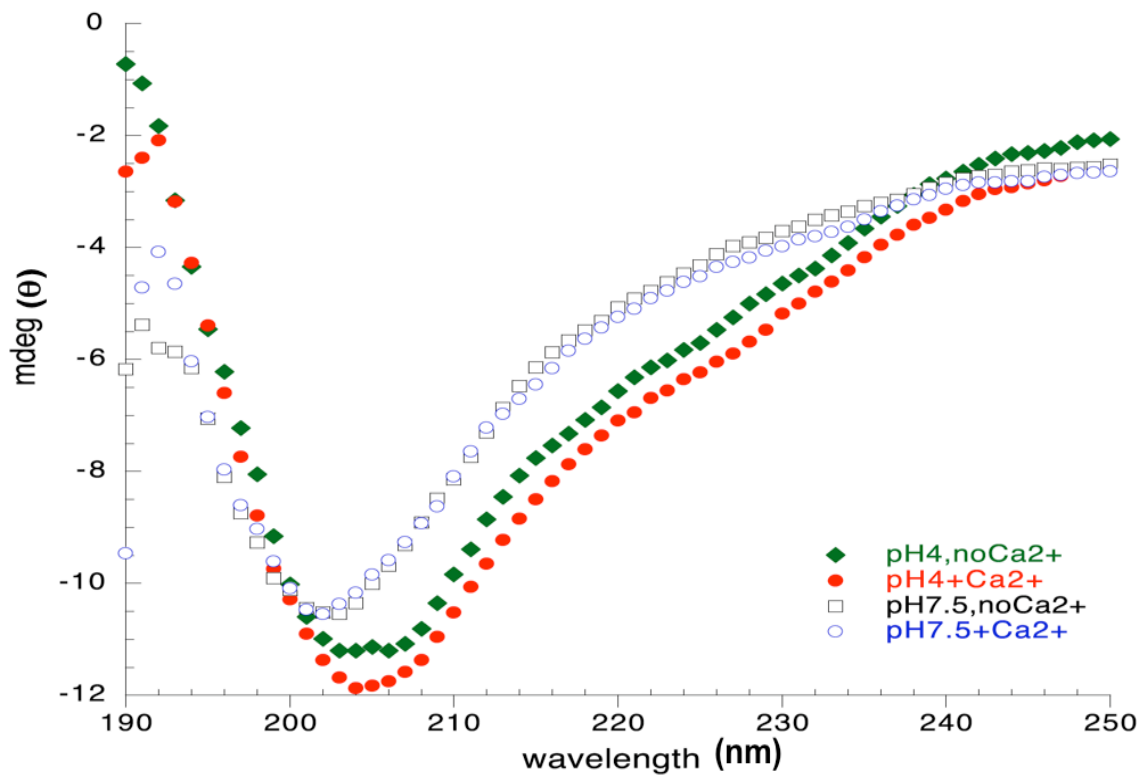


Figure 3.

The far-UV circular dichroism (CD) spectra of LRAP in the absence or presence of calcium ions, at different pH values.

The CD spectra of 500 μ L LRAP [28 μ M] in HEPES [10 mM], pH 7.5 and in acetate [10 mM], pH 4.0 at 25 $^{\circ}$ C in the absence or presence of calcium ions (4 μ L CaCl_2 , 50 mM added) showed that LRAP maintained its random-coiled conformation when bound to Ca^{2+} .

Proteins	Ca⁺² Binding	HAP Binding	Protein Structure	Regulation of Mineralization	Cell Signaling
LRAP	Yes	Yes	Random-Coil	No	Yes
rH174	Yes	Yes	β-turns & β-spiral	Yes	No

Table 2.

Comparison the proposed functions between LRAP and rH174.

Both LRAP and rH174 bind to Ca⁺² and hydroxyapatite. However, LRAP functions as a cell-signaling molecule, while full-length amelogenin (rH174) directly regulates biomineralization.

Chapter 8. Amelogenins in Human Developing and Mature Dental Pulp to Affect Cell Proliferation

INTRODUCTION:

In developing tooth enamel, amelogenins are the principal matrix proteins comprising more than 90% of the extracellular matrix protein in the secretory stage of enamel formation (Fincham *et al.*, 1999). Amelogenins are characterized by heterogeneity, which results in part from alternative splicing of the primary RNA transcript (Bonass *et al.*, 1994; DenBesten and Li, 1992; Simmer *et al.*, 1994). Alternative splicing of amelogenins generates a group of protein variants whose proportions change during tooth formation (Yuan *et al.*, 1996).

Several early studies using immunohistochemistry identified amelogenins in endocytotic vesicles and lysosomes within odontoblasts before mineralization of mantle dentin in mouse (Nakamura *et al.*, 1994), along the cell surfaces and processes of odontoblasts (Sawada and Nanci, 1995), and in young odontoblasts of hamster (Karg *et al.*, 1997). Recently, amelogenin mRNA transcripts have been amplified from mouse dental mesenchyme and immortalized odontoblast-like cells (Papagerakis *et al.*, 2003), and porcine odontoblasts (Nagano *et al.*, 2003). Studies of rodent teeth by *in situ* hybridization failed to find amelogenin transcripts in odontoblasts (Karg *et al.*, 1997; Torres-Quintana *et al.*, 2005), suggesting that transcripts may be present at very low levels.

The isolation and identification of low-molecular-weight amelogenins in rat dentin, as a chondrogenic stimulating factor, brought rapid attention to the potential role of amelogenins in mesenchymal cell signaling (Nebgen *et al.*, 1999; Veis *et al.*, 2000; Veis, 2003). The expression pattern of the alternatively spliced amelogenins in human dentin-pulp complex has not yet been reported, and the role of amelogenins in the human dentin formation and dental pulp repair remains unclear.

The objective of this study was to elucidate the expression and function of amelogenins in the human dentin-pulp complex. Developing human tooth buds were immunostained for amelogenin, and mRNA was detected by *in situ* hybridization. The effects of recombinant amelogenins on dental pulp cell (DPC) proliferation were measured by 5-bromo-2'-deoxyuridine (BrdU) incorporation immunoassay, and cell differentiation was monitored by alkaline phosphatase (ALP) expression. Amelogenin protein was found in the forming dentin matrix, and amelogenin mRNA was localized in the dentin, presumably in the odontoblast processes. Proliferation of dental pulp cells was enhanced by the treatments of recombinant human leucine-rich amelogenin peptide (LRAP), and LRAP+exon4 (exon 4 encoded for additional 14 amino acids, NSHSQAINVDRTAL), but no effect by full-length amelogenin (rH174). These studies suggest that odontoblasts actively synthesize and secrete amelogenin protein during human tooth development, and that low-molecular-weight amelogenins enhance dental pulp cell (DPC) proliferation.

MATERIALS AND METHODS

Immunohistochemical localization of amelogenins

Developing human tooth buds were obtained from approximately 21-week old fetal tissue through the tissue-sharing program within the University of California at San Francisco, CA, USA. The teeth were frozen and cryo-sectioned. An adult non-cariou premolar was obtained from patient who had given his written consent. Immediately after extraction, it was fixed by immersion in 10% neutral formalin for 24 h, decalcified in 17% buffered EDTA, and processed routinely for paraffin embedding. Sections were blocked with 10% fetal bovine serum (FBS) and 0.1% Triton X-100, and immunostained with anti-amelogenin antibody raised from rH174 (Li *et al.*, 2001), or pre-immuned rabbit serum (1:200) diluted in the same blocking solution. All sections were labeled by the secondary antibody, anti-rabbit IgG-Alexfluor594 (Sigma, St. Louis, MO, USA). Nuclei were counterstained with 0.5 µg/ml Hoechst 33324 (Invitrogen, Carlsbad, CA, USA).

***In situ* hybridization of amelogenin mRNA**

Incisor tooth buds were fixed in 4% paraformaldehyde and processed for *in situ* hybridization as described (Albrecht *et al.*, 1997) with ³⁵S-labeled human amelogenin and a type I collagen riboprobes. The amelogenin probe was prepared by amplifying the full-length amelogenin cDNA from a human ameloblast cDNA library. Sections were counter-stained with a nuclear stain (Hoechst Stain, Sigma). Hybridization signals were detected using dark-field optics and the nuclear stain was visualized using epifluorescence.

Identification of alternatively apliced amelogenins in dental pulp cells *in vitro*

Dental pulp cells (DPC) were obtained from adult human pulp tissues as previously described (Gronthos *et al.*, 2000). DPC were cultured in alpha-modified Eagle's Medium (Cell Culture Facility, UCSF, San Francisco, CA), supplemented with 10% fetal bovine serum (FBS, Invitrogen), 100 U/mL penicillin, and 100 mg/mL streptomycin at 37 °C in 5% CO₂ on Lab-Tek chamber slides (Nalge, Rochester, NY, USA). The DPC were collected and fixed in 95% methanol and 5% acetic acid for 30 min at -20 °C, and immunostained by initial incubation with anti-amelogenin antibody (1:1000), followed by anti-rabbit IgG-FITC antibody (Sigma).

Alternatively spliced amelogenin mRNA expressed by these cells was identified by reverse-transcription of 2 µg total RNA, which was extracted using RNAase Mini kit (Qiagen, Valencia, CA, USA) with SSR reverse-transcriptase (Invitrogen). Two primers- Amg U01 (5'-TGGGGACCTGGATTTTATTTG-3') and Amg D02 (5'-CTCTTCCTCCCGCTTGGTC-3')-located at the 5' and 3' termini of amelogenin gene (primers bind at regions of exon 2 and exon 7) were used to amplify spliced amelogenins. A PCR reaction of 30 cycles, with annealing temperature of 55 °C for 45 seconds was performed. The PCR products were separated on 1.5% agarose gels, sub-cloned into the TOPO-Blunt II vector (Invitrogen) and sequenced.

Dental pulp cell proliferation in the presence of alternatively spliced amelogenins.

Human recombinant full-length amelogenin (rH174) was prepared as previously described (chapter 4). Human LRAP and LRAP+exon4 cDNA's were amplified using two primers, Amg U13 (5'-AGCTGGATCCATGCCTCTACCACCTCATCCT-3') and

Amg D08 (5'-ATTAGAATTCTTAATCCACTTCCTCCCGCTTG-3'), containing two restriction enzyme cutting sites *BamH I* and *Eco RI* at their respective 5' termini, cloned into pGEX-4T-1 vector (Invitrogen) using rapid ligation kit (Amersham, Biosciences, NJ, USA). The plasmids were transformed into BL21 DE3 *E. coli* (Invitrogen) and cultured in LB broth supplemented with 50 $\mu\text{g}/\text{mL}$ ampicillin at 37 °C. At optical density (O.D.) of 0.6, the protein expressions were induced by 0.8 mM IPTG for 4 h. After sonication and centrifugation, the supernatants containing the expressed proteins were loaded onto a glutathione-Sepharose affinity column (Amersham) according to the manufacturer's instructions, and the fusion proteins were then digested with 100 U of thrombin (Amersham) at 25 °C for 5 h. The eluted proteins were further purified by reverse-phase HPLC using a C18 column (Varian, Lake Forest, CA, USA) eluting with a gradient of acetonitrile (ACN) and 0.1% trifluoroacetic acid (TFA).

The expressed amelogenin proteins (LRAP, LRAP+exon4 and rH174) were characterized by SDS-PAGE and Western blots using the anti-amelogenin antibody and an anti-rabbit LRAP antibody raised from synthetic LRAP peptide. Mass spectrometry (Biomolecular Resource Center Mass Spectrometry Facility, UCSF, San Francisco, USA) was used to further definitively confirm the identity of the expressed proteins (data not shown).

Cells were cultured in clear-bottom black 96-well plates (Falcon, USA) at a density of 2×10^3 cells / well until 60% confluence, serum starved for 24 h, and recombinant full-length amelogenin (rH174) and its alternatively spliced variants (LRAP and LRAP+exon4) were added in triplicate in cell culture media at a concentrations of 0 to

1000 ng/mL, without FBS. Cells were maintained in this medium for 24 h, and cell proliferation was measured using an ELISA BrdU kit (Roche, Mannheim, Germany) according to the manufacturer's instructions.

Statistical analysis between groups was performed by ANOVA with Dunnet's post-test analysis using GraphPad Prism version 3.0a for Macintosh (GraphPad Software, San Diego, CA, USA).

Cell-cycle Gene SuperArray™ analysis

Cell-cycle Gene SuperArray™ A GEMArray Q series human cell-cycle gene array kit was obtained from SuperArray Inc. (Bethesda, MD, USA). Dental pulp cells were plated at a density of 2×10^5 cells /dish, cultured until 60% confluence and serum-starved for 24 h. The cells were divided into two groups, an experimental group with 10 nM LRAP added and a control group without peptide addition. After 24 h, total RNA was isolated using RNeasy Mini Kit (Qiagen) and 3 µg total RNA were used as a template to generate Biotin-16-dUTP-labeled cDNA probes, which were hybridized to the SuperArray membrane according to the manufacturer's instructions (SuperArray Corp., <http://www.superarray.com>). Duplicated assays were analyzed with ScanAlyze software (shareware, <http://rana.lbl.gov/EisenSoftware.htm>), and the signal intensity from the membrane was compared with Gearray analyzer program as previously described (Liu *et al.*, 2004).

Cell differentiation assay

Cells were cultured and grown to confluence. Full-length amelogenin (rH174) and alternatively spliced amelogenins (LRAP and LRAP+exon4) of 10 nM were added to the culture dishes for 48 h in triplicate assays. Relative levels of alkaline phosphatase (ALP) and dentin sialoprotein (DSP) were determined by Western blots and semi-quantitative reverse-transcription (RT)-PCR, and compared with the control as described below.

For Western blot analysis, cells were scrapped from the tissue culture dishes, lysed with ice-cold lysis buffer containing 50 mM Tris-HCl (pH 7.6), 1% NP-40, 150 mM NaCl, 0.25% Na-deoxycholate, 1 mM EDTA, 1 mM PMSF, 1 mM NaF, 1 mM Na₃VO₄. Cell debris was eliminated by centrifugation of 12,000 r.p.m. for 15 min. The proteins in the supernatants were determined by the Bradford method with a protein assay reagent (Bio-Rad, Hercules, CA, USA). Equal amounts proteins were loaded and separated by 12% SDS- PAGE and transferred to a Duralon-UV™ membrane (Stratagene, La Jolla, CA, USA). Western blots were done with anti-DSP (1:200 dilution of LF-151) (Gronthos *et al.*, 2000), anti-ALP (1:75 dilution)(Zymed, South San Francisco, CA, USA) or anti-actin (1:1000)(Santa Cruz Biotechnology, Santa Cruz, CA, USA). Protein bands were visualized using chemiluminescence detection provided by ECL Plus kit (Amersham) and exposed to autoradiograph film. The relative intensity of DSP-specific and ALP-specific bands were digitalized and compared using a shareware program, NIH Image (<http://rsb.info.nih.gov/nih-image/>). The actin expression was used as a control.

For semi-quantitative reverse-transcription (RT)-PCR, total RNA was isolated using RNeasy Mini Kit (Qiagen). The same amount of total RNA was used for reverse-transcription using an oligo-dT primer, followed by PCR with a 50- μ l reaction system: 30 of μ l H₂O, 5 μ l of 10X PCR buffer, 1.5 μ l of 50 mM MgCl₂, 1 μ l of 10 mM dNTP, 0.5 μ l of Taq polymerase, 2 μ l of template, 5 μ l of sense primer, 5 μ l of anti-sense primer. Primers for ALP (416-bp product) are: sense: 5'-GACCCGTCACTCTCCGAGATG-3', anti-sense: 5'-CTGCGCCTGGTAGTTGTTGTG-3'; for DSP (312-bp product) are: sense: 5'-ATGGCATCCAGGGACAAGTAA-3', anti-sense: 5'-CCAGGCCAGCATCTTCTCCAG-3'; and for G3DPH (432-bp product) are: sense 5'-ACCACAGTCCATGCCATCAC-3', anti-sense 5'-TCCACCACCCTGTTGCTGTA-3'. PCR reactions were incubated in an Eppendorf Mastercycler cyler (Eppendorf, Westbury, NY, USA) at 94°C for 3 min for one cycle and then 94 °C 30 sec, 55 °C 30 sec for GAPDH and ALP and 58 °C 30 sec for DSP, 72 °C 1 min for 35 cycles, with a final 10-min extension at 72 °C. After amplification, the reaction was analyzed by 1% agarose gel electrophoresis.

RESULTS

Amelogenins are expressed in dental pulp cells

Immunostaining of a developing tooth organ showed amelogenin protein in the developing dentin in a tooth bud where enamel matrix formation had not yet been initiated (Fig 1B). Similar diffuse staining of the odontoblast layer was found in the adult human dentin (results not shown).

In Situ hybridization showed that amelogenin mRNA was localized in the dentin matrix, and in the secretory ameloblasts (Fig 1D). The pattern of amelogenin mRNA localization in the dentin matrix, opposing the unlabeled acellular enamel matrix, was in contrast to the Type I collagen-positive control (Fig 1E) mRNA, which was localized in the odontoblast cell bodies lining the forming dentin.

Alternatively spliced patterns of amelogenin in dental pulp cells

RT-PCR amplification of amelogenin mRNA from cultured dental pulp cells (DPC) resulted in two apparent different bands on 1.5 % gel, ~216-bp and ~525-bp products (Fig. 2A). Subsequent subcloning, bacterial transformation, colony screening by PCR (Fig. 2B) and DNA sequencing of these amplified cDNA products showed 3 specific amelogenin spliced variants: LRAP, LRAP+exon4, and the full-length amelogenin (H174) (DNA sequencing data not shown). Therefore, the 525-bp encoded for H174, while the 174-bp and 216-bp “apparent” products encoded for LRAP and LRAP+exon4, respectively. Since LRAP and LRAP+exon4 are different by only 14 amino acids (NSHSQAINVDRTAL) coded by exon 4 (42-bp exon), this small bp difference was not initially distinguishable on 1.5% gel separating RT-PCR products (Fig. 2A). As a control, PCR amplification of human fetal tooth cDNA library also resulted in identical amelogenin isoforms (LRAP, LRAP+exon4 and H174) as seen in DPC, and three other additional spliced variants (H136, H159 and H169) that were already previously identified (Salido *et al.*, 1992) (data not shown).

Effect of alternatively spliced amelogenins on dental pulp cell proliferation

Both LRAP and LRAP+exon4 significantly stimulated dental pulp cell proliferation at an optimal concentration of 200 ng/mL (Fig. 3A and B), while full-length amelogenin (rH174) had no significant effects on the proliferation of these cells ($P > 0.05$) (data not shown).

Cell-cycle Gene SuperArray™ data using dental pulp cells showed that 3 genes, including cyclin-dependent kinase 6 (CDK6), cullin-4 (CUL4) and Neural Precursor Cell Expressed Developmentally Down-regulated Gene 8 (NEDD8), were up-regulated two-fold by 10 by the treatment of 10 nM of LRAP (Fig. 3C).

Effect of amelogenins on cell differentiation characterized by ALP and DSP mRNA expression

Dental pulp cells were initially positive for alkaline phosphatase (ALP) and dentin sialoprotein (DSP) at both mRNA and protein levels (Fig. 4A and B, lane 4). Addition of recombinant amelogenins (LRAP, LRAP+exon4 and rH174) into these cell cultures did not alter the initial mRNA expression or protein synthesis of either of these differentiation markers (ALP and DSP) in dental pulp cells (Fig. 4A and B, lane 1, 2 and 3). G3DPH was used as a control for gene expression, and actin was used as a control for Western analysis.

DISCUSSION

Immunohistochemical localization of amelogenin at the interface of the inner-enamel epithelium and the mesenchymal cells of the dental papilla is similar to reports from

studies of rat (Bronckers *et al.*, 1993; Janones *et al.*, 2005). Some previous studies have suggested that amelogenins secreted by developing ameloblast-lineage cells may diffuse into the predentin matrix (Inai *et al.*, 1991; Uchida *et al.*, 1989). However, our studies using both *in situ* hybridization and immunohistochemistry indicated that the odontoblasts synthesized amelogenins and secreted these proteins at the epithelial/enamel interface.

It is interesting that amelogenin mRNA localization in the dentin layer containing the odontoblastic processes is different from Type I collagen mRNA localization to the odontoblast cell bodies. The localization of amelogenin mRNA by *in situ* hybridization differs from the negative results reported for rodent teeth (Karg *et al.*, 1997; Torres-Quintana *et al.*, 2005), possibly related to differences between rodents and humans, or to differences in sensitivity of the *in situ* hybridization assay. These results suggest that amelogenins may not directly interact with pulp cells during development, but may have a role in epithelial/mesenchymal interactions related to enamel and dentin formation.

The incisal end of dental papilla adjacent to the amelogenin-positive epithelium contained more differentiated columnar, polarized cells, which was expected since tooth development progresses in an incisal to apical gradient. These cells were amelogenin-immunopositive, while the more apical ones were negative. A similar stage-specific expression of amelogenin was found in mouse molars, where amelogenin was expressed only by young odontoblasts (Papagerakis *et al.*, 2003).

Amelogenin transcripts identified in our study are similar to those found in dentin tissues in other species: human full-length amelogenin (H174) and LRAP are counterparts of P173 and P56, found in porcine odontoblasts (Nagano *et al.*, 2003), while LRAP and LRAP+exon4 are identical to [A-4] and [A+4] found in rat (Veis *et al.*, 2000). We did not find the human amelogenin transcript corresponding to the P41 in porcine odontoblasts, which could be species-specific, nor H185 previously reported by Salido *et al.* (Salido *et al.*, 1992).

It is interesting that we found LRAP+exon4 in dental pulp cells. Amelogenin mRNA splice variants containing exon 4 have been reported to be in relatively low abundance in other species (Brookes *et al.*, 1995), suggesting that the amelogenin protein encoded by the LRAP+exon4 mRNA, may have a specific role in early dentin formation.

Papagerakis and coworkers (Papagerakis *et al.*, 2003) reported that only odontoblast cell lines express amelogenin transcripts, with no expression in dental pulp and mature odontoblast cell lines. Our *in vivo* results support this finding, however, we did find amelogenin expressed in pulp cells grown *in vitro*. Since pulp cells are known to differentiate into odontoblast-like cells *in vitro*, it is possible that the amelogenin transcripts were specific to these differentiated cells.

Repeated analyses of the effect of LRAP on dental pulp cells showed a specific effect on the up-regulation of the cell cycle related genes: CDK6, CUL4 and NEDD8. CDK6 can promote cell-cycle progression by accelerating G1/S transition (Malumbres *et al.*, 2004).

CUL4 is a component of E3 ubiquitin ligase complexes, which mediate the ubiquitination and the degradation of short-lived regulatory proteins, including cyclins and other cell cycle regulator such as the p27^{KIP1}, regulates the cell cycle and signaling (Nakayama *et al.*, 2001). NEDD8-modifying pathway, which is essential to E3 ubiquitin ligase complexes, plays a key role in the Ub-mediated pathway with respect to cell-cycle regulation (Hochstrasser, 1998). Up-regulation of these 3 genes had a positive effect on the cell cycle progression, while the mechanism by which LRAP alters expression of these proteins to affect the cell cycle is not known, and requires further study.

ALP and DSP expression increased when dental pulp cells differentiate into odontoblasts (Couple *et al.*, 2000; Veis *et al.*, 2000; Yokose *et al.*, 2000). In our study of human dental pulp cells, there were no significant effects of recombinant amelogenins on cell differentiation. This is in contrast to previously reported finding that [A+4] (counterpart of LRAP+exon4) stimulated the production of type I collagen by odontoblasts in cultured mouse tooth germs, while [A-4] (counterpart of LRAP) did not (Tompkins *et al.*, 2005). Likewise, Veis and coworkers showed that embryonic muscle fibroblast differentiation into chondrocytes was enhanced by additional of recombinant rat [A+4] (or LRAP+exon4) (Nebgen *et al.*, 1999). Viswanathan and coworkers found that murine full length amelogenin promoted BSP expression by a mouse cementoblast cell line at 0.1 µg/mL and decreased BSP expression at 10 µg/mL (Viswanathan *et al.*, 2003). The reasons for the discrepancies between our results, showing no effects on cell differentiation, and these reported studies are not immediately apparent, but may be species-related.

It is important to note that the Cell-cycle Gene SuperArray™ results for determining the effects of amelogenins on cell proliferation, and the RT-PCR data showing no effects of amelogenins on cell differentiation can be further strengthened with the future corresponding data obtained from qualitative real-time PCR in order to accurately draw a more definitive conclusion.

In summary, our studies are the first to identify specific alternatively spliced amelogenin fragments and their effects on adult human dental pulp cells grown in culture.

Amelogenin mRNA transcripts and amelogenin proteins are present in the developing human dentin matrix, though the role of amelogenin in dentin matrix formation is not known. Cells from the dental pulp can increase proliferation in response to low molecular weight amelogenins such as LRAP and LRAP+exon4, though it is not apparent whether sufficient amounts of protein are present in the dental pulp to modify or direct dentin formation. However, the effects of low-molecular-weight amelogenins on dental pulp cell proliferation suggests the potential applications of these proteins to be used as agents to promote proliferation of dental pulp tissue in the presence of injury, resulting in the formation of reparative dentin.

REFERENCES

Alberch UEG, Helm JA, Lin H. (1997), Visualization of gene expression patterns by in situ hybridization. In. *Molecular and Cellular Methods in Developmental Toxicology*. GP Daston, editor. Boca Raton, Florida: CRC Press, pp.23-48

- Bonass WA, Kirkham J, Brookes SJ, Shore RC, Robinson C (1994). Isolation and characterisation of an alternatively-spliced rat amelogenin cDNA: LRAP--a highly conserved, functional alternatively-spliced amelogenin? *Biochim Biophys Acta* 1219(3):690-2.
- Bronckers AL, D'Souza RN, Butler WT, Lyaruu DM, van Dijk S, Gay S, Woltgens JH (1993). Dentin sialoprotein: biosynthesis and developmental appearance in rat tooth germs in comparison with amelogenins, osteocalcin and collagen type-I. *Cell Tissue Res* 272(2):237-47.
- Brookes SJ, Robinson C, Kirkham J, Bonass WA (1995). Biochemistry and molecular biology of amelogenin proteins of developing dental enamel. *Arch Oral Biol* 40(1):1-14.
- Couple ML, Farges JC, Bleicher F, Perrat-Mabillon B, Boudeulle M, Magloire H (2000). Odontoblast differentiation of human dental pulp cells in explant cultures. *Calcif Tissue Int* 66(2):129-38.
- DenBesten PK, Li RS (1992). Characterization of amelogenin mRNA from secretory- and maturation-stage rat incisor enamel. *Arch Oral Biol* 37(12):1097-100.
- Fincham AG, Moradian-Oldak J, Simmer JP (1999). The structural biology of the developing dental enamel matrix. *J Struct Biol* 126(3):270-99.
- Gronthos S, Mankani M, Brahim J, Robey PG, Shi S (2000). Postnatal human dental pulp stem cells (DPSCs) in vitro and in vivo. *Proc Natl Acad Sci U S A* 97(25):13625-30.
- Hochstrasser M (1998). There's the rub: a novel ubiquitin-like modification linked to cell cycle regulation. *Genes Dev* 12(7):901-7.
- Inai T, Kukita T, Ohsaki Y, Nagata K, Kukita A, Kurisu K (1991). Immunohistochemical demonstration of amelogenin penetration toward the dental pulp in the early stages of ameloblast development in rat molar tooth germs. *Anat Rec* 229(2):259-70.
- Janones DS, Massa LF, Arana-Chavez VE (2005). Immunocytochemical examination of the presence of amelogenin during the root development of rat molars. *Arch Oral Biol* 50(5):527-32.
- Karg HA, Burger EH, Lyaruu DM, Woltgens JH, Bronckers AL (1997). Gene expression and immunolocalisation of amelogenins in developing embryonic and neonatal hamster teeth. *Cell Tissue Res* 288(3):545-55.
- Li W, Gibson CW, Abrams WR, Andrews DW, DenBesten PK (2001). Reduced hydrolysis of amelogenin may result in X-linked amelogenesis imperfecta. *Matrix Biol* 19(8):755-60.

- Liu H, Li W, Gao C, Kumagai Y, Blacher RW, DenBesten PK (2004). Dentonin, a fragment of MEPE, enhanced dental pulp stem cell proliferation. *J Dent Res* 83(6):496-9.
- Malumbres M, Sotillo R, Santamaria D, Galan J, Cerezo A, Ortega S, Dubus P, Barbacid M (2004). Mammalian cells cycle without the D-type cyclin-dependent kinases Cdk4 and Cdk6. *Cell* 118(4):493-504.
- Nagano T, Oida S, Ando H, Gomi K, Arai T, Fukae M (2003). Relative levels of mRNA encoding enamel proteins in enamel organ epithelia and odontoblasts. *J Dent Res* 82(12):982-6.
- Nakamura M, Bringas P, Jr., Nanci A, Zeichner-David M, Ashdown B, Slavkin HC (1994). Translocation of enamel proteins from inner enamel epithelia to odontoblasts during mouse tooth development. *Anat Rec* 238(3):383-96.
- Nakayama KI, Hatakeyama S, Nakayama K (2001). Regulation of the cell cycle at the G1-S transition by proteolysis of cyclin E and p27Kip1. *Biochem Biophys Res Commun* 282(4):853-60.
- Nebgen DR, Inoue H, Sabsay B, Wei K, Ho CS, Veis A (1999). Identification of the chondrogenic-inducing activity from bovine dentin (bCIA) as a low-molecular-mass amelogenin polypeptide. *J Dent Res* 78(9):1484-94.
- Papagerakis P, MacDougall M, Hotton D, Bailleul-Forestier I, Oboeuf M, Berdal A (2003). Expression of amelogenin in odontoblasts. *Bone* 32(3):228-40.
- Salido EC, Yen PH, Koprivnikar K, Yu LC, Shapiro LJ (1992). The human enamel protein gene amelogenin is expressed from both the X and the Y chromosomes. *Am J Hum Genet* 50(2):303-16.
- Sawada T, Nanci A (1995). Spatial distribution of enamel proteins and fibronectin at early stages of rat incisor tooth formation. *Arch Oral Biol* 40(11):1029-38.
- Simmer JP, Hu CC, Lau EC, Sarte P, Slavkin HC, Fincham AG (1994). Alternative splicing of the mouse amelogenin primary RNA transcript. *Calcif Tissue Int* 55(4):302-10.
- Tompkins K, Alvares K, George A, Veis A (2005). Two related low molecular mass polypeptide isoforms of amelogenin have distinct activities in mouse tooth germ differentiation in vitro. *J Bone Miner Res* 20(2):341-9.
- Torres-Quintana MA, Gaete M, Hernandez M, Farias M, Lobos N (2005). Ameloblastin and amelogenin expression in postnatal developing mouse molars. *J Oral Sci* 47(1):27-34.
- Uchida T, Tanabe T, Fukae M (1989). Immunocytochemical localization of amelogenins in the deciduous tooth germs of the human fetus. *Arch Histol Cytol* 52(5):543-52.

Veis A, Tompkins K, Alvares K, Wei K, Wang L, Wang XS, Brownell AG, Jengh SM, Healy KE (2000). Specific amelogenin gene splice products have signaling effects on cells in culture and in implants in vivo. *J Biol Chem* 275(52):41263-72.

Veis A (2003). Amelogenin gene splice products: potential signaling molecules. *Cell Mol Life Sci* 60(1):38-55.

Viswanathan HL, Berry JE, Foster BL, Gibson CW, Li Y, Kulkarni AB, Snead ML, Somerman MJ (2003). Amelogenin: a potential regulator of cementum-associated genes. *J Periodontol* 74(10):1423-31.

Yokose S, Kadokura H, Tajima Y, Fujieda K, Katayama I, Matsuoka T, Katayama T (2000). Establishment and characterization of a culture system for enzymatically released rat dental pulp cells. *Calcif Tissue Int* 66(2):139-44.

Yuan ZA, Collier PM, Rosenbloom J, Gibson CW (1996). Analysis of amelogenin mRNA during bovine tooth development. *Arch Oral Biol* 41(2):205-13.

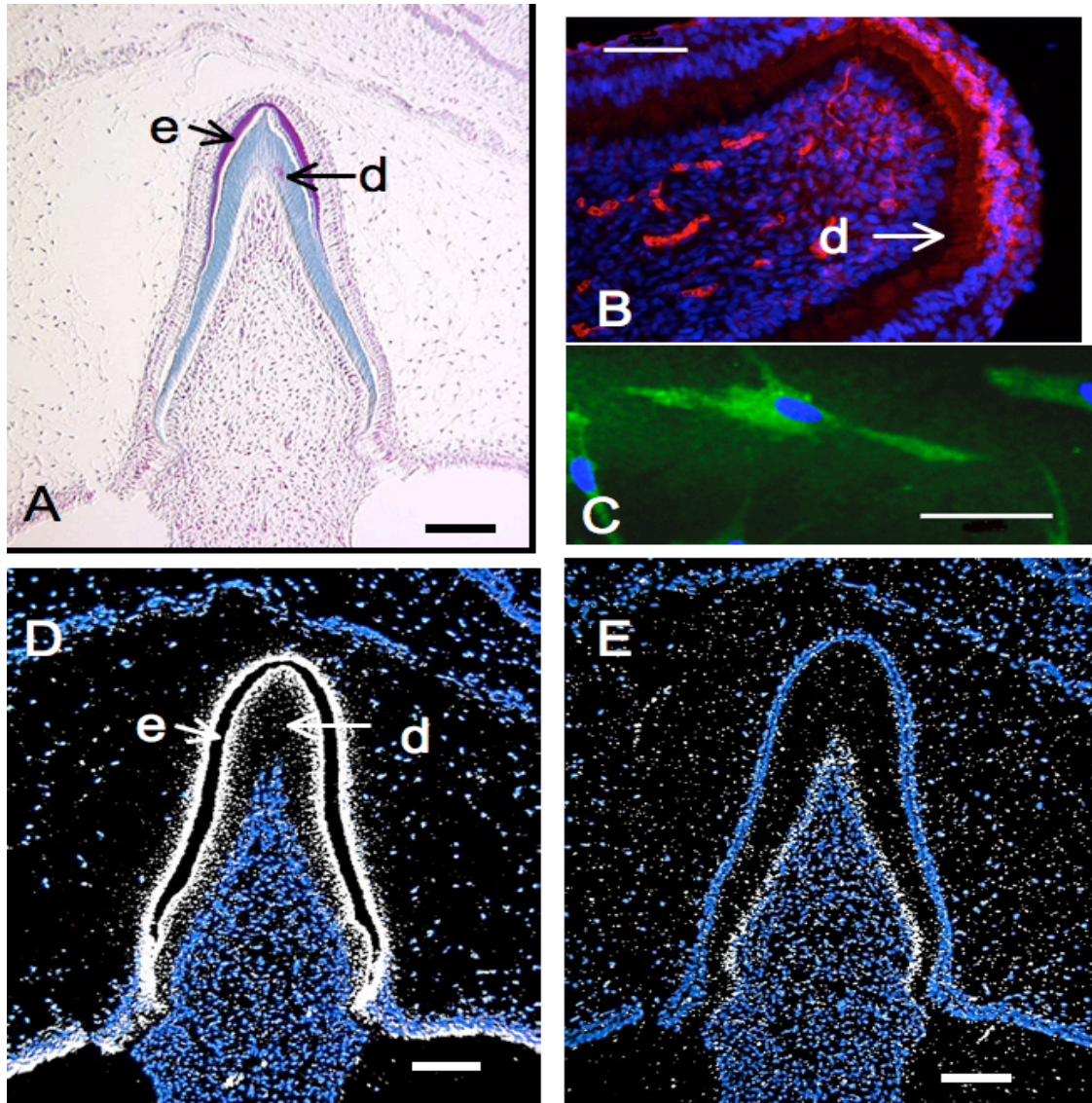


Figure 1.

Amelogenin in human dental pulp tissue.

A) Trichrome stained section of a late bell-stage of tooth organ. B) Amelogenin immunolocalization on a frozen section of an early bell-stage tooth organ shows amelogenin (red) in the forming dentin matrix (d). C) Dental pulp cells grown *in vitro* show positive amelogenin immunostaining (green) in the cytoplasm. D) *In situ* hybridization of amelogenin mRNA on a section of the same tooth as shown in panel A. Positive signal is correlated to the ameloblast cell layer, and the dentin matrix (d), separated by the negative (black) enamel matrix (e). E) Type I collagen *in situ* hybridization shows positive signal in the odontoblast layer lining the forming dentin matrix. Bars = 50 μm .

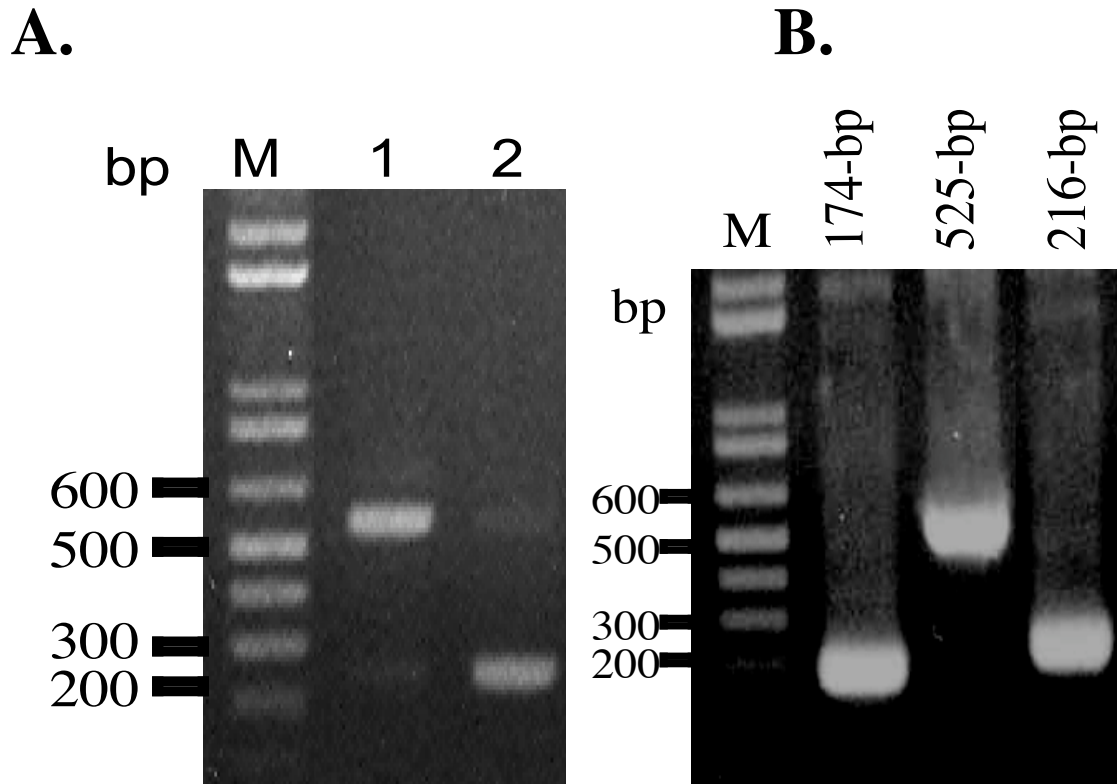


Figure 2.

RT-PCR amplification to detect mRNA of amelogenin spliced variants in dental pulp cells.

A) Polyacrylamide gel (1.5%) contained ethidium bromide showed RT-PCR products as two apparent different bands with sizes of ~216-bp and ~525-bp. Lane 1 and 2 indicated that RT-PCR amplifications were conducted at two separate occasions with different optimization conditions. B) PCR products were randomly subcloned into TOPO-Blunt II vectors (Invitrogen), followed by bacterial transformation and colony screening using PCR amplification. The amplified products of ~174-bp, ~216-bp, ~525-bp bands were visible on gel electrophoresis, and subsequent DNA sequencing showed that they encoded for 3 amelogenin spliced variants: LRAP, LRAP+exon4 and H174 (full-length amelogenin), respectively (DNA sequencing data not shown).

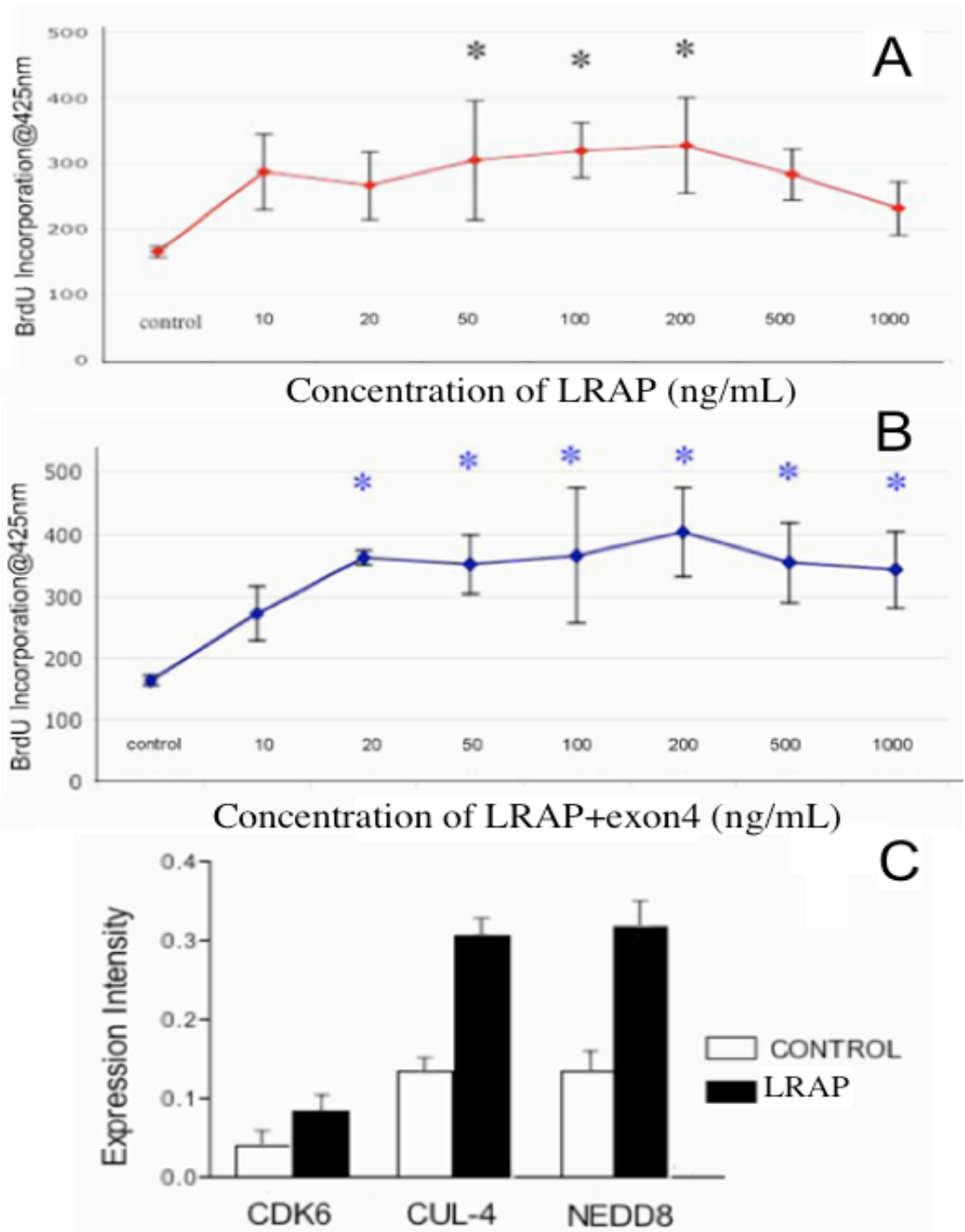


Figure 3.

The effect of amelogenins on dental pulp cell proliferation as measured by BrdU incorporation assay.

(A) Proliferation as measured by BrdU incorporation was significantly increased under the treatment of LRAP at concentrations from 50 to 200 ng/mL, with 200 ng/mL as the

optimal concentration. (B) LRAP+exon4 also enhanced DPC proliferation at concentrations from 20-1000 ng/mL, with 200 ng/mL as optimal. (C) Cell-cycle Superarray™ results showed CKD6, CUL4 and NEDD8 of DPC were up-regulated more than 2 times by LRAP treatment. Results represent the means ± SE. Asterisks show significant differences. *P < 0.05 vs. control. N (for each cell of data) = 3.

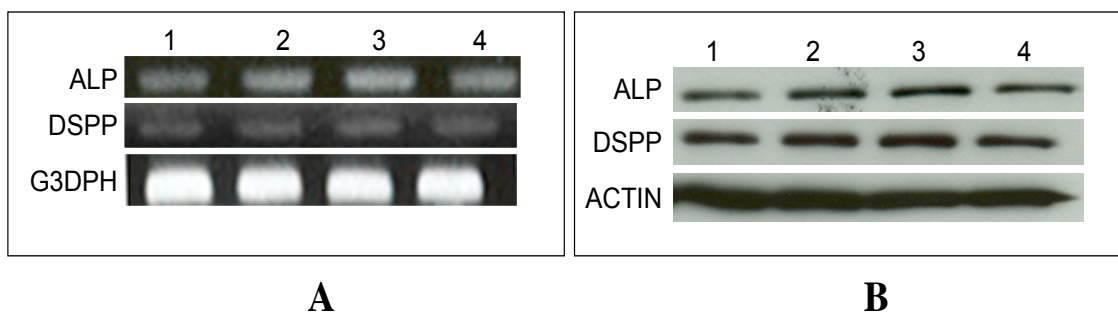


Figure 4.
The effect of amelogenins on dental pulp cell differentiation as measured by alkaline phosphatase (ALP) and dentin sialoprotein (DSP) expression.
 A) RT-PCR to detect ALP and DSP mRNA expression and B) their respective protein syntheses were not altered significantly under the treatments of LRAP (lane 1), LRAP+exon4 (lane 2), or rH174 (lane 3), and control with no added amelogenins (lane 4). ($P > 0.05$).

Chapter 9. Proteolytic Processing of Leucine-rich Amelogenin Peptide and Functional Analysis of Its Proteolytic Products

INTRODUCTION

Amelogenins, secreted by ameloblasts, comprise greater than 90% of the enamel extracellular matrix proteins that function as regulators of enamel biomineralization (Fincham *et al.*, 1999). Amelogenins are categorized into two major groups, high and low-molecular-weight components, ranging in sizes from 5–25 kDa (Fincham *et al.*, 1982). Fincham *et al.* first isolated and characterized leucine-rich amelogenin peptide (LRAP) as one of the principal components of lower-molecular-weight amelogenins (5-6 kDa) in the secretory enamel matrix proteins (Fincham *et al.*, 1981). Using polymerase chain reaction to amplify bovine tooth amelogenin cDNA, Gibson *et al.* showed that the origin of LRAP resulted from alternative splicing of the primary transcript of amelogenin gene (Gibson *et al.*, 1991). LRAP is encoded by exons 2, 3, 5, 6d (3'-end segment of exon 6) and 7, resulting in 58-residue polypeptide, which correspond to the first 33 and the last 25 amino acids of the full-length amelogenin (Fig. 1). Thus, LRAP is identical to the full-length amelogenin at its amino- and carboxyl-termini, but lacks the majority of the central domain encoded by the entire exon 6.

After secretion, a 58-residue precursor LRAP undergoes proteolytic cleavage remove the hydrophilic 11-residue C-telopeptide, yielding a hydrophobic 47-residue polypeptide (Fincham *et al.*, 1981). Similarly, in the enamel matrix, carboxyl-terminal cleavage at the same scissile bond was also detected in the full-length amelogenin (~20 kDa), resulting in

a truncated amelogenin product (~18.7 kDa) (Takagi *et al.*, 1984). The protease that is responsible for the proteolysis of amelogenins was identified as matrix metalloproteinase 20 (MMP-20 or enamelysin) (Fincham *et al.*, 1991; Li *et al.*, 1999; Ryu *et al.*, 1999). It is likely that LRAP might contain other MMP-20 cleavage sites that have not yet been identified.

The C-terminal polypeptide, produced by amelogenin proteolysis, has not been isolated from the enamel matrix, presumably due to its relatively small size (1.3 kDa). Thus, the function of C-terminal domain remains largely elusive. However, there evidence suggests that a synthetic C-terminal polypeptide mediates protein-apatite interaction and potentially functions to inhibit hydroxyapatite crystal growth in simulated secretory enamel fluid (Aoba *et al.*, 1989).

LRAP does not appear to have a major role in enamel crystal growth. Synthetic LRAP failed to promote enamel-like crystal formation *in vitro* (Habelitz *et al.*, 2006). LRAP knock-in has failed to rescue hypoplastic (thin) enamel defect phenotype in amelogenin-null mice (Chen *et al.*, 2003). However, LRAP has been reported to regulate chondrocyte cell proliferation and/or differentiation (Tompkins *et al.*, 2005; Veis *et al.*, 2000; Veis, 2003; Ye *et al.*, 2006).

The observation that LRAP can modulate mesenchymal cell function, suggests a role for this alternatively spliced amelogenin in cell signal transduction. In tooth related cells, LRAP has been demonstrated to regulate cementogenesis (Boabaid *et al.*, 2004). LRAP

can also stimulate dental pulp cell (DPC) proliferation, suggesting that LRAP potentially has important roles in dentinogenesis (chapter 8). However, LRAP function in enamel formation is largely unknown.

In this study, I analyzed MMP-20-mediated proteolysis of LRAP and determined how amelogenin hydrolyzes LRAP. I also completed functional analyses of LRAP and its proteolytic products to interacting with apatites and effecting ameloblast-lineage cell (ALC) function. This study of LRAP proteolysis and its functional analysis provide new insights into the mechanism of LRAP degradation and the functions of its proteolytic products in protein-apatite interaction and cell proliferation and/or differentiation that regulates tooth enamel development.

MATERIALS & METHODS

Expression, purification and characterization of LRAP, sLRAP and activated MMP-20

cDNA's of LRAP and sLRAP (lacking the 3' nucleotide sequence encoded for the last 11 C-terminal residues, STDKTKREEVD, of LRAP) were amplified from a human ameloblast cDNA library, cloned into pGEX-4T-1 vectors (Amersham Biosciences, Piscataway, NJ, USA) and transformed into BL21 (DE3) pLysS competent *E. coli* (Stratagene, La Jolla, CA, USA). The subsequent expression and purification of recombinant LRAP and sLRAP were conducted according to our methods previously published (Le *et al.*, 2006) (chapter 4). Both purified peptides were characterized by SDS-PAGE, Western blot, and reconfirmed by mass spectrometry.

Recombinant bovine MMP-20 was expressed, purified and activated according to methods previously described by our group (Li *et al.*, 1999).

MMP-20 mediated proteolysis of LRAP

LRAP was dissolved in 1X assay buffer (50 mM Tris/HCl, 10 mM CaCl₂, 10 μM ZnCl₂, 150 mM NaCl, pH 7.5). LRAP (200 μl of 29.2 μM) were hydrolyzed by activated MMP-20 (3 μl of 0.4 μg/μl or 8.6 μM) at 37 °C. At specific time points of 0 min, 10 min, 30 min, 1 h, and 3 h, reaction aliquots (25 μl) were collected. The proteolytic LRAP products were run on SDS-PAGE using 10 μl of reaction sample and 10 μl 2X SDS loading buffer per well. The remaining proteolytic samples were analyzed by mass spectrometry.

Properties analyses of LRAP and its MMP-20 mediated proteolytic products

Protein assembly analysis by spectrophotometer

In each well of 96-well plate, activated MMP-20 (5 μl of 4.3 μM) was added into 180 μl of LRAP (19.0 μM) dissolved in 1X assay buffer and incubated at 37 °C for proteolysis. The absorbance (O.D. at λ 340 nm, optimal wavelength) of the digested LRAP was measured at specific time points for a period of 2 h using SpectraMax Plus-384 (Molecular Devices, Sunnyvale, CA, USA). Samples containing either MMP-20 only (no LRAP substrates), or LRAP only (without MMP-20) dissolved in 1X assay buffer were used as controls. Assay buffer only (1X) was used as a blank. All analyses were

done in triplicate ($n = 3$). The data was analyzed using Softmax software 4.7.1 (Molecular Devices). Standard deviations were calculated.

Size analysis using Dynamic Light Scattering (DLS)

DLS analysis of LRAP and its proteolytic products were carried out using a DynaPro MS/X laser photometer molecular sizing instrument equipped with temperature control and a MicroSampler (ProteinSolutions Inc., Charlottesville, VA, USA). An 18- μ l of LRAP (19.0 μ M) dissolved in 1X assay buffer was injected into a chamber quartz cuvette. After DynaPro instrument was blanked with 1X assay buffer and equilibrated to the desired temperature of 25 °C or 37 °C, the hydrodynamic radius R_h (nm) of LRAP were determined at 25 °C and 37 °C in the absence or presence of activated MMP-20 (1 μ l of 2.1 μ M). Approximately 10 to 15 DLS measurements were obtained for each sample to provide adequate data analysis. The collected data were analyzed by Dynamics software version 5.25.44 (ProteinSolutions, Inc., Lakewood, NJ, USA). The results were displayed as the means of hydrodynamic radius, R_h (nm).

LRAP and synthetic carbonated apatite (CAP) interaction

Synthetic CAP was prepared and characterized according to methods previously described (Nelson and Featherstone, 1982). The surface areas of CAP were measured to be 74.68 ± 0.31 m²/g (Micrometrics instrument, Norcross, GA, USA). The C-terminal peptide treated CAP was produced by using synthetic CAP (3 mg) to incubate with excessive amount (\sim 240 μ g) of synthetic C-terminal peptide, STDKTKREEVD, the last 11 C-terminal amino acids of LRAP (GeneScript Corporation, Piscataway, NJ, U.S.A.) in

a final volume of 500 μ l of Tris/HCl (20 mM), pH 7.5, for 2 h at 25 °C, allowing protein-apatite interaction. The C-termini treated CAP was then carefully washed 4 times to remove the unbound peptides and resuspended in 500 μ l of the same Tris/HCl buffer. These C-termini bound CAP and free CAP were used for the subsequent binding experiments with recombinant LRAP and sLRAP.

The C-termini bound CAP (150 μ g) and free CAP (150 μ g) were incubated separately with LRAP (7.65 μ g) or sLRAP (7.65 μ g) in a final volume of 40 μ l of 20 mM Tris/HCl, pH 7.5 for 2 h at 25 °C to facilitate the binding interactions, which were run in triplicate (n=3). After binding, peptide-bound CAP samples were washed 4 times with Tris/HCl (20 mM), pH 7.5 by centrifugation to remove the unbound proteins in the supernatants, while avoiding to disturbing the pellets. The amounts of bound peptides were analyzed using SDS-PAGE and Bradford protein assay kit according to manufacturer's instruction (Bio-Rad Lab, Inc., Hercules, CA, USA). Statistical analysis was done with unpaired t-test with $p < 0.05$ (n=3) to be considered significant, using an InStat software (GraphPad software, Inc., San Diego, CA, USA).

Effects of LRAP on cell proliferation and differentiation

Isolation of ameloblast-lineage cells (ALC)

Human primary ameloblast-lineage cells (ALC) were obtained according to our previously published protocol (Yan *et al.*, 2006). Specifically, the tooth organs were rinsed with phosphate-buffered saline (PBS), followed by digestion with 2 mg/mL collagenase/dispace (Roche, Indianapolis, IN, USA) in PBS for 1 h with continuous

rotation of 35 r.p.m. at 37 °C. The tissue/cell mass was then collected by centrifugation at 1000 r.p.m. for 5 min, washed with PBS, and further digested with STV (0.05% trypsin, 0.025% versene) for 5 min at 37 °C. The cell suspensions were filtered through a 70-µm cell strainer (BD Biosciences, San Jose, CA, USA). The cells were centrifuged, the pellet was washed with PBS, and 1×10^5 cells were plated on a 100-mm Primaria tissue culture dish (Becton Dickinson Labware, Franklin Lakes, NJ, USA). Supplemented keratinocyte growth media 2 (KGM-2) (Cambrex, Walkersville, MD, USA) with 1% penicillin/streptomycin was used to select epithelial-lineage cells. This epithelial-derived cell population was further enhanced by removing fibroblast-like cells using a trypsin-impregnated cloning disc (Scienceware, Savannah, GA, USA). These selected epithelial-derived cells were previously identified as ameloblast-lineage cells (ALC) by immunocytochemistry using cytokeratin-14 and amelogenin antibodies (DenBesten *et al.*, 2005; Yan *et al.*, 2006).

Cell proliferation

In a clear-bottom black 96-well plate (BD Biosciences, Franklin Lakes, NJ, USA), ALC were cultured at a density of 2.5×10^3 cells/well in keratinocyte growth media 2 (KGM-2) (Cambrex) supplemented with 1% penicillin/streptomycin incubated at 37 °C in 5% CO₂. As positive controls for cell proliferation, adult dental pulp cells (DPC) were cultured in Alpha-modified Eagle's Medium (α-MEM) (UCSF Cell Culture Facility, San Francisco, CA, USA) containing 1% penicillin/streptomycin and 10% fetal bovine serum (FBS) (HyClone, Logan, UT, USA) (chapter 8).

At 60% confluence, ALC were synchronized in keratinocyte basal media 2 (KBM-2) (Cambrex) for 16 h. However, dental pulp cells (DPC) were synchronized in α -MEM, supplemented with 2% FBS. To both ALC and DPC cultures, recombinant LRAP, sLRAP and synthetic C-terminal domain were added in triplicate at various final concentrations (0, 10, 30, 90, 180 nM). Cells were maintained in these media for another 24 h, and cell proliferation was measured using an ELISA BrdU-labeling kit (Roche, Indianapolis, IN, USA) according to the manufacturer's instructions. Statistical analyses between groups were performed by ANOVA with Tukey's post-test analysis using GraphPad Prism version 4.0a (GraphPad Software, San Diego, CA, USA).

Cell differentiation

Human fetal primary ameloblast-lineage cells (ALC) were also cultured in glass chamber slides (Lab-Tek, Naperville, IL, USA) in KGM-2 (Cambrex) supplemented with 1% penicillin/streptomycin, incubated at 37 °C in 5% CO₂. At 60% confluence, cells were synchronized in KBM-2 (Cambrex) for 16 h, followed by addition of LRAP, sLRAP and C-terminal peptide to a final concentration of 180 nM per chamber. Cells without any peptide treatment were used as controls. The protein-treated and control cells were incubated for another 24 h at 37 °C. Immunofluorescent staining for amelogenin and Notch1 was conducted for evidence of cell differentiation.

ALC cultured on glass slides were fixed with a mixture of 5% acetic acid and 95% methanol for 30 min at -20 °C. Non-specific binding sites were blocked by incubating samples with 10% horse serum for 1 h, followed by incubation for 1 h at room

temperature with primary antibody against amelogenin and Notch1. Amelogenin antibody (used at 1/1000 dilution) was purified from serum of a rabbit immunized with recombinant human amelogenin by Protein A affinity chromatography. Rabbit anti-human Notch1 (Santa Cruz Biotechnology, Santa Cruz, CA, USA) was purchased and used at 1/100 dilution. After washing to remove unbound primary antibodies, the samples were incubated for another 1 h in the dark with fluorescence-conjugated anti-rabbit IgG-FITC as a secondary antibody (1/500 dilution) (Sigma, St. Louis, MO, USA). The slides were then washed with PBS, and cell nuclei were counterstained with 1 μ g/mL bis-benzimide or Hoechst dye (Molecular Probes, Eugene, OR, USA) for 5 min. After removing the unbound bis-benzimide with PBS, these slides were mounted using SlowFade anti-fading agent (Molecular Probes, Eugene, OR, USA) and observed under a Nikon Eclipse E800 fluorescent microscope and photographed using SimplePCI Version 5.3.1 software (Compix, Cranberry Township, PA, USA).

RESULTS

Characterization of recombinant LRAP and sLRAP

Recombinant LRAP and sLRAP appeared as two bands (\sim 6.8 and 5.5 kDa) in SDS-PAGE (Fig. 2A) and Western blots (Fig. 2B). It should be noted that because thrombin was used to cleavage the GST-LRAP and GST-sLRAP fusion proteins, the resultant two additional residues, Gly and Ser, should be added to the N-terminal of the recombinant peptides. The mass spectrometric results showed that the mass values of LRAP and sLRAP were 6838.68 and 5546.84 Da (Fig. 2C), which matched the theoretical mass of 6838.48 and 5546.85 Da for both proteins, respectively.

Progressive C-terminal proteolysis of LRAP by MMP-20

Proteolytic products of LRAP were analyzed after a time-controlled hydrolysis by MMP-20 over periods of 0 min, 10 min, 30 min, 1 h, and 3 h, at 37 °C . The hydrolysis products showed two distinct bands on SDS-PAGE, at 6.8 kDa and 5.5 kDa, whose Coomassie Blue staining gradually decreased over times (Fig. 3). LRAP incubated without MMP-20 as a control indicated no evidence of LRAP hydrolysis.

Mass spectrometric analysis of the proteolytic products at specific time points showed that LRAP had three identifiable MMP-20 cleavage sites, AWP/STD, DLT/LEA and PLP/PML, which were located very closely to each other (5-7 residues apart) at the C-terminal tail (Table 2). A controlled digestion also revealed that proteolysis of LRAP occurred in a sequence that includes an initial cleavage at AWP/STD, followed by cleavage at DLT/LEA and finally at PLP/PML (Table 2). MMP-20 proteolysis of LRAP at AWP/STD generated the hydrophobic N-terminal peptide known as short LRAP (sLRAP) and the hydrophilic C-terminal peptide of 11 residues. Both sLRAP and C-terminal motif were used in subsequent experiments for their functional analysis.

LRAP proteolytic products enhanced protein assembly and sizes

MMP-20 proteolysis of LRAP resulted in an initial rapid increase of absorbance (λ 340 nm) within the first 20-min of digestion with evidence of solution turbidity due to protein assembly or aggregation (Fig. 4A). Prolonged digestion of LRAP did not result in an eventual decrease in absorbance values, suggesting that the N terminus (the first 34-

residue domain) of proteolytic LRAP was a very stable motif, containing no other MMP-20 cleavage sites. LRAP without MMP-20 was used as background controls, showing no significant changes of turbidity, which remained much lower than proteolytic LRAP throughout the experimental period (Fig. 4A).

The average hydrodynamic radii (R_h) of LRAP were analyzed using DLS analysis. At 25 °C, the average R_h of LRAP was determined to be 104.5 ± 15.1 nm (Fig. 4B). As the temperature increased to 37 °C, R_h of LRAP was also significantly increased to 153.0 ± 28.8 nm. When incubating in the presence of activated MMP-20 at 25 °C and 37 °C, R_h of proteolytic LRAP products were dramatically increased to 222.3 ± 18.9 nm and 325.7 ± 46.9 nm, respectively (Fig. 4B). These results showed that temperature and LRAP proteolytic products ultimately determined the sizes of the protein assembly.

C-terminal domain mediated the binding of LRAP to synthetic carbonated hydroxyapatite (CAP)

The amount of LRAP bound to CAP (23.52 ± 2.98 $\mu\text{g}/\text{mg}$ CAP) was significantly greater than that of LRAP bound to C-terminal peptide pre-treated CAP (5.04 ± 1.54 $\mu\text{g}/\text{mg}$ CAP/C-term), showing an increased binding by 79% (Fig. 5A, B). However, there was no significant difference between the amounts of sLRAP bound to CAP (2.67 ± 1.13 $\mu\text{g}/\text{mg}$ CAP) and C-terminal pre-treated CAP (2.58 ± 0.80 $\mu\text{g}/\text{mg}$ CAP/C-term) (Fig. 5C, D). In a cross comparison, the amount of bound LRAP to CAP was significantly greater than that of bound sLRAP to CAP, showing increased binding by LRAP of more than 88%.

Effects of LRAP and its proteolytic products on ameloblast-lineage cell (ALC) proliferation and/or differentiation

LRAP, sLRAP and synthetic C-terminal peptide at various concentrations (0, 10, 30, 90, 180 nM) were added to human primary ameloblast-lineage cells (ALC). Dental pulp cells (DPC) were used as positive controls for cell proliferation (chapter 8). We found that LRAP, sLRAP and C-terminal domains had no effect on stimulating ameloblast-lineage cell proliferation ($P > 0.05$) (Fig. 6D, E and F). However, both LRAP and sLRAP significantly stimulated dental pulp cell proliferation as positive controls at concentrations greater than 30 nM ($P^* < 0.05$) (Fig. 6A, B). The C-terminal peptide did not enhance DPC proliferation (Fig. C).

Treatment of ALC with LRAP, sLRAP and C-terminal peptide, phase-contrast images showed that LRAP and sLRAP altered cell morphology causing cells to become larger and non-proliferating (Fig. 7A and B) as compared to the control of no peptide-treated smaller cells (Fig. 7D). The C-terminal treated cells (Fig. 7C) did not appear to change cell morphology, retaining their original small cobblestone-like shapes, similar to the control cells.

Immunofluorescent staining showed that ALC treated with LRAP and sLRAP showed much stronger immunoreactivity for amelogenins (cell differentiation marker), localized mainly in the larger, non-proliferating cells (Fig. 7E and F) as compared to immunonegative staining for amelogenin in the control cells (Fig. 7H). The C-terminal

peptide treated cells (Fig. 7G) did not have enhanced amelogenin synthesis, and the undetectable immunostaining for amelogenin was comparable to the control cells.

In contrast, LRAP and sLRAP treatment to ALC decreased immunopositive staining for Notch1 (stem cell marker). Decreased Notch1 immunostaining seemed relating to an increasing numbers of larger cells (Fig. 7I, J). Similar changes were not detected in the C-terminal treated and untreated control cells (Fig. 7K and L).

DISCUSSION

In this study, we analyzed MMP-20 mediated proteolysis of LRAP and the effect of this hydrolysis on protein assembly. The roles of these peptides in enamel formation were further explored by completing functional analyses of LRAP and its proteolytic products (i.e. sLRAP and C-terminal tail) to interacting with apatites and effecting cell functions that regulate tooth enamel development.

The purified recombinant LRAP and sLRAP, characterized by SDS-PAGE, Western blots and mass spectrometry, were found to be similar to the predicted sizes of 6.8 and 5.5 kDa. In Western analysis, a weaker sLRAP showed less immunoreactivity was most likely due to differences in antigenicity of the sLRAP as compared to LRAP.

Incubation of LRAP with active MMP-20 at 37 °C over a 3-h period yielded 2 distinct bands on SDS-PAGE, indicating hydrolysis of LRAP by MMP-20. Mass spectrometric analysis of LRAP proteolytic products showed that LRAP contained a total of three

specific cleavage sites (AWP/STD, DLT/LEA, and PLP/PML) at the C-terminal end of the protein (Table 1). The fact that these three cleavage sites were closely located (only 5-7 residues apart) may explain the reason why only one digested band (~ 5 kDa) appeared on SDS-PAGE following MMP-20 proteolysis of LRAP.

Time-controlled progressive proteolysis revealed that MMP-20 initially hydrolyzed LRAP at AWP/STD, followed by DLT/LEA and finally PLP/PML (Table 1).

Interestingly, AWP/STD and DLT/LEA were rapidly hydrolyzed first by MMP-20 because these scissile bonds are located in a highly hydrophilic charged C-terminal region of LRAP. This result is in agreement with a previous report by Moradian-Oldak *et al.*, indicating that the C-terminal motif of full-length amelogenin was exposed to the surface of amelogenin nanospheres, thus increasing surface accessibility of the proteases (Moradian-Oldak *et al.*, 2001). In fact, these C-terminal proteolytic products were predominantly detected to be in the supernatant portion of the enzymatic reaction solution, supporting the hydrophilic properties of the C terminus (data not shown).

Scissile bonds AWP/STD and DLT/LEA of human LRAP are equivalent to those previously identified cleavage sites (AWP/ATD and ELP/LEA) in full-length porcine and mouse amelogenins (Ryu *et al.*, 1999). Only prolonged MMP-20 proteolysis (> 1 h) resulted in cleavage of PLP/PML, a novel cleavage site, whose significance is currently unknown. I hypothesize that the delayed digestion of PLP/PML maybe because this cleavage site is located in a much more hydrophobic region than the locations of the other two scissile bonds (AWP/STD and DLT/LEA), thus inhibiting accessibility of MMP-20.

Turbidity measurements supported the evidence of that LRAP hydrolysis products aggregate in solution. Proteolysis of LRAP by MMP-20 resulted in a rapid increase turbidity or absorbance within the initial 20-min of digestion and then plateaued. This suggests that proteolytic LRAP underwent an initial protein assembly or aggregation, mediated by hydrophobic-hydrophobic interaction between the N-terminal proteolytic fragments after cleaving the hydrophilic C-terminal tails. This observation was supported by the evidence that the C-terminal truncated amelogenin formed significantly larger nanospheres than the full-length amelogenin precursors via hydrophobic interaction (Moradian-Oldak *et al.*, 2002).

Prolonged proteolysis of LRAP for nearly 2 h did not result in a significant decrease in absorbance values. This suggests that the N-terminal domain (the first 34-residue fragment), resulting from sequential cleaving of AWP/STD, DLT/LEA and PLP/PML, formed stable proteolytic products that may contain no additional MMP-20 cleavage sites. Besides the 3 cutting sites identified in the C-terminal region, mass spectrometric analysis of LRAP proteolytic products revealed no additional MMP-20 cleavage sites in this N-terminal domain.

DLS data revealed that changing the temperature from 25 °C to 37 °C increased the average R_h of LRAP from 104.5 ± 15.1 nm to 153.0 ± 28.2 nm, respectively.

Temperature appeared to have a significant effect on protein assembly of LRAP, stimulating larger protein-complex formation. However, the average R_h values reported

in this study were greater than those values of full-length mouse and porcine amelogenins (rM179 $R_h = 22.9 \pm 8.8$ nm, rP172 $R_h = 13 \pm 2.1$ nm) in a previous report (Moradian-Oldak *et al.*, 2002).

These differences in the values of R_h between our study that that of Moradian-Oldak *et al.* (Moradian-Oldak *et al.*, 2002) could be because LRAP and the full-length amelogenins were studied in different buffer conditions. In our study, LRAP was dissolved in 1X assay buffer (50 mM Tris-HCl, pH 7.5, 10 mM CaCl_2 , 10 μM ZnCl_2 , 150 mM NaCl), which was necessary for MMP-20 enzymatic activity. Ca^{2+} ions have been shown to interact directly LRAP via its C-terminal domain (Le *et al.*, 2006) (chapter 6). Based on this collective evidence, I propose that the divalent Ca^{2+} ions might enhance protein-complex formation by acting as ionic salt bridges, linking amelogenins together via the charged C-terminal domains to form the larger aggregates reported in this study.

During early proteolysis (the initial 5- to 10-min) of LRAP at 25 °C and 37 °C, the average R_h of digested LRAP were dramatically increased to 222.3 ± 18.9 nm and 325 ± 46.9 nm, respectively. Increase the average R_h values is the result of aggregation of proteolytic LRAP products, facilitated by N-terminal hydrophobic interaction. This observation was also supported by the turbidity data during the very early linear phase of increase absorbance. It is important to emphasize that the DLS analysis of proteolytic LRAP could not be performed under a prolonged proteolysis because the large protein aggregates prevented the accurate measurements of DLS. Thus, the scattering light would be operationally out-of-range for detection.

LRAP and carbonated hydroxyapatite (CAP) binding experiments definitively showed that LRAP interacts with apatites by the C-terminal motif, suggesting LRAP functions in matrix-mediated enamel biomineralization. Although using different experimental approaches, C-terminal domain-apatite interaction results of this study were similar with those of previous reports (Aoba *et al.*, 1989; Shaw *et al.*, 2004). The C-terminal motif has been demonstrated to inhibit mineralization *in vitro*, suggesting its role as a negative regulator of enamel crystal growth (Aoba *et al.*, 1989). Even though LRAP can bind directly to apatites, LRAP failed to stimulate enamel-like crystal formation when incubated in simulated secretory enamel fluid in the presence of fluoroapatite substrates (Habelitz *et al.*, 2006). An *in vivo* study reported that LRAP knock-in has failed to rescue the hypoplastic enamel defect of amelogenin-null mice; however, this study did not report any changes at cellular levels (Chen *et al.*, 2003). Thus, LRAP appears to have no enamel structural implications. This negative result leads me to investigate the function of LRAP and its proteolytic products as cell signaling molecules.

In this subsequent portion of this study, I showed that LRAP acts as a cell-signaling molecule to effect cell functions. The ability of LRAP and its proteolytic products (i.e. sLRAP and C-terminal motif) to stimulate odontogenic cell proliferation and/or differentiation *in vitro* was investigated. When adding LRAP, sLRAP or C-terminal domain to ameloblast-lineage cell (ALC) cultures, cell proliferation was not enhanced, though similar amounts of LRAP and sLRAP did stimulate dental pulp cell (DPC) proliferation. There was no effect of the C-terminal motif on cell proliferation.

In chapter 8, I showed that LRAP significantly stimulated DPC proliferation by up-regulating cell-cycle related genes (CDK6, CUL4 and NEDD8), which together accelerated cell cycle progression to stimulate cell division. In the presence of LRAP and sLRAP, ameloblast-lineage cells became larger and non-proliferating, coupled with increasing amelogenin, but decreasing Notch1 synthesis as compared to their untreated controls, suggesting that LRAP may function to control ALC differentiation. C-terminal motif treatment had no significant effects on alteration of cell morphology and synthesis of differentiation markers.

This study was the first to report the function of LRAP in stimulating ALC differentiation, suggesting that LRAP also plays critical roles in regulation of amelogenesis. Based on the ability of LRAP and sLRAP to stimulate ALC differentiation and DPC proliferation, I suggest that the biologically active site responsible for cellular effects is located in the N-terminal domain of LRAP. I propose that LRAP functions through its receptor, LAMP-1, which was identified in mesenchymal-derived mouse myoblasts (Tompkins *et al.*, 2006).

In summary, LRAP and its N-terminal proteolytic product sLRAP can stimulate DPC proliferation and ALC differentiation, suggesting their important functions in dentinogenesis and amelogenesis. LRAP appears to have little effect on crystal growth within the enamel matrix, though when it is hydrolyzed, LRAP forms large aggregates with sLRAP as the functional unit. This sLRAP, which forms a large insoluble protein

complex, may have a role in cell signaling at the dentinal enamel junction, as ameloblast differentiation is initiated. Additional studies to determine the specific down-stream signaling pathways that control cell proliferation and differentiation processes require further investigation.

REFERENCES

- Aoba T, Moreno EC, Kresak M, Tanabe T (1989). Possible roles of partial sequences at N- and C-termini of amelogenin in protein-enamel mineral interaction. *J Dent Res* 68(9):1331-6.
- Boabaid F, Gibson CW, Kuehl MA, Berry JE, Snead ML, Nociti FH, Jr., Katchburian E, Somerman MJ (2004). Leucine-rich amelogenin peptide: a candidate signaling molecule during cementogenesis. *J Periodontol* 75(8):1126-36.
- Chen E, Yuan ZA, Wright JT, Hong SP, Li Y, Collier PM, Hall B, D'Angelo M, Decker S, Piddington R, Abrams WR, Kulkarni AB, Gibson CW (2003). The small bovine amelogenin LRAP fails to rescue the amelogenin null phenotype. *Calcif Tissue Int* 73(5):487-95.
- DenBesten PK, Machule D, Zhang Y, Yan Q, Li W (2005). Characterization of human primary enamel organ epithelial cells in vitro. *Arch Oral Biol* 50(8):689-94.
- Fincham AG, Belcourt AB, Termine JD, Butler WT, Cothran WC (1981). Dental enamel matrix: sequences of two amelogenin polypeptides. *Biosci Rep* 1(10):771-8.
- Fincham AG, Belcourt AB, Lyaruu DM, Termine JD (1982). Comparative protein biochemistry of developing dental enamel matrix from five mammalian species. *Calcif Tissue Int* 34(2):182-9.
- Fincham AG, Hu Y, Lau EC, Slavkin HC, Snead ML (1991). Amelogenin post-secretory processing during biomineralization in the postnatal mouse molar tooth. *Arch Oral Biol* 36(4):305-17.
- Fincham AG, Moradian-Oldak J, Simmer JP (1999). The structural biology of the developing dental enamel matrix. *J Struct Biol* 126(3):270-99.
- Gibson CW, Golub E, Ding WD, Shimokawa H, Young M, Termine J, Rosenbloom J (1991). Identification of the leucine-rich amelogenin peptide (LRAP) as the translation product of an alternatively spliced transcript. *Biochem Biophys Res Commun* 174(3):1306-12.

Habelitz S, Denbesten PK, Marshall SJ, Marshall GW, Li W (2006). Self-assembly and effect on crystal growth of the leucine-rich amelogenin peptide. *Eur J Oral Sci* 114 Suppl 1(315-9).

Le TQ, Gochin M, Featherstone JD, Li W, Denbesten PK (2006). Comparative calcium binding of leucine-rich amelogenin peptide and full-length amelogenin. *Eur J Oral Sci* 114 Suppl 1(320-6).

Li W, Machule D, Gao C, DenBesten PK (1999). Activation of recombinant bovine matrix metalloproteinase-20 and its hydrolysis of two amelogenin oligopeptides. *Eur J Oral Sci* 107(5):352-9.

Moradian-Oldak J, Jimenez I, Maltby D, Fincham AG (2001). Controlled proteolysis of amelogenins reveals exposure of both carboxy- and amino-terminal regions. *Biopolymers* 58(7):606-16.

Moradian-Oldak J, Bouropoulos N, Wang L, Gharakhanian N (2002). Analysis of self-assembly and apatite binding properties of amelogenin proteins lacking the hydrophilic C-terminal. *Matrix Biol* 21(2):197-205.

Nelson DG, Featherstone JD (1982). Preparation, analysis, and characterization of carbonated apatites. *Calcif Tissue Int* 34 Suppl 2(S69-81).

Ryu OH, Fincham AG, Hu CC, Zhang C, Qian Q, Bartlett JD, Simmer JP (1999). Characterization of recombinant pig enamelysin activity and cleavage of recombinant pig and mouse amelogenins. *J Dent Res* 78(3):743-50.

Shaw WJ, Campbell AA, Paine ML, Snead ML (2004). The COOH terminus of the amelogenin, LRAP, is oriented next to the hydroxyapatite surface. *J Biol Chem* 279(39):40263-6.

Takagi T, Suzuki M, Baba T, Minegishi K, Sasaki S (1984). Complete amino acid sequence of amelogenin in developing bovine enamel. *Biochem Biophys Res Commun* 121(2):592-7.

Tompkins K, Alvares K, George A, Veis A (2005). Two related low molecular mass polypeptide isoforms of amelogenin have distinct activities in mouse tooth germ differentiation in vitro. *J Bone Miner Res* 20(2):341-9.

Tompkins K, George A, Veis A (2006). Characterization of a mouse amelogenin [A-4]/M59 cell surface receptor. *Bone* 38(2):172-180.

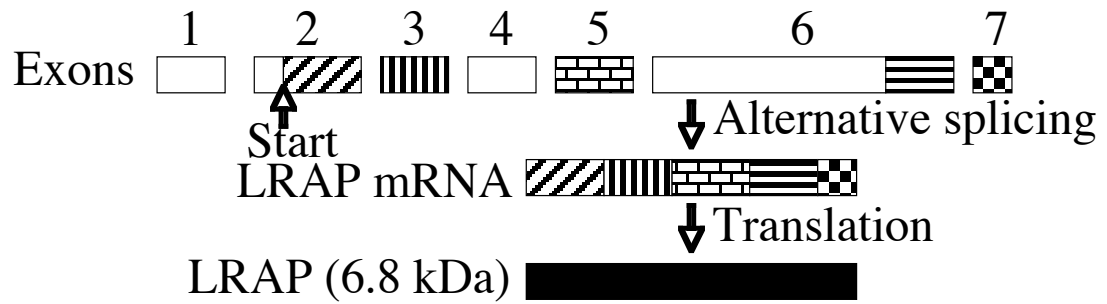
Veis A, Tompkins K, Alvares K, Wei K, Wang L, Wang XS, Brownell AG, Jengh SM, Healy KE (2000). Specific amelogenin gene splice products have signaling effects on cells in culture and in implants in vivo. *J Biol Chem* 275(52):41263-72.

Veis A (2003). Amelogenin gene splice products: potential signaling molecules. *Cell Mol Life Sci* 60(1):38-55.

Yan Q, Zhang Y, Li W, Denbesten PK (2006). Differentiation of human ameloblast-lineage cells in vitro. *Eur J Oral Sci* 114 Suppl 1(154-8).

Ye L, Le TQ, Zhu L, Butcher K, Schneider RA, Li W, Besten PK (2006). Amelogenins in human developing and mature dental pulp. *J Dent Res* 85(9):814-8.

Amelogenin mRNA



MPLPPHPGHPGYINFSYEVLTPKWKYQSIRPPPLP
PMLPDLTLEAWPSTDKTKREEVD (LRAP sequence)

Figure 1.

Alternatively spliced pattern of human LRAP and its amino acid sequence.

LRAP is encoded by exons 2, 3, 5, 6d and 7, resulting in a 58-residue alternatively spliced peptide, whose amino acid sequence is identical to the first 33 and the last 25 residues of the full-length amelogenin.

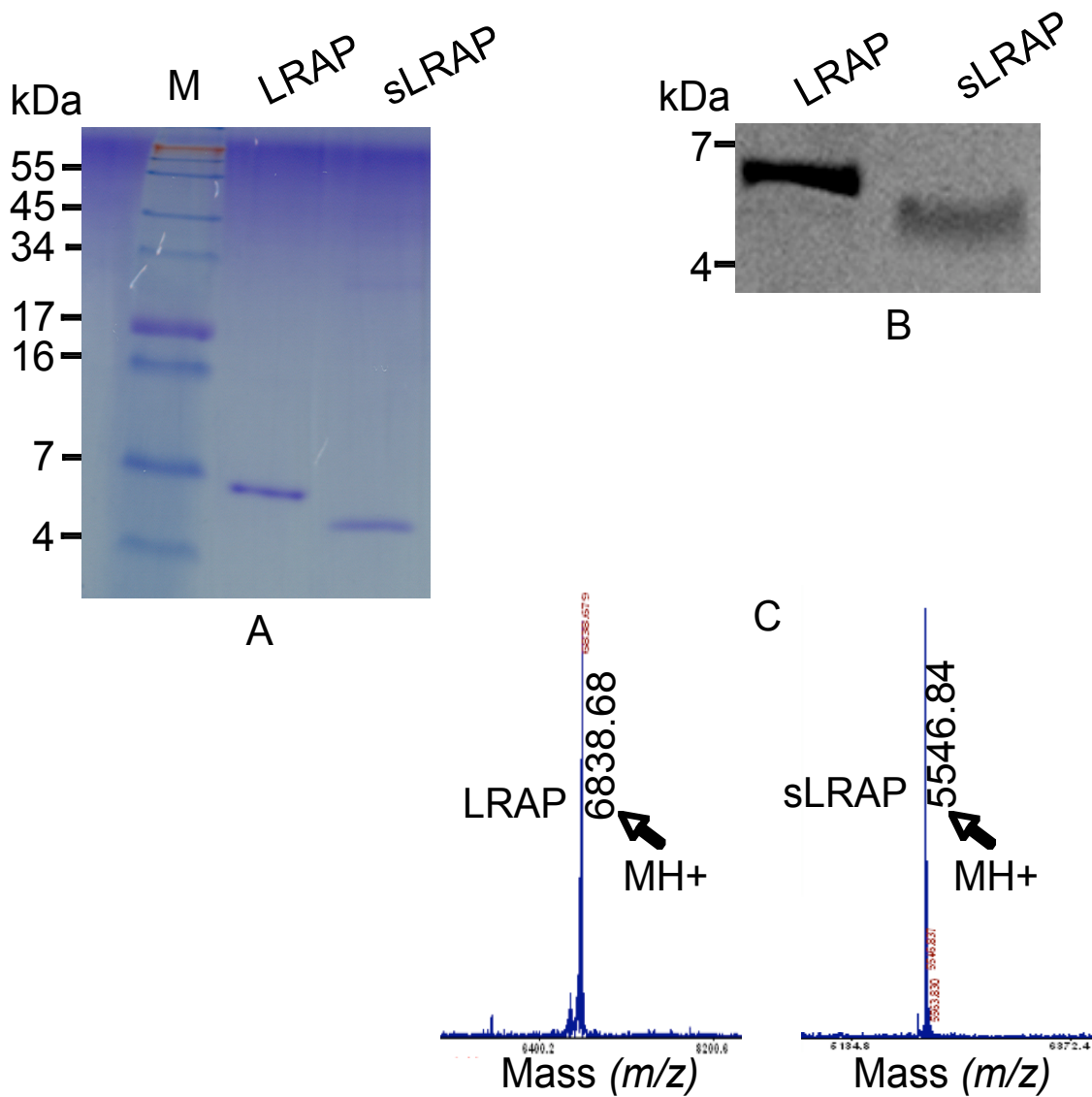


Figure 2.

Characterization of purified LRAP and C-terminal truncated or short LRAP (sLRAP).

A) SDS-PAGE analysis LRAP and sLRAP, showing ~ 6.8 kDa and ~ 5.5 kDa, respectively. B) Western blot to confirm the identities of purified LRAP and sLRAP. M, SeeBlue Plus2 marker standard (Invitrogen). C) Ion-spray mass spectrometry of LRAP and sLRAP.

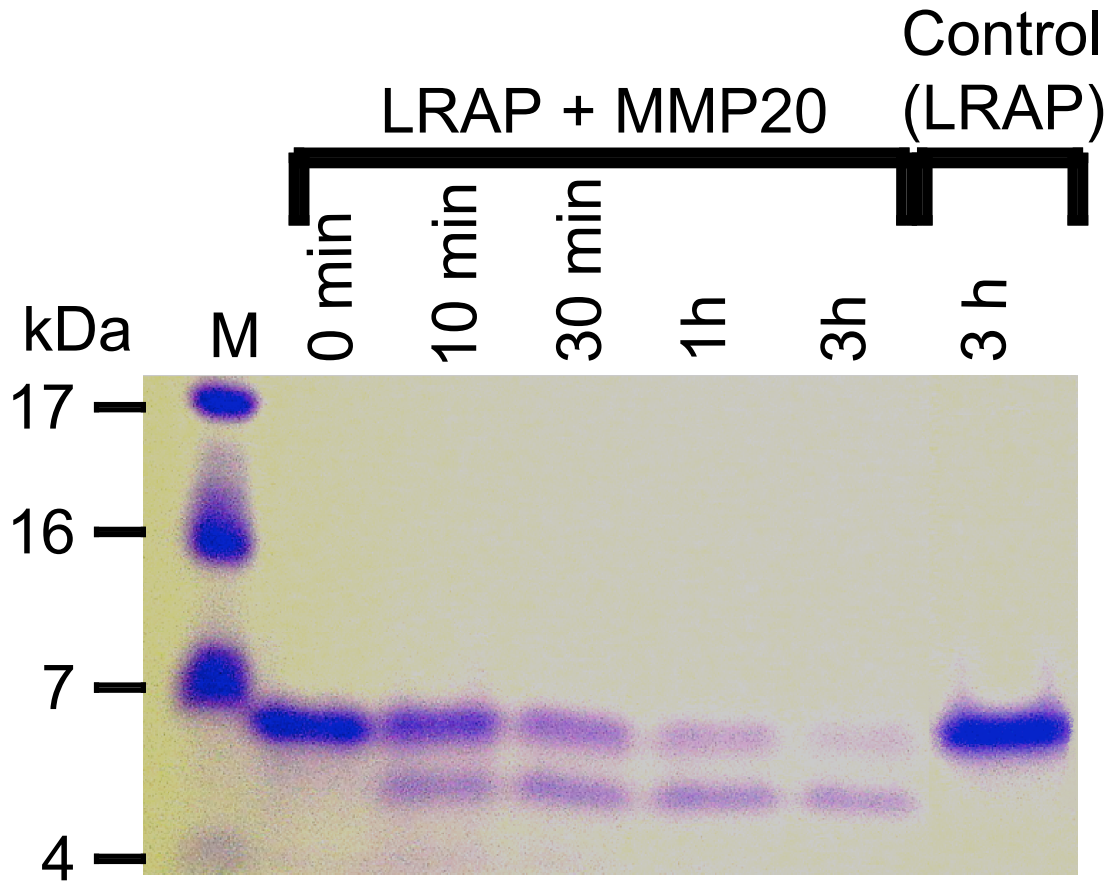


Figure 3.

MMP-20 mediated progressive proteolysis of LRAP.

LRAP was digested by activated MMP-20 over a time course of 0 min, 10 min, 30 min, 1 h, and 3 h. The proteolytic products of LRAP were analyzed on SDS-PAGE, indicating that LRAP was a specific substrate of MMP-20. LRAP incubated for 3 h without the protease as a control indicated no evidence of proteolysis.

MPLPPHPGHPGYINFSYEVLTPWKWYQSIRPPPLP PMLP
 DLT LEAWP STDKTKREEVD

Cleavage sites	Time of cleavage-site 1 st detected	Measured N-term (m/z) Da	Measured C-term (m/z) Da	Predicted N-term (m/z) Da	Predicted C-term (m/z) Da
AWP/STD	0-10 min	5546.89	1307.67	5546.85	1307.64
DLT/LEA	10-60 min	4950.65	1904.89	4950.55	1903.94
PLP/PML	> 1 h	4187.01	2674.26	4185.91	2673.03

Table 1.

Mass spectrometry analysis of a time-controlled progressive proteolysis of LRAP.

After MMP-20 mediated progressive proteolysis, LRAP was analyzed by mass spectrometry, showing that LRAP contained 3 specific MMP-20 cleavage sites closely located at the C-terminal tail. These scissile bonds were sequentially cleaved at AWP/STD, DLT/LEA and PLP/PML.

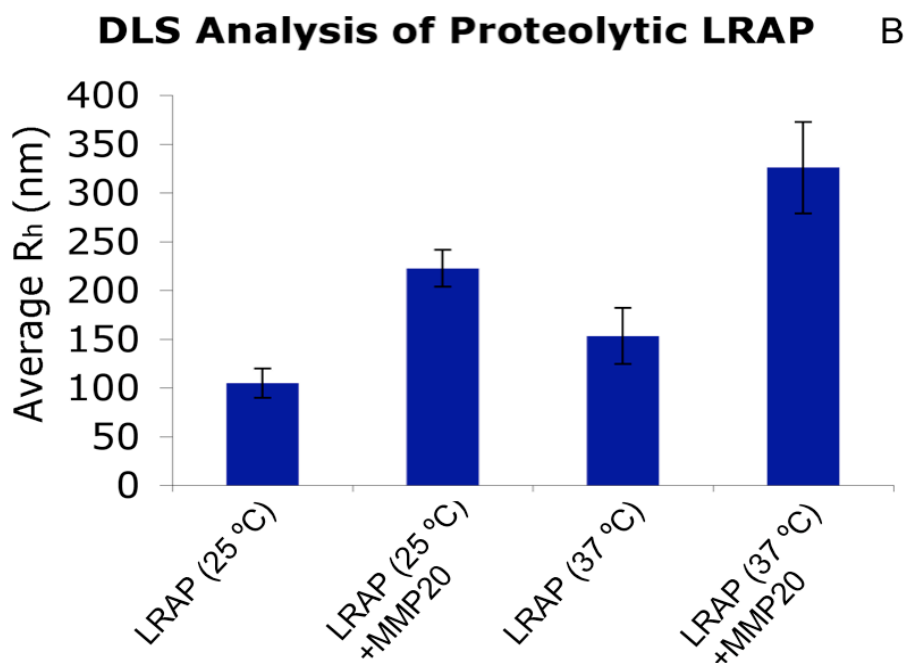
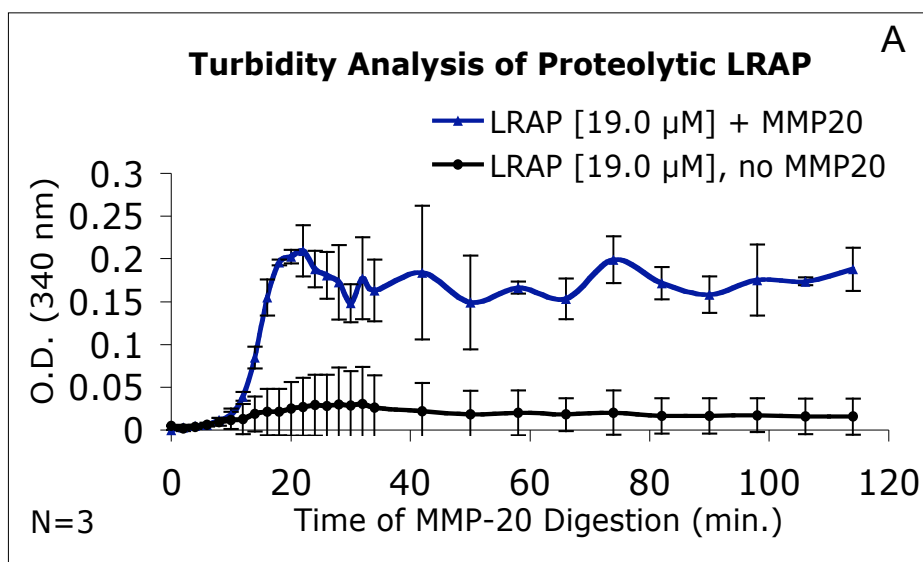


Figure 4.

LRAP proteolytic products enhanced protein assembly and sizes.

A) Turbidity measurement (absorbance at λ 340 nm) of progressive proteolysis of LRAP at 37 °C over 2-h period showed increase absorbance or turbidity during the initial 20-min of digestion, then plateau. The control (LRAP without MMP-20) did not result in any significant increase in turbidity. B) Dynamic light scattering (DLS) analysis of LRAP showed that increasing temperature from 25 °C to 37 °C induced protein assembly, indicated by increasing R_h (nm) of LRAP. MMP-20 mediated proteolysis of LRAP at 25 °C and 37 °C further enhanced protein aggregate formation.

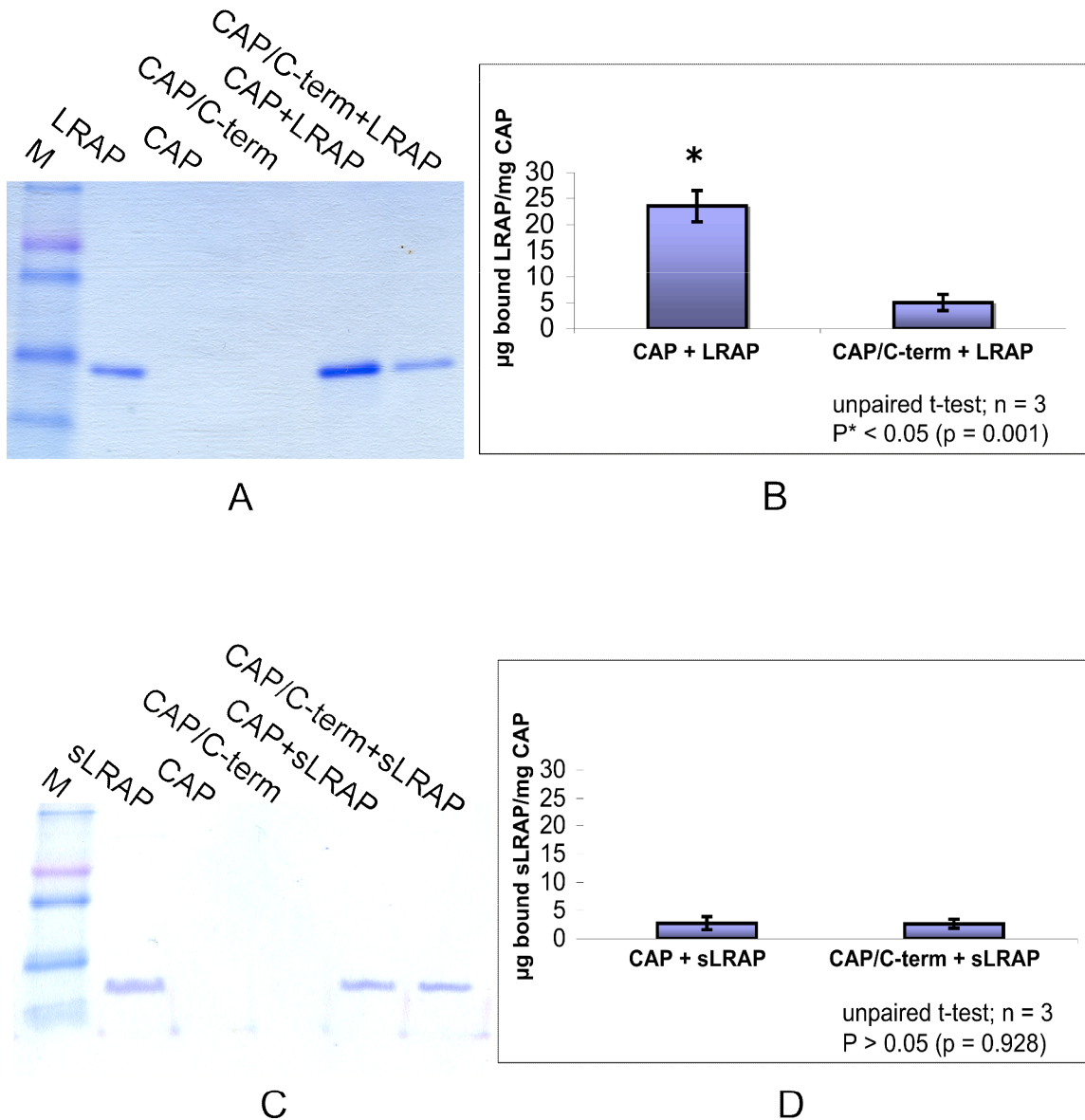


Figure 5.

C-terminal motif mediated the binding of LRAP to CAP.

A) SDS-PAGE of bound LRAP to CAP and C-terminal pre-treated CAP. B) Quantification of the amount of bound LRAP to CAP and C-terminal pre-treated CAP. Results represented the mean \pm S.E. and $P^* < 0.05$, showing significant difference. C) SDS-PAGE to visualize the amount of bound sLRAP to CAP and C-terminal pre-treated CAP. D) Quantification of the amount of bound sLRAP to CAP and C-terminal pre-treated CAP. Results represented the mean \pm S.E. and $P > 0.05$, showing no significant difference.

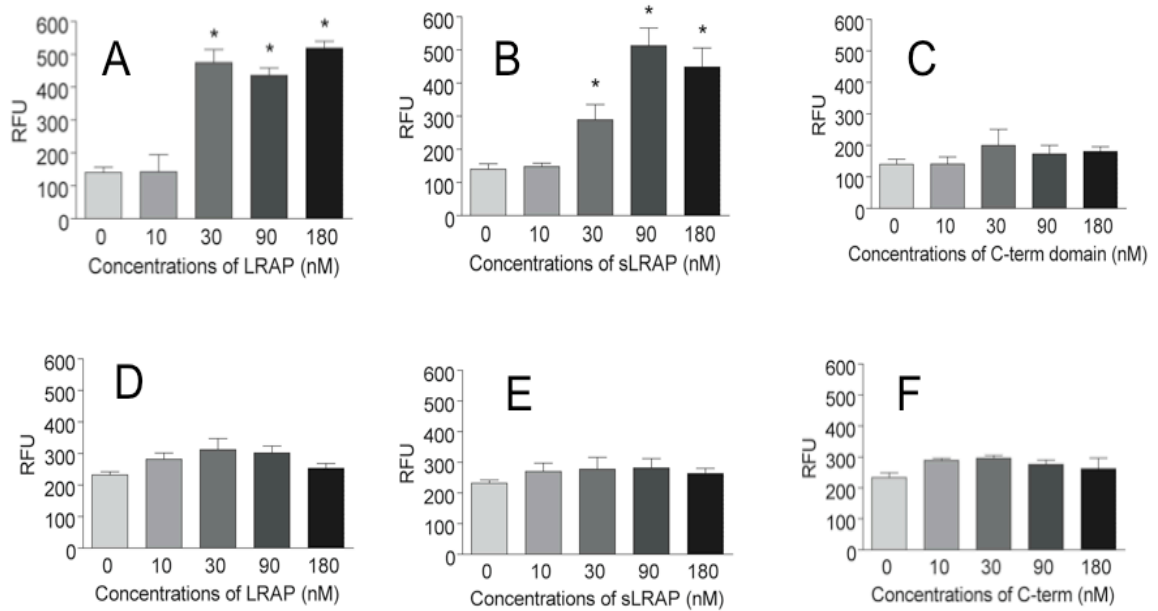


Figure 6.

LRAP and its proteolytic products (sLRAP and C-terminal peptide) significantly stimulated dental pulp cell (DPC) proliferation, but had no effects on ameloblast-lineage cell (ALC) proliferation.

A) LRAP, B) sLRAP at different concentrations (0, 10, 30, 90, 180 nM) were added to dental pulp cells (DPC) as positive controls significantly stimulated DPC proliferation ($P^* > 0.05$); however, C) C-terminal peptide failed to enhanced DPC proliferation. In the experimental samples using similar peptide treatments to ALC indicated that D) LRAP, E) sLRAP and F) C-terminal peptide had no effects on ALC proliferation ($P > 0.05$). (*) Asterisk indicates statistical significant difference as compared to the untreated control cells.

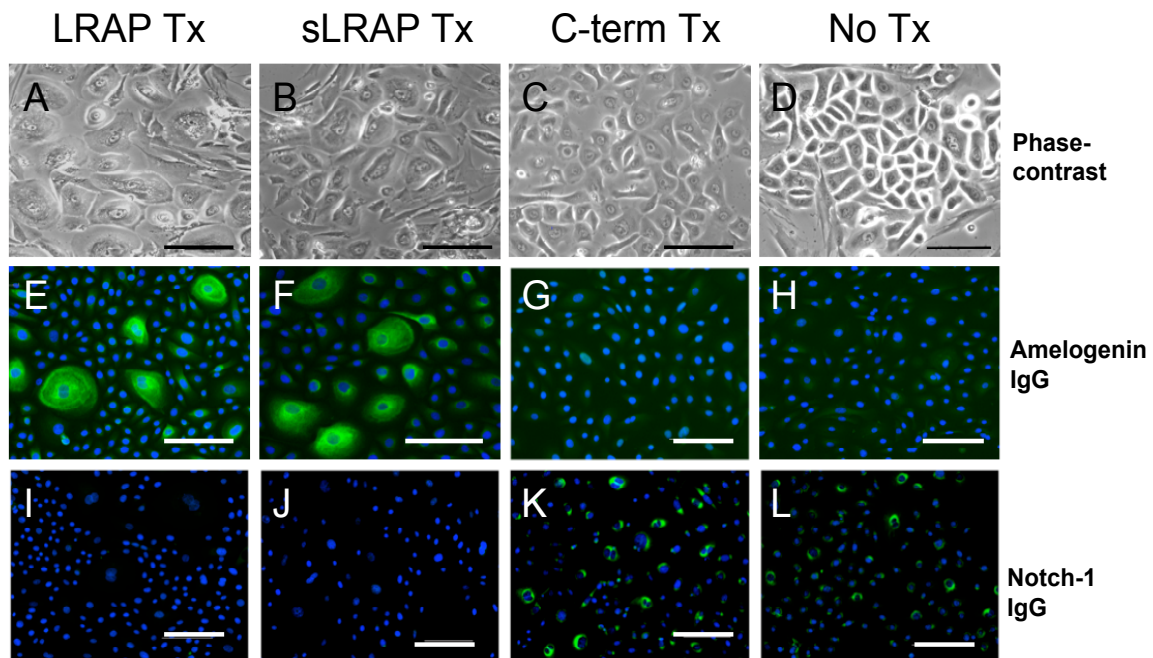


Figure 7.

LRAP and sLRAP treatments altered ALC morphology and stimulated cell differentiation.

Phase-contrast images showed that under the treatment of LRAP (A) and sLRAP (B), ALC became rounded, larger and non-proliferating. The C-terminal domain treatment (C) did not change cell morphology, retaining similar shapes as the control non-treated cells (D). LRAP and sLRAP treated ALC increased immunopositive staining for amelogenin (E and F), but decreased immunostained for Notch-1 (I and J) as compared to their corresponding untreated controls stained with similar antibodies (H and L). The C-terminal peptide treated ALC (G and K) resulted in similar immunostaining for amelogenin and Notch-1 as that observed in the untreated controls (H and L). Bars = 50 μm .

Chapter 10: The Effect of Leucine-rich Amelogenin Peptide on Ameloblast-lineage Cell Differentiation

INTRODUCTION

Leucine-rich amelogenin peptide (LRAP) was first isolated and characterized as one of the principal components of lower-molecular-weight amelogenins (5-6 kDa) in the secretory enamel matrix proteins (Fincham *et al.*, 1981). LRAP was identified as a 58-residue peptide generated by alternative splicing of amelogenin pre-mRNA. LRAP is identical to the full-length amelogenin at its amino and carboxyl termini, but lacks a majority of exon-6-coded segment found in the central region of the full-length protein (Gibson *et al.*, 1991). The precise function of LRAP in enamel formation is still unknown.

LRAP cDNA is detected in rat odontoblasts, and the peptide can be extracted from mineralized dentin (Veis *et al.*, 2000). In studies by Veis and Tompkins (Tompkins and Veis, 2002; Tompkins *et al.*, 2005; Veis *et al.*, 2000; Veis, 2003), LRAP was identified as a chondrogenic and osteogenic promoting factor, suggesting its role in mesenchymal cell signaling. We reported that LRAP can stimulate dental pulp cell proliferation *in vitro* (Ye *et al.*, 2006). More recently, cell-surface receptors of LRAP have been identified and characterized in mesenchymal-derived mouse myoblasts as lysosome-associated membrane protein 1 (LAMP-1) (Tompkins *et al.*, 2006).

A study of mouse epithelial-derived mammary cells (HC11 cells) demonstrated that LAMP-1 is a novel differentiation marker. Specifically, there was a significant increase of LAMP-1 in HC11 cells following the treatment of lactogenic hormones (i.e. glucocorticoids) (Cella *et al.*, 1996). Upregulation of lysosomal-associated membrane glycoproteins may function in cellular remodeling, which is a major hallmark of cell differentiation (Cella *et al.*, 1996). In addition, upregulated LAMP-1 expression in human keratinocytes is also strongly associated with cell differentiation (Sarafian *et al.*, 2006). In contrast, the molecular signal Notch1 has been shown to regulate the maintenance of dental epithelial stem cells in the cervical loop of continuously growing mouse incisor (Harada *et al.*, 1999; Harada and Ohshima, 2004).

In these studies, we used LAMP-1 and Notch1 to track changes in differentiation of ALC, and propose that LRAP may function to regulate ameloblast differentiation. This study provides new insights into the effect of LRAP on the synthesis of proteins that control the process of ameloblast differentiation, regulating tooth enamel formation.

MATERIALS & METHODS

Expression, purification and characterization of LRAP

Expression and purification of human recombinant LRAP was conducted according to our methods previously published (Le *et al.*, 2006). Briefly, LRAP cDNA was amplified from a human ameloblast cDNA library, cloned into a vector pGEX-4T-1 (Amersham Biosciences, Piscataway, NJ, USA) and transformed into BL21 (DE3) pLysS competent *E. coli* (Stratagene, La Jolla, CA, USA). After synthesis of recombinant LRAP by *E. coli*,

LRAP fusion protein was purified using an affinity column of glutathione Sepharose beads (Amersham Biosciences), and LRAP was eluted after cleaving the glutathione S-transferase (GST)-tag by thrombin (Amersham Biosciences). LRAP was further purified by reverse-phase HPLC on a C18 column (Varian, Lake Forest, CA, USA) and eluted with a gradient of acetonitrile + 0.1% trifluoroacetic acid (TFA). The purified LRAP was characterized by SDS-PAGE, Western blots and mass spectrometry.

Localization of LAMP-1 in human enamel organ

Tooth organs were obtained from 21-week old human fetal tissue, which was embedded in optimal cutting temperature (O.C.T) compound (Tissue-Tek, Hatfield, PA, USA) within 3 h of collection, frozen in a mixture of dry ice/2-methylbutane and cryo-sectioned for immunocytochemistry. Tissue collection was conducted according to guidelines and approval of the University of California San Francisco (UCSF) committee on human research. Frozen tissue sections were fixed with a mixture of 5% acetic acid and 95% methanol for 30 min at -20°C . Non-specific binding sites were blocked by incubating samples with 10% horse serum for 1 h, followed by incubation for 1 h at room temperature with primary antibody against LAMP-1 (rabbit anti-human LAMP-1 immunoglobulin, 1/500 dilution) (Abcam, Cambridge, MA, USA). After washing to remove unbound primary antibodies, the samples were incubated for another 1 h in the dark with fluorescence-conjugated anti-rabbit IgG-FITC as a secondary antibody (1/500 dilution) (Sigma, St. Louis, MO, USA). The slides were then washed with PBS, and cell nuclei were counterstained with 1 $\mu\text{g}/\text{mL}$ bis-benzimide or Hoechst dye (Molecular Probes, Eugene, OR, USA) for 5 min. After removing the unbound dyes with PBS, these

slides were mounted using SlowFade anti-fading agent (Molecular Probes, Eugene, OR, USA) and observed under a Nikon Eclipse E800 fluorescent microscope and photographed using SimplePCI Version 5.3.1 software (Compix, Cranberry Township, PA, USA).

RT- PCR for LAMP-1 expression in ameloblast-lineage cells (ALC)

Human primary ameloblast-lineage cells (ALC) were isolated from the remaining fetal tooth organs and selectively cultured in keratinocyte growth media (KGM-2) (Cambrex, Walkerville, MD, USA), according to our methods described previously (Yan *et al.*, 2006). The detailed method for isolation of ameloblast-lineage cells was also described in chapter 9.

ALC were plated in 100-mm Primaria tissue culture dishes (Becton Dickinson Labware, Franklin Lakes, NJ, USA). At 60% confluence, total RNA was isolated from ALC cultures using RNeasy Mini Kit (Qiagen, Valencia, CA, USA). The purified total RNA (3 μ g) was used for reverse-transcription (RT) using an oligo-dT primer according to SuperScript II RT kit (Invitrogen), followed by PCR in 50- μ l reaction tubes: 30 μ l H₂O, 5 μ l 10X PCR buffer, 1.5 μ l of 50 mM MgCl₂, 1 μ l of 10 mM dNTP, 0.5 μ l Taq polymerase, 2 μ l DNA template, 5 μ l sense primer, and 5 μ l anti-sense primer. A pair of primers (a sense primer 5'-CCTCATCGTCCTCATCGCCTA-3' and an anti-sense primer 5'-CTCAGAGACAGCGGCATTCCA-3') was used for amplification of a segment of LAMP-1 cDNA, resulting in 513-bp PCR product. Human enamel organ cDNA library (2 μ l) was used as a positive control, while 2 μ l of dH₂O was used as a negative control.

PCR reactions were incubated in an Eppendorf Mastercycler cycler (Eppendorf, New York, NY, USA). The cycles for PCR were 1 cycle at 94 °C for 3 min, 34 cycles of 94 °C for 30 s, 65 °C for 30 s, and 72 °C for 2 min. The final extension time was 7 min at 72 °C. After amplification, the reactions were analyzed by 1.5% agarose gel electrophoresis.

Characterization of ameloblast-lineage cells (ALC) cultured with LRAP

ALC were also grown on glass chamber slides (Lab-Tek, Naperville, IL, USA) in KGM-2 media (Cambrex). At 60% confluence, cells were synchronized in KBM-2 media (Cambrex) for 16 h, followed by addition of recombinant LRAP to a final concentration of 180 nM per chamber. Cells without LRAP treatment were used as controls. The protein-treated and control cells were incubated for another 24 h at 37 °C. Cells were immunofluorescent stained with rabbit anti-human LAMP-1 (1/500 dilution) (Abcam, Cambridge, MA, USA), anti-human Notch1 (1/100 dilution) (Santa Cruz Biotechnology, Santa Cruz, CA, USA), and anti-human amelogenin antibodies (1/1000 dilution). Amelogenin antibody was purified from serum of a rabbit immunized with recombinant human amelogenin by Protein A affinity chromatography. .

RESULTS

Characterization of purified human recombinant LRAP

Purified recombinant LRAP appeared as a single band in SDS-PAGE at an apparent molecular weight of 6.8 kDa (Fig. 1A), and confirmed by Western blot (Fig. 1B) and mass spectrometry (Fig. 1C). It should be noted that because thrombin was used to

cleave the GST-LRAP fusion protein, there are two additional residues, Gly and Ser, at the N-terminus of the peptides. Mass spectrometric analysis showed that the measured mass of LRAP was 6838.68, which matched the predicted mass of 6838.48 (Fig. 1C).

LAMP-1 detected in stratum intermedium of tooth enamel organ

Immunofluorescent staining of tooth enamel organ showed a positive staining for LAMP-1 localized in stratum intermedium layers (Fig. 2). However, inner enamel epithelium and well-differentiated ameloblast cells did not produce detectable LAMP-1 signals (Fig. 2).

Expression of LAMP-1 at mRNA and protein levels in ALC

LAMP-1 expression detected in ALC by RT-PCR (Fig. 3A). Immunofluorescent analysis showed weakly positive staining for LAMP-1 in ALC (Fig. 3B). In the negative control, ALC stained by pre-immuned IgG was immunonegative for LAMP-1 (Fig. 3C).

LRAP treatment stimulated ALC differentiation by upregulating LAMP-1 and amelogenin, while downregulating Notch1

LRAP treatment did result in a significant change in cell morphology. Cells became larger and appeared more differentiated (Fig. 4B) as compared to the smaller, proliferating, cobblestone-like shapes of the control cells (Fig. 4A).

Immunofluorescent staining showed a strong increase of LAMP-1 staining after the cells were incubated with LRAP (Fig. 4D), while the untreated cells showed weakly positive

staining for LAMP-1 (Fig. 4C). Amelogenin immunostaining was also upregulated under LRAP treatment (Fig. 4F); however, the control untreated cells were amelogenin negative (Fig. 4E). In contrast, LRAP treatment resulted in immunonegative staining for Notch1 (Fig. 4H) as compared to Notch1 positive in the untreated control cells (Fig. 4G).

DISCUSSION

In the present study, we showed positive expression of LAMP-1 at both mRNA and protein levels in epithelial-derived ameloblast-lineage cell (ALC) and stratum intermedium layers of the developing enamel organ. This finding is in agreement with a study by Tompkins and co-workers, who used “Far Western” immunohistochemistry with biotin-labeled LRAP as primary ligand, showing that LAMP-1 immunostaining was most prominent in the stratum intermedium (Tompkins *et al.*, 2006).

LAMP-1 was initially identified in mesenchymal-derived mouse myoblasts as a receptor for LRAP (Tompkins *et al.*, 2006), which induces these cells to undergo the chondrogenic and osteogenic transformation (Nebgen *et al.*, 1999; Veis, 2003). These results along with our previous study showing that LRAP stimulates dental pulp cell proliferation (Ye *et al.*, 2006) suggests that the LAMP-1 receptors may also be present in the dental mesenchymal-derived cells, mediating the regulatory signaling of LRAP in these cells.

In this study, we found that LRAP upregulated LAMP-1 to promote differentiation of ameloblast-lineage cells. These LRAP-treated cells appeared to be rounded, larger and

non-proliferating as compared to the proliferating smaller, cobblestone-shaped of untreated control cells. Similar to our results, upregulation of LAMP-1 expression in epithelial-derived mammary cells and keratinocytes is correlated with cell differentiation (Cella *et al.*, 1996; Sarafian *et al.*, 2006). Thus, LAMP-1, which is upregulated as epithelial cells differentiate, may have a role in mediating the differentiation of ameloblast-lineage cells in the developing enamel organ.

It is interesting that Tompkins *et al.* reported that LRAP inhibited epithelial-derived ameloblast polarization and development in organ culture (Tompkins *et al.*, 2005). These results may reflect the stage-specific effects of LRAP on epithelial cell differentiation. Our *in vivo* immunostaining data showed the absence of LAMP-1 in the more differentiated ameloblasts, suggesting that LAMP-1 expression was downregulated as cells further differentiated. However, whether the prolonged treatment of LRAP to ameloblast-lineage cells (ALC) *in vitro* would eventually result in downregulation of LAMP-1, suggesting that ALC may ultimately differentiate into ameloblast-like cells, is currently unknown. It is possible that LRAP secreted by odontoblasts at the dentoenamel junction (DEJ) could promote early differentiation of ameloblast-lineage cells lining the DEJ, to form stratum intermedium in the initial stages of enamel organ differentiation. Clearly, further studies are needed to understand the role of LAMP-1 in differentiation of cells and in enamel organ development.

Notch1 functions in the maintenance of undifferentiated epithelial stem cells (Harada *et al.*, 1999). Expression of Notch1 at both mRNA and protein level has been reported in

dental epithelial stem cells, located in the stellate reticulum and stratum intermedium cells (Harada *et al.*, 1999; Harada and Ohshima, 2004). These studies suggest that Notch1 is downregulated as enamel organ epithelial cells differentiate. In our present study, immunofluorescent staining showed that ALC produced Notch1 signal, suggesting that these are young and undifferentiated epithelial-derived cells. However, LRAP-treated ALC resulted in decreasing Notch1, but increasing amelogenin immunostaining, supporting the evidence of cell differentiation under the effect of LRAP.

Ameloblast-lineage cells are epithelial-derived cells isolated from the embryonic enamel tooth organ (Yan *et al.*, 2006). The specific stage of ALC development is unclear, but the fact that these are proliferating cells suggests that they are early undifferentiated cells. Initially, these epithelial-derived ALC are largely immunonegative for amelogenins. However, after LRAP treatment, ALC appeared to be more differentiated by showing that Notch1 was downregulated, and both LAMP-1 and amelogenin were upregulated. Increasing amelogenin synthesis as ameloblast-lineage cell differentiating has been reported previously (Yan *et al.*, 2006). In addition, expression patterns and tissue distribution of amelogenins show amelogenins present in stratum intermedium (Iacob and Veis, 2006; Papagerakis *et al.*, 2005). In view of these results we suggest that ALC are undifferentiated ameloblast-lineage cells, which can differentiate to stratum intermedium in the presence of LRAP.

In conclusion, this study shows LAMP-1 receptors are localized in the stratum intermedium cell layer of the developing tooth organ. This receptor is upregulated by

LRAP and promotes tooth organ epithelial cell differentiation *in vitro*. These results suggest that rather than a structural role in enamel formation, LRAP signals early epithelial cell differentiation.

Taken together the results of this chapter and those of chapters 8 and 9, I propose that LRAP is initially synthesized and secreted by odontoblasts at the dentoenamel junction (DEJ), where LRAP is cleaved by MMP-20 and functions to promote ameloblast-lineage cell differentiation. The hydrophilic C-terminal domain may aid in protein packaging and secretion, enhance solubility for diffusion and binding apatite to modulate enamel-crystal growth.

REFERENCES

- Cella N, Cornejo-Uribe RR, Montes GS, Hynes NE, Chammas R (1996). The lysosomal-associated membrane protein LAMP-1 is a novel differentiation marker for HC11 mouse mammary epithelial cells. *Differentiation* 61(2):113-20.
- Fincham AG, Belcourt AB, Termine JD, Butler WT, Cothran WC (1981). Dental enamel matrix: sequences of two amelogenin polypeptides. *Biosci Rep* 1(10):771-8.
- Gibson CW, Golub E, Ding WD, Shimokawa H, Young M, Termine J, Rosenbloom J (1991). Identification of the leucine-rich amelogenin peptide (LRAP) as the translation product of an alternatively spliced transcript. *Biochem Biophys Res Commun* 174(3):1306-12.
- Harada H, Kettunen P, Jung HS, Mustonen T, Wang YA, Thesleff I (1999). Localization of putative stem cells in dental epithelium and their association with Notch and FGF signaling. *J Cell Biol* 147(1):105-20.
- Harada H, Ohshima H (2004). New perspectives on tooth development and the dental stem cell niche. *Arch Histol Cytol* 67(1):1-11.
- Iacob S, Veis A (2006). Identification of temporal and spatial expression patterns of amelogenin isoforms during mouse molar development. *Eur J Oral Sci* 114 Suppl 1(194-200); discussion 201-2, 381.

Le TQ, Gochin M, Featherstone JD, Li W, Denbesten PK (2006). Comparative calcium binding of leucine-rich amelogenin peptide and full-length amelogenin. *Eur J Oral Sci* 114 Suppl 1(320-6).

Nebgen DR, Inoue H, Sabsay B, Wei K, Ho CS, Veis A (1999). Identification of the chondrogenic-inducing activity from bovine dentin (bCIA) as a low-molecular-mass amelogenin polypeptide. *J Dent Res* 78(9):1484-94.

Papagerakis P, Ibarra JM, Inozentseva N, DenBesten P, MacDougall M (2005). Mouse amelogenin exons 8 and 9: sequence analysis and protein distribution. *J Dent Res* 84(7):613-7.

Sarafian V, Jans R, Poumay Y (2006). Expression of lysosome-associated membrane protein 1 (Lamp-1) and galectins in human keratinocytes is regulated by differentiation. *Arch Dermatol Res*.

Tompkins K, Veis A (2002). Polypeptides translated from alternatively spliced transcripts of the amelogenin gene, devoid of the exon 6a, b, c region, have specific effects on tooth germ development in culture. *Connect Tissue Res* 43(2-3):224-31.

Tompkins K, Alvares K, George A, Veis A (2005). Two related low molecular mass polypeptide isoforms of amelogenin have distinct activities in mouse tooth germ differentiation in vitro. *J Bone Miner Res* 20(2):341-9.

Tompkins K, George A, Veis A (2006). Characterization of a mouse amelogenin [A-4]/M59 cell surface receptor. *Bone* 38(2):172-180.

Veis A, Tompkins K, Alvares K, Wei K, Wang L, Wang XS, Brownell AG, Jengh SM, Healy KE (2000). Specific amelogenin gene splice products have signaling effects on cells in culture and in implants in vivo. *J Biol Chem* 275(52):41263-72.

Veis A (2003). Amelogenin gene splice products: potential signaling molecules. *Cell Mol Life Sci* 60(1):38-55.

Yan Q, Zhang Y, Li W, Denbesten PK (2006). Differentiation of human ameloblast-lineage cells in vitro. *Eur J Oral Sci* 114 Suppl 1(154-8).

Ye L, Le TQ, Zhu L, Butcher K, Schneider RA, Li W, Besten PK (2006). Amelogenins in human developing and mature dental pulp. *J Dent Res* 85(9):814-8.

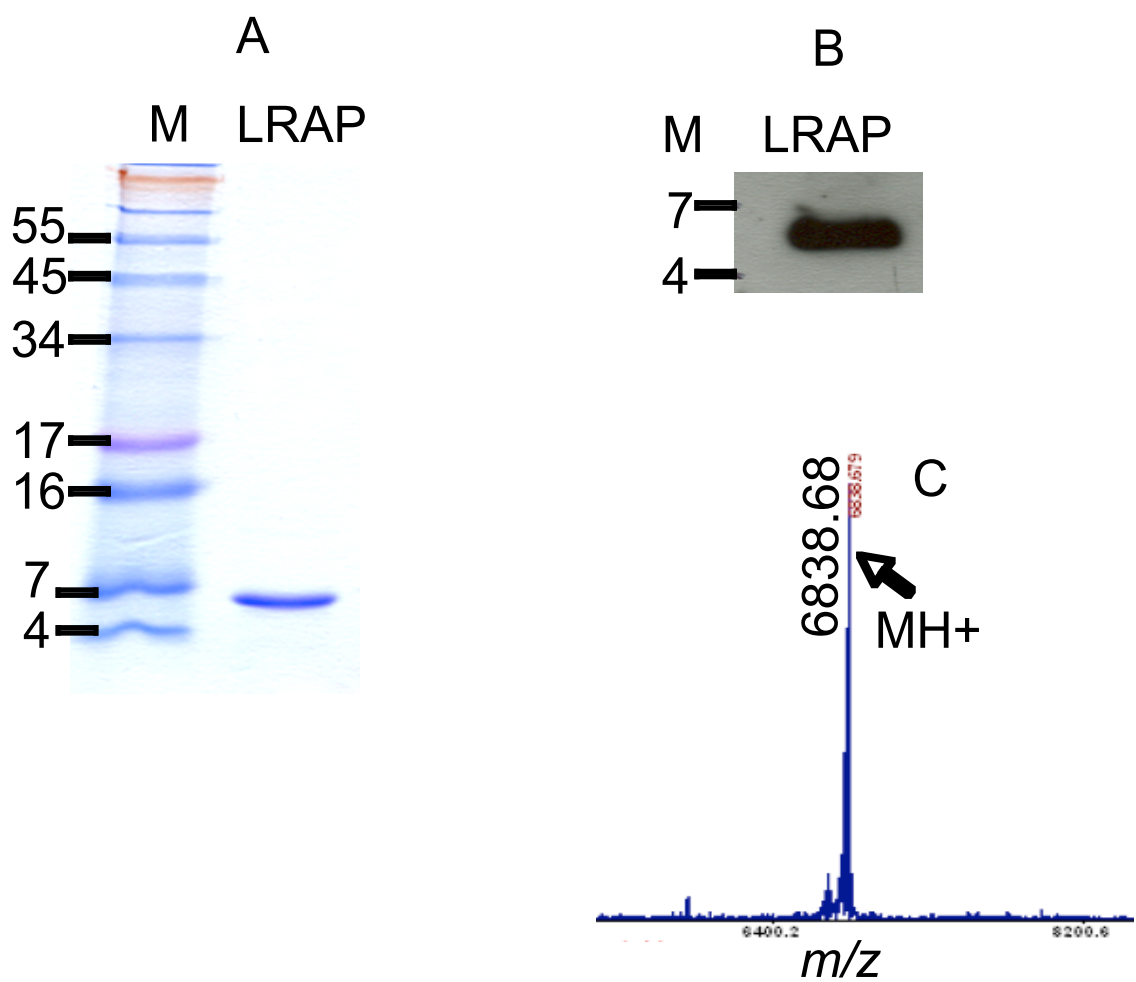


Figure. 1.

Characterization of human recombinant purified LRAP.

(A) SDS-PAGE and (B) Western blot of purified LRAP as a single band at ~6.8 kDa.

(C) Mass spectrometric analysis of LRAP to reconfirm its identity as a peak (arrow) representing 6838.68 ($M/z = \text{Da}$), which matched its theoretical mass of 6838.48 ($M/z = \text{Da}$).

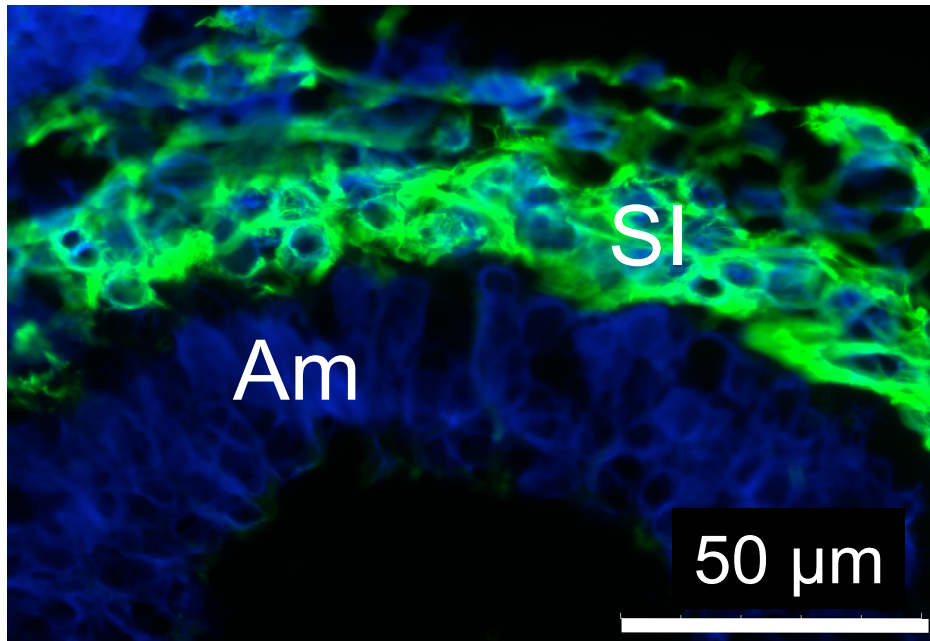


Figure 2.

LAMP-1 detected in stratum intermedium of tooth enamel organ.

Immunofluorescent staining of LAMP-1 showed a strong positive staining for LAMP-1 in stratum intermedium (SI) layers of a frozen section of a human enamel organ, while immunostained for LAMP-1 in ameloblasts (Am) was not detectable. Cell nuclei were counterstained with Hoechst dye (blue).

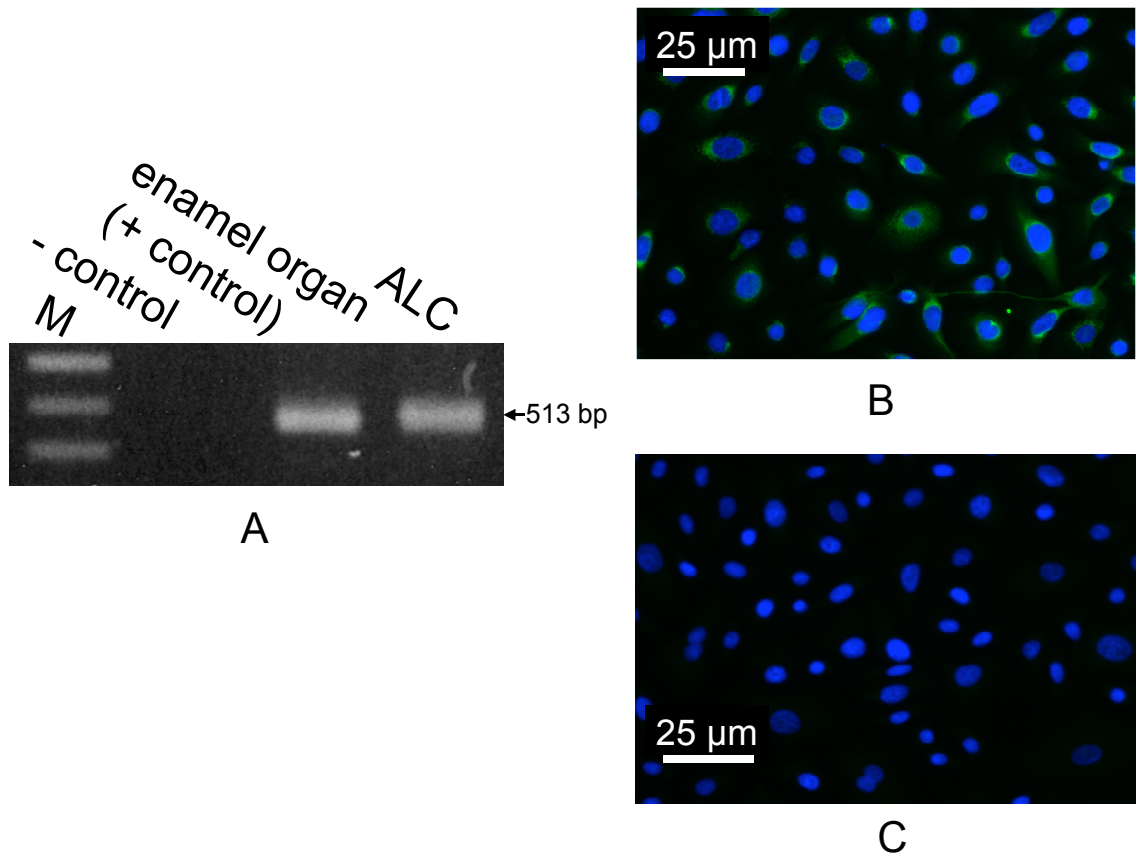


Figure 3.
Reverse-transcription (RT)-PCR to detect mRNA expression and immunostaining of LAMP-1 in ALC.
 (A) RT-PCR product showed positive LAMP-1 expression, indicating by 513-bp band in 1% gel. Human enamel organ cDNA library was used as a positive control, while no addition of cDNA template was used a negative control. (B) A weak positive staining (green) of LAMP-1 in cytoplasm of primary ALC. (C) Pre-immuned IgG staining in ALC showed immunonegative for LAMP-1. Cell nuclei were counterstained with Hoechst dye (blue).

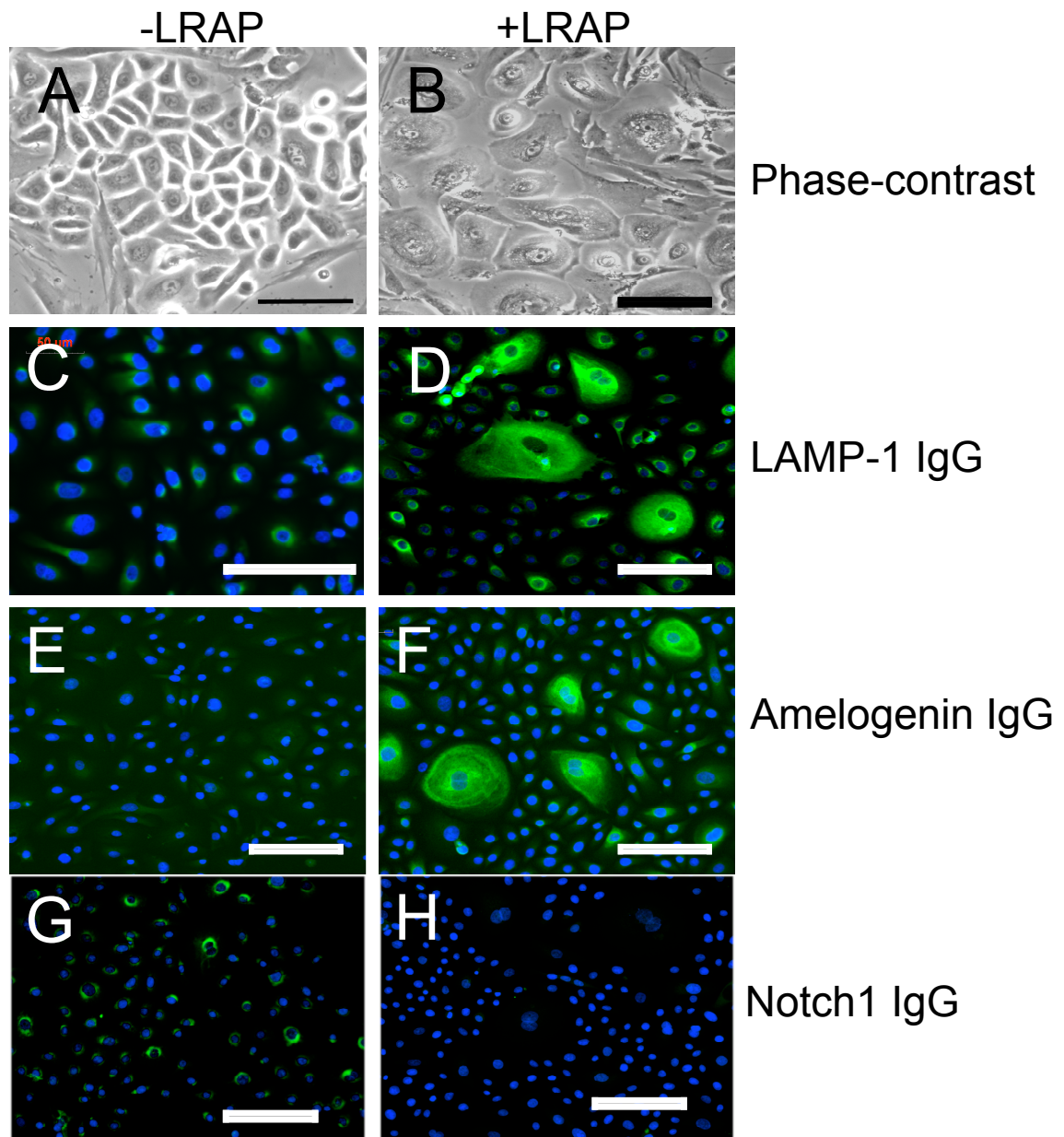


Figure 4.

Characterization of LRAP-treated ameloblast-lineage cells (ALC).

Phase-contrast images showed that under the treatment of LRAP (B), ALC became rounded, larger and non-proliferating, while the untreated control cells (A) retained their small, cobblestone-like shapes. Immunofluorescent results indicated strong positive staining for LAMP-1 (D) and amelogenin (F), but decreased immunostaining for Notch1 (H) in LRAP-treated ameloblast-lineage cells. The untreated control cells were stained weakly for LAMP-1 (C) and negative immunostaining for amelogenin (E), but immunopositive for Notch1 (G). Cell nuclei were counterstained with Hoechst dye (blue). Bars = 50 μ m.

Chapter 11 Conclusion and Future Studies

It has been a challenging and rewarding research thesis project, which provided me with a tremendous opportunity to learn during my graduate training. I began my research study using proteins, antibodies, odontogenic cells and carbonated hydroxyapatites that were not commercially available. As a result, I spent a substantial amount of effort to learn how to produce and characterize these proteins and biological materials from the very basic levels. However, the outcomes were highly satisfactory.

The topic of my dissertation is primarily focused on the functional analysis of amelogenins and specific alternatively spliced variants, called leucine-rich amelogenin peptide (LRAP) and LRAP+exon4 (briefly), whose functions in tooth development are completely unknown. I began my research in Dr. Den Besten's lab with the hypothesis that post-translationally modified full-length amelogenin (phosphorylation of Ser-16) may function as a signaling molecule and/or mineral inducer.

After one year of investigating, I was not successful with this project. Despite the fact that I have used various cell lines (i.e. immortalized porcine and human ameloblast-like cells and odontoblasts), different vectors and various retroviral approaches for transfection, I could only produce such a small amount of phosphorylated amelogenins, that it was not practical to propose using this material for future studies. Although I made several attempts to increase the efficiency of protein expression and production scale, I was not able to produce a high-yield amount of phosphorylated amelogenin that

could be used for functional studies in my subsequent experiments (not included in this thesis). Other investigators, who have utilized insects and other mammalian cell lines to express amelogenin, also experienced similar challenges. Currently, the function of phosphorylated amelogenin in tooth development remains obscure. With improved technology and methods in the future to overcome this obstacle, the functions of post-translational modified amelogenins should be investigated.

I then changed my research focus from the role the phosphorylated Ser-16 to study the function of the smaller alternatively spliced amelogenins, such as LRAP, relative to the longer amelogenins derived from splice variants that included the entire exon 6 (i.e. rH174 or full-length amelogenin). These amelogenins were synthesized by *E. coli*, and purified using a combination of chromatographic techniques. My first hypothesis was to test whether or not amelogenins specifically interact with carbonated hydroxyapatite to induce protein-mediated enamel-like crystal growth *in vitro*.

To begin, I successfully synthesized and characterized carbonated hydroxyapatite using various methods such as FTIR and X-ray diffraction in Dr. Featherstone's lab (chapter 3). This synthetic carbonate hydroxyapatite has been proven to be similar in composition and property of dental enamel, and thus was used as an enamel substitute. This synthetic carbonated hydroxyapatite was critical for the subsequent protein-apatite interaction experiments done as a part of this thesis project.

My next goal was to produce several different human recombinant amelogenins (full-length and fragments of alternatively spliced variants). The purification of these amelogenins has proven to be the most difficult task because of their high degree of hydrophobicity. However, utilizing two-step purification approach, glutathione-beads affinity column and followed by C18 reverse-phase HPLC, purified amelogenins were successfully obtained and subsequently characterized (chapter 4). These proteins have proven to be instrumental for investigating the mechanism of amelogenin-apatite interaction that guided enamel-like crystal growth *in vitro*. Such protein-matrix interaction may play a critical role in regulating a highly-controlled process of enamel formation (chapter 5). I definitively showed that amelogenins bind directly to the surface of carbonated hydroxyapatite by the C-terminal domains. However, unlike LRAP, only full-length amelogenin (rH174) can promote enamel-like crystal growth *in vitro*. Since LRAP is different from the full-length amelogenin in that it lacks the central domain encoded by majority of exon 6. This region presumably includes a β -spiral structure that maybe important for mineralization. Future studies should focus on the functions of this central region of the full-length amelogenin in its ability to guide enamel-like crystal formation.

Although amelogenins bind specifically to the surface of apatites, it is important to understand the mechanism of this interaction. Since the surfaces of apatites are saturated with calcium ions, it is logical to study the binding between the negatively charged amelogenins and calcium ions. To determine the calcium binding to amelogenins, it was necessary to optimize the isothermal titration microcalorimetry (ITC) experimental

conditions by first studying the interaction between negatively-charged and highly phosphorylated and non-phosphorylated proteins such as phosphovitin (PV) and bovine serum albumin (BSA), respectively (chapter 6). Subsequently, the bindings of full-length amelogenin and LRAP to calcium ions were also determined (chapter 6). Moreover, a similar interaction was also detected between calcium ions and the synthetic C-terminal peptide, implicating that amelogenins interact with calcium ions via the negatively charged hydrophilic C-terminal domain. Since carbonated hydroxyapatite surface is highly saturated with calcium, it is most likely that the C-termini of amelogenins bind apatite surface by interacting with calcium ions via ionic interactions.

To further understand the possible role of calcium in amelogenin structure, the structure of LRAP was studied with the presence and absence of calcium ions using CD and NMR. I found that in the presence of calcium in solution, LRAP maintained its random-coiled conformation (chapter 7). Yet, it is still possible that under a specific buffer condition similar to that found in the enamel matrix, LRAP may be induced to fold into a well-defined structure. Such structural folding was not been detected in the buffer conditions that I studied. Future studies should aim at determining the specific conditions that would allow LRAP to fold into a specific structure (i.e. α -helix and /or β -sheet). Subsequently, LRAP crystallization for X-ray crystallography study is a worthwhile research pursuit.

Since LRAP had no structural function to promote crystal growth, this lead to my second hypothesis. I hypothesized that LRAP may function as a signaling molecule by binding

to its specific cell-surface receptor to regulate cell proliferation and differentiation that is responsible for tooth enamel development. In chapter 8, I showed definitively that dental pulp cells (DPC) express alternatively spliced amelogenin mRNA's that encoded for LRAP and LRAP+exon4. Functional analysis of LRAP and LRAP+exon4 showed that these low-molecular-weight amelogenins significantly stimulated dental pulp cell proliferation, but had no effect on cell differentiation *in vitro*. These results suggest that alternatively spliced amelogenins may play a role in early dentinogenesis. Because the biological effects of LRAP and LRAP+exon4 on pulp cell proliferation were not significantly different, LRAP was chosen for subsequent functional analysis due to its higher yield during recombinant protein expression and purification.

In contrast to the effects on dental pulp cells, LRAP had no effect on ameloblast-lineage cell (ALC) proliferation (chapter 9 and 10). However, LRAP stimulated ALC differentiation by up-regulating LRAP's receptor LAMP-1 (chapter 10) and other cell differentiation markers (chapter 9), implicating its role in amelogenesis. The effects of LRAP+exon4 on ALC proliferation and differentiation were not studied because the synthesis and purification of recombinant LRAP+exon4 was a challenge, resulting in such a low yield due to its highly hydrophobic property.

After discovering that LRAP was a biological active molecule, my third hypothesis was that LRAP contained a biological active domain located on the N-terminal region of the peptide. This hypothesis was formulated based on the fact that N-terminal motif is highly hydrophobic fragment, which would be most likely interact with LAMP-1 receptor,

presumably via hydrophobic-hydrophobic interaction. To test this hypothesis, several LRAP enzymatic products were created by controlled MMP-20 proteolysis. LRAP was progressively hydrolyzed (3 specific MMP-20 cleavage sites) from the C-terminal end (chapter 9). The structural mechanism by which MMP-20 recognizes and binds LRAP substrates to facilitate cleavage is a subject of current investigation using surface plasmon resonance (SPR) based technology (Biacore, Piscataway, NJ, USA) and X-ray crystallography. I showed that the N-terminal proteolytic product of LRAP contains the biological functional domain (chapter 9) to promote ameloblast-lineage cell differentiation.

We are currently embarking on additional collaborative studies to determine precisely which specific amino acid fragments (< 10-residue motifs) within this N-terminal domain are responsible for the biological effects on cells. Subsequently, these specific peptides will be immobilized onto specific biomaterials, onto which odontogenic cells are seeded, to study the specific signaling transduction pathway that controls tooth development. These novel findings are critical for future tissue engineering application to regenerate enamel and dentin.

In brief, this thesis work has provided new insights into process of amelogenin proteolysis by MMP-20, the functions of amelogenin and its alternatively spliced variants on enamel-like crystal growth, and their specific effects on cell proliferation and/or differentiation that ultimately regulate tooth formation. Although further studies are needed to better understand these amelogenin structure/function relationships, the

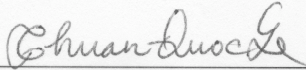
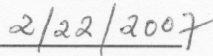
findings described in this thesis have resulted in a deeper understanding of tooth development. This knowledge is critical for further studies of tooth regeneration and the use of amelogenins in biomineralization.

Publishing Agreement

It is the policy of the University to encourage the distribution of all theses and dissertations. Copies of all UCSF theses and dissertations will be routed to the library via the Graduate Division. The library will make all theses and dissertations accessible to the public and will preserve these to the best of their abilities, in perpetuity.

Please sign the following statement:

I hereby grant permission to the Graduate Division of the University of California, San Francisco to release copies of my thesis or dissertation to the Campus Library to provide access and preservation, in whole or in part, in perpetuity.

 _____	 _____
Author Signature	Date